Chair of Energy Geosciences

Master's Thesis

Systematic analysis of sediments, gas seeps and sludge gas at Lake Neusiedl

Christoph Bähr, BSc

September 2024

MONTANUNIVERSITÄT LEOBEN
www.unileoben.ac.at

EIDESSTATTLICHE ERKLÄRUNG

Ich erkläre an Eides statt, dass ich diese Arbeit selbstständig verfasst, andere als die angegebenen Quellen und Hilfsmittel nicht benutzt, den Einsatz von generativen Methoden und Modellen der künstlichen Intelligenz vollständig und wahrheitsgetreu ausgewiesen habe, und mich auch sonst keiner unerlaubten Hilfsmittel bedient habe.

Ich erkläre, dass ich den Satzungsteil „Gute wissenschaftliche Praxis" der Montanuniversität Leoben gelesen, verstanden und befolgt habe.

Weiters erkläre ich, dass die elektronische und gedruckte Version der eingereichten wissenschaftlichen Abschlussarbeit formal und inhaltlich identisch sind.

Datum 14.09.2024

Bähr Christoph

Unterschrift Verfasser/in
Christoph Bähr

Acknowledgments

Besonderer Dank gilt meinen Eltern, ohne eure Unterstützung wäre das Studium nicht möglich gewesen. Ein großer Dank geht auch an meine Schwester Selina, Markus Gruber, Christoph Baschny, und Philipp Tremmel, die mich tatkräftig und selbstlos bei der Probenahme unterstützt haben und Janine Pink für das Korrekturlesen. Zusätzlich noch ein Dankeschön an den gesamten Lehrstuhl für Energy Geosciences. Die erfahrene Unterstützung und Hilfsbereitschaft sind nicht selbstverständlich!

Abstract

Permanent gas seeps at Lake Neusiedl are indicated in literature, but not very well characterized in terms of their origin. This study aimed at analysing the source of the apparently permanent seeps and comparing their geochemical signature with sludge gas that is a common by-product of organic matter degradation in the lake sediments. The main research questions were if a thermogenic gas source exists, and if all gases of biogenic origin share a common source or can be distinguished by their organic-geochemical signature.

Molecular and stable carbon and hydrogen isotope compositions were measured to analyse the origin of the gas. Methane was the only hydrocarbon that was detected, indicating the absence of a thermogenic contribution of higher hydrocarbon components. Stable hydrogen and carbon isotope signature of methane and CO_2 confirm a purely biogenic source for seep gas and sludge gas. A systematic difference in isotope composition between these two types could not be detected, so a common origin of all gases, presumably associated with organic matter degradation in the lake sediments, is indicated. It is still under question why some of the gas shows seem to occur permanently at the same spot, and if this observation holds true at all. No evidence was found that permanent shows are related to a shallow microbial reservoir associated with organic-rich strata underlying the recent lake sediments.

Another point of investigation were systematic changes of mineralogy and bulk geochemical parameters across the W-E lake axis. Sediment samples along two profiles between Breitenbrunn and Podersdorf were analysed via X-ray diffraction, as well as for their total organic carbon (TOC) content and pH. The composition of the lake sediments is dominated by quartz, feldspar, clay minerals and varying carbonate minerals. Carbonate minerals present are calcite, low magnesium calcite, high magnesium calcite and protodolomite. The X-ray diffractograms showed broadened peaks for low magnesium calcite, and protodolomite. The formation of high magnesium calcite and protodolomite is currently only occurring in specific regions of the lake. The pH decreases towards the lake centre, while TOC increases accordingly, arguing for more favourable conditions for organic matter preservation.

Kurzfassung

Permanente Gasaustritte am Neusiedlersee wurden zwar in der Literatur erwähnt, jedoch noch nicht ausreichend auf die Herkunft des Gases untersucht. Diese Studie zielte darauf ab, den Ursprung dieser permanenten Gasaustritte zu untersuchen und diese mit der geochemischen Signatur des Schlammgases, welches ein gewöhnliches Beiprodukt der Degradation von organikreichem Seesediment ist, zu vergleichen. Die vorrangige Forschungsfrage war herauszufinden, ob eine thermogene Gasquelle existiert, und ob alle biogenen Gase einen gleichen Ursprung haben oder durch die organisch-geochemische Signatur unterschieden werden können.

Die Zusammensetzung der molekularen und stabilen Kohlenstoff-, und Wasserstoff-Isotope wurde gemessen, um die Herkunft des Gases zu analysieren. Methan wurde als einziger Kohlenwasserstoff nachgewiesen, was auf die Abwesenheit eines thermogenen Einflusses von höheren Kohlenwasserstoffkomponenten hinweist. Die stabile Wasserstoff-, und Kohlenstoff-Isotope Signatur von Methan und CO_2 bestätigen eine rein biogene Quelle für das permanent austretende Gas und Schlammgas. Ein systematischer Unterschied in der Zusammensetzung der Isotope zwischen den beiden Typen wurde nicht gefunden, was auf einen gemeinsamen Ursprung aller Gase hinweist, welcher vermutlich mit der Degradation von organischer Materie im Seesediment verbunden ist. Es stellt sich noch immer die Frage, warum manche Gasaustritte anscheinend dauerhaft am gleichen Ort auftreten, falls das überhaupt zutrifft. Kein Nachweis wurde bei den permanenten Gasaustritte dafür gefunden, dass sie in Verbindung mit oberflächennahen mikrobiellen Reservoirs, welche in Zusammenhang mit einer organikreichen Schicht, die unter den rezenten Seesedimenten liegt, stehen.

Ein weiterer Punkt war die Untersuchung der systematischen Unterschiede der Mineralogie und unterschiedlichen geochemischen Parametern über die West-Ost Achse des Sees. Sediment Proben wurden in zwei Profilen zwischen Breitenbrunn und Podersdorf genommen und mittels Röntgendiffraktometrie, dem gesamten organischen Kohlenstoffgehalt (TOC) und pH analysiert. Die Zusammensetzung des Seesediments wird von Quarz, Feldspat, Tonminerale und unterschiedlichen Karbonaten dominiert. Die Karbonate setzen sich aus Kalzit, Kalzit mit geringem Magnesiumgehalt, Kalzit mit hohem Magnesiumgehalt und Protodolomit zusammen. Die Röntgendiffraktogramme zeigten verbreiterte Peaks für Kalzit mit geringem Magnesiumgehalt und Protodolomit. Kalzit mit hohem Magnesiumgehalt und Protodolomit bilden sich momentan nur in gewissen Bereichen des Sees. Der pH sinkt in Richtung Seemitte, für TOC steigen die Werte, was auf günstige Bedingungen für die Erhaltung von organischer Materie hinweist.

Content

1 Introduction

"Kochbrunnen" at Lake Neusiedl have a long research history, from early interpretation as hydrothermal vents (Sauerzopf, 1959; Tauber, 1959; Gattinger, 1979; see Rank et al., 1985) to recent recognition as gas seeps (Rank et al., 1986; Häusler et al., 2010). While a shallow biogenic source of the gas shows is most likely, it is still not clear if a deeper thermogenic source could also play a role, considering the gas seeps have existed for decades. The work herein will attempt to answer these questions with modern molecular compositional and carbon and hydrogen stable isotope geochemical investigations of gas samples from permanent seeps (e.g. located at Rust) and the lake mud.

Furthermore, to gain an understanding of the composition of the lake sediments and their organic matter content, sediment profiles roughly across the W_E axis of the lake were analysed. Samples were collected at the eastern and western lake margins along two sub-profiles towards the lake centre starting from Breitenbrunn and Podersdorf, respectively. Changes in sediment mineralogy and particularly carbonate content were investigated by X-ray diffraction and additionally total organic carbon (TOC) content and pH measurements were performed.

Protodolomite is forming at Lake Neusiedl at the sediment-water interface, but the responsible mechanisms are still not fully understood (Fussmann et al., 2020; Meister et al., 2023; Neuhuber et al., 2024). Potential influencing factors could be the mineralogical composition of the sediment, or the pH conditions at the respective location. The samples were screened for protodolomite content in order to find potential links to systematic compositional or geographical influences on the presence of protodolomite.

2 Lake Neusiedl

2.1 Geographical overview

Lake Neusiedl is situated at the border between Austria and Hungary with its major part being located in the Austrian province Burgenland (Fig. 1).

Figure 1: Map of Lake Neusiedl with the most important locations for this study.

The lake covers an area of ~300 km² with a maximum water depth of ~1.8 m depending on the seasonal water level (Wolfram & Herzig, 2013). Lake Neusiedl is a very shallow steppe lake with varying water levels and high salinity. This leads to a unique biodiversity, especially of birds. About half of it is covered in reeds (Herzig, 2014) and Podersdorf am See is the only location without a reed belt at the lake shore and a direct connection to the beach. The importance of Lake Neusiedl for the province Burgenland in terms of tourism as well as biodiversity is immense. The main tributary water comes from the Wulka River from the western side (Herzig, 2014). There are also other influxes and a drainage system at the Hungarian side to control the lake level. Recently an artificial influx of Danube River water to the lake has been discussed due to the concerns that the lake may dry out due to decreased precipitation and increasing mud levels. Introducing water from a different water body however would create new risks to biodiversity due to changes in the water chemistry and possible introduction of invasive species (Dinka et al. 2004; Wolfram & Herzig 2013; Wolfram et al., 2014).

2.1.1 Temperature

The current annual temperature in Burgenland is approximately 12°C (Fig. 2) with higher temperatures in the north. Compared to the period of 1940 – 1980 there is an increase of about 2°C in average temperature at Neusiedl am See (Fig. 1). The continued increase in the average temperature at the area of Lake Neusiedl is also shown in Eitzinger et al. (2009; Fig. 2) and Hiebl & Orlik (2023; Fig. 3).

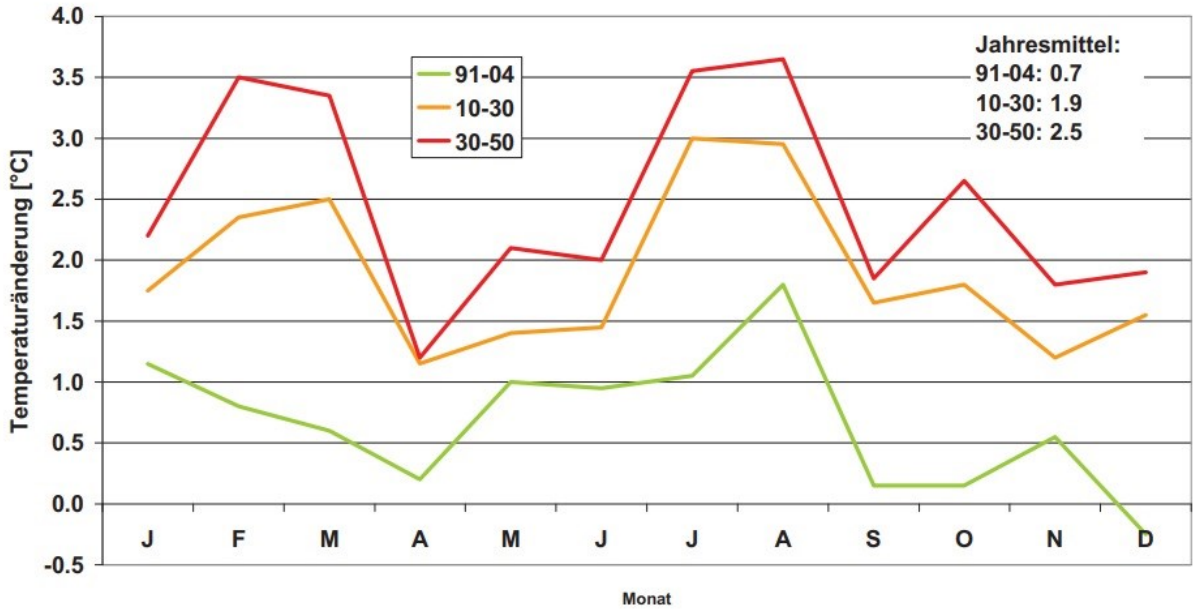

Figure 2: Mean temperature change for specific time periods (1991 – 2004 in green, 2010 – 2030 in orange, 2030 – 2050 in red) at Neusiedl am See compared with the period 1961 – 1990. The x-axis indicates the month and the y-axis the change in the average temperature compared to the period 1961 – 1990 (Eitzinger et al., 2009).

2.1.2 Precipitation

The annual precipitation is approximately 700mm/yr (Fig. 3) but can strongly vary. The northern part of the Burgenland shows a more arid climate compared to the south. Figure 3 shows no clear ongoing trend in one way or the other and the research of Eitzinger et al. (2009) also shows no indication of a future trend.

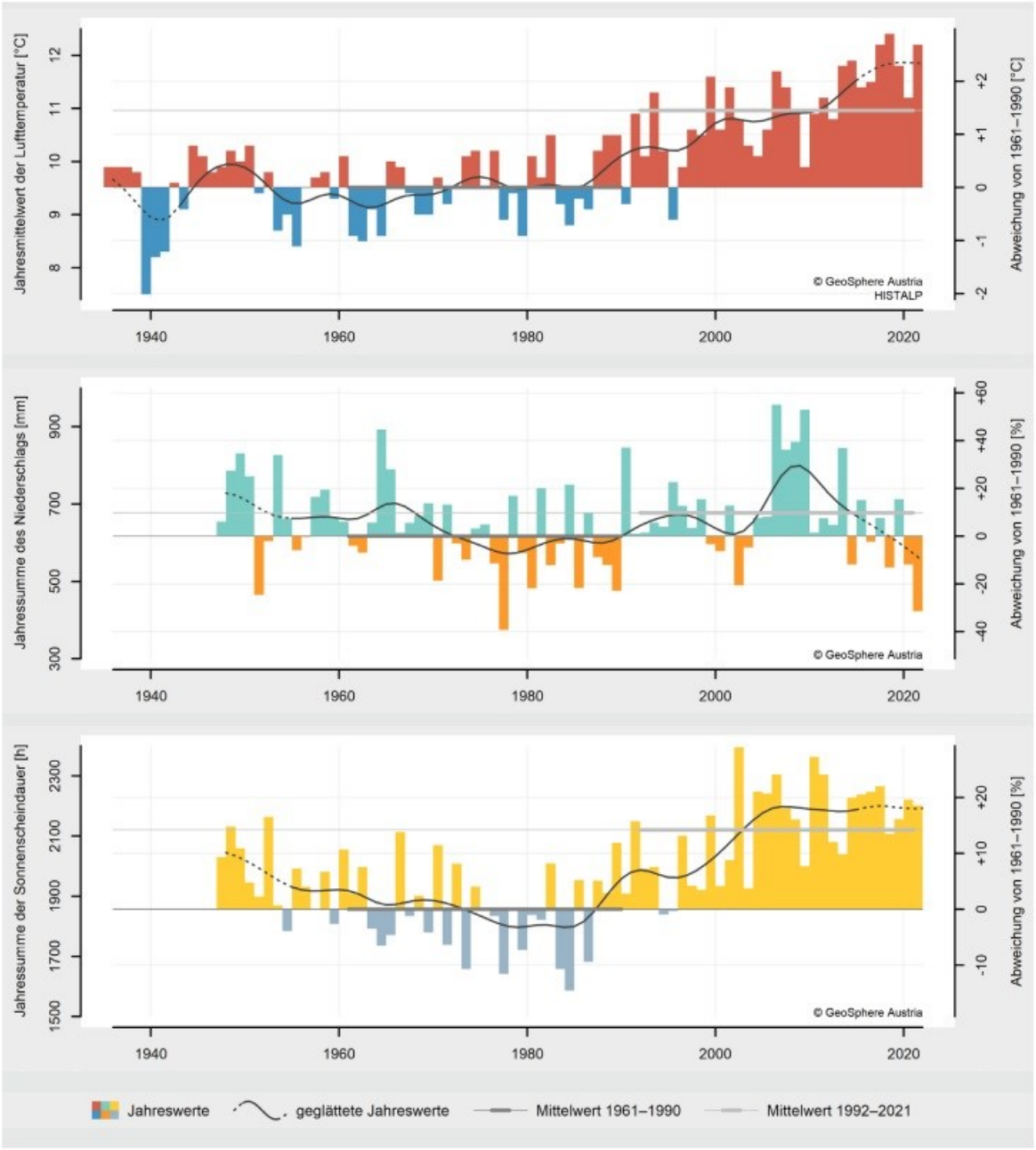

Figure 3: Annual sum and mean of the temperature (top), precipitation (middle) and duration of sunshine (bottom) with the mean values of the time period 1961 - 1990 (dark grey) and 1992 - 2021 (light grey) (Hiebl & Orlik, 2023).

2.2 Wind currents

Lake Neusiedl is in general prone to strong wind. The main wind direction is northwest, but in late autumn and winter changes to southeast (Herzig, 2014). This also explains the continental, dry and hot Pannonian climate. The low relief leads to wind currents that are only minor orographically influenced (Dobesch & Neuwirth, 1978). The average wind force is the strongest directly above the lake and higher at the eastern shore compared to the western shore (Dobesch & Neuwirth, 1978). Long term thermal stratification is prevented due to the lake being strongly exposed to wind currents and with no barrier in the proximity, as well as the low average water level of the lake (Herzig, 2014). The strong wind currents lead to turbulence and resuspension of the lake sediments. These currents and the resulting piling up of ice layers in the Holocene are the reasons for formation of lake dams in the eastern part of up to 0.5 m at this low lake level (Häusler, 2007).

2.3 Water level

The average water depth in Lake Neusiedl is about 1.2 m with a maximum of ~1.8 m in the deepest part (Herzig, 2014). The water level fluctuates in general between 115 and 116 m above the Adriatic Sea level. A very low water level in the last years has led to significantly reduced water depths, which was conquered by mud extraction from the lake margins. Insertion of river water from the Danube River is currently being discussed to maintain the water level at the height required for tourism and agriculture. The lake is very dependent on precipitation. Years or decades of low influx of rain and drainage water can seriously decrease the water column or eventually lead to a drying out of the lake. Twenty-two percent of the recharge are contributed by surface influx (mean 1965-2012; Kubu & Kramer, 2014) with the Wulka River as main contributor with 14 %, the remainder is provided from the Kroisbach River, Golser Kanal and some streams from the Ruster Hügelland and the Hügelland von Boz (Herzig, 2014). Underground inflow and outflow have only a minor impact (Kubu & Kramer, 2014). The different evaporation events since the year 1600 can be seen in Figure 4. The Einser-Kanal was constructed in 1909-1911 and led to a more regulated water level.

Figure 4: Water level of Lake Neusiedl since 1600 reconstructed based on historical data (Jubiläumsschrift „40 Jahre Österreichisch-Ungarische Gewässerkommission“, 1996; see Eitzinger et al., 2009).

2.4 Water currents

Because of the shallowness of Lake Neusiedl, wind direction and intensity are the controlling factors for water movement (Sauerzopf, 1959). There are two different driving factors: the water current and the drift of the whole water body (Sauerzopf, 1959). If the wind direction is northwest, the wind circulates the water current on the eastern shore to flow south, and on the western shore an opposing water current is created directed to north (Fig. 5; Sauerzopf, 1959). At inlets like at Rust swirls and deviations can form (Sauerzopf, 1959). The reed belts also show a directed current (Sauerzopf, 1959). These currents are also the reason for a mud-free sea gate at Mörbisch (Sauerzopf, 1959). The occurrence of longitudinal shaped gravel deposits seems also to be one of the results of the currents (Sauerzopf, 1959). Long-lasting strong storms lead to a drift of the water body into the direction of the wind, and this leads to an inclination of the water column (Sauerzopf, 1959).

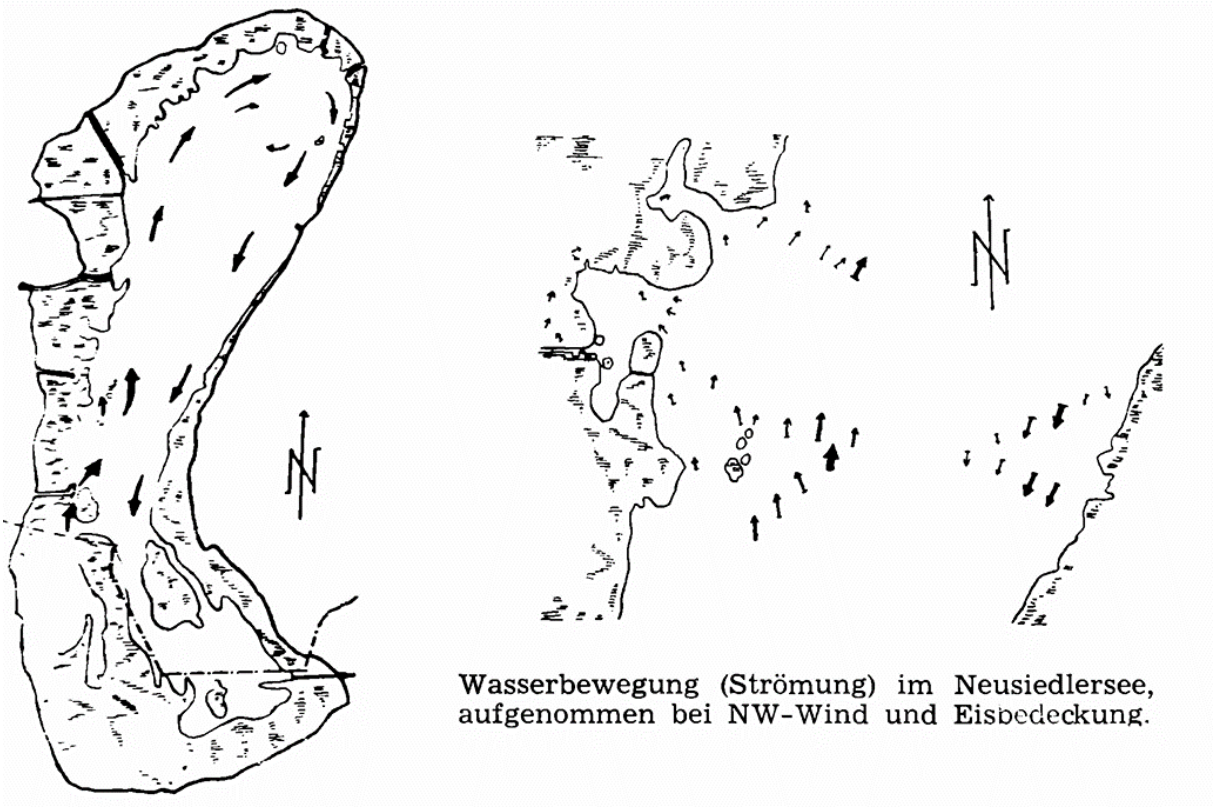

Figure 5: Water currents at Lake Neusiedl due to wind in northwest direction and when covered by ice (Sauerzopf, 1959).

2.5 Water geochemistry

Lake Neusiedl is a rather saline lake. Reasons for this are the semiarid climate, the hydrological characteristics, saline tertiary sediments and the connection to deep groundwater by tectonic fault lines (Wolfram, 2006; see Herzig, 2014). The current salt content amounts to approximately 1.2 g/l and an alkaline character with a pH > 8 (Herzig, 2014). This classifies the lake water as oligohaline according to the Venice classification (Tab. 2). The salinity increased up to 16 g/l during low water levels in the last century according to Herzig (2014). The total dissolved solids of the lake water consist mostly of sodium, magnesium, bicarbonate, sulphate and chloride (Tab. 1; Wolfram & Herzig, 2013). Because soda-hydrogen carbonate is dominant and pH is high, it is considered a soda lake. The strong saline brines around the lake have an evaporation residue of over 2 g/l (Schroll, 1959).

Morphometrische Kenndaten		
Maximale Oberfläche (bei Pegel 116,0 m ü.A.)	315	km^2
davon: offener See	48	%
Schilfgürtel	52	%
Einzugsgebiet	1.120	km^2
Mittlerer Wasserspiegel	115,45	m ü.A.
Maximale Wassertiefe	1,8	m
Mittlere Wassertiefe	1,2	m
Maximales Volumen (bei Pegel 116,0 m ü.A.)	$367,5 \times 10^6$	m^3
Volumen bei Pegel 115,0 m ü.A.	$114,9 \times 10^6$	m^3
Physikal.-chemische / hydrochemische Kenndaten		
elektrische Leitfähigkeit	2.249 (1.300-3.200)	$\mu S\ cm^{-1}$
pH-Wert	8,7 (8,0–9,1)	$-\log[H^+]$
Sauerstoff	10,3 (5,8–17,2)	$mg\ L^{-1}$
Wassertemperatur	14,7 (0,2–28,7)	°C
Calcium Ca^{2+}	31 (3–119)	$mg\ L^{-1}$
Magnesium Mg^{2+}	144 (17–199)	$mg\ L^{-1}$
Natrium Na^+	363 (207–684)	$mg\ L^{-1}$
Kalium K^+	39 (15–67)	$mg\ L^{-1}$
Karbonat CO_3^{2-}	39 (3–97)	$mg\ L^{-1}$
Hydrogenkarbonat HCO_3^{2-}	610 (346–1139)	$mg\ L^{-1}$
Chlorid	253 (141–406)	$mg\ L^{-1}$
Sulfat-S	163 (90–270)	$mg\ L^{-1}$
Ammonium-N NH_4-N	33 (1–377)	$\mu g\ L^{-1}$
Nitrat-N NO_3-N	157 (2–941)	$\mu g\ L^{-1}$
Gesamtphosphor	73 (14–552)	$\mu g\ L^{-1}$

Table 1: Physical, chemical and hydro chemical data of Lake Neusiedl (Wolfram & Herzig, 2013).

Salinity [ppt]	Salinity term	Typical environment
0-0.5	Limnetic	Freshwater
0.5-5	Oligohaline	Near mouth of river or stream
5-18	Mesohaline	Upper estuary
18-30	Polyhaline	Middle to lower estuary
30-40	Euhaline	Marine
>40	Hypersaline	Shallow bodies of saltwater

Table 2: Venice system for classification of water bodies according to salinity values (after Winqard, 2004).

2.6 Paleo salinity trend

The salinity changed drastically since the Upper Tortonian, during which the lake was euhaline with a salinity of 36-38 g/l. Salinity decreased in the Sarmatian to 15-20 g/l and again in the Pannonian to 3-12 g/l (Schroll & Tauber, unpublished; see Schroll, 1959), which are still drastically elevated from current values. Lake Neusiedl is most comparable to the inner Asiatic steppe lakes that resemble the Aral type (Schroll, 1959).

2.7 Biodiversity

Because of the present biodiversity with special habitats for plants and animals, Lake Neusiedl is a Natura 2000 nature reserve area. Parts of it are protected areas and it is part of the Ramsar-area for conservation of wetland habitats. Especially striking are the reed belts, more accurately Phragmites australis, that covers over half of the lake. There is only one location, besides the lake centre, that is mostly free from reed, which is Podersdorf am See. At other locations there are artificial accesses or even canals necessary to cross the reed belts. The reeds tend to increase their growth in general with decreasing water level (Herzig, 2014). In the 1950's and 60's it even seemed possible that the whole lake would be covered by reed (Herzig, 2014). While the nutrient content is high in the lake water, the high amount of suspension and the resulting limitation of sun light strongly impacts the growth rate of algae (Herzig, 2014). The dominating phytoplankton species are green algae, diatoms and blue algae and the picoplankton has a high abundance (Herzig, 2014). Crustaceans are the dominant biomass for zooplankton (Herzig, 2014). In terms of zoobenthos the dominant species are nematodes, ostracods, benthic cladocerans, oligochaetes and chironomids (Herzig, 2014). The reed belts are preferably inhabited by zoobenthos compared to the mostly depleted offshore wind exposed areas of the lake (Schiemer, 1979; Wolfram 1996).

2.8 Sediment

2.8.1 Mud

The general composition of the lake sediment is quartz, feldspar, mica, dolomite, calcite, protodolomite, clay minerals and pyrite (Tauber & Wieden, 1959). Plagioclase is the dominant member of the feldspar group and muscovite dominates the mica content (Tauber & Wieden, 1959). The dominant clay minerals are very likely illite, chlorite and montmorillonite (Tauber & Wieden, 1959). Pyrite only appears in minor concentrations (Tauber & Wieden, 1959). The uppermost lake sediments are oxidized and not in a reduced state due to the turbulent water that introduces oxygen (Tauber & Wieden, 1959). Pyrite forms only under reduced conditions, which means the formation of pyrite occurred under different conditions at an earlier period when reduced conditions prevailed (Tauber & Wieden, 1959). Sediment is likely eroded at the lake centre and deposited at the outer ridge of the lake. (Tauber & Wieden, 1959).

2.8.2 Protodolomite

In recent years protodolomite formation in a lake environment under surface conditions became a research focus (Fussmann et al., 2020; Meister et al., 2023; Neuhuber et al., 2024). The formation of protodolomite at Lake Neusiedl by the support of bacteria was described in 1958 by Neher and Rohrer. Today it is still unclear how the dolomite formation overcomes the kinetic barrier at surface conditions. Protodolomite has a similar composition to dolomite, but calcium and magnesium are not ordered in alternating layers. Initiated by the strong seasonally changing hydro chemistry in Lake Neusiedl forms magnesium-calcite first that slowly recrystallizes to protodolomite (Meister et al., 2023). On the phase boundaries where calcite is recrystallizing to protodolomite, dolomite nanocrystals might form from protodolomite (Fig. 6; Meister et al., 2023). The energy barrier for nanoparticles might be lower compared to particles in general, that otherwise hinder the growth of dolomite due to the high energy barrier (Meister et al., 2023). According to Neuhuber et al. (2024) the unconsolidated sediments contain a continuum of magnesium-calcite phases with 10 to 20 mol% high-magnesium calcite and 40 to 50 mol% protodolomite and a lesser amount of low-magnesium calcite. The amount of low-magnesium calcite increases in older lake sediments, while it decreases for protodolomite (Neuhuber et al., 2024). Protodolomite particles found by Neuhuber et al. (2024) are in general authigenic. Radiocarbon dating suggests that carbonate crystals are also currently growing, but at an extremely low speed (Neuhuber et al., 2024). Protodolomite formation by “ripening” of high-magnesium calcite is suggested, due to an increase of protodolomite in older grain-size fractions, while in the youngest fractions high-magnesium calcite is present (Neuhuber et al., 2024). The variation of humid and evaporative climate combined with a high pH and salinity are the main reason behind the authigenic

formation (Neuhuber et al., 2024). Transformation of high-magnesium calcite to protodolomite may be a result of sudden repetitive changes in the environmental conditions (Neuhuber et al., 2024).

The research regarding protodolomite uncovers also new information about the formation of Lake Neusiedl. According to the extrapolated nucleation age, it is likely that a lake was already present at over 25 ka BP during the last glacial maximum (Neuhuber et al., 2024). At least in some periods a higher water column with less magnesium, but still controlled by evaporation, must have been present (Neuhuber et al., 2024). Lake Neusiedl in its modern form has been present since most of the Holocene with an extremely low sedimentation rate, due to an estimated nucleation age between 3.6 and 8 ka BP (Neuhuber et al, 2024).

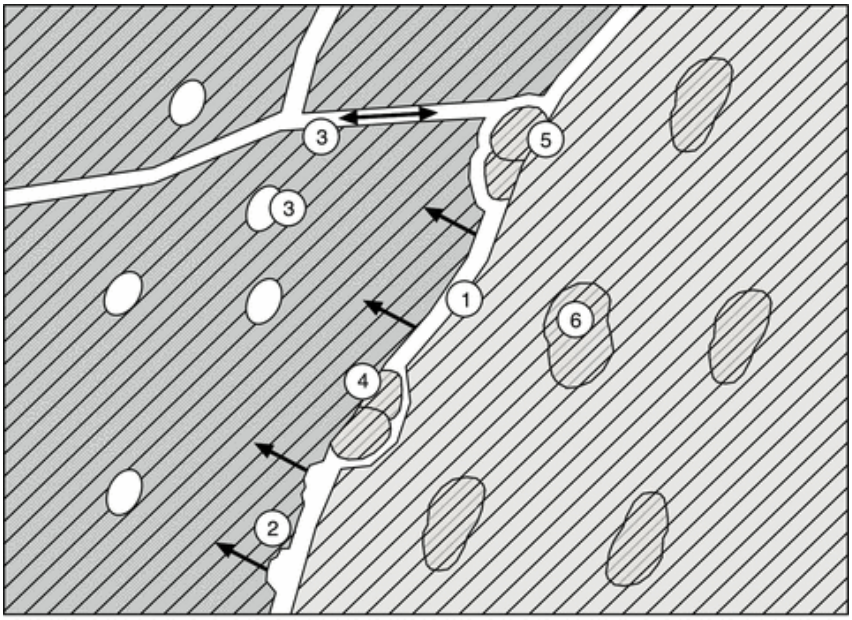

Figure 6: Current model of protodolomite and dolomite formation from Mg-calcite under surface conditions at Lake Neusiedl (Meister et al., 2023).

2.9 Gas seeps

The so called Kochbrunnen at Lake Neusiedl are characterized by uprising bubbles and in many cases a ring-like ice free area when the rest of the lake is frozen solid (Fig. 7). As the term Kochbrunnen implies hydrothermal activity (Sauerzopf, 1959; Tauber, 1959; Gattinger, 1979; see Rank et al., 1985) and is therefore misleading and the observed features actually represent gas seeps, the terminology “gas show” or “gas seep” is used throughout this thesis.

Figure 7: Gas seep at Lake Neusiedl with bubbles rising from the lake floor and an ice-free circle, when the lake is mostly frozen solid (Tanzberger, 2005).

Some of these gas seeps can be observed near Rust, but they also cover different parts of the lake. While there are some that are producing bubbles permanently, there are others that are not bubbling all the time or only every few seconds. The same bubbles can be observed when pressure is applied at the sludge near the reed belts, but only in areas not influenced by waves. Analysis of the isotopy, conductivity and element concentration of water samples near the gas seeps and at different lake locations was performed, but no significant difference could be detected (Rank et al., 1985) (Tab. 3 & 4; Fig. 8). The ice-free ring-like structures are a result of upwelling of gas and the resulting turbulence (Rank et al., 1985).

	Datum	^{3}H(TE)	$\delta^{2}H$(‰)	$\delta^{18}O$(‰)	Leitf.(µS)	Temp.(°C)
Kochbrunnen B	20.2.84	35,8	-29,7	2,80	2056	1,6
Kochbrunnen F	20.2.84	35,4	-28,7	- 2,77	-	-
Neusiedlersee,Podersdorf	20.2.84	34,8	-29,7	- 3,25	-	-
Qu. Hottergraben, Rust	9.2.84	11,5	-72,7	- 9,80	637	11,0
Grundwasseraustritt Purb.	15.2.84	20,6	-79,9	-11,13	466	10,0
Wulka, Wulkaprodersdorf	18./24.2.84	49,6	-71,2	-10,08	-	-
Kochbrunnen A	17.1.85	30,4	-32,8	3,94	3150	0,7
Kochbrunnen B	17.1.85	29,6	-33,7	3,96	3020	0,7
Kochbrunnen C	17.1.85	28,6	-34,1	- 3,97	3220	0,6
Kochbrunnen D	17.1.85	30,5	-35,0	- 4,01	3160	0,8
Kochbrunnen E	17.1.85	28,4	-32,9	- 4,01	3130	0,6
Kochbrunnen F	17.1.85	27,9	-35,4	3,91	3140	0,6
Neusiedlersee, Rust	17.1.85	30,7	-32,5	3,95	3190	0,7
Neusiedlersee,Podersdorf	19.1.85	29,9	-36,5	3,94	-	-
Qu. Hottergraben, Rust	17.1.85	10,7	-70,3	- 9,79	634	10,4
Qu. Sportplatz, Mörbisch	17.1.85	7,4	-72,6	-10,19	1187	6,4
Wulka, Wulkaprodersdorf	12./18.1.85	45,7	-71,3	-10,15	-	-

Table 3: Isotope ratios, conductivity and temperature measurements at Lake Neusiedl, comparing the water of the gas seeps with water of Lake Neusiedl, springs and Wulka River (Rank et al., 1985).

	Datum	Na mg/l	K mg/l	Li µg/l	Ca mg/l	Mg mg/l	Sr µg/l	Ba µg/l	Cl^{-} mg/l
Kochbrunnen B	20.2.84	357	41	140	22,4	134	460		
Neusiedlersee,Podersdorf	20.2.84	350	40	140	22,2	132	470		
Kochbrunnen A	17.1.85	425,3	46,3	124	19,7	158,0	509	16	220
Kochbrunnen B	17.1.85	424,3	44,5	117	19,0	158,2	502	16	240
Kochbrunnen C	17.1.85	429,4	42,7	105	18,4	160,0	475	15	210
Kochbrunnen D	17.1.85	426,3	42,4	110	19,3	160,3	481	16	240
Kochbrunnen E	17.1.85	422,2	40,0	101	18,6	158,2	453	15	240
Kochbrunnen F	17.1.85	420,7	41,9	100	18,6	157,4	466	15	260
Neusiedlersee, Rust	17.1.85	411,3	41,4	99	17,8	155,7	455	14	170
Neusiedlersee,Podersdorf	19.1.85	465,4	45,6	110	25,6	160,8	505	16	240
Qu. Hottergraben, Rust	17.1.85	10,5	1,6	<10	66,3	34,0	320	41	5
Qu. Sportplatz, Mörbisch	17.1.85	38,0	21,4	<10	136,9	39,1	486	85	20
Wulka, Wulkaprodersdorf	12./18.1.85	16,2	6,0	<10	104,1	36,7	338	55	-

Table 4: Elemental concentration of gas seeps at Lake Neusiedl, springs and the Wulka River (Rank et al., 1985).

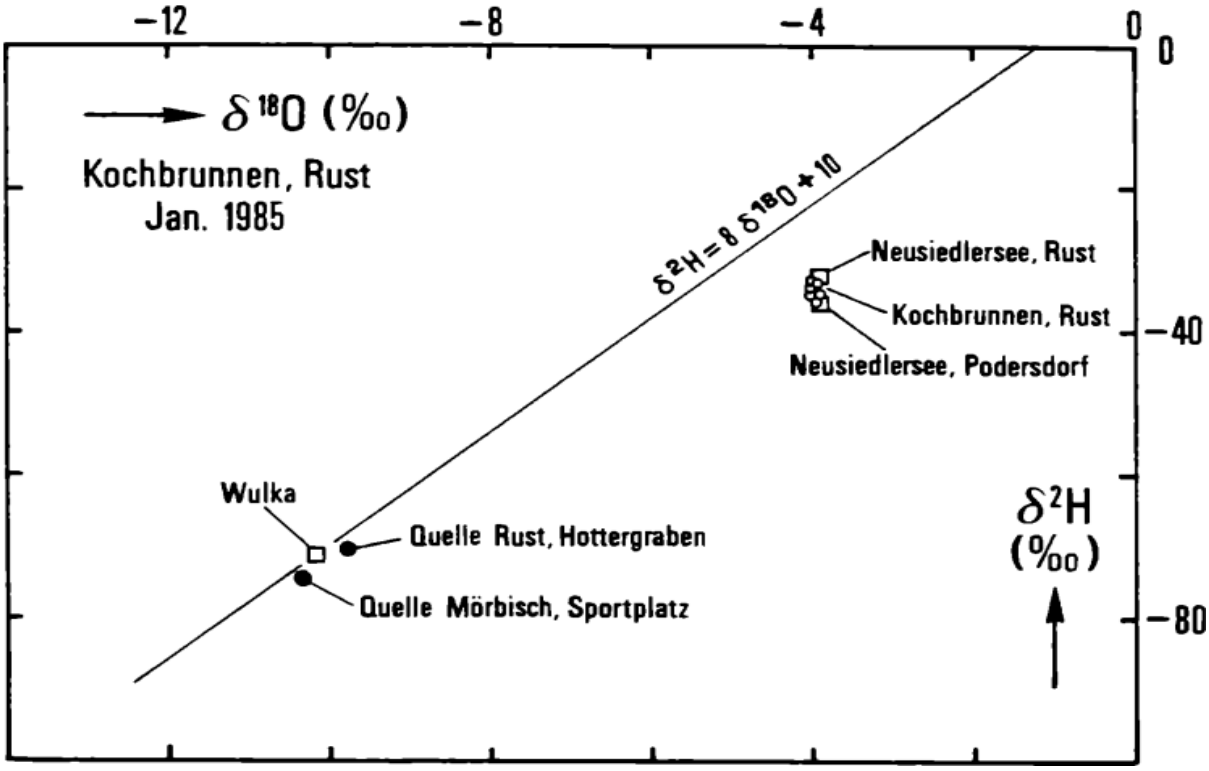

Figure 8: δ^2H - $\delta^{18}O$-diagram of the gas seeps at Lake Neusiedl, springs and the Wulka River (Rank et al., 1985).

Further research regarding water discharge at these gas seeps with temperature measurements (Tanzberger, 2005) did not find any significant anomaly either. The uprising gas was also measured, and it was found that the gas consists mainly of methane (Tab. 5). According to Schoell (1980; see Rank et al., 1986) the gas has a biogenic origin. C-14 dating results in an age of over 30.000 years and there is no relation to the modern Lake Neusiedl (Rank et al., 1986). The gas should have a tertiary origin because of the composition of the gas (79.36 % CH_4, 16.87 % N_20, 0.77 % O_2+Argon and the rest water vapour) and the carbon isotope ratio with -$\delta^{13}C$ = -58 ‰ (Rank et al., 1986). According to Häusler et al. (2010) the gas upwelling at the gas seeps might be related to faults and the gas is emerging from deep structures, or they might be related to the Upper Pannonian coal layers. There should be a different origin for the sludge gas that emits irregularly at the reed belts and the permanent discharge of gas at the gas seeps (Häusler et al., 2010). In 2021 the stable carbon isotopes of methane and carbon dioxide of sludge gas at Lake Neusiedl near Illmitz were measured by Baur et al. (2024). The sludge gas has a biogenic origin and should be dominated by acetoclastic methanogenesis (Fig. 9; Baur et al., 2024). Zámolyi et al. (2017) interpreted a gas chimney in lake seismic sections taken at Lake Neusiedl close to Neusiedl am See (Fig. 10).

	Kochbrunnen im Neusiedlersee (350 m vom Schilfrand)			Sumpfgas am Ufer
	1984 02 20	1985 01 17	1985 08 23	1959 11 02
CH_4 (%)	77,16	79,36	82,58	76,1
N_2 (%)	19,06	16,87	15,75	14,1
O_2 (%)	1,66	0,77	0,14	3,0
CO_2 (%)	0,20	0,62	0,39	6,8
δ^2H (‰)	-	-	-206,9	-
$\delta^{13}C$ (‰)	-	-57,4	- 54,5	-
^{14}C-Alter (a)	-	-	>30.000	-

*) Rest Wasserdampf

Table 5: Chemical composition and isotopy of gas, with the first three rows of the gas seeps and the last row with sludge gas from near the shore (BVFA-Arsenal, 1960; see Rank et al., 1986).

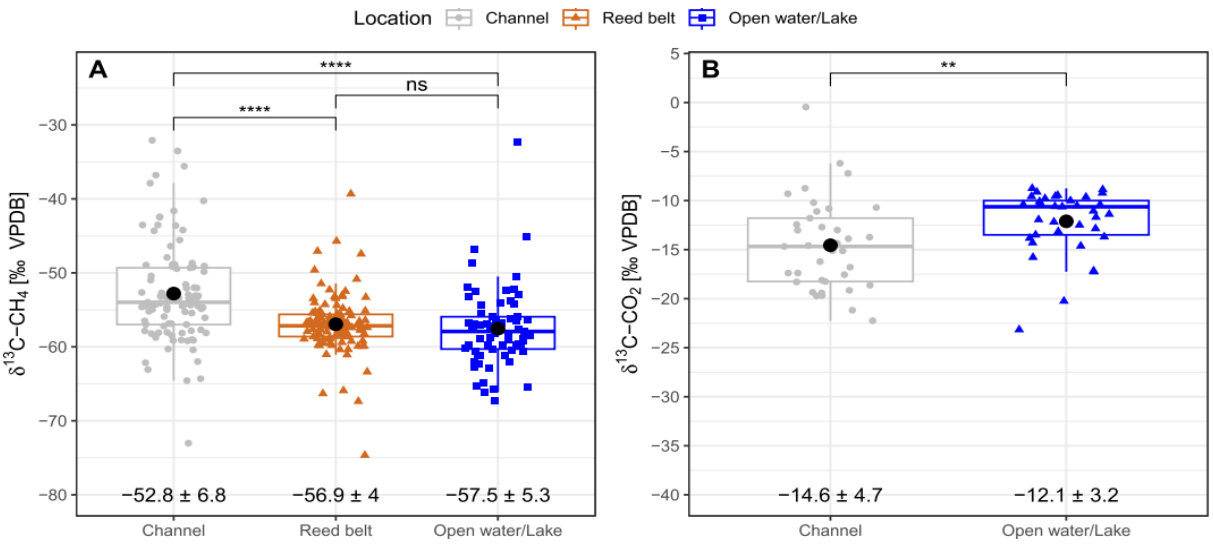

Figure 9: Results of the stable carbon isotopes of CH_4 and CO_2 close to Illmitz at Lake Neusiedl (Baur et al., 2024).

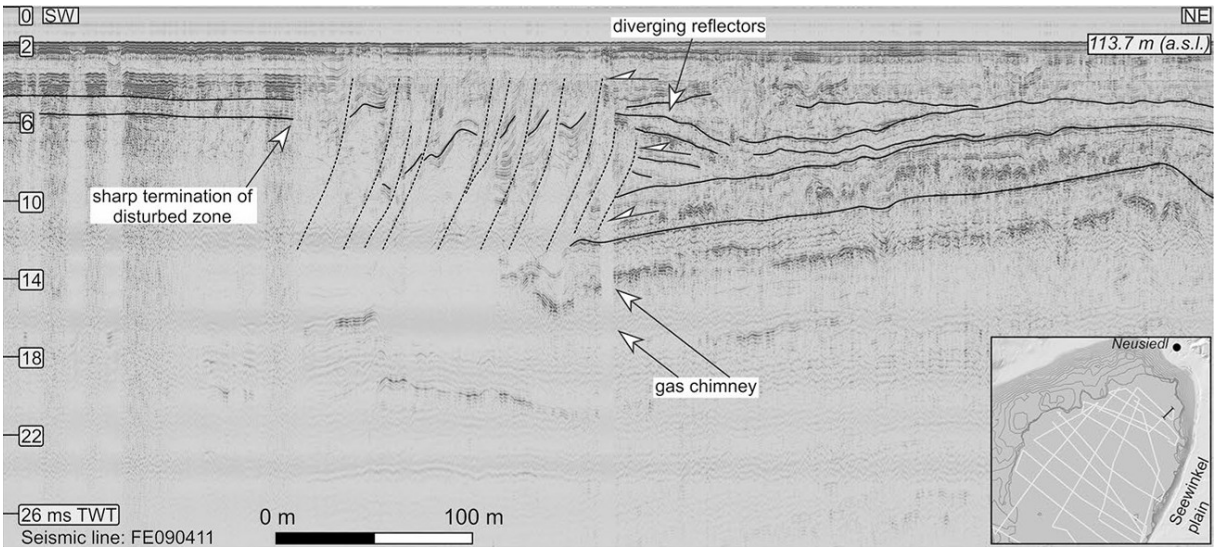

Figure 10: Lake seismic section that displays sedimentological and tectonic features beneath Lake Neusiedl close to Neusiedl am See. Additionally, a gas chimney was interpreted from the data (Zámolyi et al., 2017).

2.10 Formation of Lake Neusiedl

Miocene

The boundary between the Karpatian and the Badenian is characterized by a long interruption of sedimentation that is related to strong erosion, which is interpreted to represent a strong sea level drop (Häusler et al., 2010). Marine clays and carbonate sediments formed in the Badenian as basin fill, with the Leithakalk as the only phase with coral reefs in the whole Paratethys (Häusler et al., 2010). The beginning of the Sarmatian is related to the isolation of the Central Paratethys from the other marine basins, which led to an extensive change in the fauna, that is characterized by mass occurrence of molluscs and large foraminifers (Häusler et al., 2010). Southeast of the Leithagebirge was still an elevated zone (Häusler et al., 2010). The main part of the Pannonian (zone A-D) is also missing in the southern elevated zones and have only been found locally in relief depressions (Fig. 11; Häusler et al., 2010).

The impact of growing continentalization in Middle and Eastern Europe in the Pannonian led to an aquatic area that was restricted in the Central Paratethys to the Pannonian Basin (Häusler et al., 2010). Lake Pannonia, a brackish and freshwater lake, a relic of the central Paratethys was formed in the Pannonian in between Alps, Carpatians and Dinarides (Häusler et al., 2010). Proximal to the shore, delta gravel, sands, light coloured marl and lignite were deposited (Häusler et al., 2010). The archipelago-like structures of the area around bay Neusiedl were lost with zone E of the Pannonian (Häusler et al., 2010). Rapid subsidence of the area Seewinkel in the direction of the small Hungarian plain started in the Upper Pannonian (Häusler et al., 2010). Silting up and the appearance of bald cypresses, lignite seams (zone F) and horizons of gravel coming from the Leithagebirge through small streams are characteristics of the limnic Upper Pannonian (Häusler et al., 2010). Zone G shows a reduction of lignite and extensive sandy and clayey sediments of the Blaue und Gelbe Serie (Pannonian G-H) and are stopping the formation of the Pannonian freshwater lake (Häusler et al., 2010).

Oberes Pannonium	GH *Viviparus*-Zone F *Congeria-neumayeri-/Congeria-zahalkai*-Zone
Mittleres Pannonium	E *Congeria-subglobosa*-Zone D *Congeria-partschi*-Zone
Unteres Pannonium	C *Congeria-hoernesi*-Zone AB *Congeria-ornithopsis-/Melanopsis-impressa*-Zone

Figure 11: Biozones in the Pannonian based on molluscs (Häusler et al., 2010).

Karpatian is the age of the partly terrestrial-fluviatile, partly limnic oldest sediments of the Lower Miocene that deposited on the crystallin mountain range of the area Rosalia, Ruster Höhenzug and the southern part of the Vienna Basin (Häusler et al., 2010). The Unterostalpin that the Leithagebirge belongs to may have also been an area of sedimentation, but gravel and sands like the Ruster Formation are missing (Häusler et al., 2010). In the Middle Miocene the subsidence of the Eisenstadt-Sopron Basin started (Fig. 12; Häusler et al., 2010).

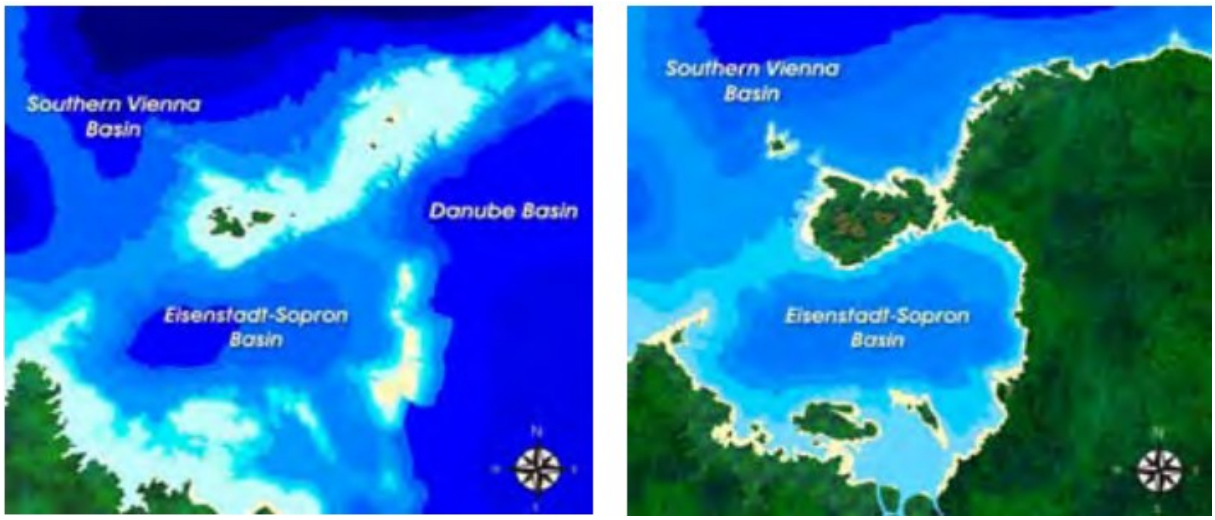

Figure 12: Right: Paleogeography of the Eisenstadt-Sopron Basin in the Early Badenian, where the eastern part of the Leithagebirge and the area east of the Ruster Hügelland were still above the water level. Left: As a result of transgression in the Middle and Upper Badenian, large areas of the Leithagebirge and the Ruster Hügelland were flooded (Harzhauser & Piller, 2005).

The Middle Miocene is characterized by extension in the Vienna Basin, that is limited by sinistral lateral displacement (Häusler et al., 2010). The early basin forming phase in the Badenian shows shallow marine, fossil-rich coarse sands and Bryozoen-calcareous sands of the Hartl formation that provide the first evidence of marine transgression (Häusler et al., 2010). River-systems formed at the northern part of the Leithagebirge by local erosion of the raised land masses (Häusler et al., 2010). These gravel deposits lead to the base of marine sediments (Häusler et al., 2010). Sedimentation of quarzitic clasts into the proximal Leithakalk-Schlammfazies was the result of continuous erosion of the Unterostalpin archipelagos (Häusler et al., 2010). Mighty Corallinaceae-limestones and coral-biostromes in the Leithakalk in the Middle and Late Badenian formed due to a high sea level that flooded the whole Leithagebirge and Ruster Höhenzug (Häusler et al., 2010). A sea level low at the Badenian – Sarmatian border led to desiccation of the Leithagebirge and its Neogene cover (Häusler et al., 2010). This resulted in extensive erosion of the Badenian Leithakalk and the formation of deeply cut in valleys (Häusler et al., 2010). Miocene volcanism is documented by volcanic tuffs in the Badenian and Sarmatian north of Fertörakos, in the Sarmatian of Breitenbrunn and in

the Badenian at the southern edge of the Vienna Basin at Mannersdorf (Zorn & Fritz, 2000). The tuffs could also have a different origin such as the volcanic area to the east like the Surianske-andesite (Häusler et al., 2010). This is followed by a sequence of pelites, sands, gravel layers and Serpulid-limestone in the Sarmatian (Häusler et al., 2010). These deposits of the Eisenstadt-Sopron area are comparable with the sequence of the southern Vienna Basin (Häusler et al., 2010). In the Sarmatian limestone with an origin of close to the shore reprocessed and redeposited Leithakalk are widespread (Häusler et al., 2010). Algae and coral limestones that were processed to limesand form the detrital Leithakalk (Häusler et al., 2010). Complex sequences of sedimentation and erosion in a coastal area that were controlled by sea level changes in the Sarmatian are documented by surf debris along Sarmatian cliffs (Häusler et al., 2010). Massive delta debris may have been the source of a river system coming from the south to the muddy coastal area, that deposited before the Leithakalk was formed (Häusler et al., 2010). This is indicated by massive sand and gravel formations at the western edge of the Ruster Höhenzug. According to Fuchs (1960) the fault structures led to the emerging of the Ruster Höhenzug to the modern extension. The formation of an extensive lake with decreasing salinity content in the Pannonian was the result of the separation of the Central Paratethys from the Miocene Sea (Häusler et al., 2010). In the Eisenstadt-Sopron Basin and the Pannonian Basin were clayey marl and sands of a Pannonian Lake deposited (Häusler et al., 2010). Lower Miocene gravel was deposited into the lake in the Middle Pannonian by a small river coming from the Leithagebirge (Häusler et al., 2010). Formation of sediments on flood plains with coal swamps and locally freshwater ponds in the Eisenstadt-Sopron Basin and the southern Vienna Basin were the result of a retraction in the Late Pannonian by the Pannonian Lake (Häusler et al., 2010). At the western edge of the Ruster Höhenzug was a reactivation in the Middle Pannonian of the Middle Sarmatian faults due to the Middle Pannonian sediments that are overlaying the Ruster Schotter (Fuchs, 1960).

Pliocene and Pleistocene

After desiccation of the Pannonian Lake the area around the Leithagebirge in the Pliocene was characterized by the deposition of fluvial-terrestric and aeolian sediments (Häusler et al., 2010). Temperate warm wet climate with cold and arid episodes, but without signs of glaciation, were the characteristics of this period (Wessely & Draxler, 2006). The Paleo-Danube was meandering in the Upper Pliocene at the northern edge of the Leithagebirge on the way to the Parndorf Plateau and was depositing gravel at Deutsch-Altenburg (Häusler et al., 2010). The Paleo-Leitha flew in the Pleistocene into eastern direction into a morphologic formed pre-Wulka Basin (Häusler et al., 2010). After the Mitterdorfer Senke caved in the Paleo-Leitha flew on the northern edge of the Leithagebirge into direction of the Paleo-Danube and a Paleo-Wulka flew into a new area between Rosaliengebirge and Leithagebirge to the east (Häusler et al., 2010). Most recent research shows an age for the beginning of lake sedimentation at least 25.000 years ago during the last glacial maximum (Neuhuber et al., 2024)

According to Zámolyi et al. (2017) the western margin of the Little Hungarian Plain is covered by Pannonian brackish clastic sediments that are overlain by coarse-grained fluvial sediments at the Parndorf Plateau and Seewinkel Plain. These sediments have an age of over 300 ka with fluvial sediments situated at the Seewinkel Plain showing Late Pleistocene age (Fig. 13). In between the Parndorf Plateau and the Seewinkel Plain normal faulting is most likely present due to the age of the deposited sediments, weathering degree, active seismicity and geomorphological features (Zámolyi et al., 2017). Today, the morphology of this area is heavily influenced by Latest Pliocene to Quaternary tectonic subsidence. To the east the Quaternary fluvial sediments become more massive according to the general inclination of the subsidence, while these sediments are controlled by the general tilt of the Parndorf Plateau (Zámolyi et al., 2017). The Quaternary sediments from the Parndorfer Plateau are likely related to the Danube, but the origin of the Late Pleistocene Seewinkel Plain sediments is still unclear. The low zircon, tourmaline and rutile ratio suggests that the distance of transport was rather low (Zámolyi et al., 2017). Fluvial and coarse-grained Quaternary sediments are missing close to the surface at Lake Neusiedl and recent lake sediments have only a sparsely lateral extension and are overlying very compacted Upper Pannonian clays to sands (Zámolyi et al., 2017). Many minor faults disrupt the truncated tilted Upper Pannonian sediments, which implies faulting in the Late Pannonian (Zámolyi et al., 2017). The formation of the lake was favoured by the non-existence of fluvial coarse grained Quaternary sediments on top of the upper marine to brackish strata, which also indicates recent subsidence (Zámolyi et al., 2017). The lack of sediment deposition led to the migration of eastward river channels due to tectonic subsidence and the elevation of the Parndorf Plateau caused by local normal faulting that denied rivers like Danube and Leitha to extent to this area (Zámolyi et al., 2017).

The fluvial cover of the Seewinkel Plain may have been formed due to a short-termed event or the repetition of fluvial events, but the combination of strong sediment pulses together with a particular cold climate might not be the underlying cause (Zámolyi et al., 2017).

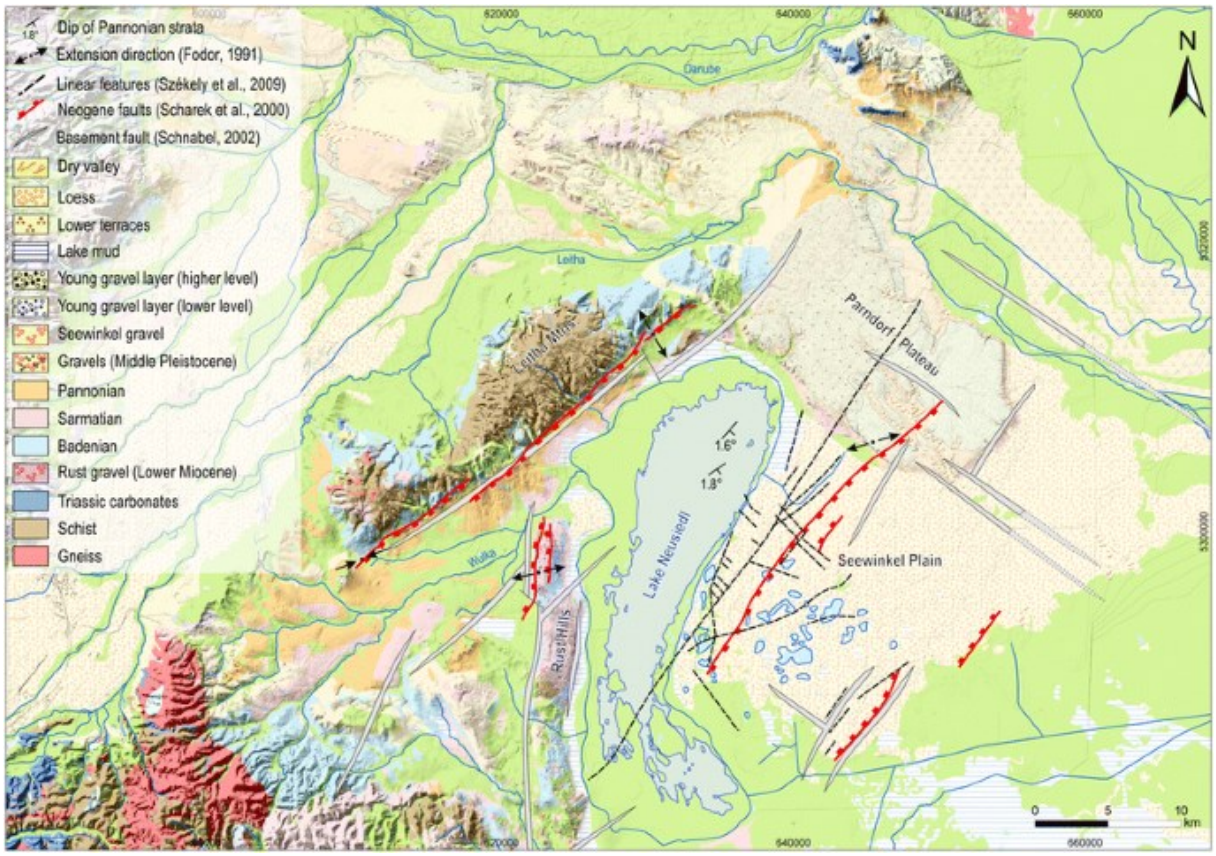

Figure 13: Geological map that provides an overview of Lake Neusiedl and surrounding areas (Zámolyi et al., 2017; after Schönlaub, 2000). The Parndorfer Plateau is covered by gravels of a Middle Pleistocene age and younger gravels that are of higher and lower level. The Seewinkel Plain is covered by a homogenous gravel layer. Faults of the Basement and Neogene are in generally oriented NE-SW and NW-SE. The extension directions of the Late Miocene to Pliocene are shown by the black arrows (Fodor, 1991; see Zámolyi et al., 2017). Tectono-geomorphic linear features are indicated as black dashed lines, which were interpreted based on an airborne laser scanned digital terrain model (Székely et al. 2009; see Zámolyi et al., 2017). Areas in green close to Lake Neusiedl are reed belts and distal from the lake Holocene floodplains.

3 Analytical Methods

3.1 Gas sampling

In total 15 gas samples were taken and analysed (Fig. 17). The samples were measured on site with the ATEX Gasanalysator Geotech BIOGAS 5000 (Fig. 14). The device measured the composition regarding the gases CH_4, CO_2, O_2, H_2 and NH_3 and collected it into a gas sampling bag (Fig. 15). The gas was collected at the water surface with a bell-shaped device (Fig. 16). This bell-shaped device was connected via a tube with the gas analysing device “Biogas 5000” and a second tube was transporting the analysed gas back into the bell-shaped device.

Figure 14: Gas analyse device on site that was used to analyse, collect and transfer the gas into the gas sampling bags.

Figure 15: Gas sampling bags where the collected gas was stored.

Figure 16: Bell-shaped device that stored the gas which enabled sampling and measurement of the collected gas.

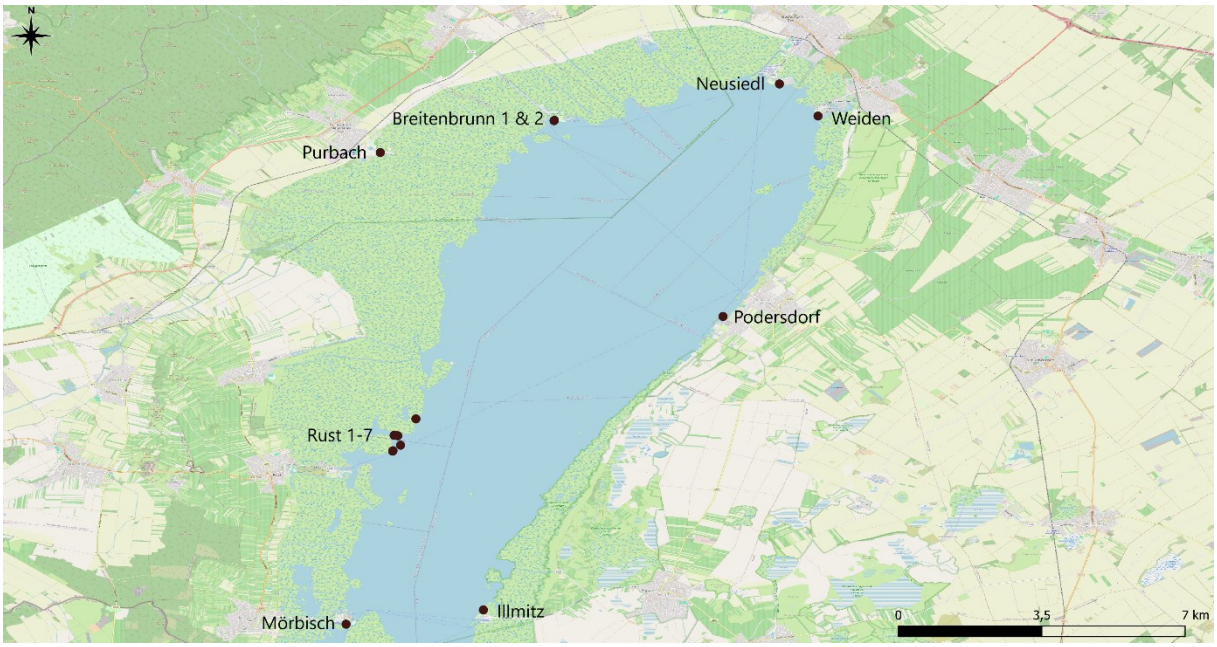

Figure 17: Gas sampling locations (black points) at Lake Neusiedl.

Seven samples were taken at and around the gas seeps near Rust (Fig. 18). Rust1 and Rust2 were taken at gas seep 1, that was constantly emitting gas in a low to average amount compared to the other sample locations. It is the only sampling location that was always emitting gas. Rust3 corresponds to gas seep 2. Only on one sampling day gas was visibly emitting to the water surface and sampling was possible. Rust4, Rust5 and Rust6 were sampled at and around gas seep 3. Gas was emitting irregularly, and the location of the up-venting bubbles did change over the course of time. Rust7 was sampled at a pathway into the reed belt near a sand shore bank. At this location the largest amount of gas was emitting.

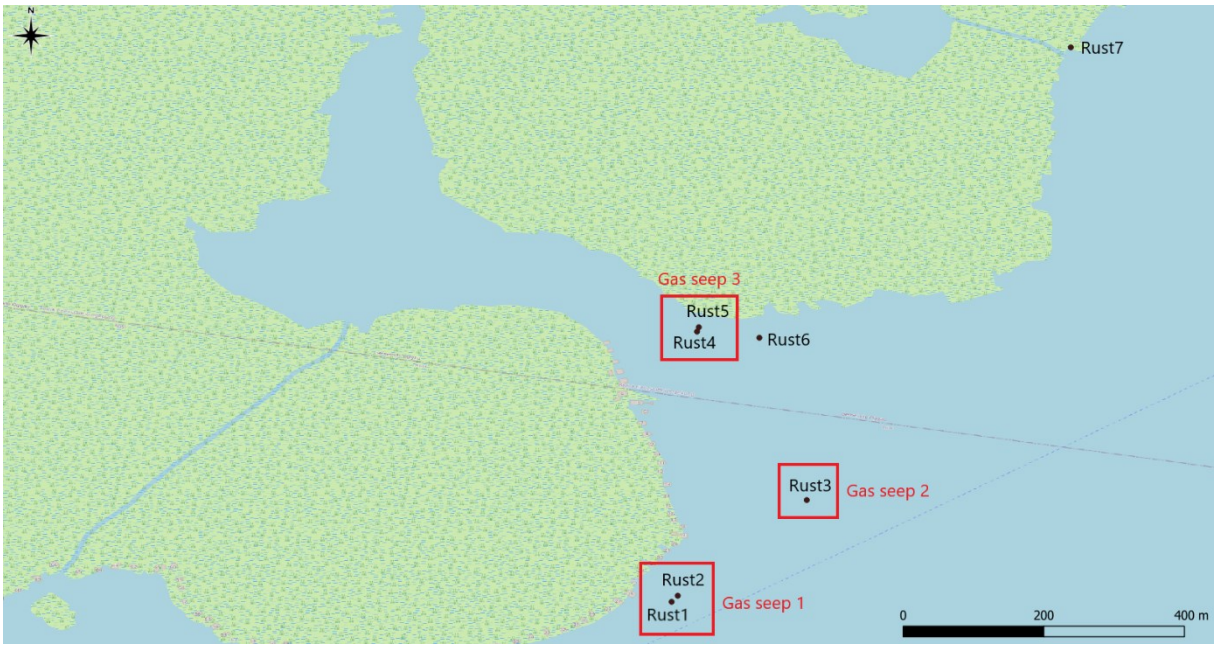

Figure 18: Gas sample locations near Rust at Lake Neusiedl.

The other eight samples were taken from different locations at Lake Neusiedl. One sample was taken at each location at Podersdorf, Neusiedl am See, Mörbisch, Illmitz, Weiden, Purbach. At Breitenbrunn two samples were taken. All these sample locations are close to the reed belts with relatively thick lake sediments and no perturbation by water currents. Gas emission from the first few decimetres of the lake mud was stimulated by agitating the sediment with a paddle.

3.2 Sediment sampling

At each gas sampling spot, except for Rust4, a sediment sample was taken. Gas samples for Rust1 and Rust2 were taken at the same spot, so one sediment sample corresponds to both gas samples. Additionally, two samples to the south of Rust in Lake Neusiedl were taken. In addition to sediment samples at the gas sampling spots, sediments were systematically sampled across two profiles. Profile 1 has a total of 31 samples with the first at the lake centre approximately 1 km away from the last sample of Profile 2 (Fig. 19). The last sample of Profile 1 is approximately 200 m away from the shore of Breitenbrunn. Profile 2 consists of 40 sediment samples with the first sample approximately 50 m away from the shore at Podersdorf and the last sample was taken at the lake centre. Spacing in-between the samples was approximately 100 m. The sediment samples were taken from the first two decimetres of the lake sediment. The samples were collected in airtight bags.

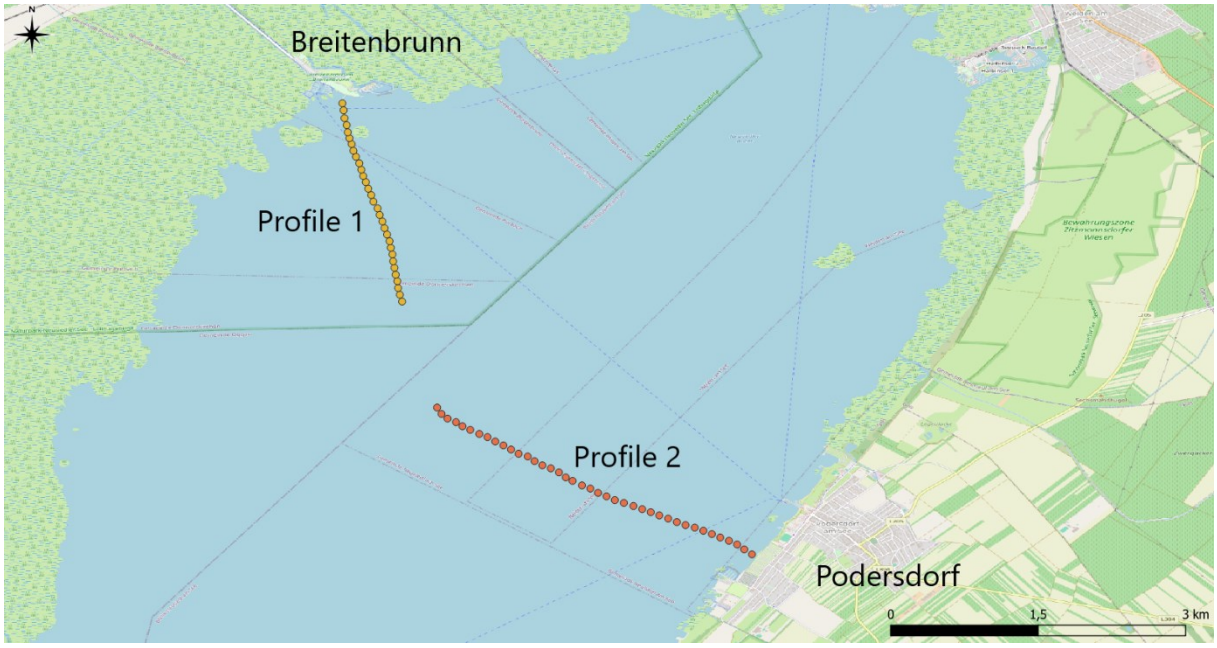

Figure 19: Sample locations of the sediment samples for Profile 1 and Profile 2.

3.3 Gas analyses

3.3.1 Gas chromatography

A gas chromatograph (GC) is comprised of an injector, columns and detectors. The sample is first dissolved in a liquid and then injected through a septum. The sample is then transported with the carrier gas through the column that is built into a GC-oven, that serves to separate the gas phases. When a substance leaves the separation system, an electrical signal is emitted to the detector and is registered as a peak. For gas chromatography the Thermo Scientific TraceGC Ultra at Montanuniversität Leoben was used. This device was used for the determination of the gas composition equipped with three detectors that could simultaneously measure gaseous hydrocarbons, H_2, N_2, O_2, CO_2 and H_2S in one run. Helium was used as a carrier gas.

3.3.2 Stable isotopes

With the Trace GC ultra gas chromatography linked to the ThermoFisher Delta-V isotope ratio mass spectrometer (IRMS) the measurements of the stable C and H isotope were undertaken with combustion and high temperature reduction interface as well (GC Isolink, ThermoFisher; Ajuaba et al., 2022). As a column for the GC, that was linked to the IRMS, the 25 m Poraplot capillary column was used (i.d. 0.32mm; 0.10 µm thickness of the film). The temperature of the oven was scheduled to increase from 30 to 180°C at 5°C per minute intervals with a subsequent isothermal phase of 5 minutes. Helium was used as a carrier gas. Calibration was done at the start and after every analysis with an injection of in-house standard gas for CO_2 and H_2 respectively. The relative ratios of $^{2}H/^{1}H$ and $^{13}C/^{12}C$ are reported in delta notation relative to Vienna Standard Mean Ocean Water (V-SMOW) and the Vienna Pee Dee Belemnite (V-PDB) standard, respectively. Reproducibility of the analyses was better than 0,4 ‰ for the stable C isotope and below 4‰ for the stable H isotope.

3.4 Sediment analyses

3.4.1 Sample preparation

At first the sediment samples were dried for about 3 days at 30°C. The samples were completely homogenized and crushed using a mortar mill. A sample quantity of about 10 g was taken from the homogenized material. After grinding, each sample was sieved with a 200 µm hand sieve. Due to the risk of damaging the crystal lattice and a resulting weaking of the diffraction reflections, the crushed sediment samples had to be treated gently.

For the preparation of the textured mounts, 0.085 g of air- dried powder and 0.045g of distilled water was mixed. The resulting paste was then smeared into a groove of a glass sample holder, which causes the clay particles to orientate parallel to the surface. This increased the basal reflections. Every textured mount was measured four times at a goniometer speed rate of 0.5 °2Θ/min and with a registration range from 2 to 42 °2Θ in untreated condition, for example air-dried, after solvation with ethylene glycol, after thermal treatment (350°C for 2 h) and after thermal treatment (550°C for 2 h).

3.4.2 X-ray Diffraction

Measurement procedure

The XRD measurements were performed using an X'pert 3 powder X-ray diffractometer (Panalytical). A copper anode was used as the radiation source to create low-energy X-rays, and a characteristic line spectrum (Kα and Kβ components) was emitted under high voltage of 40 kV and a current of 40 mA. Monochromators were used to change the K component to the Kα1 wavelength. The acquired angular range was between 2.51°2Θ and 65.99°2Θ, the step size of the measurements covered 0.0167°Θ, and the goniometer speed was 0.5°2Θ/minute.

Evaluation of the XRD analyses

Mineral phases were characterized by the diffraction pattern (intensity versus Bragg angle °2Θ). The crystal structure was specified by the position and intensity of the hkl reflections. Each mineral phase's hkl reflections were included. The samples were evaluated for maximum peak height and area. The strongest diffraction line was normalized to 100 %. The intensities were compared with the reference database ICDD (International Centre for Diffraction Data) by ADM software (version 7, Wassermann Röntgenanalytik). The ADM software quantifies all phases that were detected in the qualitative analysis. The scaling factors were corrected by the Reference Intensity Ratio (RIR). The result was displayed as wt.% that summed up to 100 wt.%. The semi-quantitative results were also confirmed with other

methods by the ADM software. The quartz content was validated with a quartz standard, that also included the mass attenuation coefficient. Mineral phases below one percent were not considered for the semiquantitative analysis. X-ray amorphous substances (e.g., organic material) were not part of the qualitative and semiquantitative analyses. The results may have been restricted by peak overlaps of mineral phases with similar crystal structure, altered minerals and solid solutions. The composition of the sediment samples was normalized to 100 %. For displaying the data, the softwares Match! version 4.0 and Profex version 5.3.0 were also used.

3.4.3 pH

The pH-values of all 87 sediment samples were measured with the Microprocessor pH-Meter pH 196 T at Montanuniversität Leoben. The pH measurement was done according to ÖNORM EN ISO 10390:2022. The dried and ground samples were used, according to EN 16179:2012. The samples were stirred with a magnetic stirrer for 10 minutes, then left in suspension for another 10 minutes. Because testing did not show a significant change in pH after stirring and suspending after more than 10 minutes, the time was shortened to 10 minutes according to ÖNORM EN ISO 10390:2022. Additionally, a test was conducted to see the difference in the pH-behaviour of the dried and ground samples and the unprepared samples. The unprepared samples showed a strong change in pH value even after a suspension time of over 1 hour. Five ml of dried and ground sample was used with distilled water as aqueous solution. Calibration was done with a pH of 7.00 and 10.01 calibration solutions. The temperature was measured as well.

3.4.4 TC, TOC and sulphur

For bulk geochemical analyses of the sediment samples total carbon (TC), total inorganic carbon (TIC), total organic carbon (TOC) and total sulphur (TS) were determined by an Eltra Helios CS elemental analyser. To prepare samples for TOC measurements, the carbonate content was removed with concentrated phosphoric acid. Remaining acid was flushed by hot water for at least 6 hours in multiple repetitions. The sediment samples were incinerated at 1350°C and the emitted CO_2 and SO_2 were determined by an infrared detector. The results are given in weight percent [wt.%] and were measured at least twice for both measurement runs (TC and TOC). TIC content was calculated from the difference between TC and TOC (TIC=TC-TOC). The calcite equivalent percentages could then be computed from the TIC: TIC * 8.334 [wt.%]. Additionally, the ratio between TOC and sulphur was calculated.

4 Results

4.1 Gas samples

4.1.1 Gas chromatography

The resulting gas composition for each gas sample location can be seen in Figure 20. Oxygen and nitrogen are related to the contribution of air in the gas samples. Hydrogen shows little variation and ranges at around 10 ppm, which is assumed to be a background signal from bacterial processes in the sediment. The four samples with the highest CO_2 content contain traces of H_2S. Methane content also vary strongly between the samples. Three of the four H_2S containing samples were part of the cluster of four samples with the highest methane content. Ethane or higher hydrocarbons were not detected. A table with all data related to the gas composition is found in appendix III.

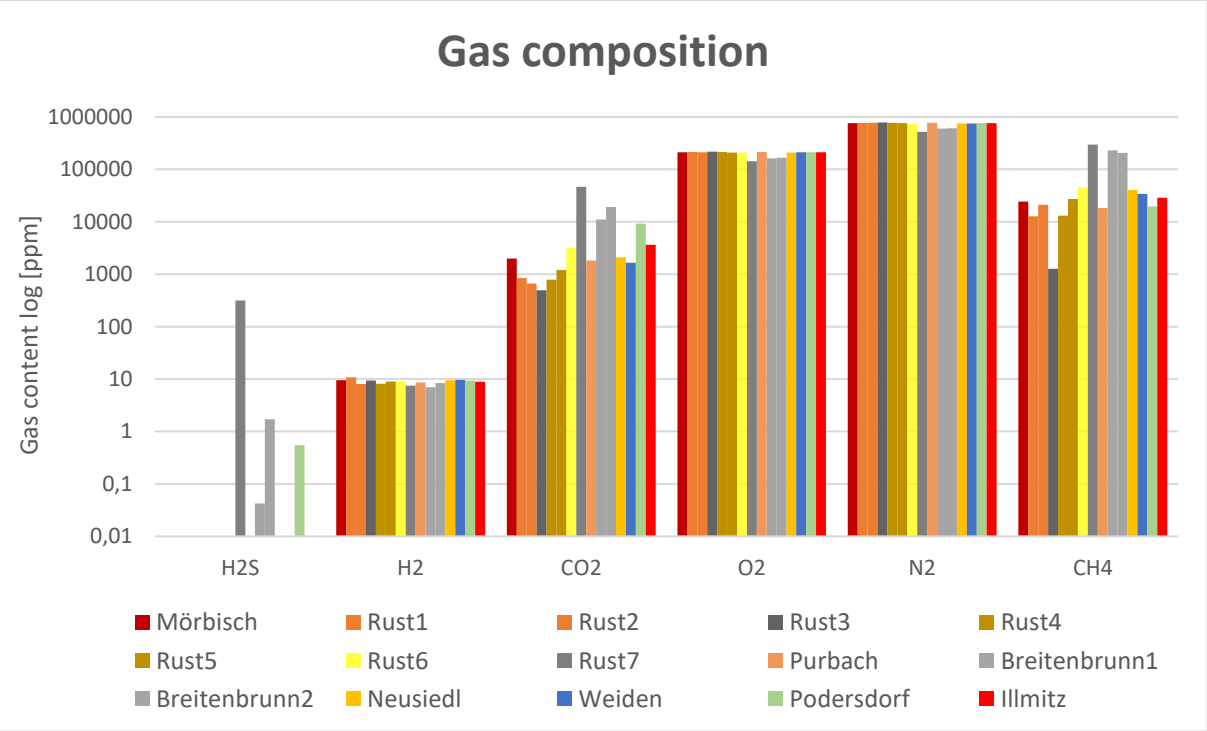

Figure 20: Gas composition in ppm of the gas samples at Lake Neusiedl with identical-coloured samples representing samples taken at the same location.

4.1.2 Stable isotopes

Twelve out of 15 samples had a $\delta^{13}C$ of methane between -56.9 and -68.5 ‰ (Fig. 21). Two samples were lighter with a $\delta^{13}C$ of -79.2 and -80.3 ‰ and one sample was very heavy with a $\delta^{13}C$ of -21.1 ‰. Samples taken at the same location (Rust1&2, Rust4&5) show only minor variation, but at Breitenbrunn1 &2 a slightly larger shift can be seen. The samples at Breitenbrunn were taken approximately 10 m apart. The hydrogen isotopy shows $\delta^{2}H$ values between -138 and -334 ‰ (Fig. 22). The $\delta^{2}H$-methane values of the gas samples at Rust and Breitenbrunn were lighter compared to samples at the other locations. Compared to the carbon isotopy the values vary strongly and it was only possible to calculate the hydrogen isotopy of methane in seven of 15 samples due to low signals of detection.

The values for the carbon stable isotopy of CO_2 are between -6.6 and -16.5 ‰ (Fig. 23). It was possible to determine values for eight out of the 15 gas samples. Strong variations were observed even for samples in close proximity.

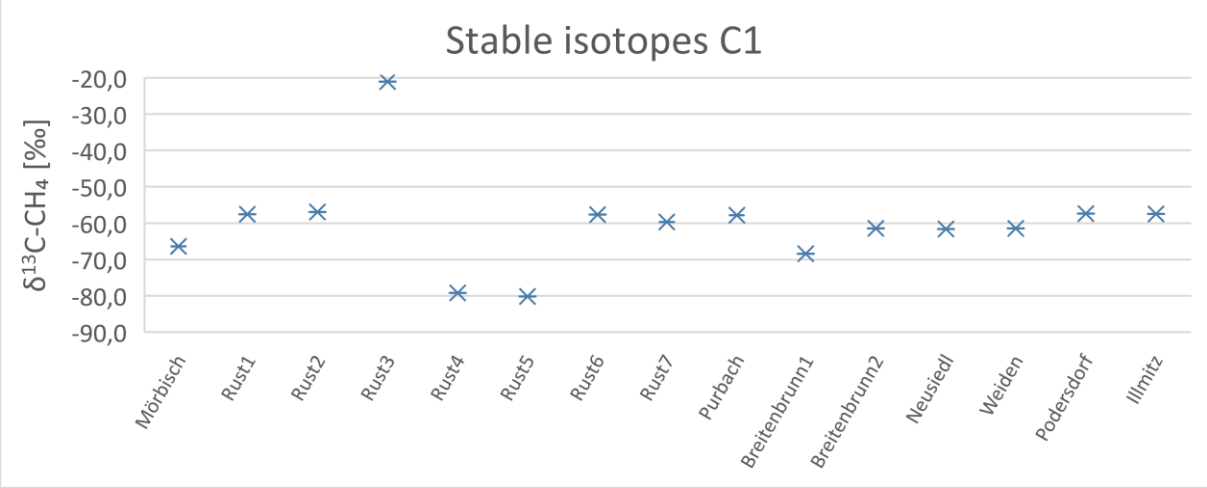

Figure 21: $\delta^{13}C$ in ‰ of methane of the gas samples at Lake Neusiedl ordered from southwest to southeast clockwise around the lake.

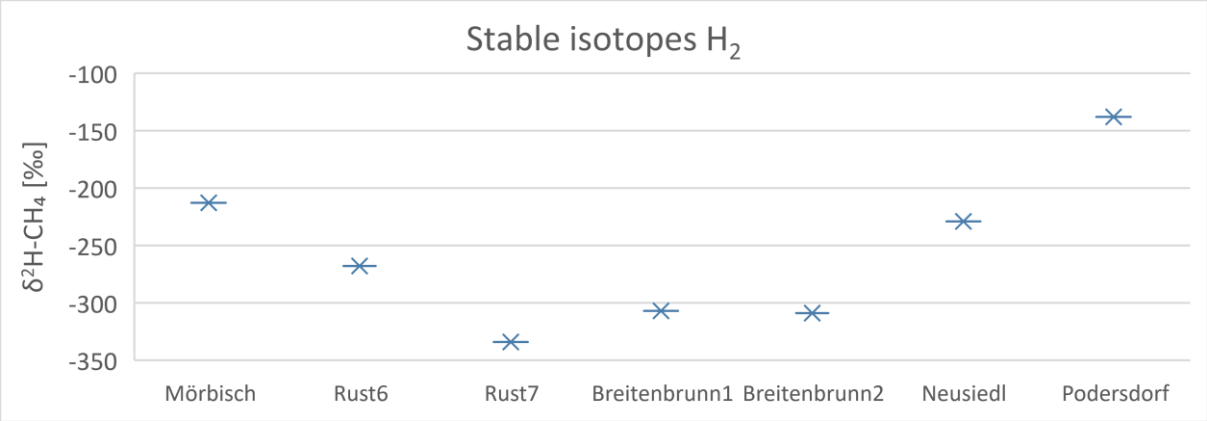

Figure 22: $\delta^{2}H$ in ‰ of methane of the gas samples at Lake Neusiedl ordered from southwest to southeast clockwise around the lake.

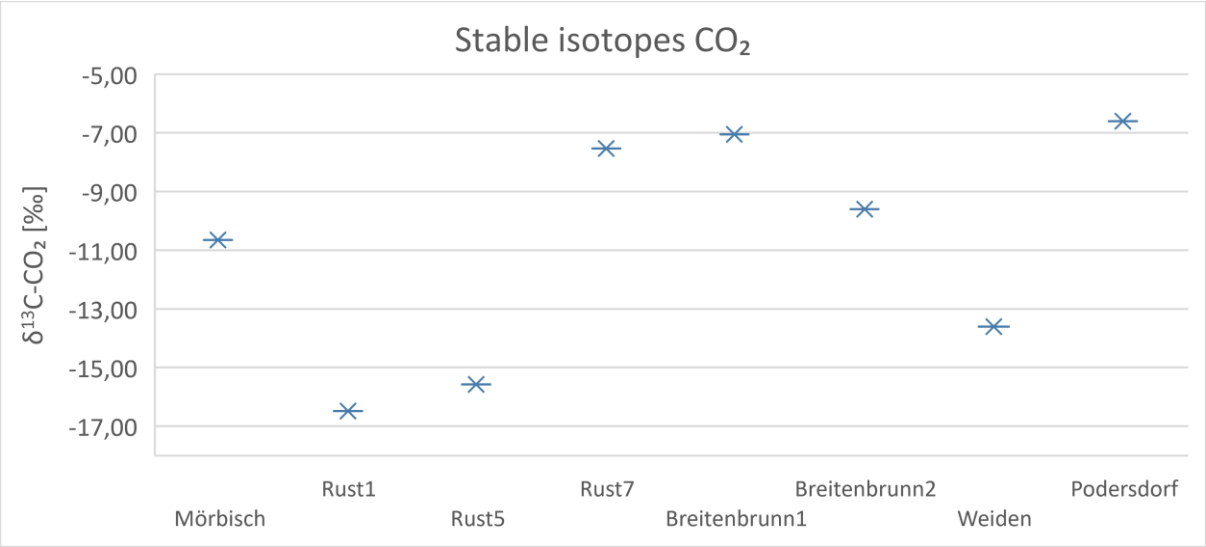

Figure 23: Clockwise ordering of $\delta^{13}C$ of CO_2 in ‰ of the gas samples at Lake Neusiedl from southwest to southeast.

4.2 Sediment samples

4.2.1 Bulk mineralogy

Carbonate minerals dominate in most samples with varying portions of calcite, low-Mg calcite, high-Mg calcite and protodolomite. Low-Mg calcite and protodolomite have the largest share of the carbonate minerals, while high-Mg calcite was also found but occur in lesser amount. Quartz, feldspar in the form of microcline and albite, illite/muscovite and chlorite were also detected. Other clay minerals were not identified. Pyrite is absent in the samples. Profile 1 (Fig. 25) is in general dominated by carbonate minerals, but their percentage varies greatly. Clay minerals (illite/muscovite and chlorite) were in most cases dominant over the sum of quartz and feldspar (Fig. 24 & Fig. 25). A table with all XRD results can be found in appendix I.

Compared to Profile 1, Profile 2 showed less variation. The carbonate content ranges in general between 60 and 70 wt.% (Fig. 25). Clay minerals were mostly between 20 and 30 wt.% and quartz and feldspar content ranges in general between 5 and 20 wt.%. Two samples close to the shore of Podersdorf showed a clearly different composition (Fig. 24).

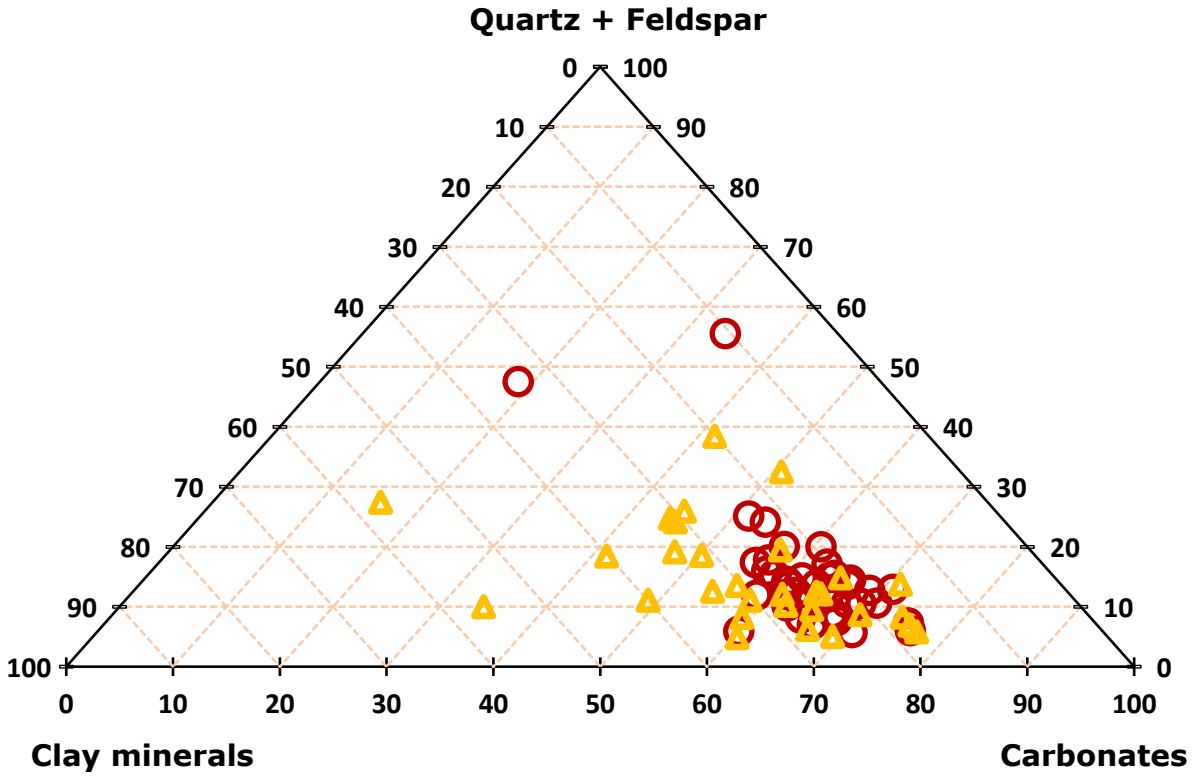

Figure 24: Ternary diagram of the mineralogical composition of samples from Profile 1 (orange triangles) and Profile 2 (red circles).

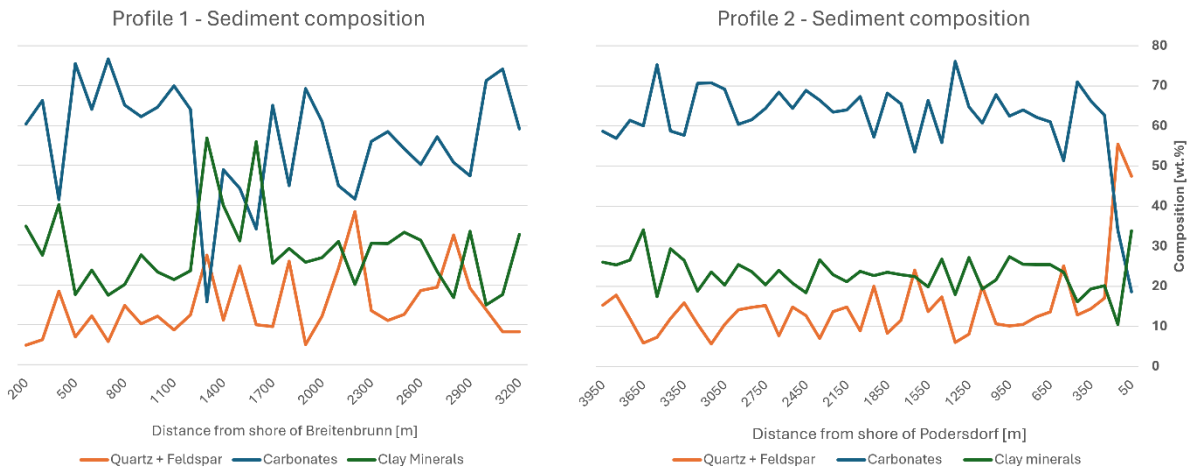

Figure 25: Sediment composition of Profile 1 and Profile 2 from Breitenbrunn (left) to Podersdorf (right).

In all samples protodolomite (PD) occurred together with either calcite or low-magnesium calcite (LMC) or both and rarely with high-magnesium calcite (HMC). While in some cases a clear peak for these carbonate minerals exists, sometimes the peak was clearly broadened. All sediment samples from both profiles were categorized into four different groups according to the existence of broadened peaks visible in the diffractograms.

Group I

Group I show a clearly defined calcite or LMC, and PD peak (Fig. 26). The presence of HMC was not detected. Group I is characterized by the absence of broadened peaks.

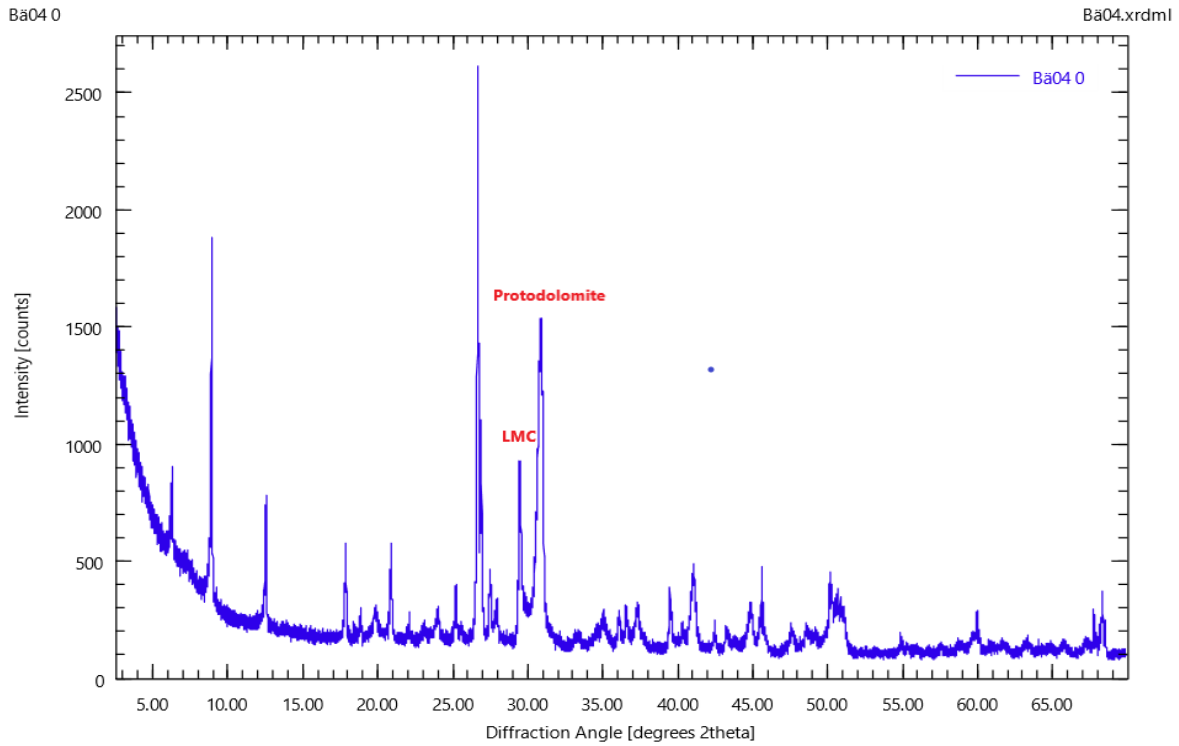

Figure 26: Group I where LMC and PD peaks exist, but HMC cannot be detected.

Group II

Group II is characterized by a broadened LMC peak and a narrow PD peak (Fig. 27).

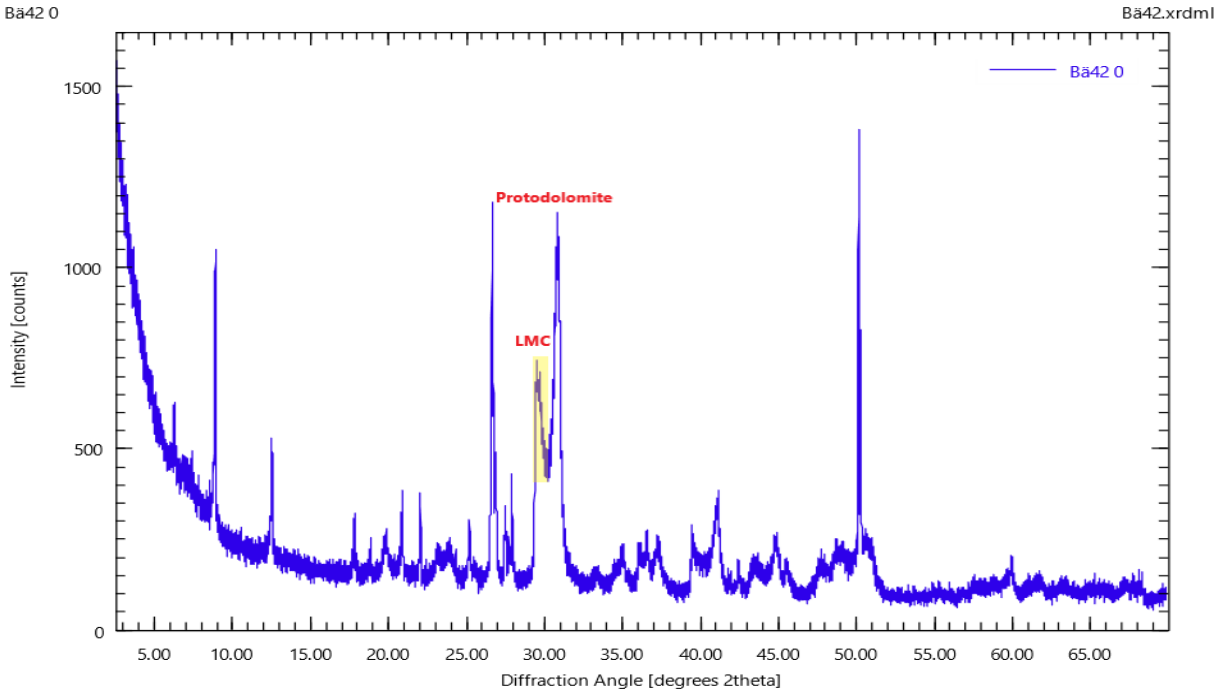

Figure 27: Group II where the LMC peak is broadened (yellow rectangle), while the PD peak is narrow.

Group III

Group III is defined by a LMC peak and a broadened PD peak (Fig. 28).

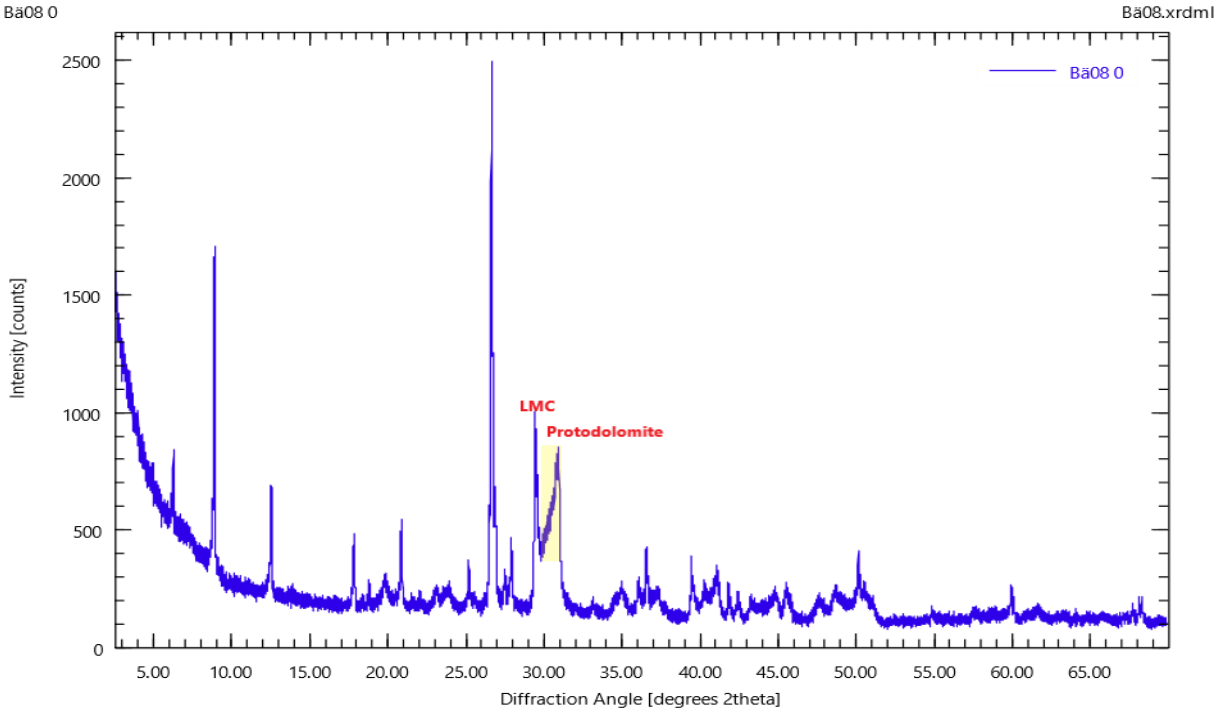

Figure 28: Group III with a LMC peak and a broadened PD peak (yellow rectangle).

Group IV

Group IV shows a LMC, HMC and PD peak (Fig. 29).

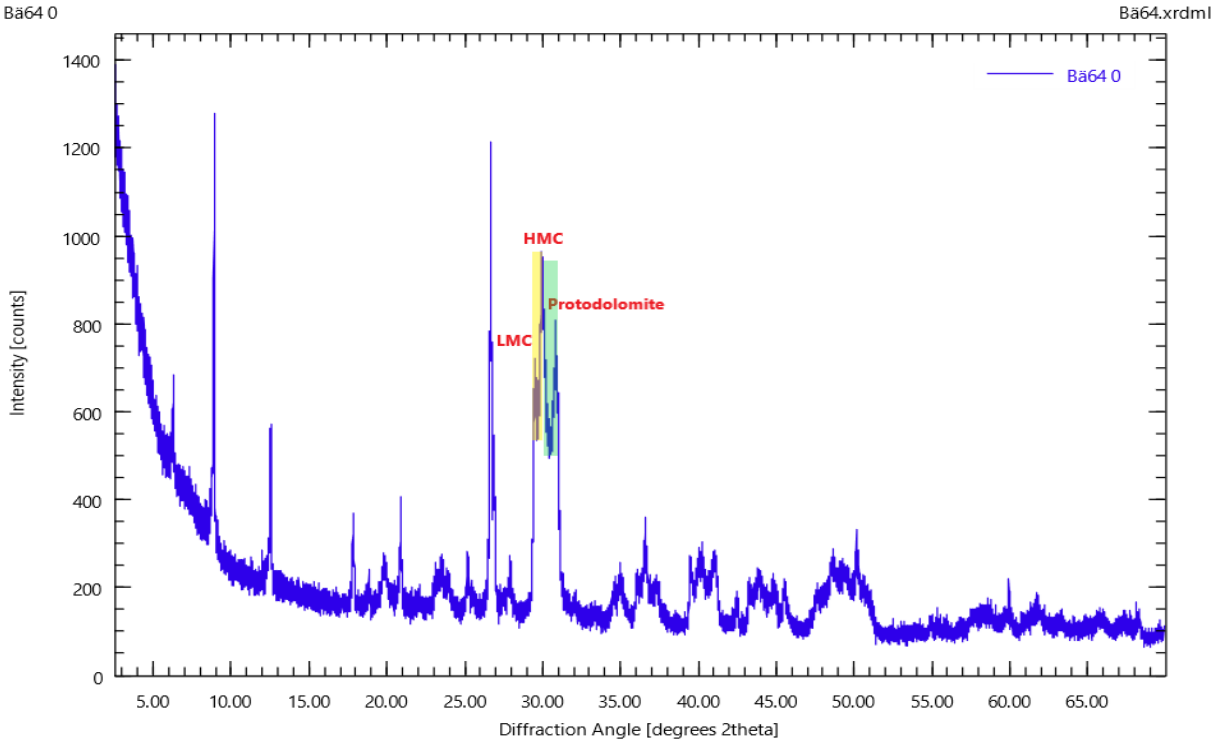

Figure 29: Group IV where LMC, HMC and PD peaks exist with broadened peaks between LMC and HMC (yellow rectangle), and between HMC and PD (green rectangle).

4.2.2 Clay mineralogy

Three samples were subjected to detailed clay mineralogical characterization. One sample was located at a distance of 4050 m from the shore of Podersdorf in the lake centre, one at a distance of 2150 m from the shore of Podersdorf and one at a distance of 1600 m from the shore of Breitenbrunn. This selection was based on the high total clay mineral percentage of the samples and the sampling locations covering the lake centre as well as the E and W margins. The XRD results of the textured mounts with temperature and ethylenglycol treatment confirm the clay mineral composition obtained from the texture-free mounts. Illite/Muscovite and chlorite were the only clay minerals that were detected. The diffractograms are found in appendix II.

4.2.3 pH

Evaluation of the pH measurements shows varying pH values between 7.4 and 8.7. The pH values were higher (more alkaline) close to the shore and became lower (more acidic) in the lake centre. Profile 1 and Profile 2 (Fig. 30) both show this trend. The pH value plotted against the carbonate content can be seen in Figure 31. A trend or correlation cannot be detected.

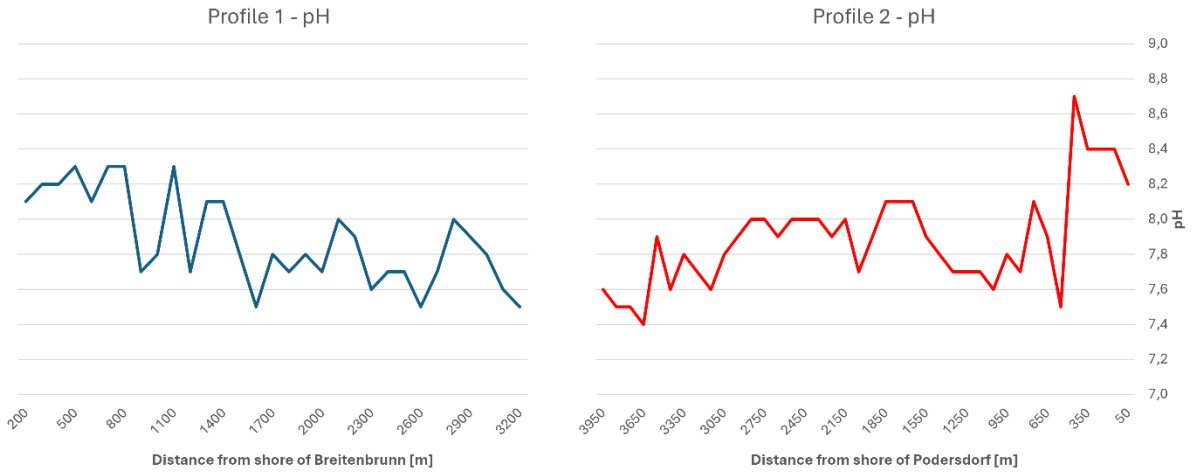

Figure 30: Distribution of pH of Profile 1 and Profile 2 from Breitenbrunn (left) to Podersdorf (right).

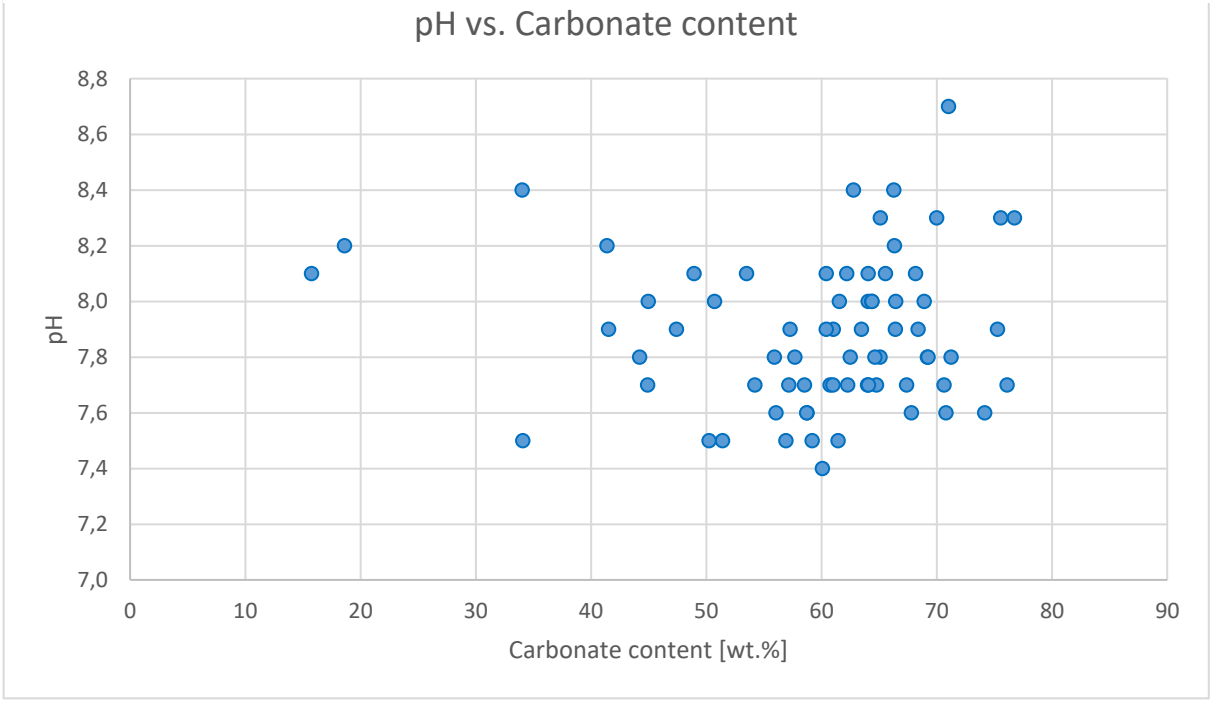

Figure 31: Crossplot of pH against carbonate content of all investigated samples from Lake Neusiedl.

4.2.4 TC, TOC and sulphur

TC contents were used to derive TOC and calcite equivalent percentages. The sulphur content varied between 0 and 0.02 wt.%. TOC had a maximum of 3.4 wt.% in Profile 1 and a minimum of 0.2 wt.% (Fig. 32). Slight variation around 2 wt.% TOC can be seen for the first 1000 m from the shore of Breitenbrunn. Thereafter, the curve behaves like an oscillation, with increasing amplitude and in general increased TOC content. Profile 2 showed in general values between 2 and 1.5 wt.% (Fig. 32). Values tend to decrease closer to the shore and there is a general increase toward the lake centre. Two minima were detected at 1650 and 3750 m distance from the shore of Podersdorf. The maximum TOC in this profile is 550 m away from the shore with a TOC of 2.3 wt.%. The TC, TOC and sulphur results are found in appendix III.

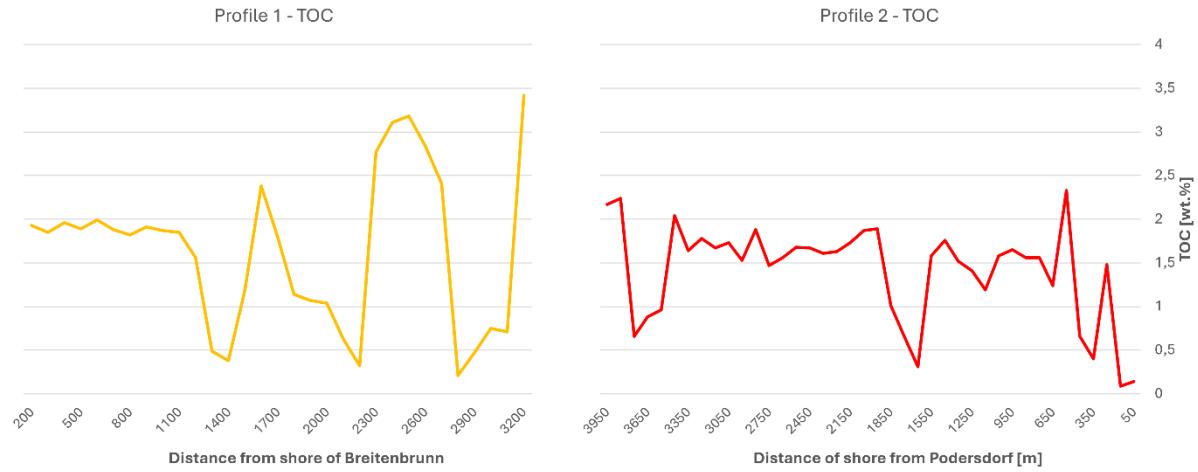

Figure 32: TOC contents of Profile 1 and Profile 2 from Breitenbrunn (left) to Podersdorf (right).

The calcite equivalent percentages that were calculated based on the TIC are plotted against carbonate contents from XRD in Figure 33. They show a generally good coincidence, although considerable scattering is visible in the data. This validates the results from XRD. Figure 34 and Figure 35 show that the calcite equivalent follows the general trend of the carbonate content.

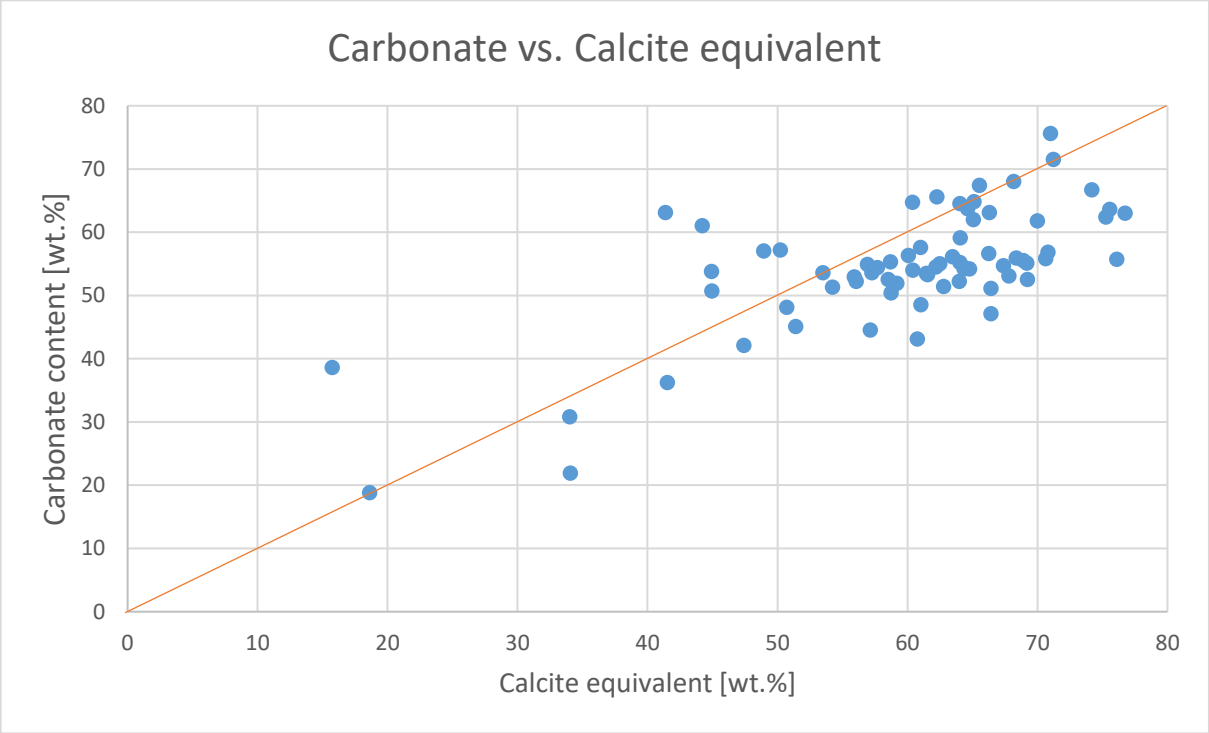

Figure 33: Crossplot of the carbonate content against the calcite equivalent percentages for the samples at Lake Neusiedl with the red line indicating a reasonable correlation.

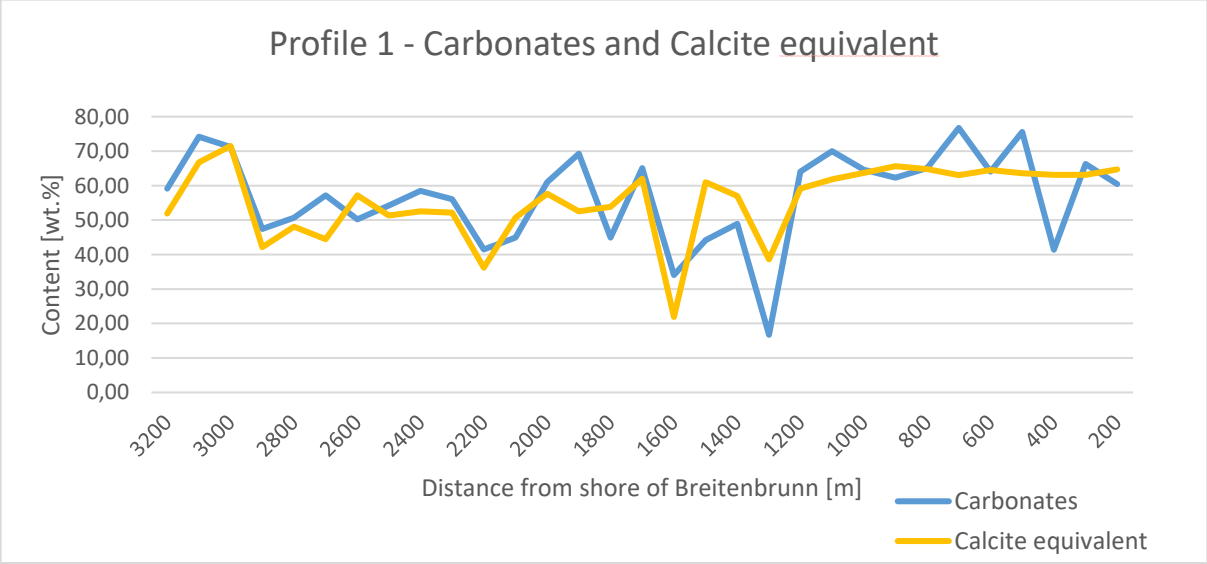

Figure 34: Profile 1 of the sediment samples at Lake Neusiedl that shows the change of carbonate content and calcite equivalent from the shore of Breitenbrunn to the lake centre.

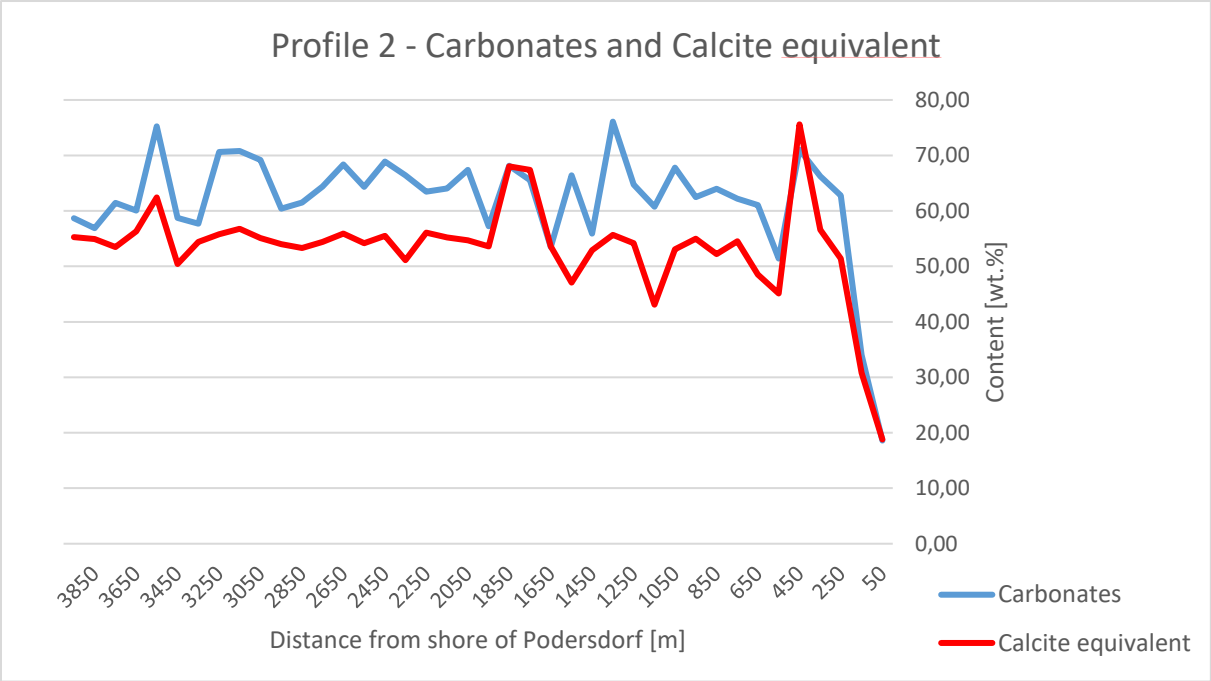

Figure 35: Profile 2 of the sediment samples at Lake Neusiedl that shows the change of carbonate content and calcite equivalent from the lake centre to the shore of Podersdorf.

The pH was also plotted against the TOC content (Fig. 36). The pH seems to decrease with increasing TOC content.

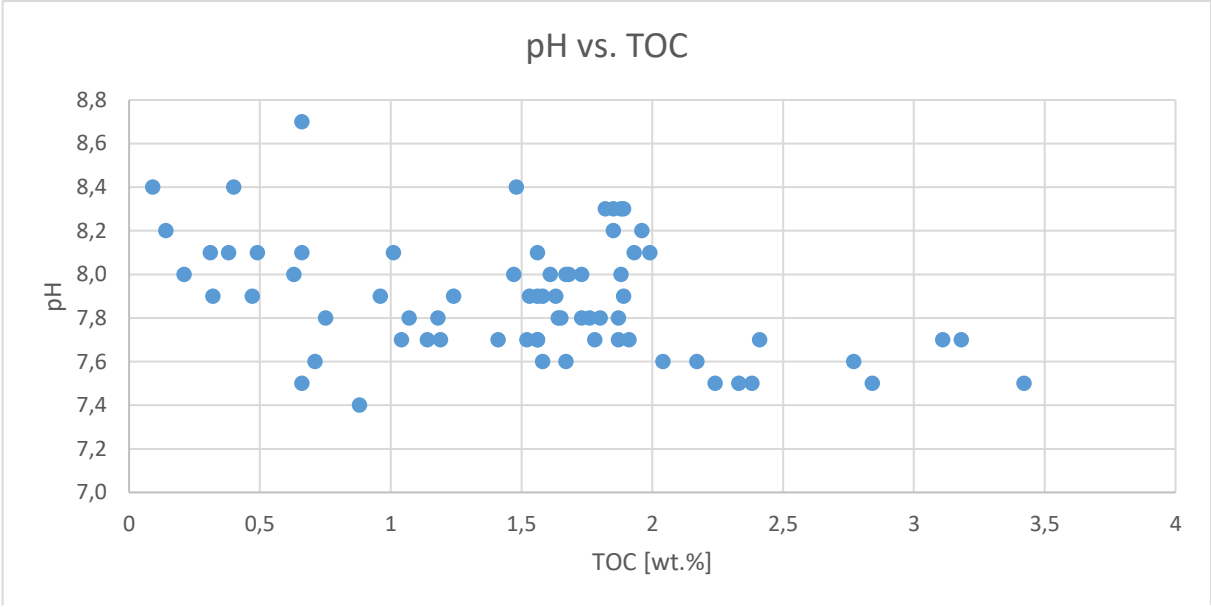

Figure 36: The pH plotted against the total organic carbon content from the sediment samples of Profile 1 and Profile 2.

5 Discussion

5.1 Gas composition and source typing

Figure 37 defines typical carbon stable isotope ranges of bacterial and thermogenic gas (Bernard et al., 1978). Gas seep 1 with the samples Rust1 and Rust2 that was not covered by lake mud and constantly emits gas provides a good indication of the origin of the gas from the gas seeps, since in case of a thermogenic source mixing with bacterial gas from organic matter decomposition within the lake sediments is minimized. The other two gas seeps were covered by lake mud and therefore a contribution of sludge gas is to be expected. The samples Rust1 and Rust2, taken over a period of several weeks, showed no contribution of higher hydrocarbons and a clearly microbial carbon stable isotope signature (-57.5 and -56.9 ‰). The only heavy isotope signature found (-21.1 ‰) was in sample Rust3 at gas seep 2; however, this sample contained no higher hydrocarbons either and a low methane concentration, and therefore the extremely heavy carbon stable isotopy which is unrealistic for a thermogenic gas from reasonable reservoir depth is likely due to measurement bias. Furthermore, there was no clear distinction between microbial gas from apparent permanent gas seeps and sludge gas sampled by stimulation of the lake mud in terms of stable carbon isotopes of methane, so a distinct source for the permanent gas shows cannot be inferred. Two sludge gas samples showed lighter carbon stable isotopy of methane, but the remaining ones showed a similar composition compared to the presumed seep gas. Therefore, it is more likely that variations in the decomposition processes active in the lake sediment cause the isotope shift in parts of the samples, rather than a distinct microbial source e.g., related to biogenic gas formation in deeper-lying strata. Also, according to Baur et al. (2024) the gas shows at Lake Neusiedl have a biogenic origin (-55.6 ±5.9 ‰ VPDB $\delta^{13}C\text{-}CH_4$).

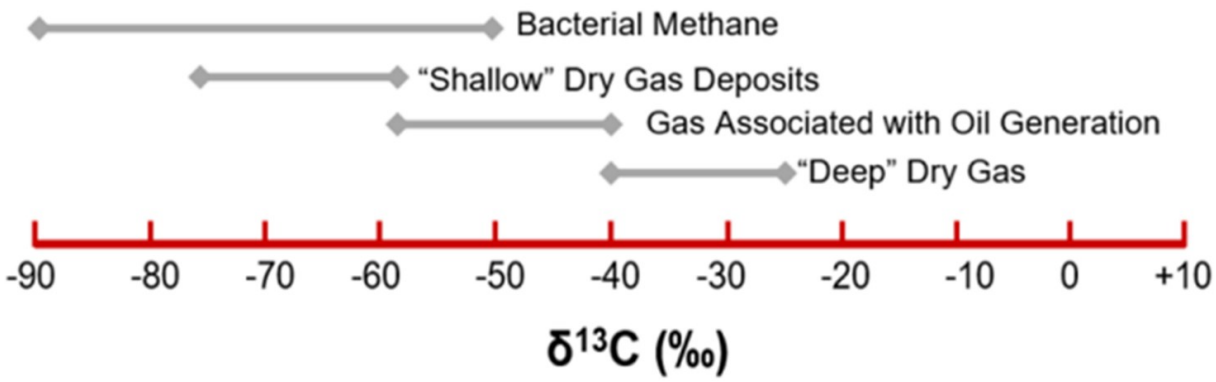

Figure 37: Classification of methane regarding the $\delta^{13}C$ of CH_4 in [‰] (modified after Caldas et al., 2022; after Bernard et al., 1978).

The hydrogen stable isotope signatures of methane also show no clear distinction between gas seeps and sludge gas. All samples plot in the field of biogenic origin, plotting between methyl-type fermentation and bacterial carbonate reduction (Figure 38; after Whiticar, 1999).

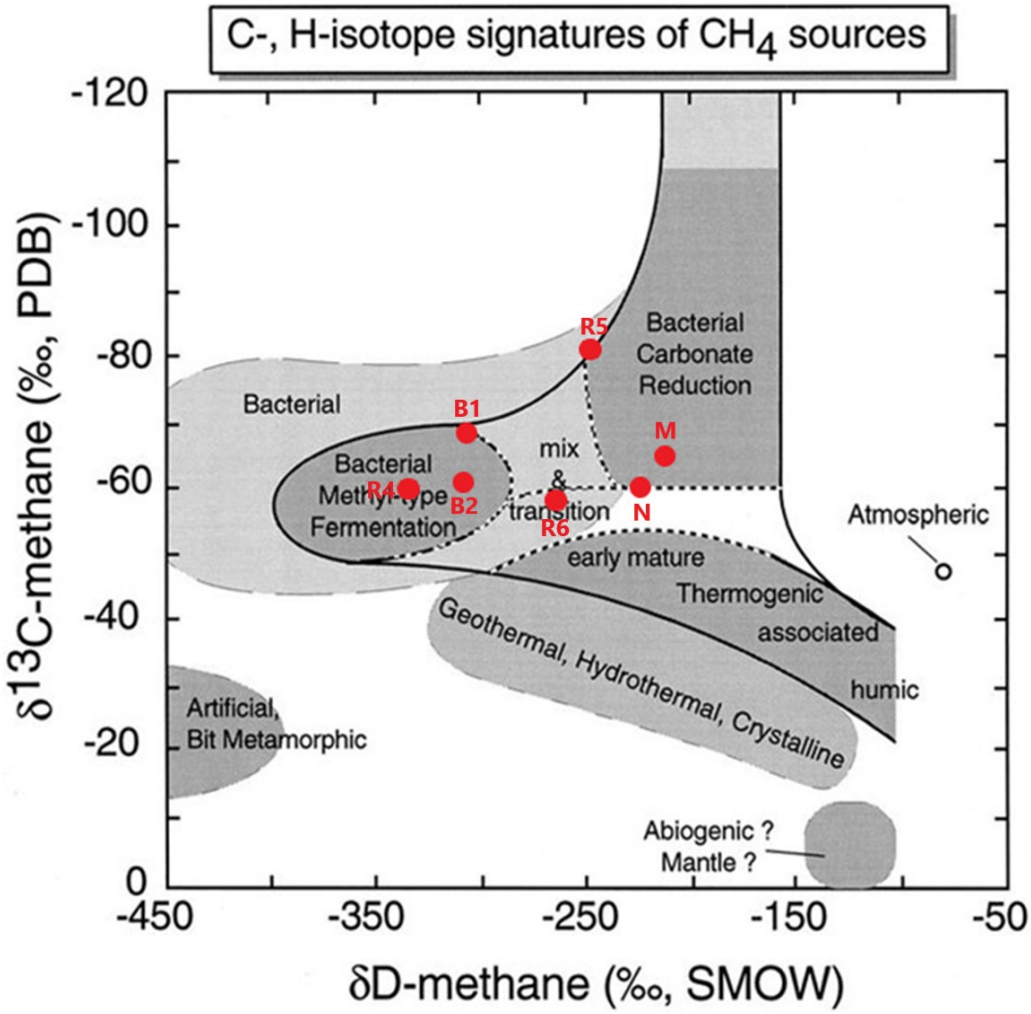

Figure 38: Crossplot of the stable isotope ratios of C and H in methane. The value –21.1 ‰ $\delta^{13}C\text{-}CH_4$ has been excluded due to unreliable measurement accuracy. (M = Mörbisch. R = Rust, B = Breitenbrunn, N = Neusiedl; modified after Whiticar, 1999).

Carbon stable isotopes of CO_2 provide further indication regarding the type of biogenic gas formation. Figure 39 indicates hydrogenotrophic processes for some samples while others plot in the field of dominant acetoclastic processes. Again, a distinction of apparent seep gas vs. sludge gas is impossible, while a gradual variation of the active processes is likely (Baur et al., 2024). While hydrogenotrophic methanogens use H_2 and CO_2 for methanogenesis, acetoclastic methanogens use acetate as an electron acceptor. Baur et al. (2024) documented that at the same location (Illmitz), the relative intensity of both processes varied over time, leading to a similar distribution of data in the crossplot of carbon stable isotope ratios of CO_2

and methane (Fig. 39). A slight shift to the field of hydrogenotrophic methanogenesis distinguishes the data from this study from the results of Baur et al. (2024).

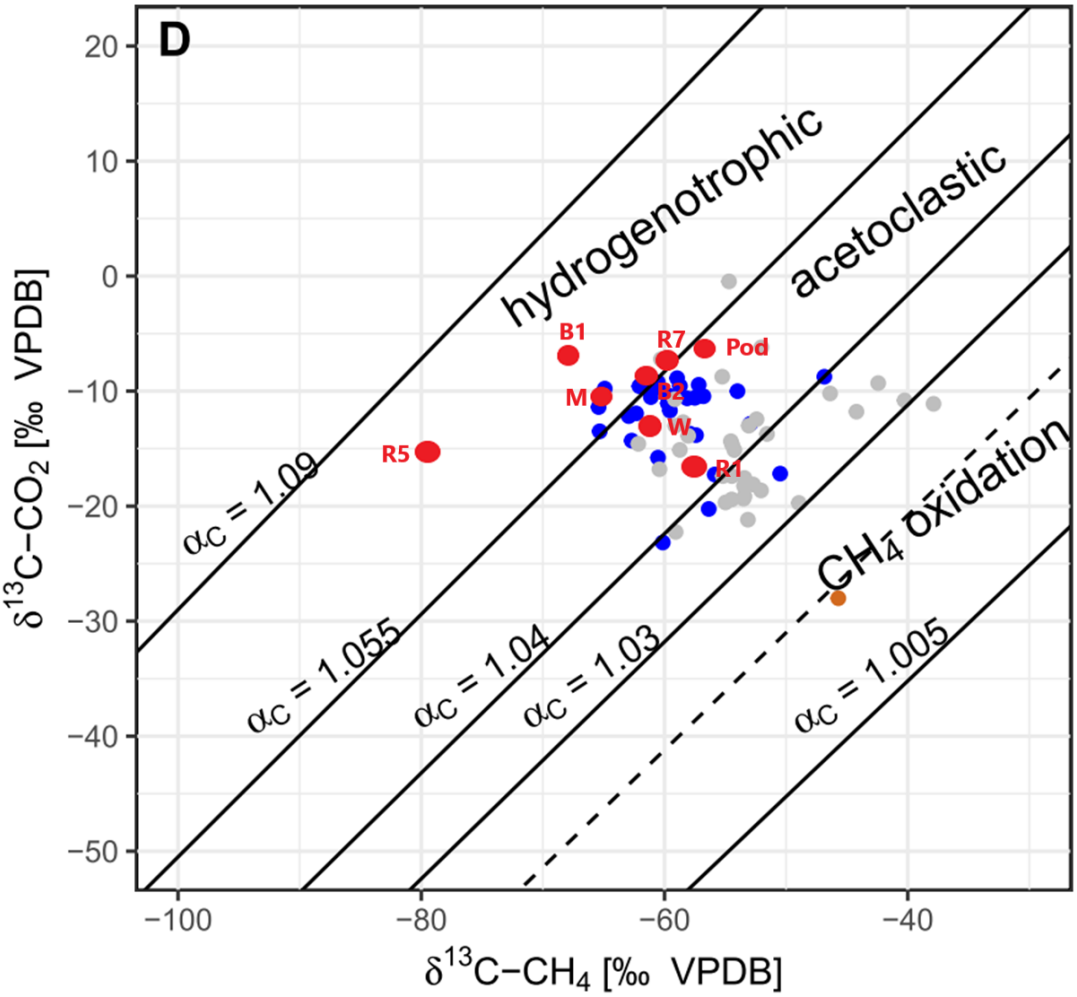

Figure 39: Methanogenic characterization where $\delta^{13}C$ of CO_2 is plotted against $\delta^{13}C$ of CH_4 with the gas samples from Lake Neusiedl as red dots; grey, blue and brown dots after Baur et al., 2024. (M = Mörbisch, R = Rust, B = Breitenbrunn, W = Weiden, Pod = Podersdorf; modified after Baur et al., 2024).

5.2 Compositional trends in lake sediments

The composition of the sediment samples is dominated by carbonate minerals, with quartz, feldspar and clay minerals representing the remaining major constituents. Pyrite was not detected, although trace amounts < 1 wt.% may have been overlooked by XRD analysis. Previous literature reports pyrite in the mud of Lake Neusiedl (Tauber & Wieden, 1959), but either pyrite may not have been formed at the sampled locations due to less reducing conditions, or traces of pyrite may have been oxidized after their initial formation in times of oxygen input by turbulent currents. The clay mineral fraction is dominated by illite/muscovite and chlorite, while other clay minerals are absent. Occasional occurrence of montmorillonite has been reported by Wieden (1963) but were not detected in this study.

Several samples with a low carbonate content and high quartz and feldspar content were detected along the W-E profile (Fig. 25). These values additionally align with low TOC values. The field observation showed occasional, roughly N-S oriented bars of gravel with a width in the range of decimetres. According to Sauerzopf (1959) longitudinal shaped gravel banks occur in Lake Neusiedl. These bars likely deposited by permanent water currents known to be present at the lake (Fig. 5; Sauerzopf, 1959). Due to the distance between the sediment sampling locations, likely the longitudinal features are only randomly covered, whereas additional bars may exist but have been overlooked in the W-E profile.

Weak trends could be observed for pH and TOC of the lake sediments; the most alkaline pH was found at the lake margin, whereas a decrease towards the lake centre could be observed (Fig. 30). TOC was the lowest at the margins and increased towards the centre (Fig. 32). This documents that conditions for organic matter preservation are slightly more favourable in the centre of the lake, where bottom waters are likely less prone to disturbance and oxygen-input by wind currents and dilution by coarser sediment input associated with recharge areas is minimized. As mentioned, the longitudinal bar-shaped gravel deposits align with minima in TOC highlighting the diluting effect of coarser sediment transported by permanent water currents.

In all samples PD was detected together with either calcite or LMC or both and occasionally HMC. Broadened peaks exist between LMC and HMC and between HMC and PD in some samples. These were categorized into four different groups according to the appearance of broadened peaks and between which minerals the broadened peak occurred. Figure 40 displays the distribution of the groups at Profile 1 and Profile 2. Group I showed no broadened peak and no HMC (Fig. 26). This suggests that HMC and PD were currently not forming. Group I generally occur in Profile 1 aligning with areas where the gravel deposits dominate and in Profile 2 towards the lake centre. Group II is characterized by a broadened LMC peak and a narrow PD peak (Fig. 27). This indicates the formation, or start of the

formation, of HMC. Group II was found at Profile 1 near Group I areas and rarely at Profile 2. Group III is defined by a LMC peak and a broadened PD peak (Fig. 28). The broadened PD peak indicates the formation of PD from HMC. It dominates Profile 2 and does not occur at Profile 1. Group IV show broadened LMC, HMC and PD peaks (Fig. 29). This suggests the simultaneous formation of HMC and PD. Group IV dominates Profile 1 and is occasionally found at Profile 2, however most commonly found at the lake centre. Formation of HMC and PD was not currently occurring throughout both profiles. The required conditions for the formation of PD were only met in some specific areas.

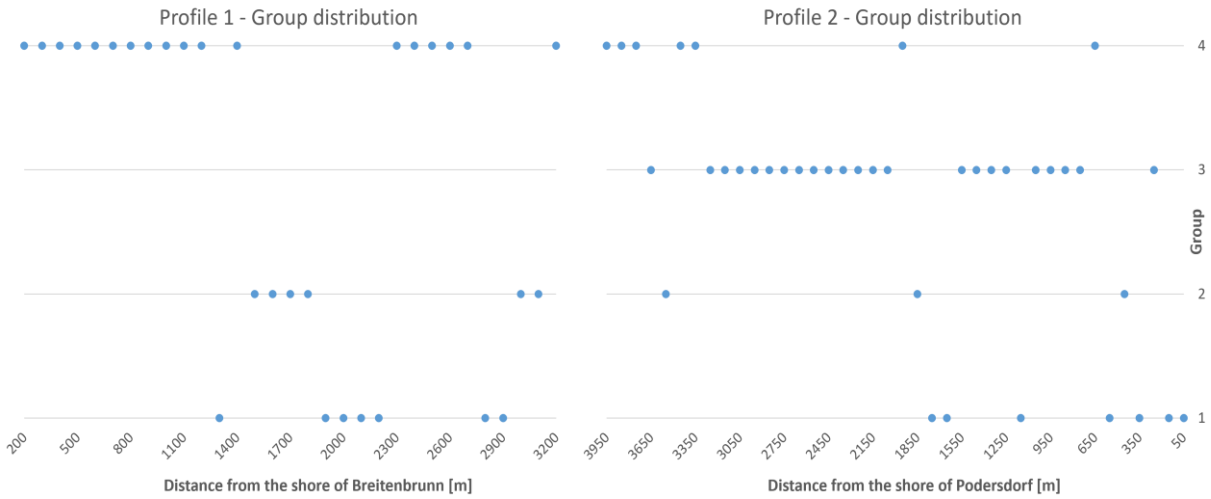

Figure 40: Group distribution of Profile 1 and Profile 2 from Breitenbrunn (left) to Podersdorf (right); Group I: LMC + PD, Group II: LMC broadened + PD, Group III: LMC + PD broadened, Group IV: LMC + HMC+ PD.

6 Conclusions

Apparently permanent gas seeps in Lake Neusiedl could not be distinguished from sludge gas obtained from the uppermost decimetres of the lake mud by manual stimulation. All samples share a purely microbial source with no indication of a thermogenic contribution in either the molecular or isotope compositional data. While a slight variation of the methanogenic processes is indicated by the scattering of organic geochemical data, it is unlikely that a distinct biogenic source e.g., related to a shallow gas accumulation associated with deeper lying strata, is responsible for the apparent permanent gas shows. The carbon stable isotope signatures of methane and CO_2 rather suggest a gradual change of methane-forming processes in the lake mud, which agrees with recent research on the isotopic composition of the sludge gas. It seems that the condition of the mud cover on the Pannonian lake basement sediments might have an influence on the release of microbial gas eventually suggesting a permanent, deeper lying source, while the formation of gas itself clearly occurs by microbial degradation of organic matter within the lake mud. Free hydrogen sulfide was only occasionally detected in sludge gas and may be associated with locally more reducing conditions in the mud cover. According to Tauber & Wieden (1959) the majority of the hydrogen sulfide is most likely produced by a breakdown of proteins due to microbial activity, but microbial reduction of sulfates is also significant (Löffler, 1959).

A substantial compositional variability was found in the sediment samples taken across to profiles roughly aligned with the W-E lake axis. Varying carbonate minerals, quartz, feldspar and clay minerals are the main components in the lake sediment. For clay minerals illite/muscovite and chlorite dominate, while other clay mineral types were not detected. Pyrite was also not to detected in the samples. TOC, pH and the general mineral composition did not vary systematically between the western and eastern lake sides, but TOC increases and pH decreases towards the lake centre. Longitudinal shaped gravel bars likely created by larger-scale lake currents were detected, reflected by high quartz and lower carbonate contents in the respective samples. These deposits also correlate with low TOC contents. Calcite, LMC, HMC and PD occur in the carbonate fraction of the sediment. Broadened peaks can be identified for LMC and PD in the X-ray diffractograms. Classification of samples into four different groups was performed based on the occurrence of these broadened peaks in the XRD data. Formation of HMC and PD occurs irregularly along the W-E profile.

7 References

Ajuaba, S., Sachsenhofer, R. F., Bechtel, A., Galasso, F., Gross, D., Misch, D., Schneebeli-Hermann, E., (2022). Biomarker and compound-specific isotope records across the Toarcian CIE at the Dormettingen section in SW Germany. International Journal of Earth Sciences, 111(5), 1631-1661.

Baur, P. A., Pinilla, D. H., Glatzel, S., (2024). Is ebullition or diffusion more important as methane emission pathway in a shallow subsaline lake?. Science of The Total Environment, Volume 912.

Bernard, B. B., Brooks, J. M., Sackett W. M., (1978). Light hydrocarbons in recent Texas continental shelf and slope sediments. Journal of Geophysical Research, 83(C8), 4053 – 4061.

BVFA-Arsenal., (1960). Analyse von Sumpfgas und Faulschlamm. Bericht S 2313 der Bundesversuchs- und Forschungsanstalt Arsenal, Wien.

Caldas, P. F. B., Snatic, J., Kronenberger, K., (2022). Quality Isotope Analysis at the Wellsite: Two Case Studies that Validate GC-C-IRMS Mud Gas Isotope Logging for Deepwater Exploration and Development. In *SPE Annual Technical Conference and Exhibition?* (p. D021S028R005). SPE. Dinka, M., Ágoston-Szabó, E., Berczik, Á., Kutrucz, G., (2004). Influence of water level fluctuation on the spatial dynamic of the water chemistry at Lake Fertő/Neusiedler See. Limnologica 34: 48-56.

Dobesch, H., Neuwirth, F., (1978). Die Windverhältnisse im Südteil des Neusiedlersees. Biologische Station Neusiedlersee, Biologisches Forschungsinstitut für Burgenland, Illmitz, BFB - Bericht 28.

EN 16179:2012: Schlamm, behandelter Bioabfall und Boden – Anleitung zur Probenvorbereitung.

Eitzinger, J., Kubu, G., Formayer, H., Haas, P., Gerersdorfer, T., Kromp-Kolb, H., (2009). Auswirkungen einer Klimaänderung auf den Wasserhaushalt des Neusiedler Sees. Endbericht im Auftrag des Amtes der Burgenländischen Landesregierung, Landeswasserbaubezirksamt Schützen am Gebirge, Institut für Meteorologie (BOKU-Met), Wien, 80 pp.

Fodor, L. (1991). Evolution tectonique et paleo-champs de contraintes soligocenes a quaternaires de la zone de transition alpes orientales-carpathes occidentales: formation et developpement des bassins de vienne et nord-pannoniens. Doctoral dissertation, Paris 6.

Fuchs, W., (1960). Geologischer Bau und Geschichte des Ruster Berglandes. Unveröff. Diss., Philosoph. Fak., Univ. Wien (Geol. Inst.), S.Wien, 104.

Fussmann, D., von Hoyningen-Huene, A. J. E., Reimer, A., Schneider, D., Babková, H., Peticzka, R., Maier, A., Arp, G., Daniel, R., Meister, P., (2020). Authigenic formation of Ca–Mg carbonates in the shallow alkaline Lake Neusiedl, Austria, Biogeosciences, 17(7), 2085-2106.

Gattinger, T., (1979). The hydrogeology of Neusiedlersee and its catchment area. Neusiedlersee: The limnology of a shallow lake in Central Europe. 21-32.

Harzhauser, M., Piller, W. E., (2005). Neogen des Wiener Beckens. The hydrogeology of Neusiedlersee and its catchment area. Neusiedlersee: The limnology of a shallow lake in Central Europe.Beckens. – 75. Jahrestagung der Paläontologischen Gesellschaft, Graz 27.8.–2.9.2005, 42 S., 32 Abb., Graz.

Häusler, H., (2007). Geologische Karte der Republik Österreich 1:50.000, Erläuterungen zu den Blättern 79 Neusiedl am See, 80 Ungarisch-Altenburg und 109 Pamhagen. Geologische Karte der Republik Österreich 1: 50.000, Erläuterungen.

Häusler, H., Figdor, H., Hammerl, C., Kohlbeck, F., Lenhardt, W., Schuster, R., (2010). Geologische Karte der Republik Österreich 1:50.000, Erläuterungen zur Geologischen Karte 78 Rust. Vienna: Geological Survey of Austria.

Hiebl, J., Orlik, A., (2023). Klimarückblick Burgenland 2022. Klimastatusbericht Österreich 2022, Hrsg. CCCA 2023, Wien.

Herzig, A., (2014). Der Neusiedler See–Limnologie eines Steppensees. Denisia, 33, 101-114.

Kubu, G., Kramer, T., (2014). Kapitel 2.2. Hydrologie und Wasserwirtschaft. —In: Wolfram, G., Deri, L., Zech, S., (Hrsg.), Strategiestudie Neusiedler See – Phase 1. Studie im Auftrag der Österreichisch-Ungarischen Grenzgewässerkommission, Wien-Szombathely, 10-21.

Löffler, H., (1959). Zur Limnologie, Entomostraken- und Rotatorienfauna des Seewinkelgebietes (Burgenland, Österreich). In: Zur Limnologie, Entomostraken- und Rotatorienfauna des Seewinkelgebietes (Burgenland, Österreich). Sitzungsberichten der Österr. Akademie der Wissenschaften. Springer, Berlin, Heidelberg.

Meister, P., Frisia, S., Dódony, I., Pekker, P., Molnár, Z., Neuhuber, S., Gier, S., Kovacs, I., Demeny, A., Pósfai, M., (2023). Nanoscale pathway of modern dolomite formation in a shallow, alkaline lake. Crystal Growth & Design, 23(5), 3202-3212.

Neher, J., Rohrer, E., (1958). *Dolomitbildung unter mitwirkung von Bakterien*. Geologisches Institut der Eidg. Technischen Hochschule und der Universität Zürich.

Neuhuber, S., Gier, S., Draganits, E., Steier, P., Bolka, M., Ottner, F., Spötl, C., Hippler, D. and Meister, P., (2024). Radiocarbon ages of microcrystalline authigenic carbonate in Lake Neusiedl (Austria) suggest millennial-scale growth of Mg-calcite and protodolomite. *Sedimentology*, *71*(3), 912-940.

ÖNORM EN ISO 10390:2022: Boden, behandelter Bioabfall und Schlamm – Bestimmung des pH-Werts.

Österreichisch- Ungarische Gewässerkommission., (1996). 40 Jahre Österreichisch-Ungarische Gewässerkommission (1956-1996), Bundesministerium f. Land- und Forstwirtschaft, A-1010 Wien; Ministerium für Verkehr, Nachrichtenwesen und Wasserwirtschaft, H-1077 Budapest, Jubiläumsschrift.

Rank, D., Tschulik, M., Papesch, W., Dolezel, P., (1985). Untersuchungen an den „Kochbrunnen“ im Neusiedlersee bei Rust. Biologisches Forschungsinstitut für Burgenland Illmitz, BFB-Bericht, 55, 45–49.

Rank, D., Papesch, W., Staudner, F., (1986). Zur Herkunft des Gases der Kochbrunnen im Neusiedlersee. *BFB-Bericht*, *58*, 93-94.

Sauerzopf, F., (1959). Landschaft Neusiedlersee. Wissenschaftliche Arbeiten aus dem Burgenland, Heft 23, Burgenländisches Landesmuseum (Hrsg.), Amt. d. Bgld. Landesregierung, Eisenstadt.

Schiemer, F. (1979). The benthic community of the open lake. In: Neusiedlersee: the limnology of a shallow lake in central Europe. Dordrecht: Springer Netherlands, 337-384.

Schoell, M., (1980). The hydrogen and carbon isotopic composition of methane from natural gases of various origins. Geochimica et cosmochimica ACTA, 44(5), 649-661.

Schönlaub, H. P., (2000). Burgenland, Erläuterungen zur Geologischen Karte des Burgenlandes 1: 200.000 Geologie der Österreichischen Bundesländer-1-130.

Schroll, E., (1959). Zur Geochemie und Genese der Wässer des Neusiedler Seegebietes. Wiss. Arbeiten aus d. Burgenland, 23, 55–64.

Schroll E., Tauber A. F., (1959). „Geochemisch-stratigraphische Beziehungen in den Neogensedimenten des Seewinkels, Burgenland“. Wissenschaft. Arbeiten aus dem Burgenland, Eisenstadt 1959, in Vorbereitg.

Székely, B., Zámolyi, A., Draganits, E., Briese, C., (2009). Geomorphic expression of neotectonic activity in a low relief area in an Airborne Laser Scanning DTM: a case study of the Little Hungarian Plain (Pannonian Basin). Tectonophysics, 474(1–2), 353–366.

Tanzberger, A., (2005). Die “Kochbrunnen” des Neusiedlersees/Ein kurzer Überblick über neue Untersuchungen. Unpublished B.Sc. Thesis. University of Vienna, Vienna.

Tauber, A. F., (1959). "Grundzüge der Tektonik des Neusiedlerseegebietes." Wissenschaftliche Arbeiten aus dem Burgenland, 23, 26-31.

Tauber, A. F., Wieden, P., (1959). Zur Sedimentschichtfolge im Neusiedlersee. *Wissenschaftliche Arbeiten aus dem Burgenland*, *23*, 68-73.

Wessely, G., Draxler, I., (2006). Pliozän und Quartär. – In: G. Wessely (Hrsg.) (2006): Niederösterreich, Geologie der österreichischen Bundesländer, Geologische Bundesanstalt Wien ,235–252, Abb. 477–513, Tab. 6.

Whiticar, M. J., (1999). Carbon and hydrogen isotope systematics of bacterial formation and oxidation of methane. Chemical Geology, 161(1-3), 291–314.

Whiticar, M. J., & Faber, E. (1986). Methane oxidation in sediment and water column environments—isotope evidence. Organic Geochemistry, 10(4-6), 759-768.

Wieden, P., (1963). Sedimentpetrographische Untersuchung des Schlammes vom Neusiedler See (Burgenland). *Tschermaks mineralogische und petrograhische Mitteilungen,* 8, 632–633.

Wingard, G. L., (2004). Changing Salinity Patterns in Biscayne Bay, Florida. US Geological Survey Fact Sheet, 3108.

Wolfram, G., (1996). Distribution and production of chironomids (Diptera: Chironomidae) in a shallow, alkaline lake (Neusiedler See, Austria). Hydrobiologia, 318(1), 103-115.

Wolfram, G., (2006). Bedeutung und Vorkommen von Salzlebensräumen. — In: Wolfram G. et al. (Hrsg.), Salzlebensräume in Österreich. Umweltbundesamt, Wien, 13-26.

Wolfram G., Herzig, A., (2013). Nährstoffbilanz Neusiedler See. — Wiener Mitteilungen 228, 317-338.

Wolfram, G., Déri, L., Zech, S., (2014). Strategiestudie Neusiedler See–Phase 1. Studie im Auftrag der Österreichisch-Ungarischen Gewässerkommission. Wien-Szombathely.

Zámolyi, A., Salcher, B., Draganits, E., Exner, U., Wagreich, M., Harzhauser, M., Gier, S., Fiebig, M., Lomax, J., Surányi, G., Diehl, M., Zámolyi, F., (2017). Latest Pannonian and Quaternary evolution at the transition between Eastern Alps and Pannonian Basin: new insights from geophysical, sedimentological and geochronological data. International Journal of Earth Sciences, 106, 1695-1721.

Zorn, I., Fritz, I., (2000). Miozäner und plio/pleistozäner Vulkanismus. – In: H.P. Schönlaub (Hrsg.): Geologie der Österreichischen Bundesländer: Burgenland. Erläuterungen zur Geologischen Karte des Burgenlandes 1 : 200.000. Geologische Bundesanstalt Wien, 28–30, Abb. 16–17, Tab. 1.

8 Appendix

I. X-ray Diffractograms

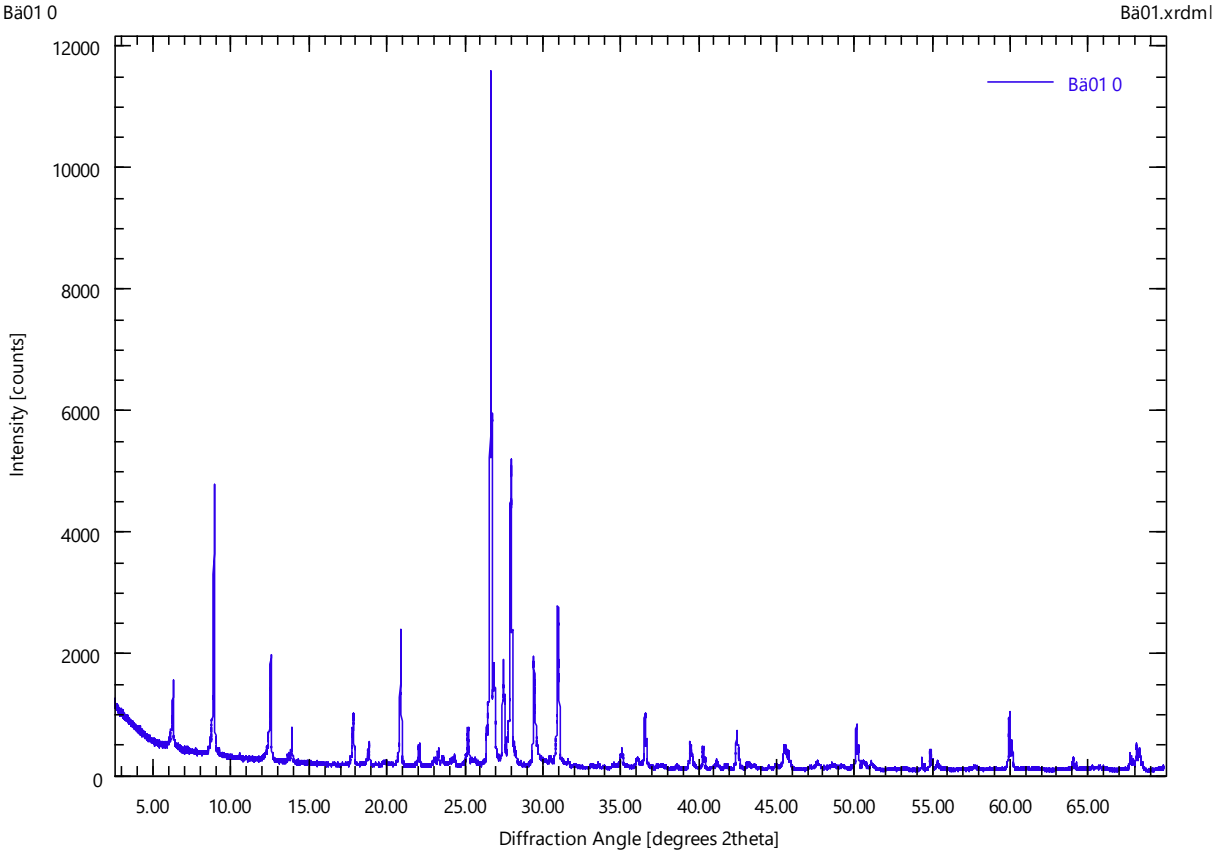

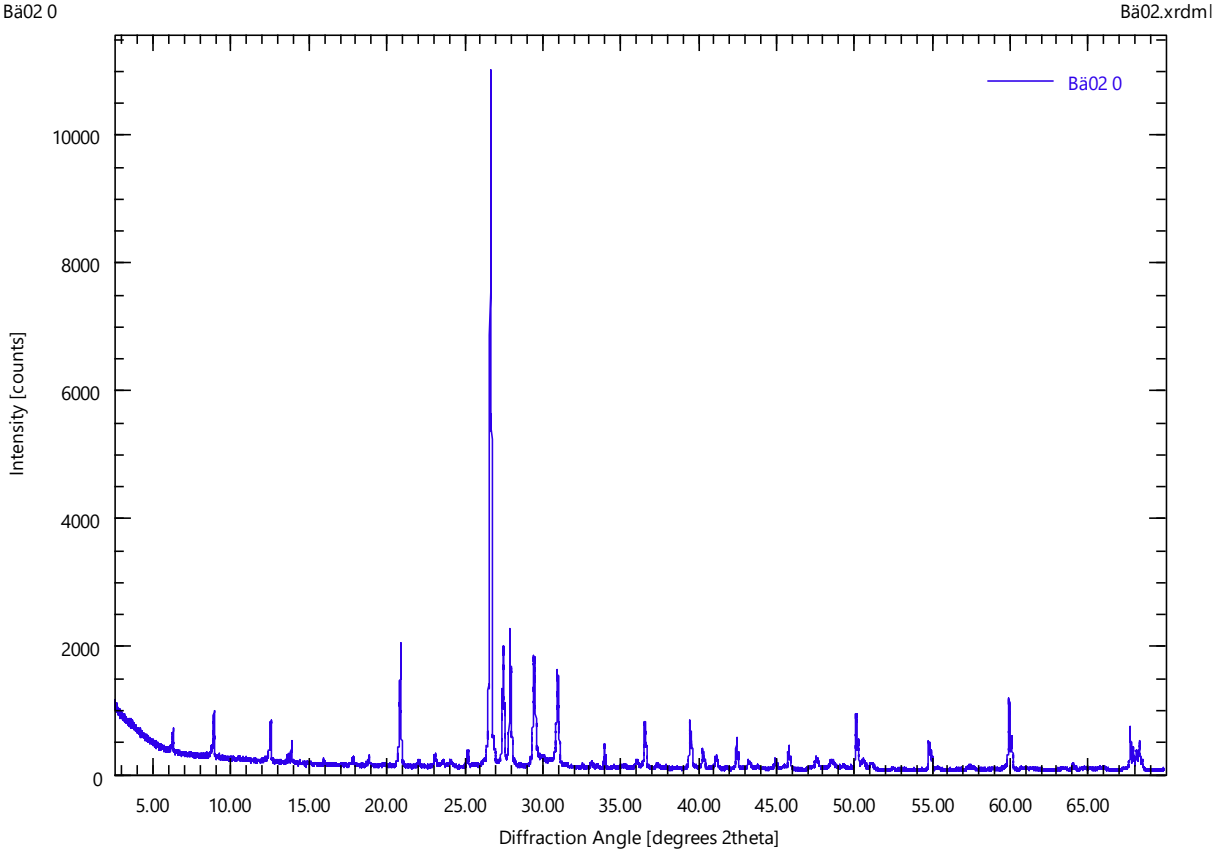

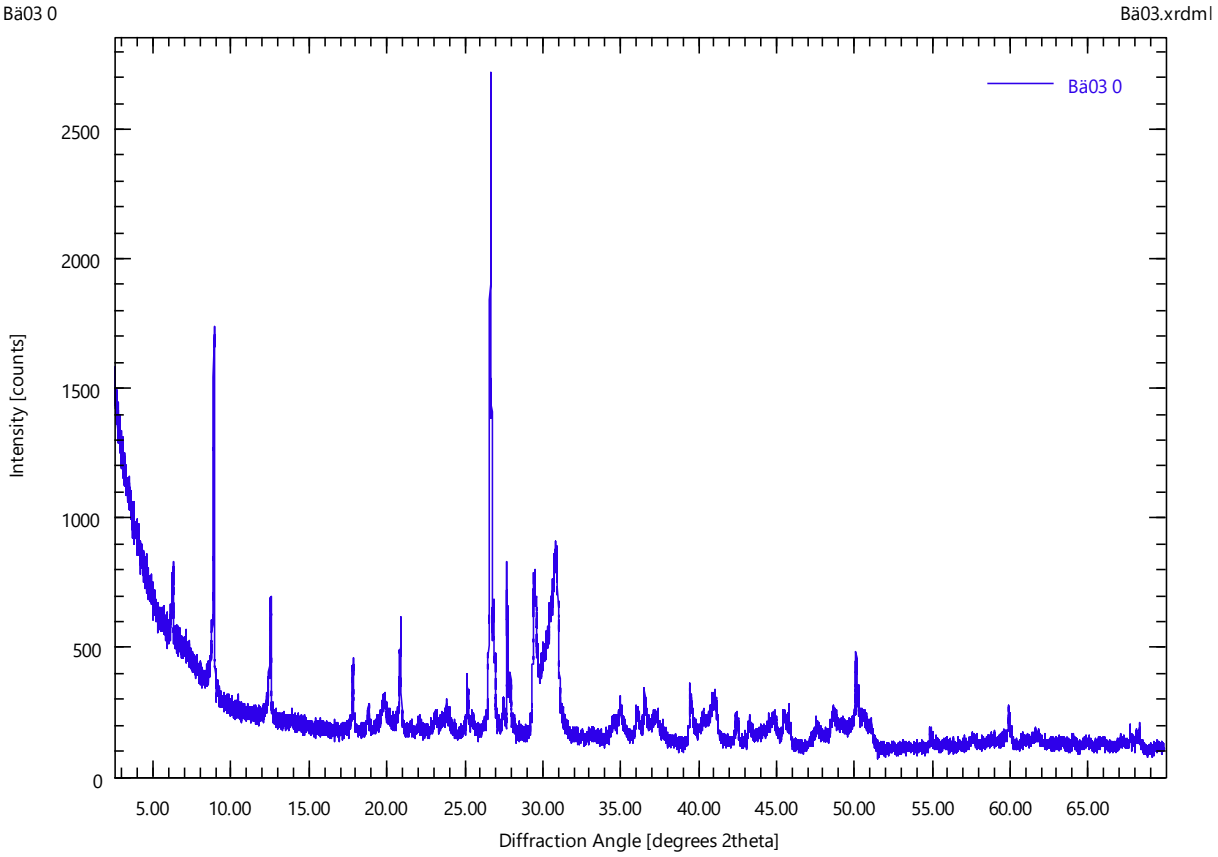
Bä03 0
Bä03.xrdml
Bä03 0
Intensity [counts]
0
500
1000
1500
2000
2500
5.00
10.00
15.00
20.00
25.00
30.00
35.00
40.00
45.00
50.00
55.00
60.00
65.00
Diffraction Angle [degrees 2theta]

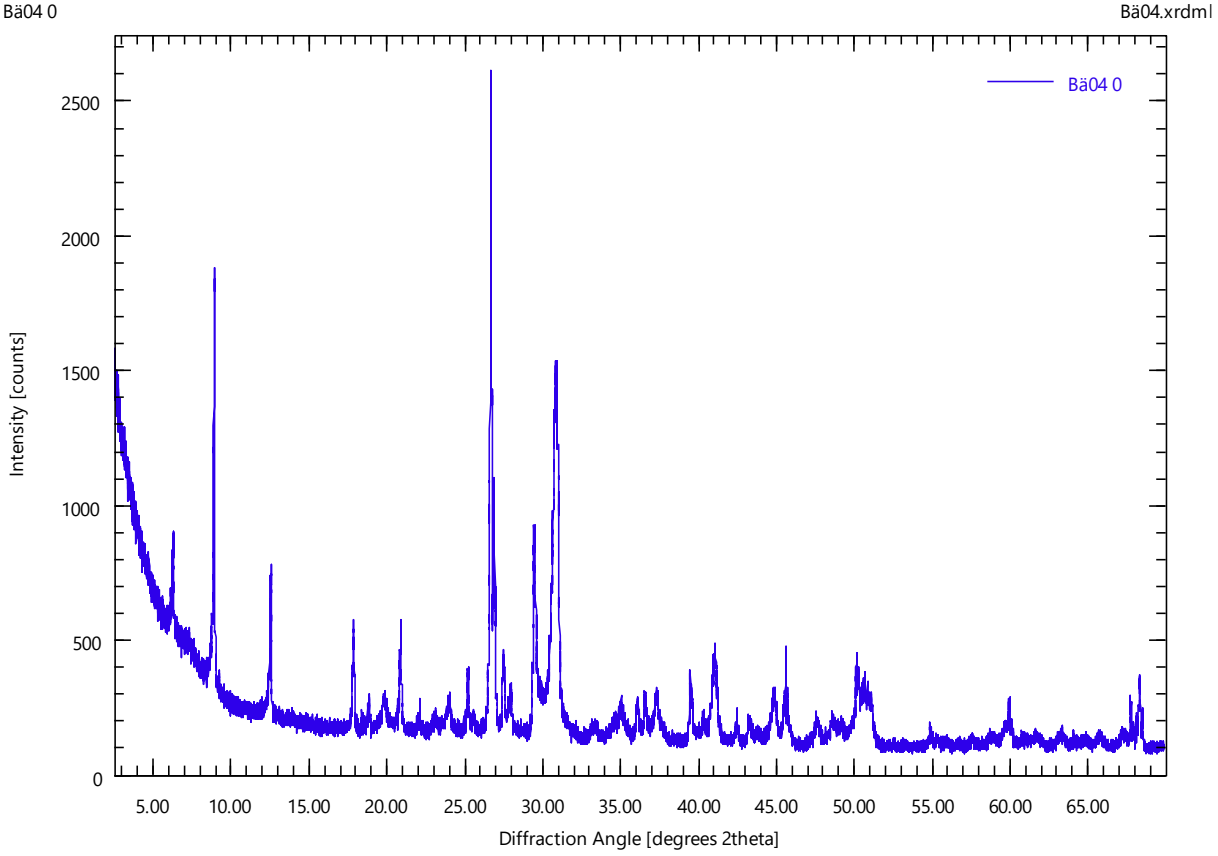
Bä04 0
Bä04.xrdml
Bä04 0
Intensity [counts]
0
500
1000
1500
2000
2500
5.00
10.00
15.00
20.00
25.00
30.00
35.00
40.00
45.00
50.00
55.00
60.00
65.00
Diffraction Angle [degrees 2theta]

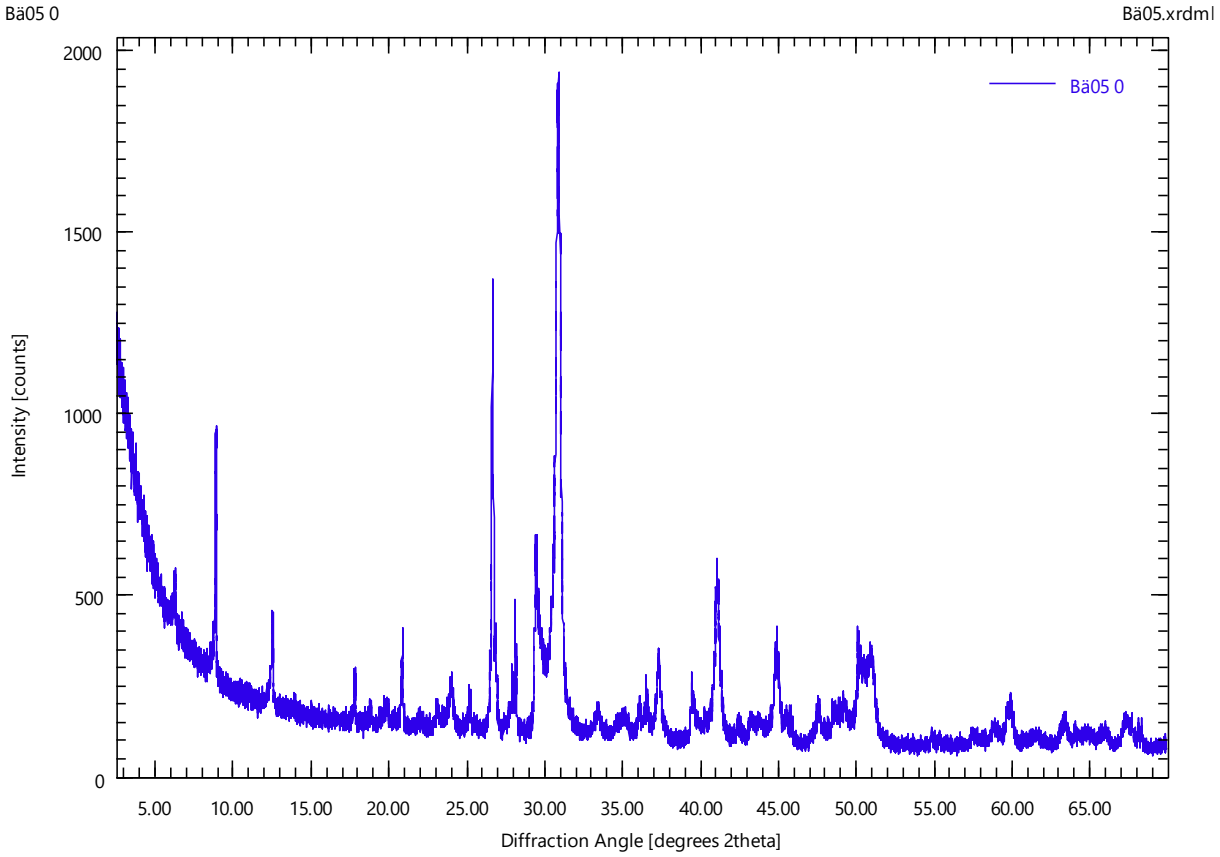
Bä05 0
Bä05.xrdml
Bä05 0
Intensity [counts]
2000
1500
1000
500
0
5.00
10.00
15.00
20.00
25.00
30.00
35.00
40.00
45.00
50.00
55.00
60.00
65.00
Diffraction Angle [degrees 2theta]

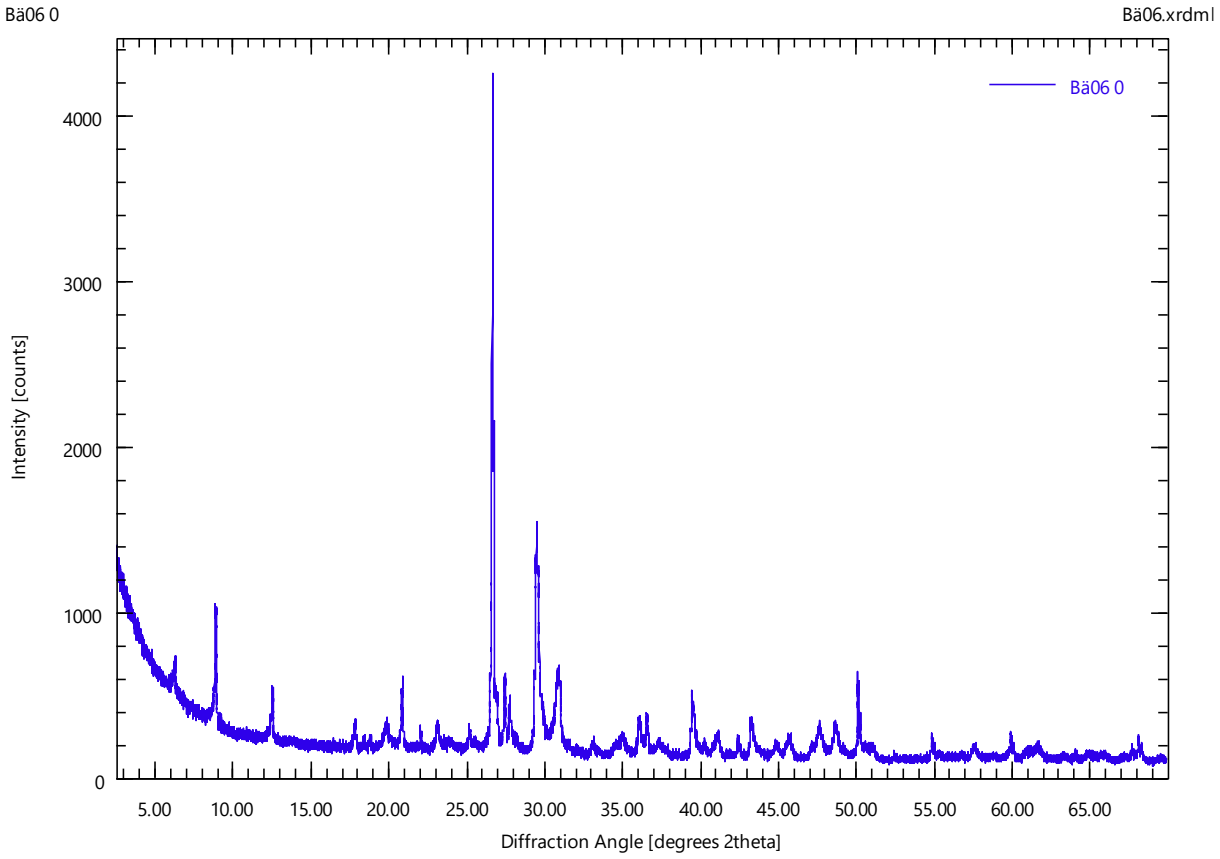
Bä06 0
Bä06.xrdml
Bä06 0
Intensity [counts]
4000
3000
2000
1000
0
5.00
10.00
15.00
20.00
25.00
30.00
35.00
40.00
45.00
50.00
55.00
60.00
65.00
Diffraction Angle [degrees 2theta]

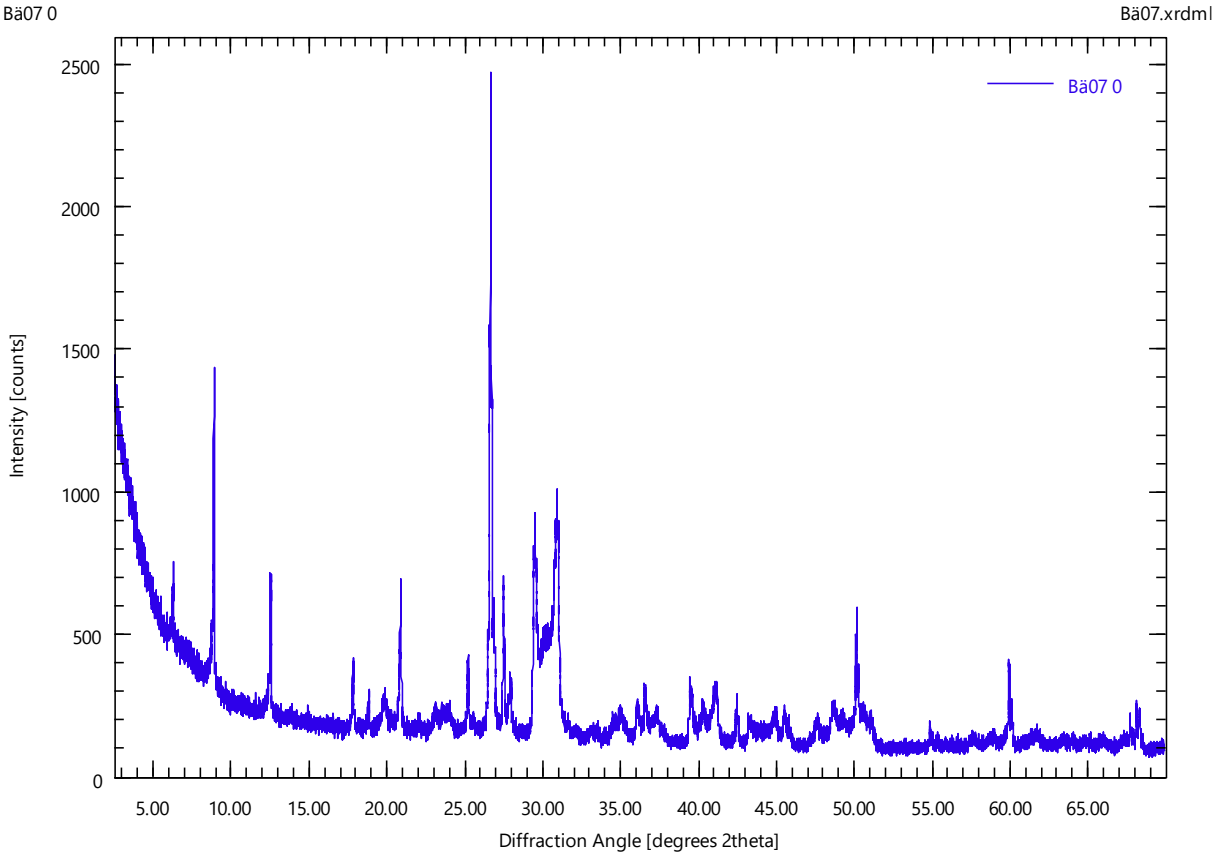
Bä07 0
Bä07.xrdml
Bä07 0
Intensity [counts]
2500
2000
1500
1000
500
0
5.00
10.00
15.00
20.00
25.00
30.00
35.00
40.00
45.00
50.00
55.00
60.00
65.00
Diffraction Angle [degrees 2theta]

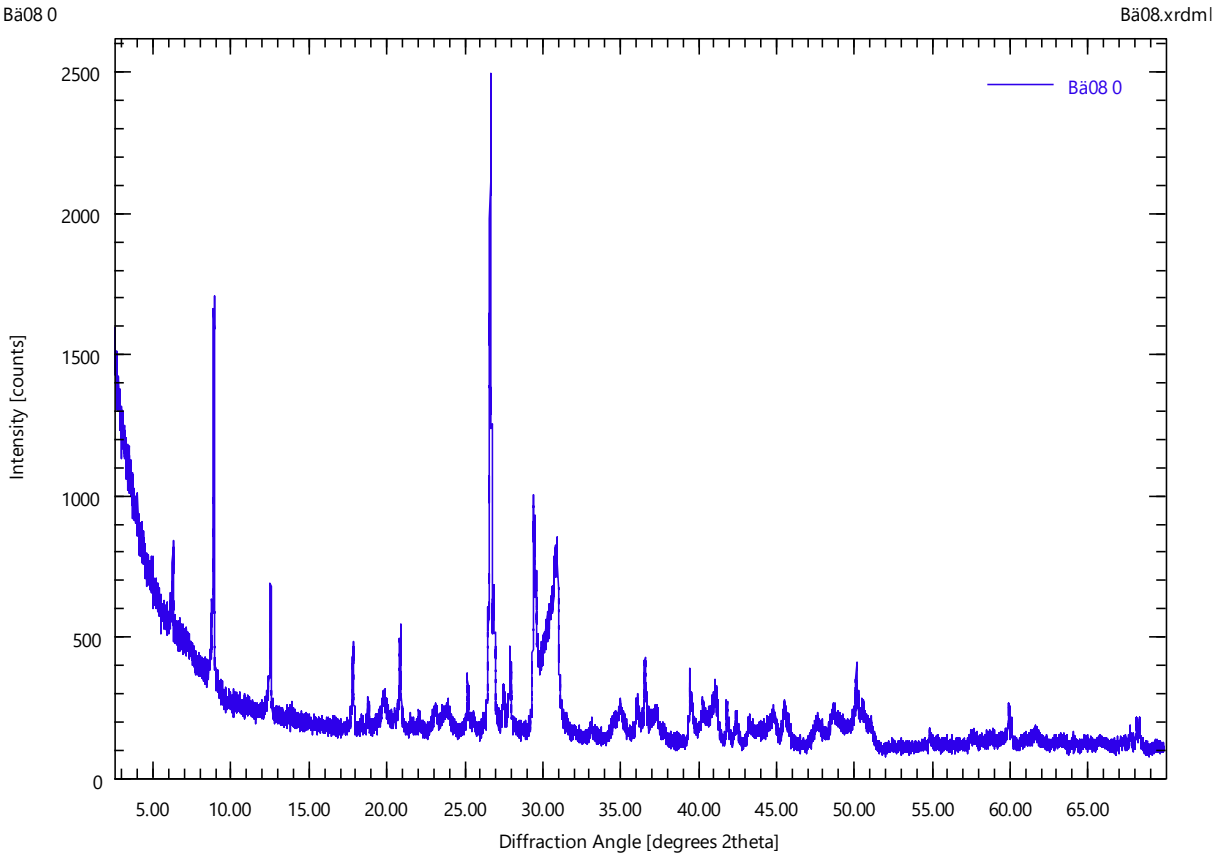
Bä08 0
Bä08.xrdml
Bä08 0
Intensity [counts]
2500
2000
1500
1000
500
0
5.00
10.00
15.00
20.00
25.00
30.00
35.00
40.00
45.00
50.00
55.00
60.00
65.00
Diffraction Angle [degrees 2theta]

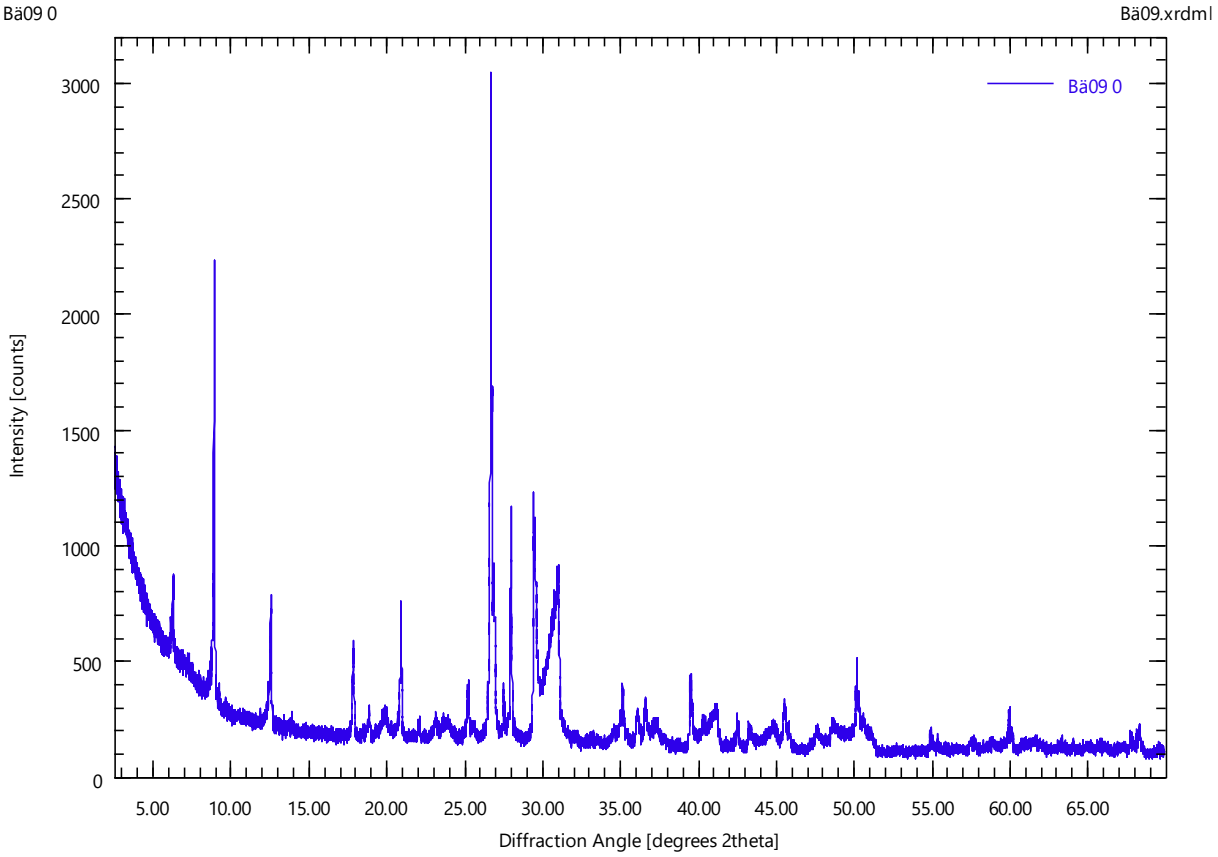
Bä09 0
Bä09.xrdml
Bä09 0
Intensity [counts]
Diffraction Angle [degrees 2theta]
0
500
1000
1500
2000
2500
3000
5.00
10.00
15.00
20.00
25.00
30.00
35.00
40.00
45.00
50.00
55.00
60.00
65.00

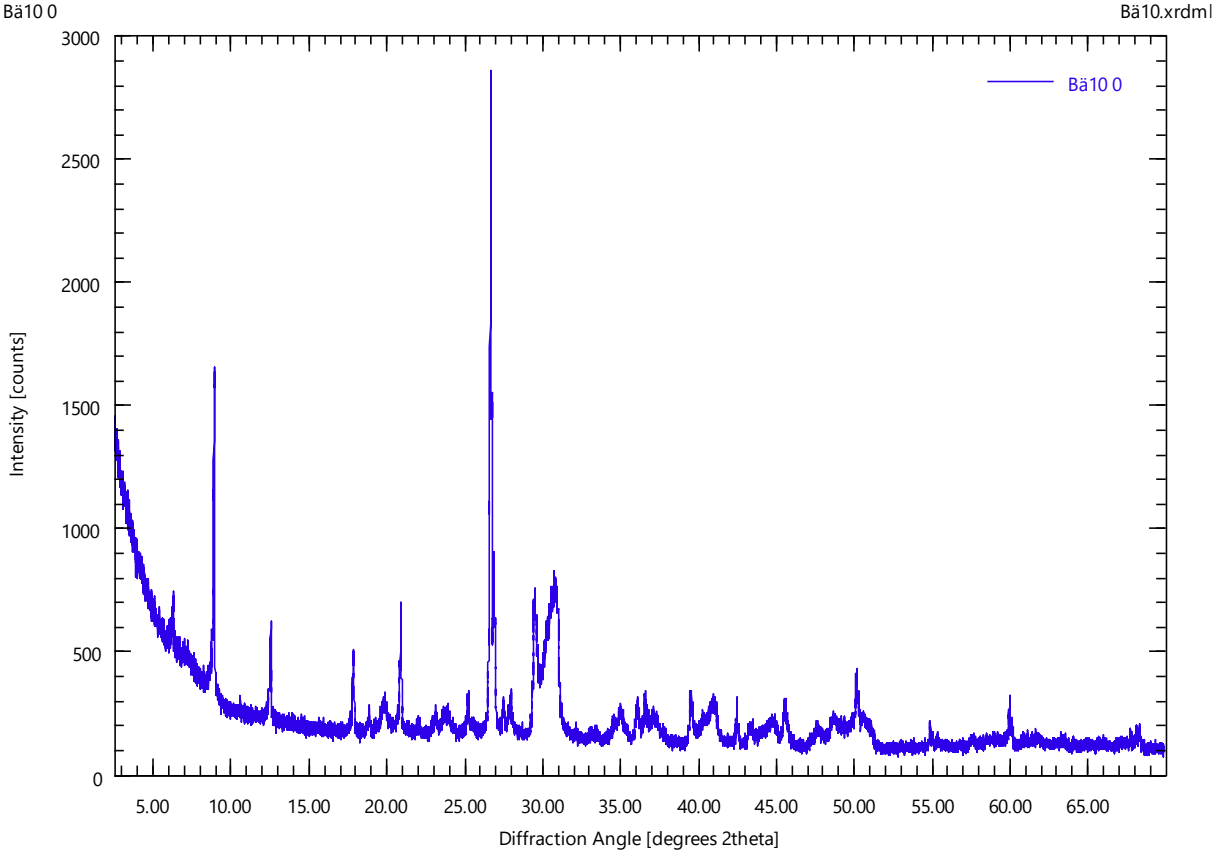
Bä10 0
Bä10.xrdml
Bä10 0
Intensity [counts]
Diffraction Angle [degrees 2theta]
0
500
1000
1500
2000
2500
3000
5.00
10.00
15.00
20.00
25.00
30.00
35.00
40.00
45.00
50.00
55.00
60.00
65.00

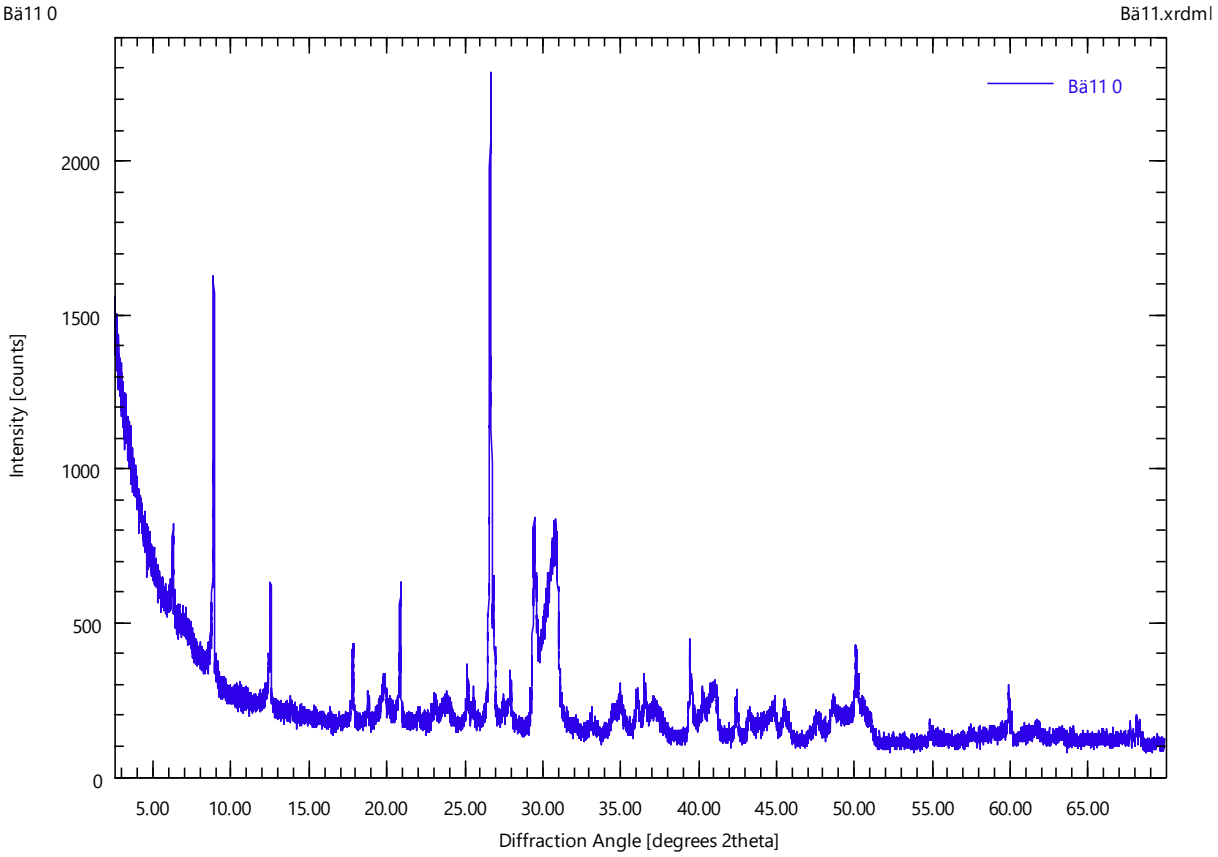
Bä11 0
Bä11.xrdml
Bä11 0
Intensity [counts]
0
500
1000
1500
2000
5.00
10.00
15.00
20.00
25.00
30.00
35.00
40.00
45.00
50.00
55.00
60.00
65.00
Diffraction Angle [degrees 2theta]

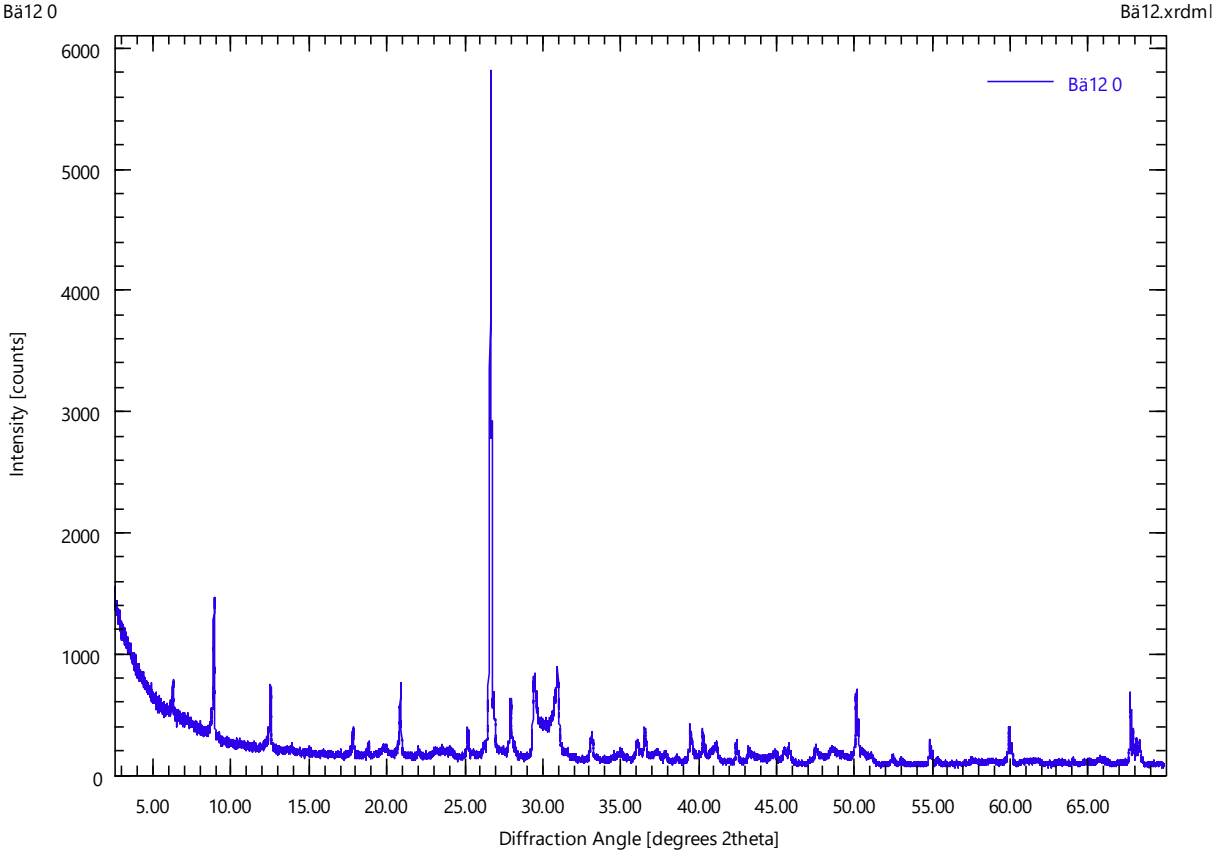
Bä12 0
Bä12.xrdml
Bä12 0
Intensity [counts]
0
1000
2000
3000
4000
5000
6000
5.00
10.00
15.00
20.00
25.00
30.00
35.00
40.00
45.00
50.00
55.00
60.00
65.00
Diffraction Angle [degrees 2theta]

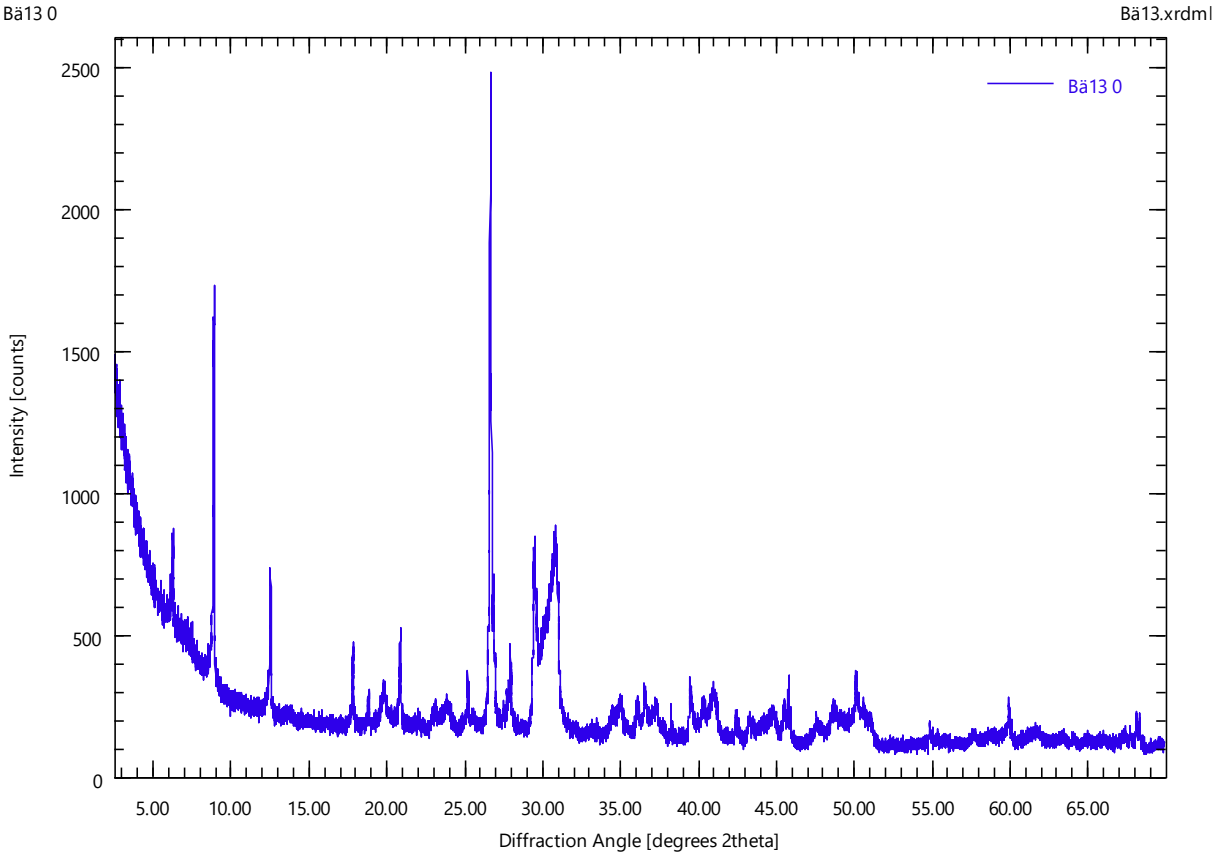
Bä13 0
Bä13.xrdml
Bä13 0
Intensity [counts]
Diffraction Angle [degrees 2theta]
0
500
1000
1500
2000
2500
5.00
10.00
15.00
20.00
25.00
30.00
35.00
40.00
45.00
50.00
55.00
60.00
65.00

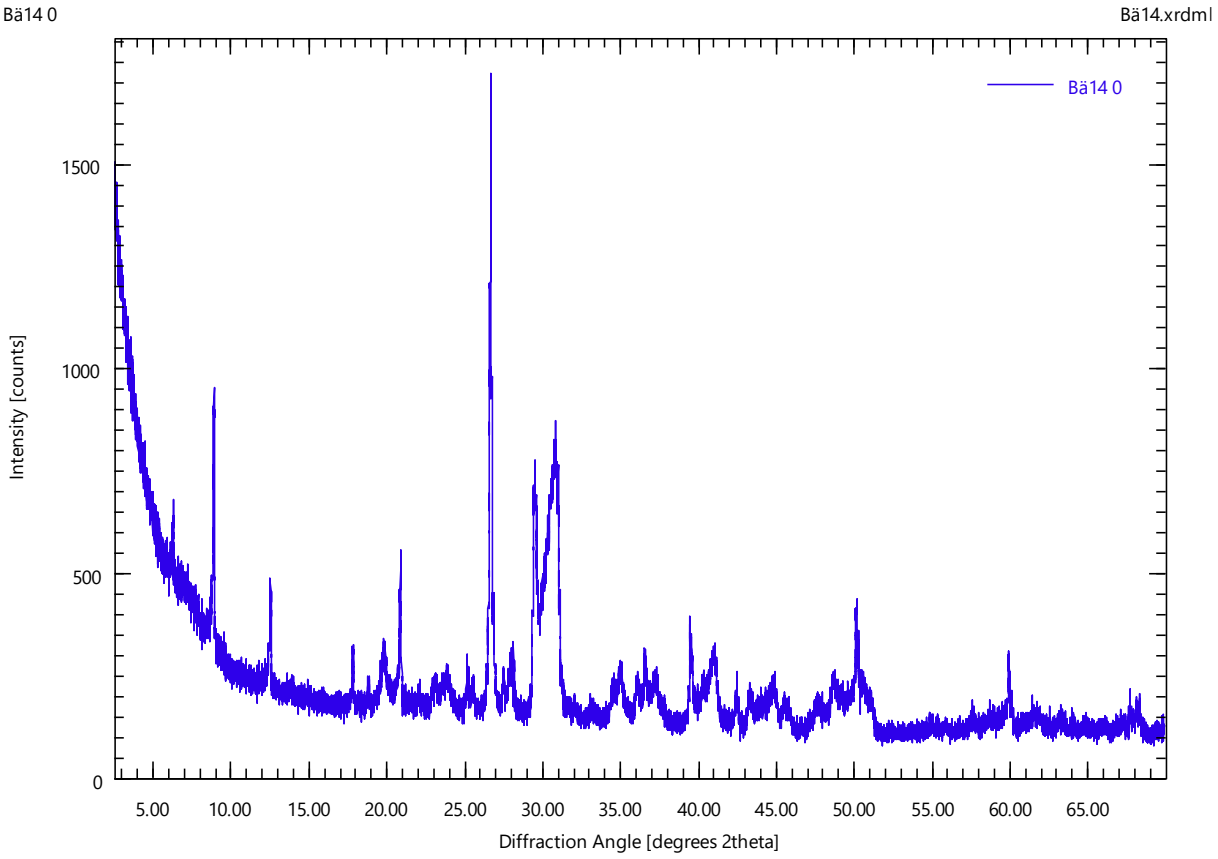
Bä14 0
Bä14.xrdml
Bä14 0
Intensity [counts]
Diffraction Angle [degrees 2theta]
0
500
1000
1500
5.00
10.00
15.00
20.00
25.00
30.00
35.00
40.00
45.00
50.00
55.00
60.00
65.00

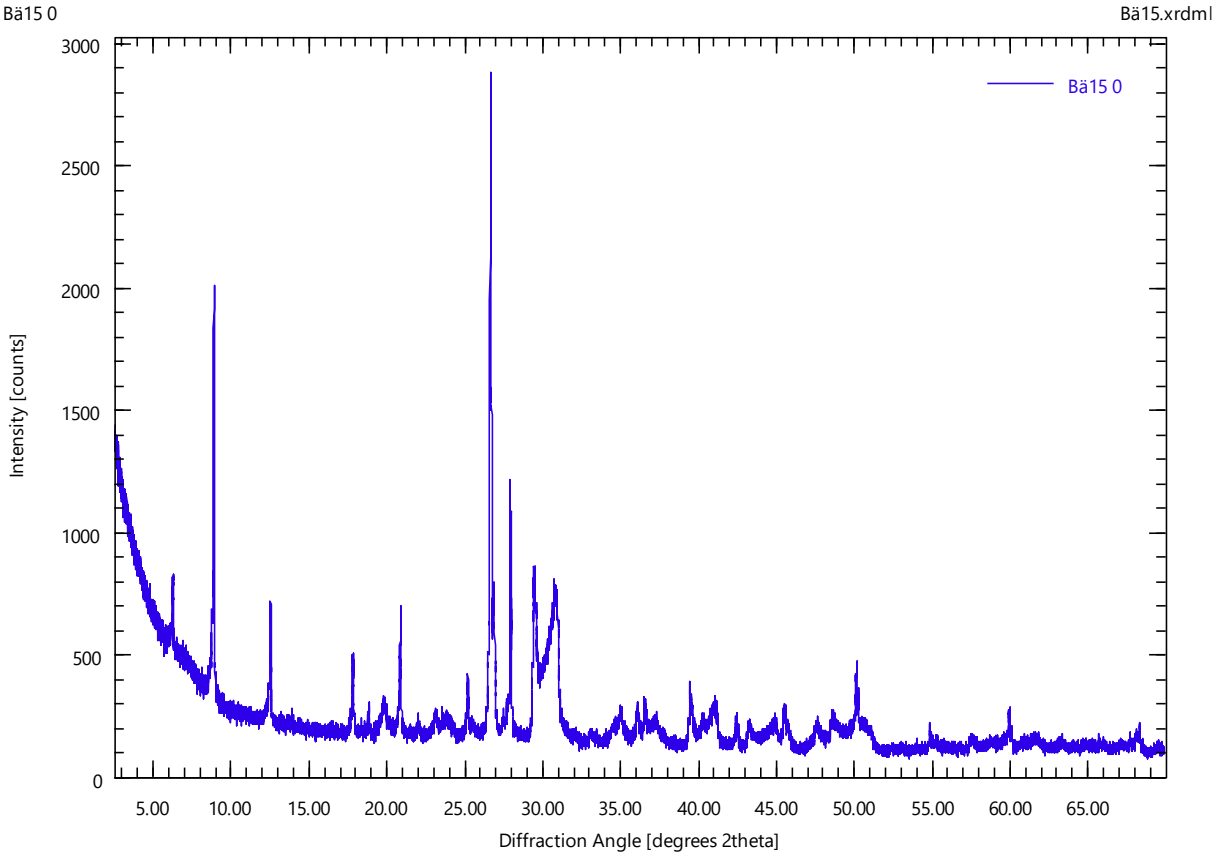
Bä15 0
Bä15.xrdml
Bä15 0
Intensity [counts]
3000
2500
2000
1500
1000
500
0
5.00
10.00
15.00
20.00
25.00
30.00
35.00
40.00
45.00
50.00
55.00
60.00
65.00
Diffraction Angle [degrees 2theta]

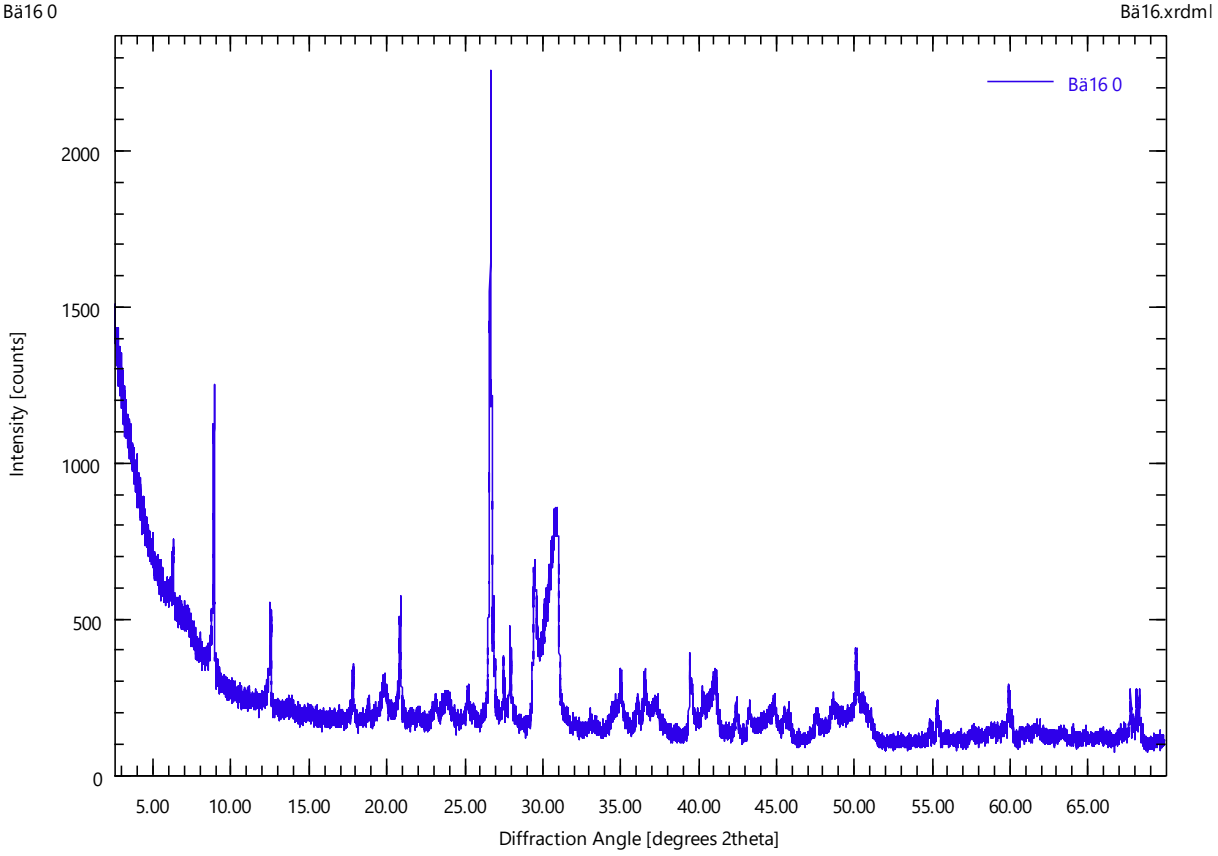
Bä16 0
Bä16.xrdml
Bä16 0
Intensity [counts]
2000
1500
1000
500
0
5.00
10.00
15.00
20.00
25.00
30.00
35.00
40.00
45.00
50.00
55.00
60.00
65.00
Diffraction Angle [degrees 2theta]

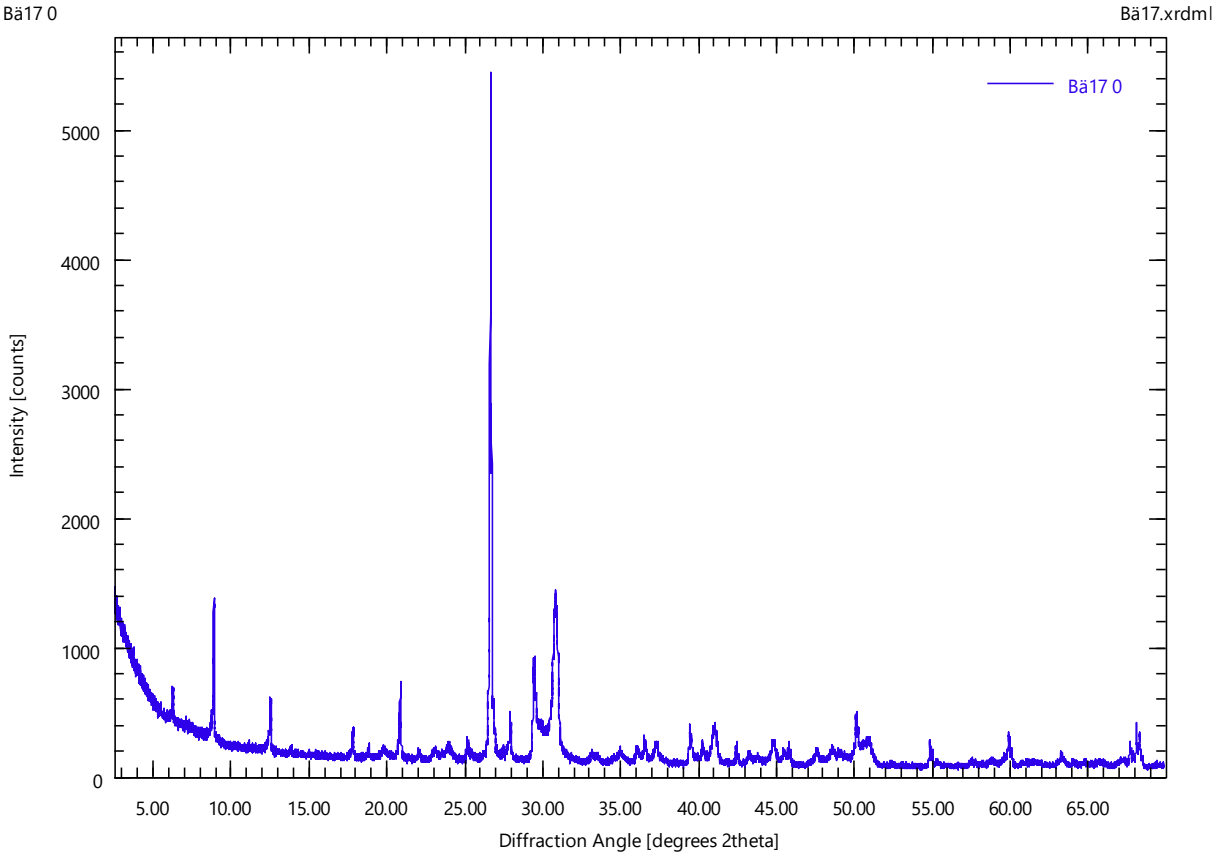
Bä17 0
Bä17.xrdml
Bä17 0
Intensity [counts]
0
1000
2000
3000
4000
5000
5.00
10.00
15.00
20.00
25.00
30.00
35.00
40.00
45.00
50.00
55.00
60.00
65.00
Diffraction Angle [degrees 2theta]

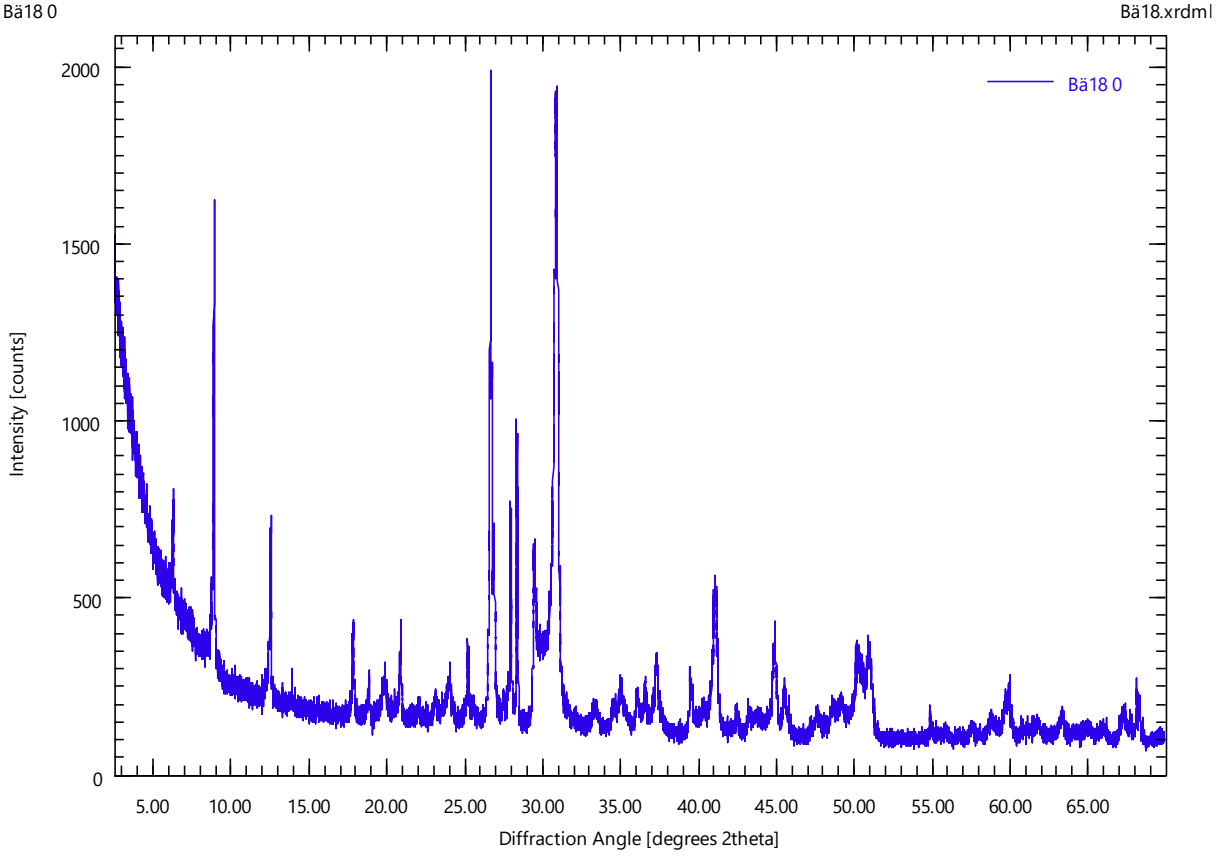
Bä18 0
Bä18.xrdml
Bä18 0
Intensity [counts]
0
500
1000
1500
2000
5.00
10.00
15.00
20.00
25.00
30.00
35.00
40.00
45.00
50.00
55.00
60.00
65.00
Diffraction Angle [degrees 2theta]

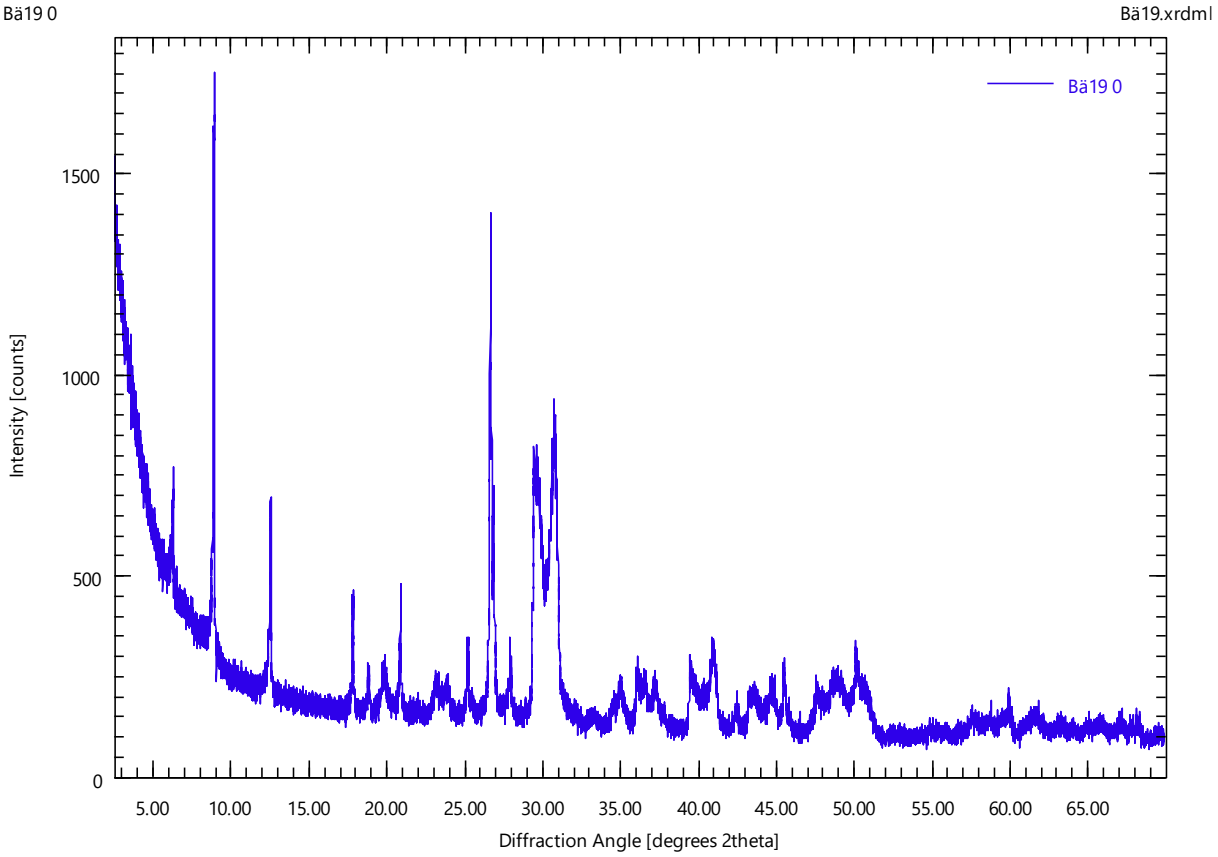
Bä19 0
Bä19.xrdml
Bä19 0
Intensity [counts]
0
500
1000
1500
5.00
10.00
15.00
20.00
25.00
30.00
35.00
40.00
45.00
50.00
55.00
60.00
65.00
Diffraction Angle [degrees 2theta]

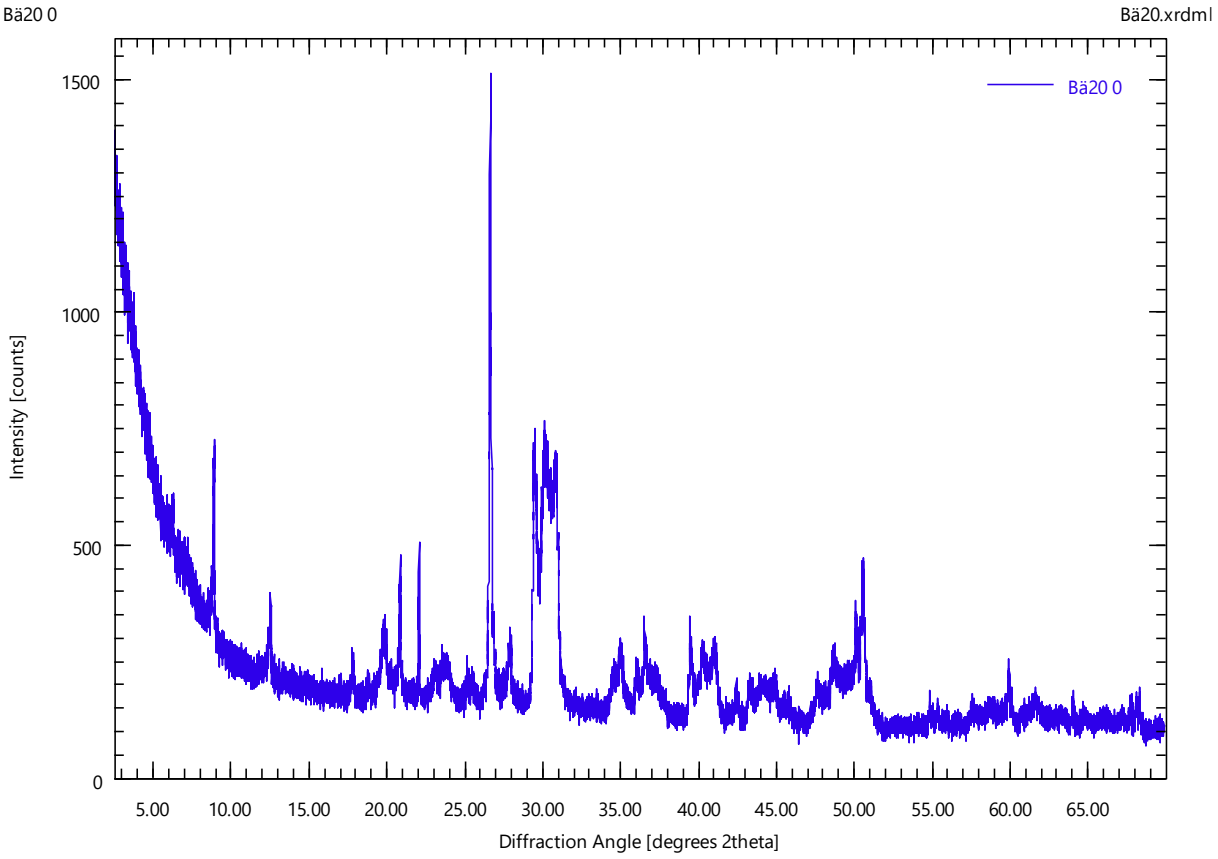
Bä20 0
Bä20.xrdml
Bä20 0
Intensity [counts]
0
500
1000
1500
5.00
10.00
15.00
20.00
25.00
30.00
35.00
40.00
45.00
50.00
55.00
60.00
65.00
Diffraction Angle [degrees 2theta]

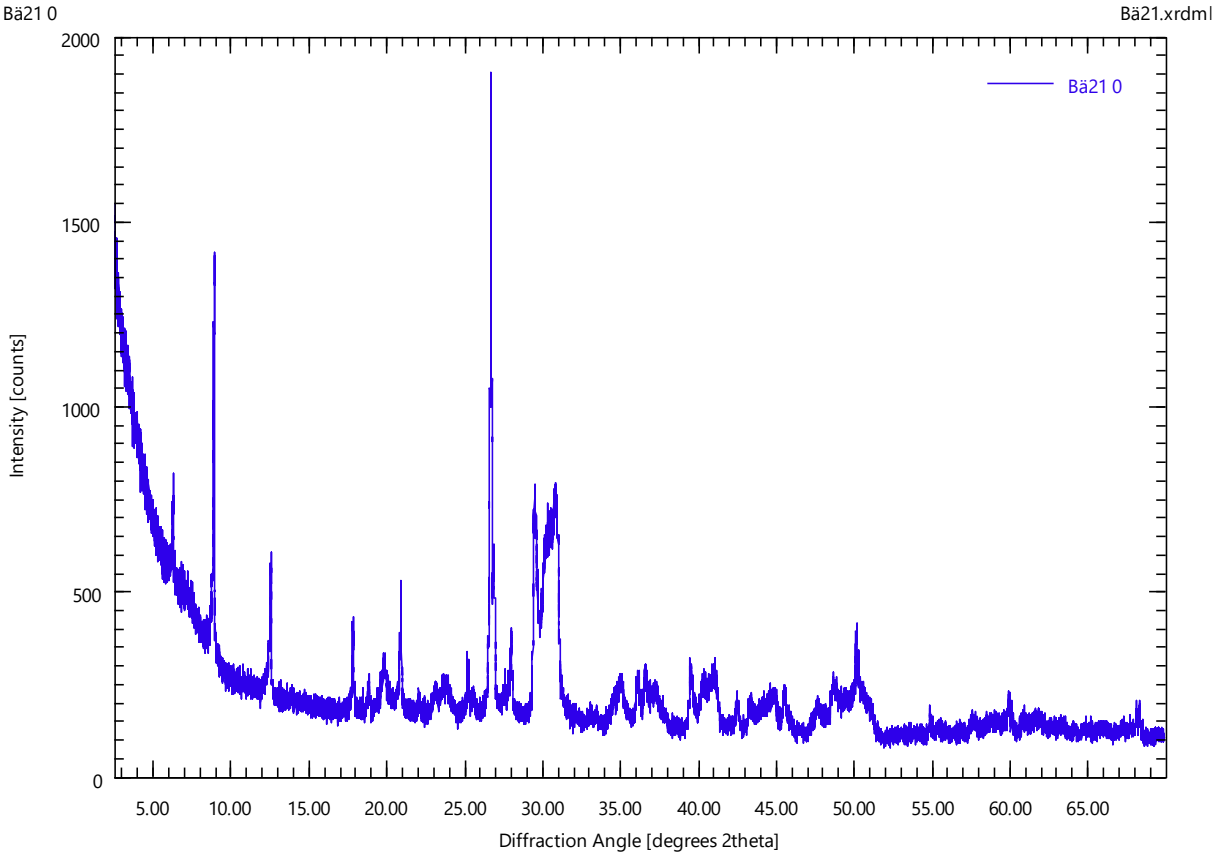
Bä21 0
Bä21.xrdml
Bä21 0
Intensity [counts]
2000
1500
1000
500
0
5.00
10.00
15.00
20.00
25.00
30.00
35.00
40.00
45.00
50.00
55.00
60.00
65.00
Diffraction Angle [degrees 2theta]

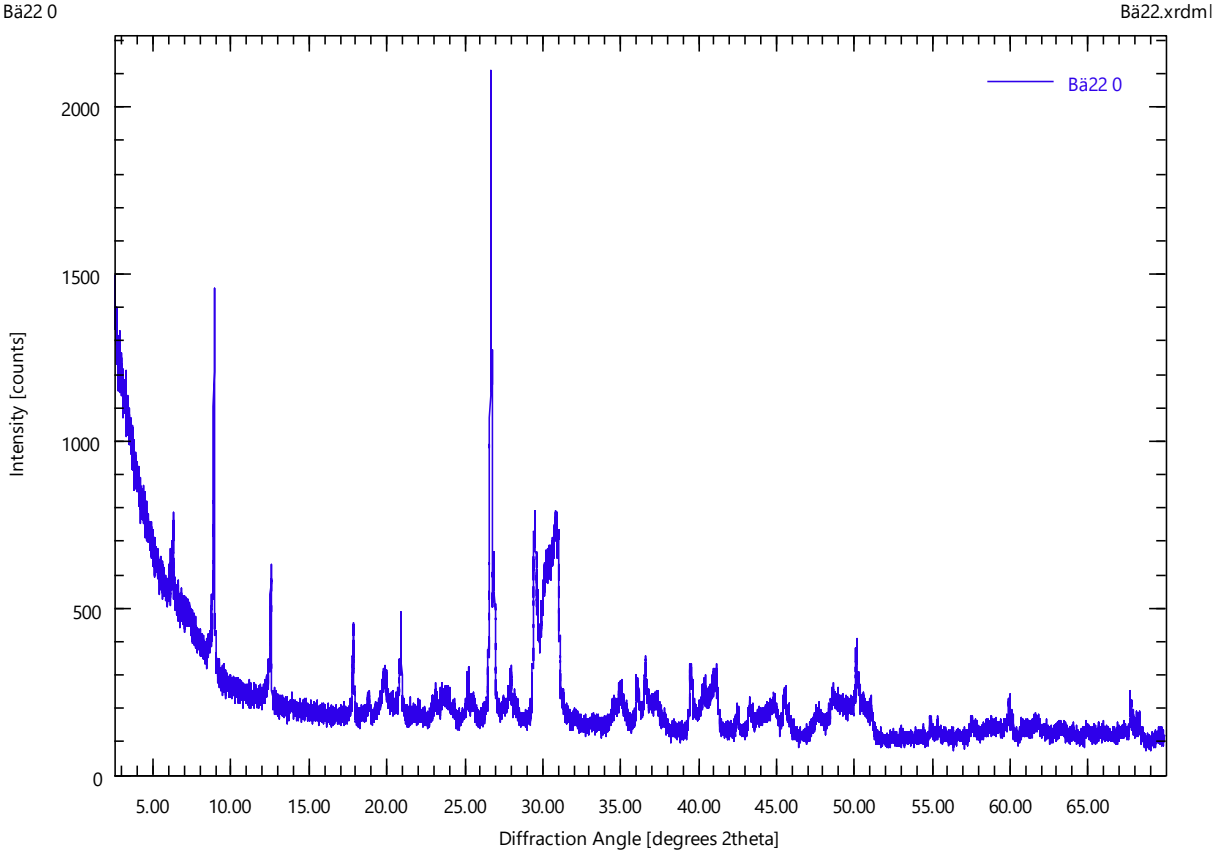
Bä22 0
Bä22.xrdml
Bä22 0
Intensity [counts]
2000
1500
1000
500
0
5.00
10.00
15.00
20.00
25.00
30.00
35.00
40.00
45.00
50.00
55.00
60.00
65.00
Diffraction Angle [degrees 2theta]

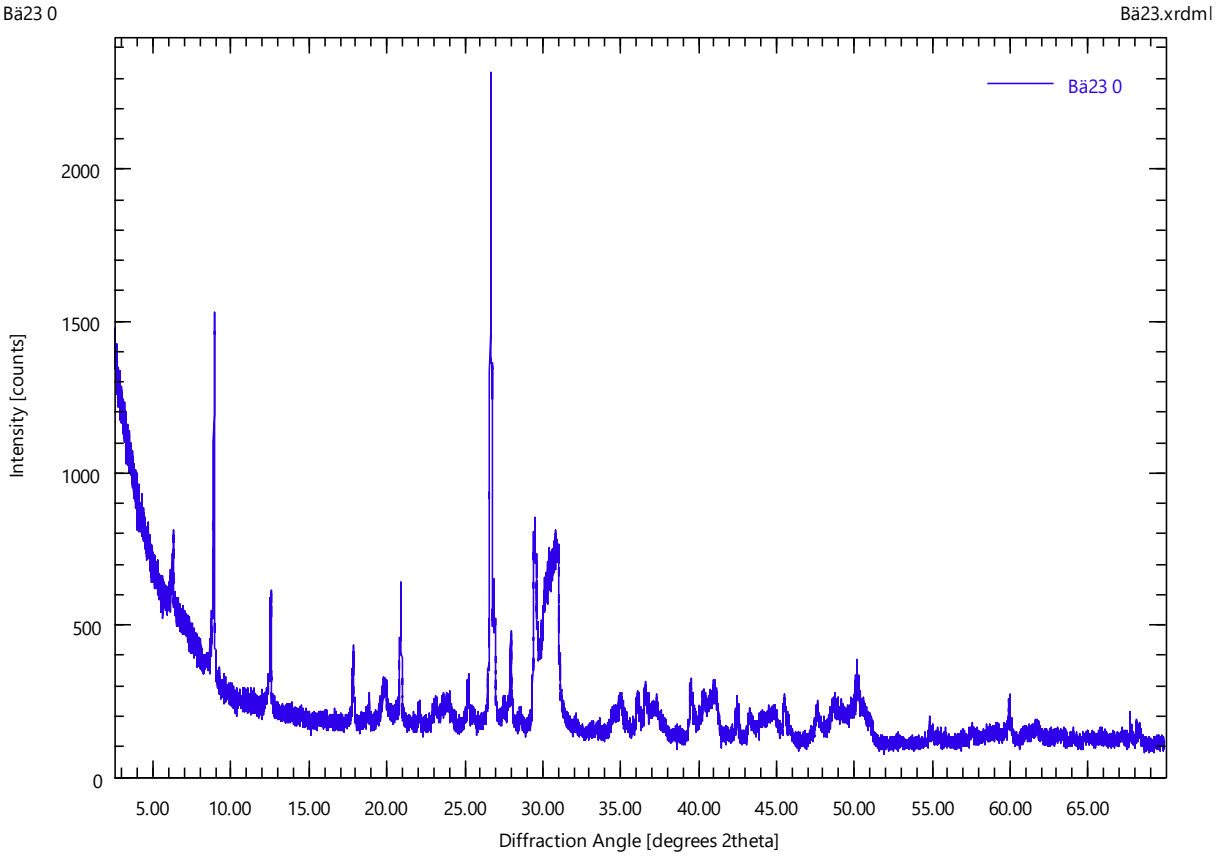
Bä23 0
Bä23.xrdml
Bä23 0
Intensity [counts]
0
500
1000
1500
2000
5.00
10.00
15.00
20.00
25.00
30.00
35.00
40.00
45.00
50.00
55.00
60.00
65.00
Diffraction Angle [degrees 2theta]

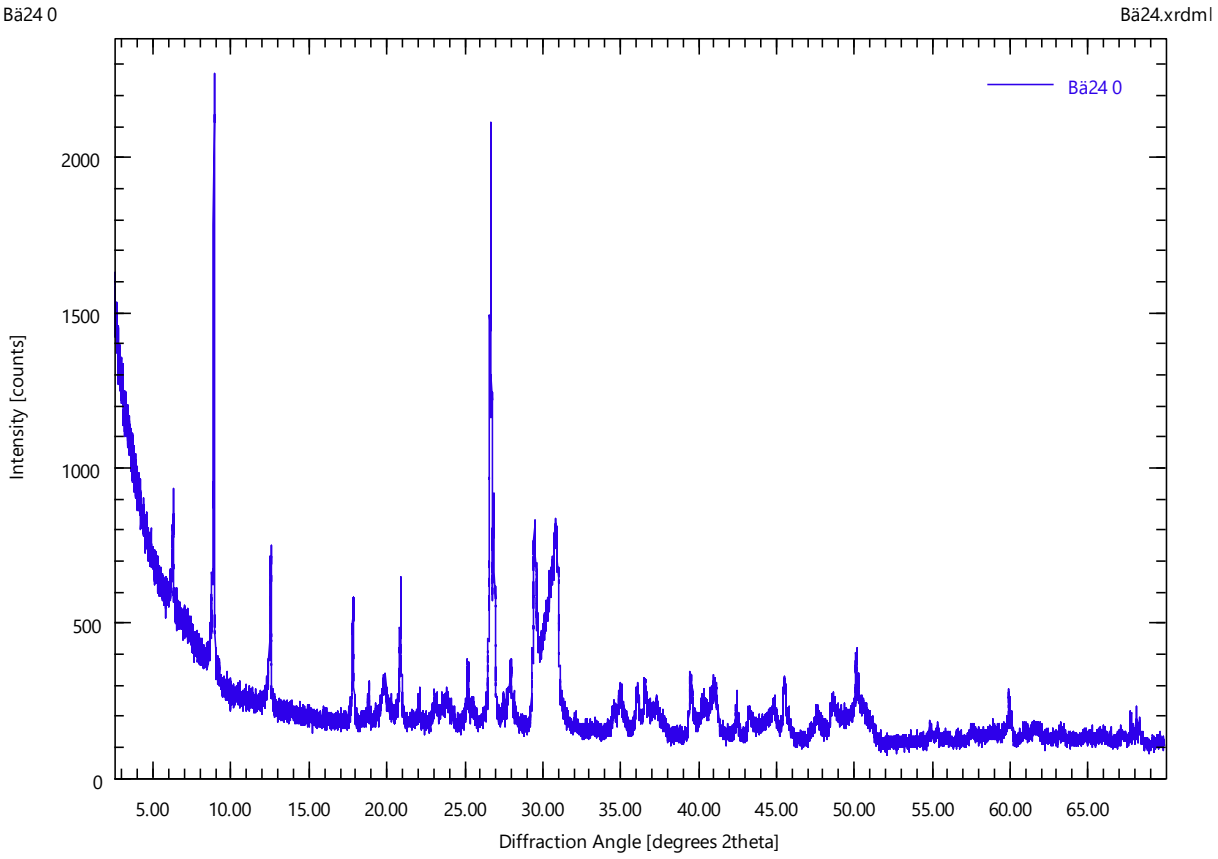
Bä24 0
Bä24.xrdml
Bä24 0
Intensity [counts]
0
500
1000
1500
2000
5.00
10.00
15.00
20.00
25.00
30.00
35.00
40.00
45.00
50.00
55.00
60.00
65.00
Diffraction Angle [degrees 2theta]

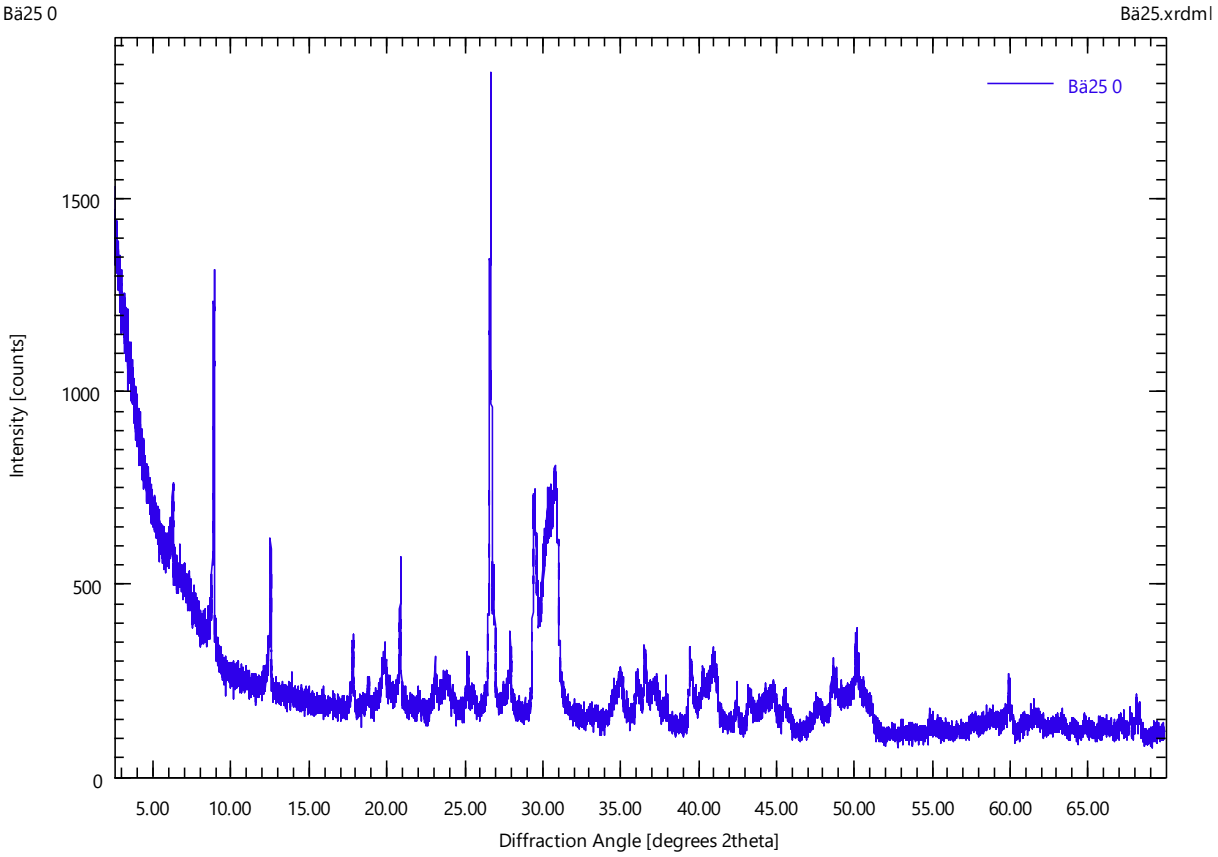
Bä25 0
Bä25.xrdml
Bä25 0
Intensity [counts]
0
500
1000
1500
5.00
10.00
15.00
20.00
25.00
30.00
35.00
40.00
45.00
50.00
55.00
60.00
65.00
Diffraction Angle [degrees 2theta]

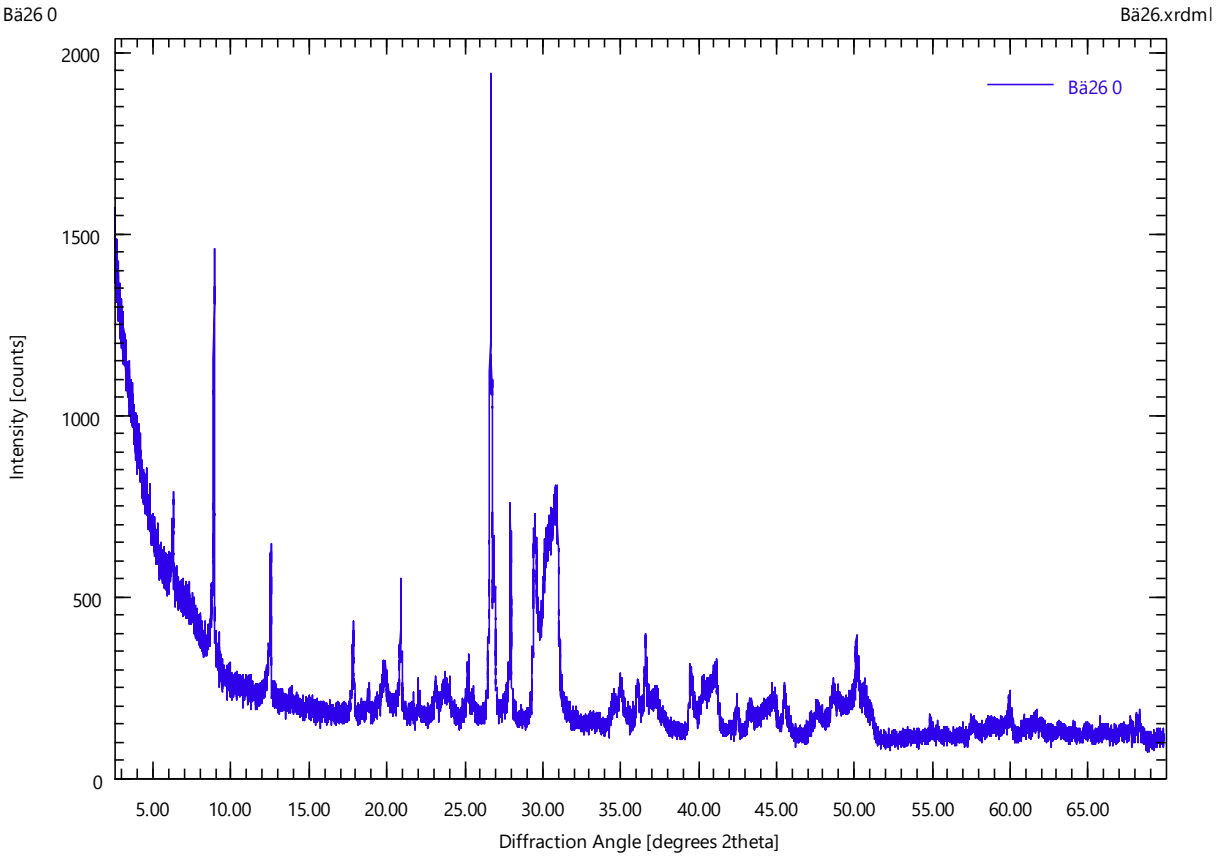
Bä26 0
Bä26.xrdml
Bä26 0
Intensity [counts]
0
500
1000
1500
2000
5.00
10.00
15.00
20.00
25.00
30.00
35.00
40.00
45.00
50.00
55.00
60.00
65.00
Diffraction Angle [degrees 2theta]

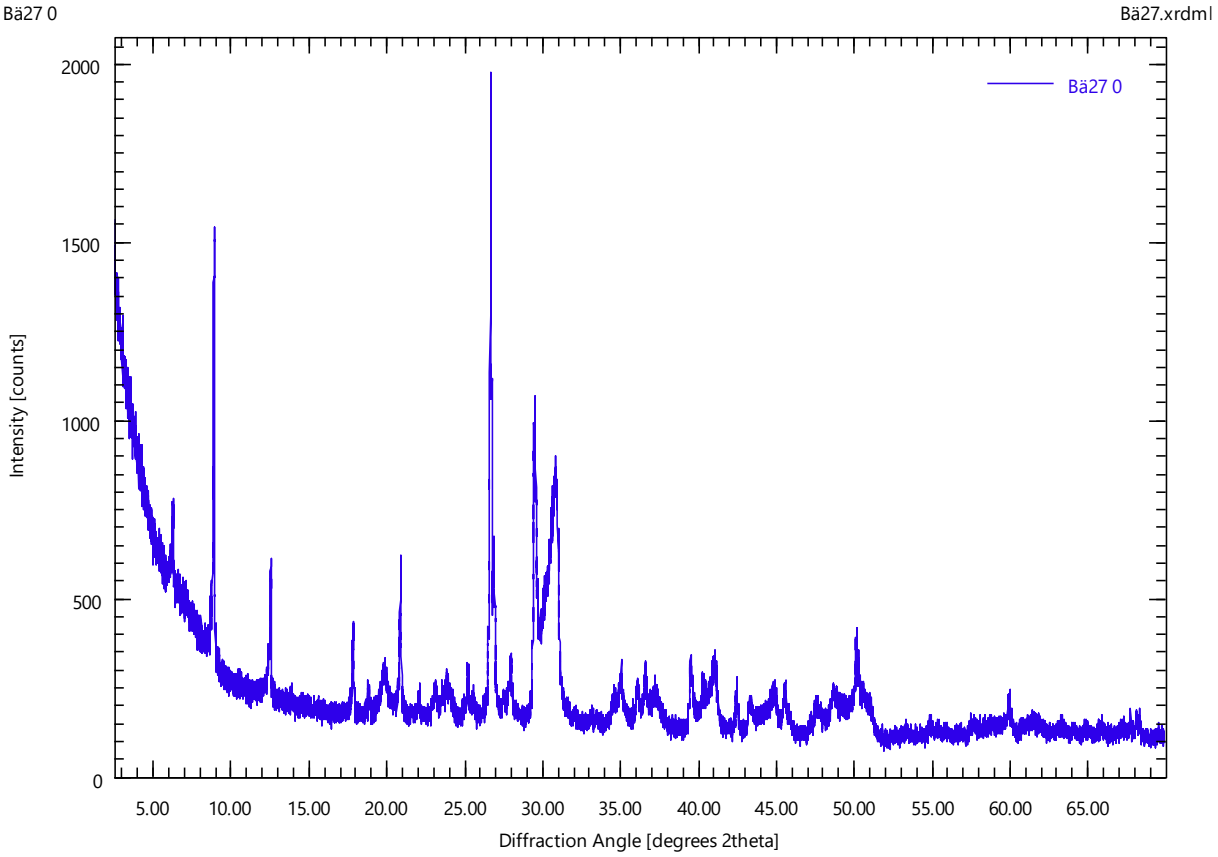
Bä27 0
Bä27.xrdml
Bä27 0
Intensity [counts]
2000
1500
1000
500
0
5.00
10.00
15.00
20.00
25.00
30.00
35.00
40.00
45.00
50.00
55.00
60.00
65.00
Diffraction Angle [degrees 2theta]

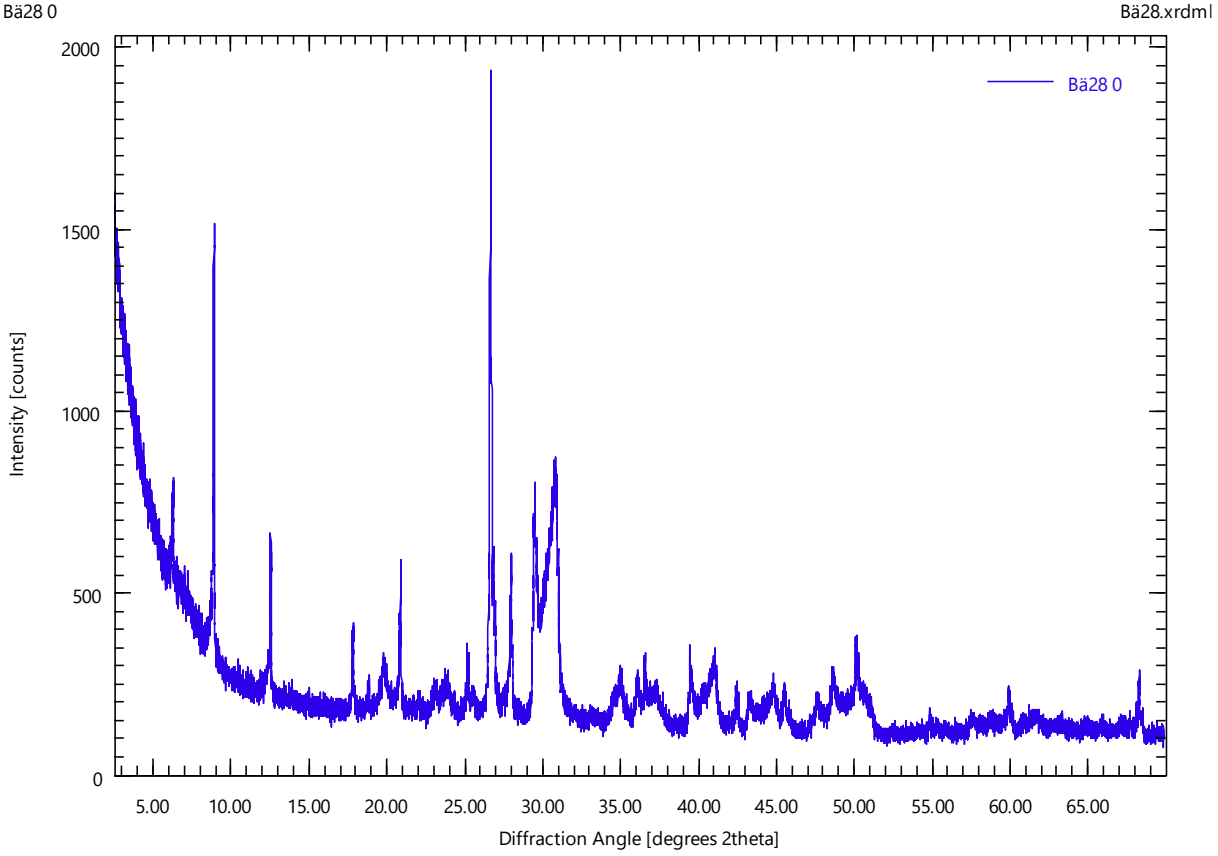
Bä28 0
Bä28.xrdml
Bä28 0
Intensity [counts]
2000
1500
1000
500
0
5.00
10.00
15.00
20.00
25.00
30.00
35.00
40.00
45.00
50.00
55.00
60.00
65.00
Diffraction Angle [degrees 2theta]

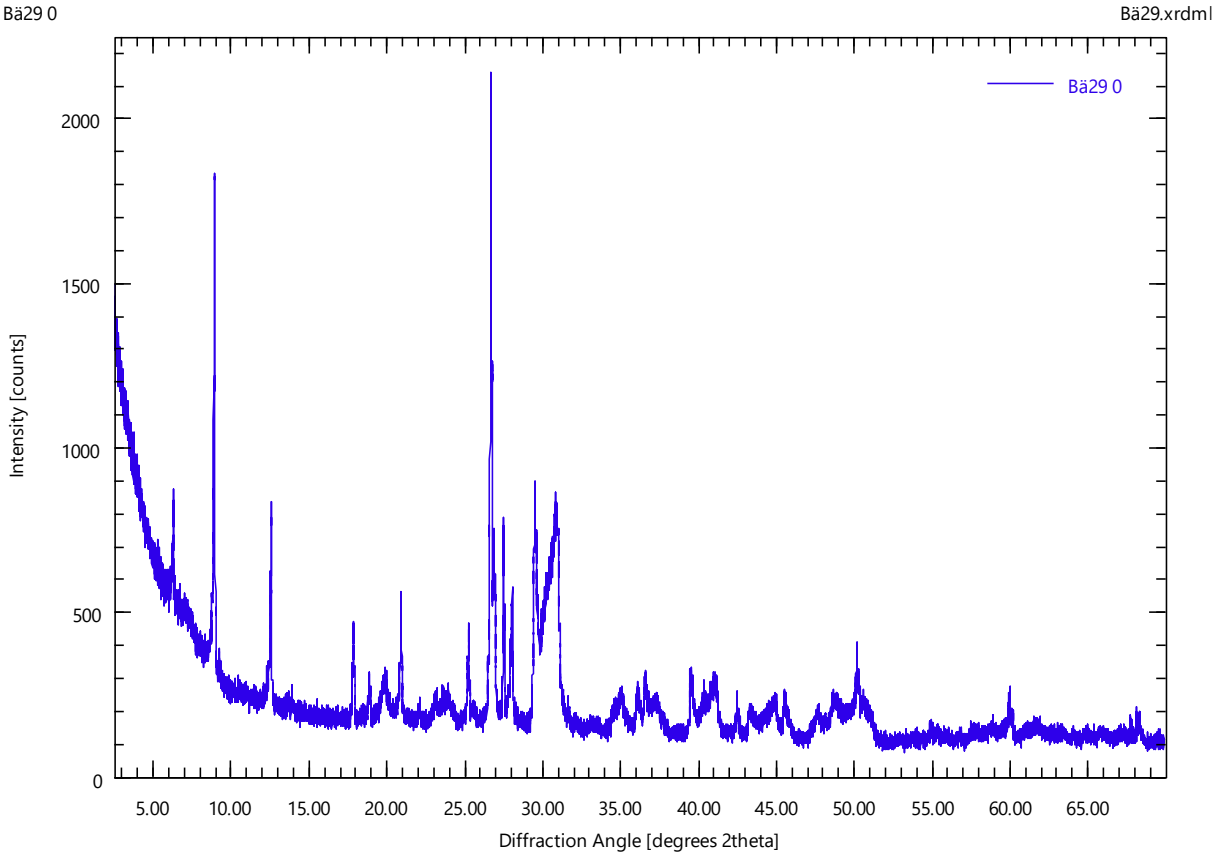
Bä29 0
Bä29.xrdml
Bä29 0
Intensity [counts]
0
500
1000
1500
2000
5.00
10.00
15.00
20.00
25.00
30.00
35.00
40.00
45.00
50.00
55.00
60.00
65.00
Diffraction Angle [degrees 2theta]

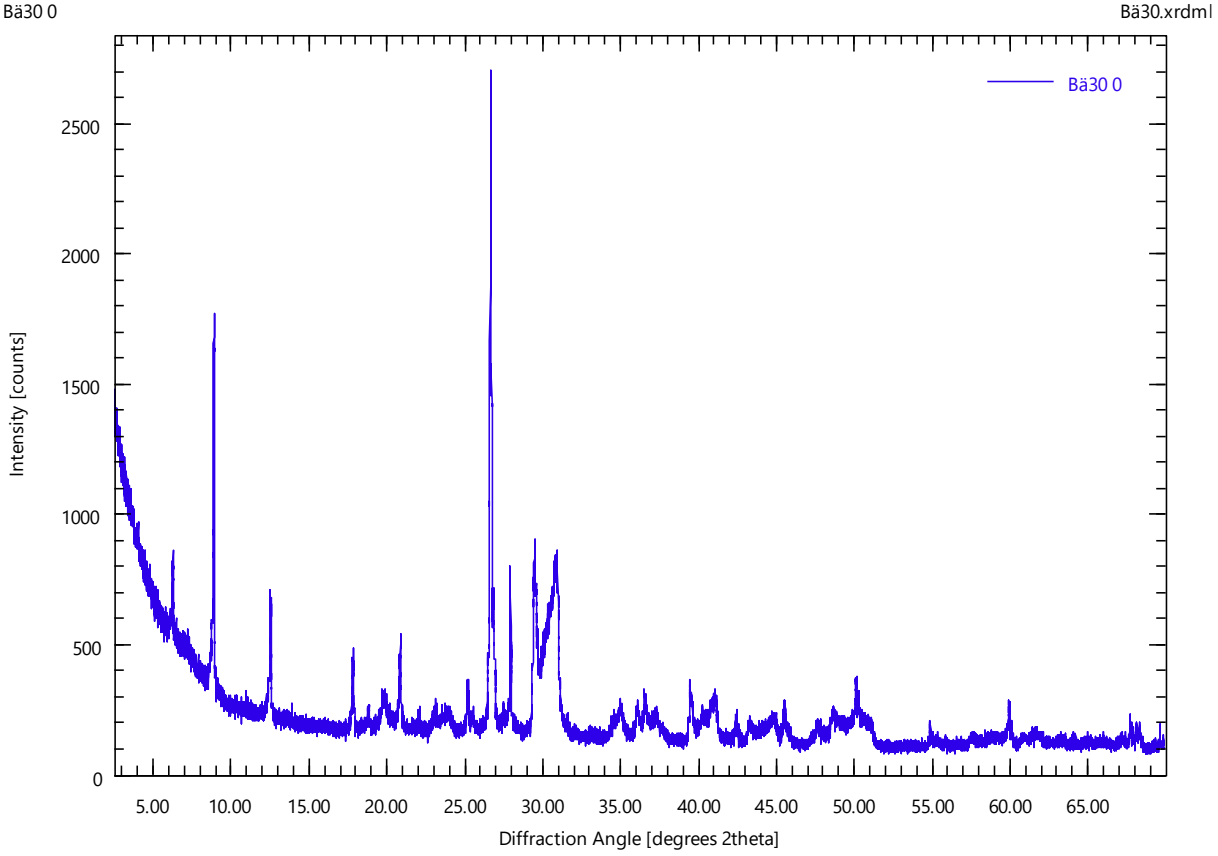
Bä30 0
Bä30.xrdml
Bä30 0
Intensity [counts]
0
500
1000
1500
2000
2500
5.00
10.00
15.00
20.00
25.00
30.00
35.00
40.00
45.00
50.00
55.00
60.00
65.00
Diffraction Angle [degrees 2theta]

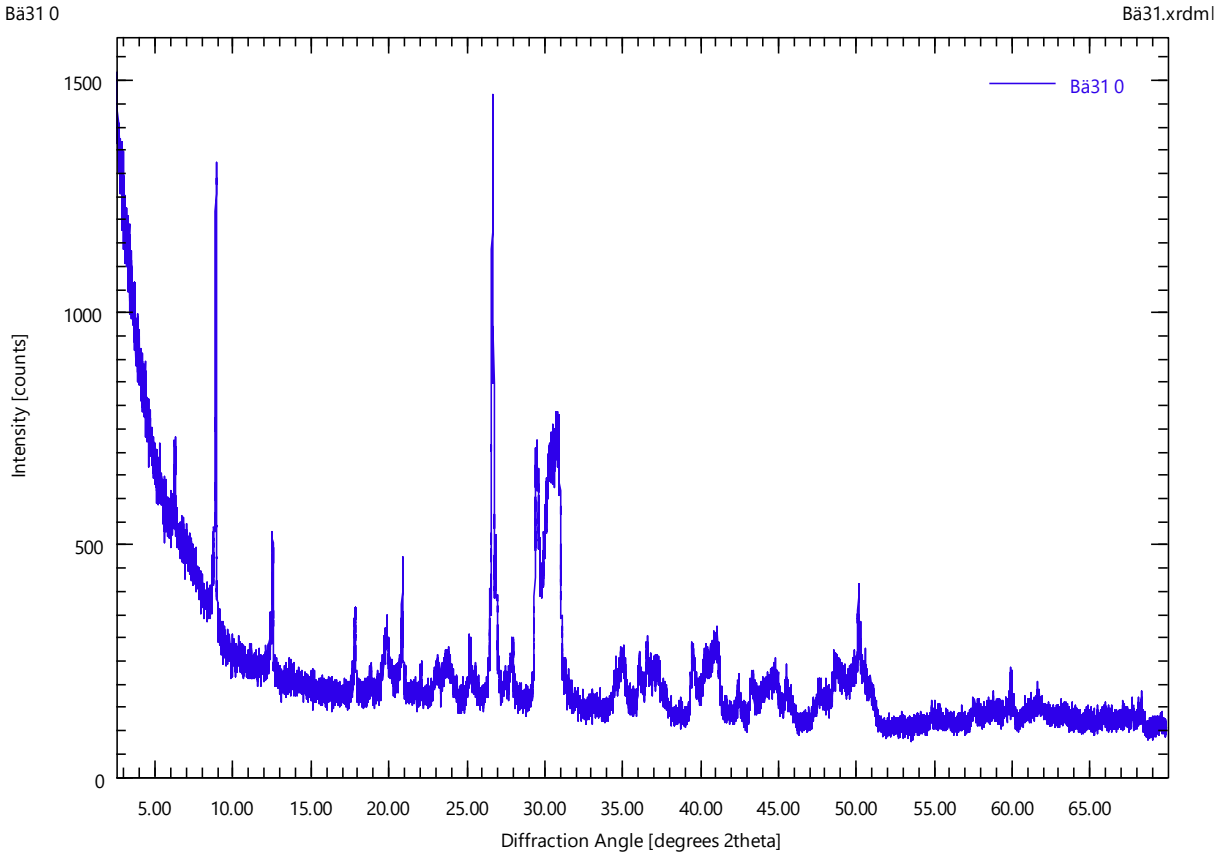
Bä31 0
Bä31.xrdml
Bä31 0
Intensity [counts]
1500
1000
500
0
5.00
10.00
15.00
20.00
25.00
30.00
35.00
40.00
45.00
50.00
55.00
60.00
65.00
Diffraction Angle [degrees 2theta]

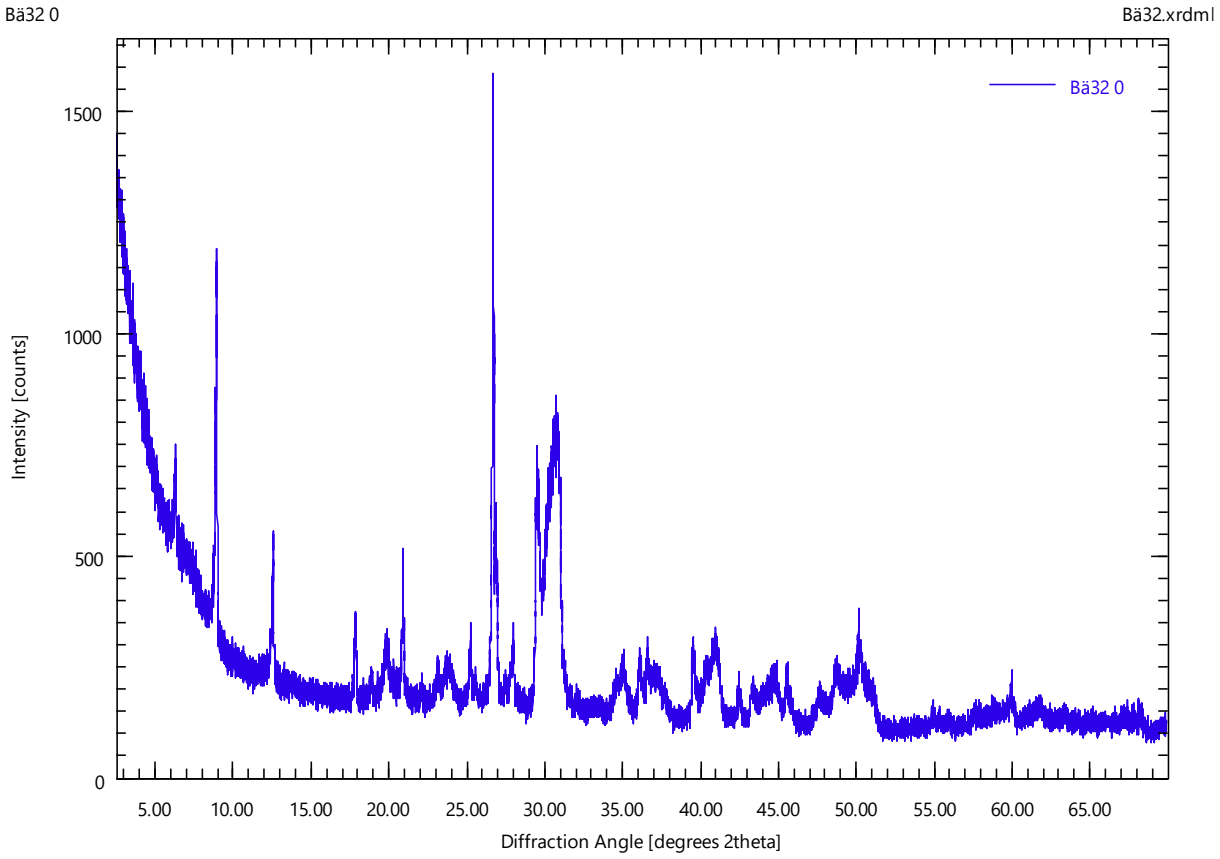
Bä32 0
Bä32.xrdml
Bä32 0
Intensity [counts]
1500
1000
500
0
5.00
10.00
15.00
20.00
25.00
30.00
35.00
40.00
45.00
50.00
55.00
60.00
65.00
Diffraction Angle [degrees 2theta]

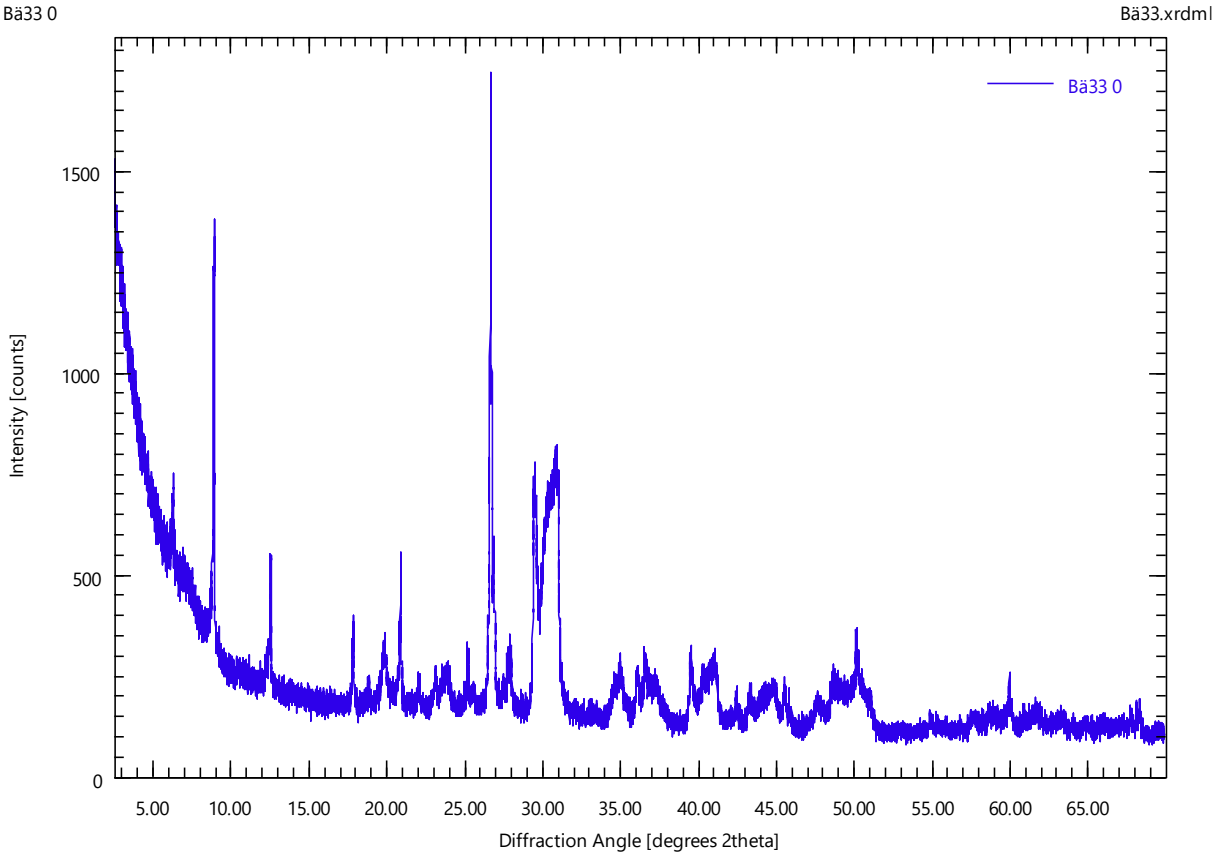
Bä33 0
Bä33.xrdml
Bä33 0
Intensity [counts]
0
500
1000
1500
5.00
10.00
15.00
20.00
25.00
30.00
35.00
40.00
45.00
50.00
55.00
60.00
65.00
Diffraction Angle [degrees 2theta]

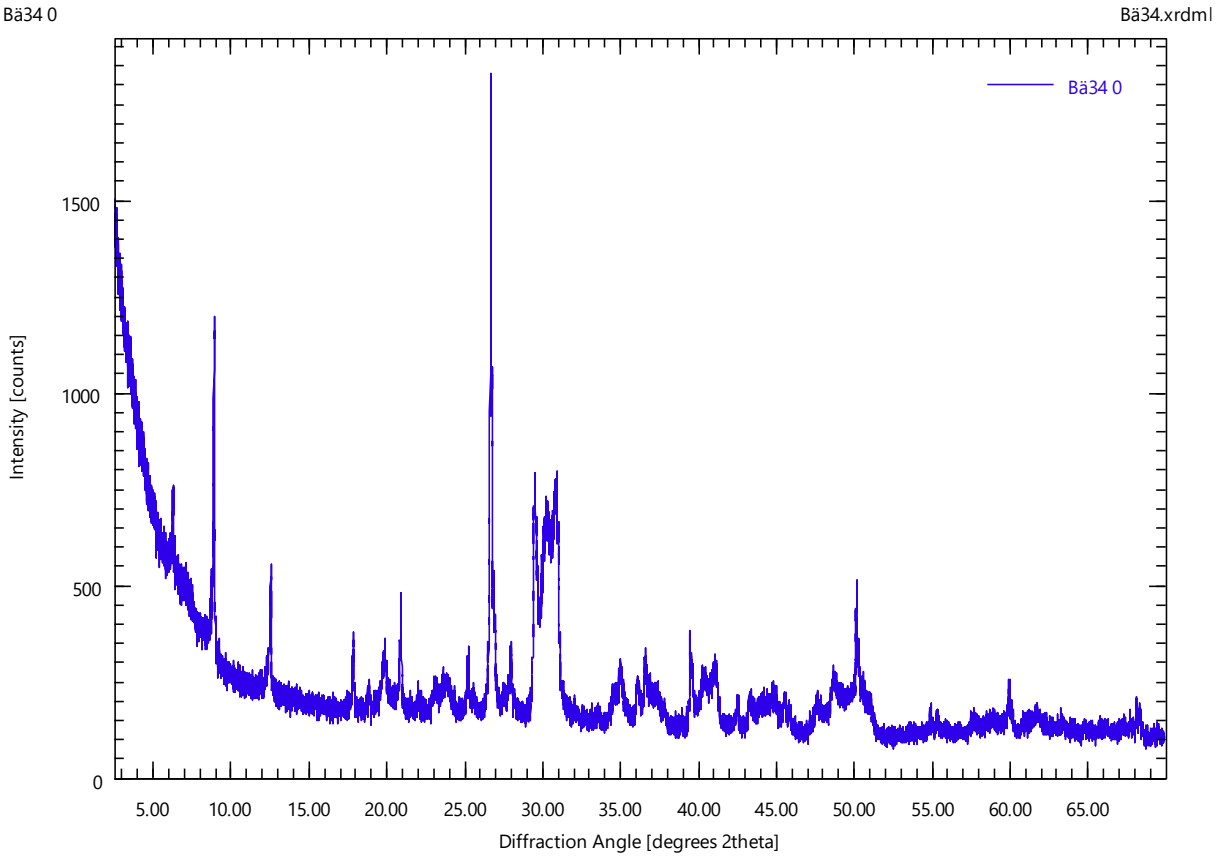
Bä34 0
Bä34.xrdml
Bä34 0
Intensity [counts]
0
500
1000
1500
5.00
10.00
15.00
20.00
25.00
30.00
35.00
40.00
45.00
50.00
55.00
60.00
65.00
Diffraction Angle [degrees 2theta]

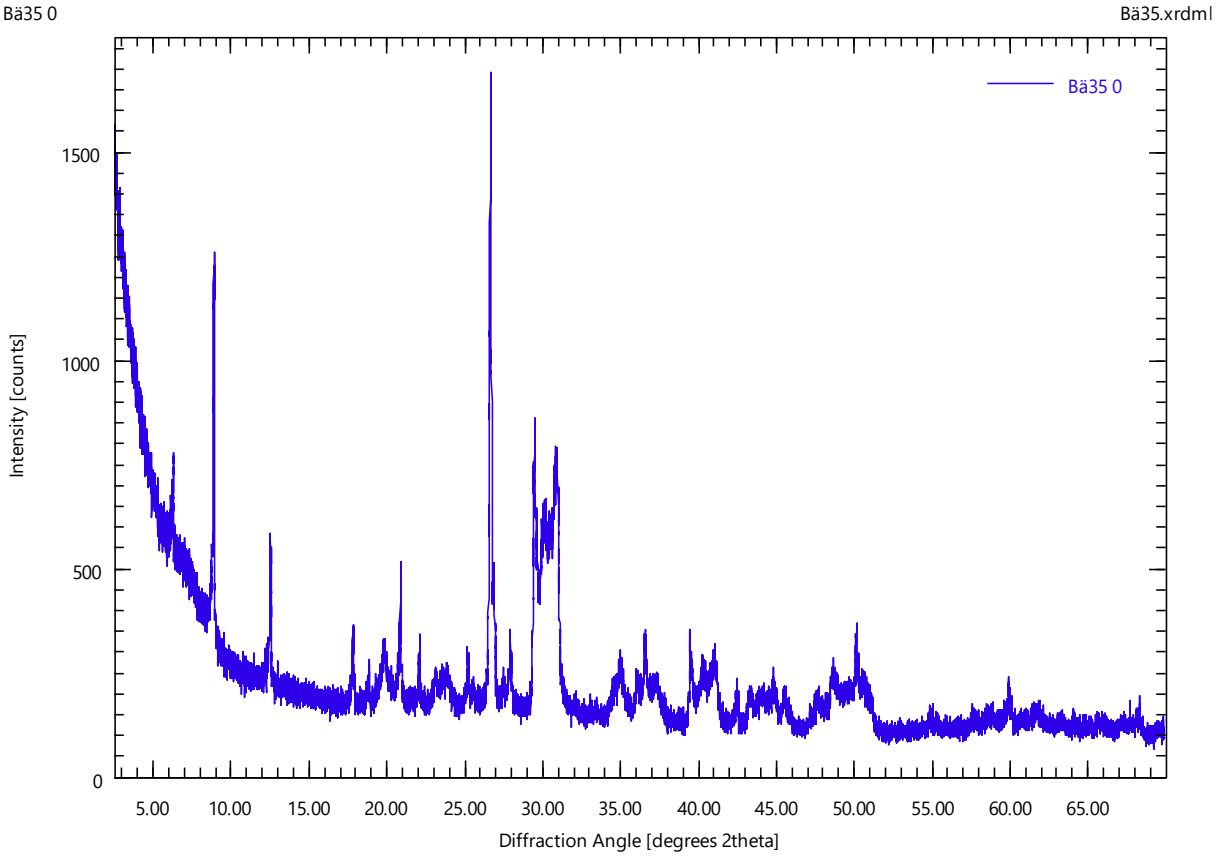
Bä35 0
Bä35.xrdml
Bä35 0
Intensity [counts]
0
500
1000
1500
5.00
10.00
15.00
20.00
25.00
30.00
35.00
40.00
45.00
50.00
55.00
60.00
65.00
Diffraction Angle [degrees 2theta]

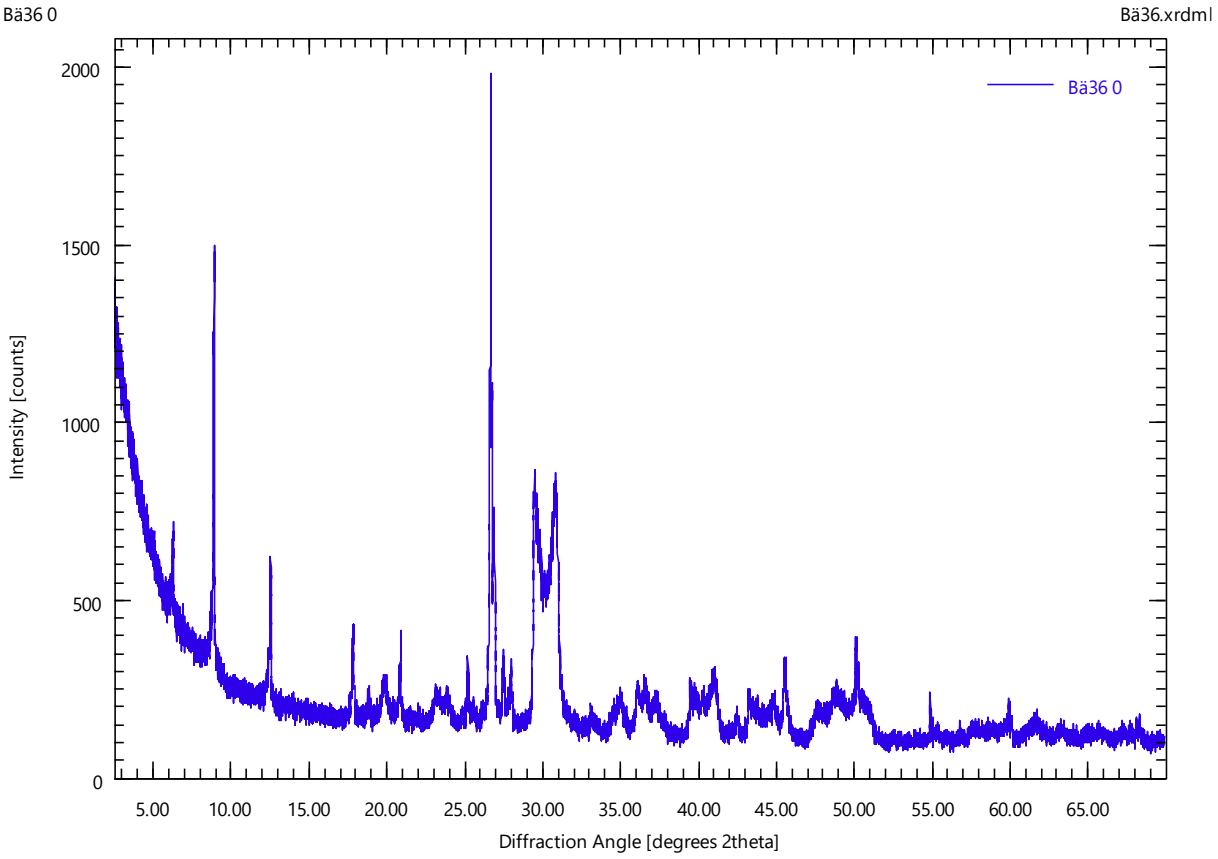
Bä36 0
Bä36.xrdml
Bä36 0
Intensity [counts]
0
500
1000
1500
2000
5.00
10.00
15.00
20.00
25.00
30.00
35.00
40.00
45.00
50.00
55.00
60.00
65.00
Diffraction Angle [degrees 2theta]

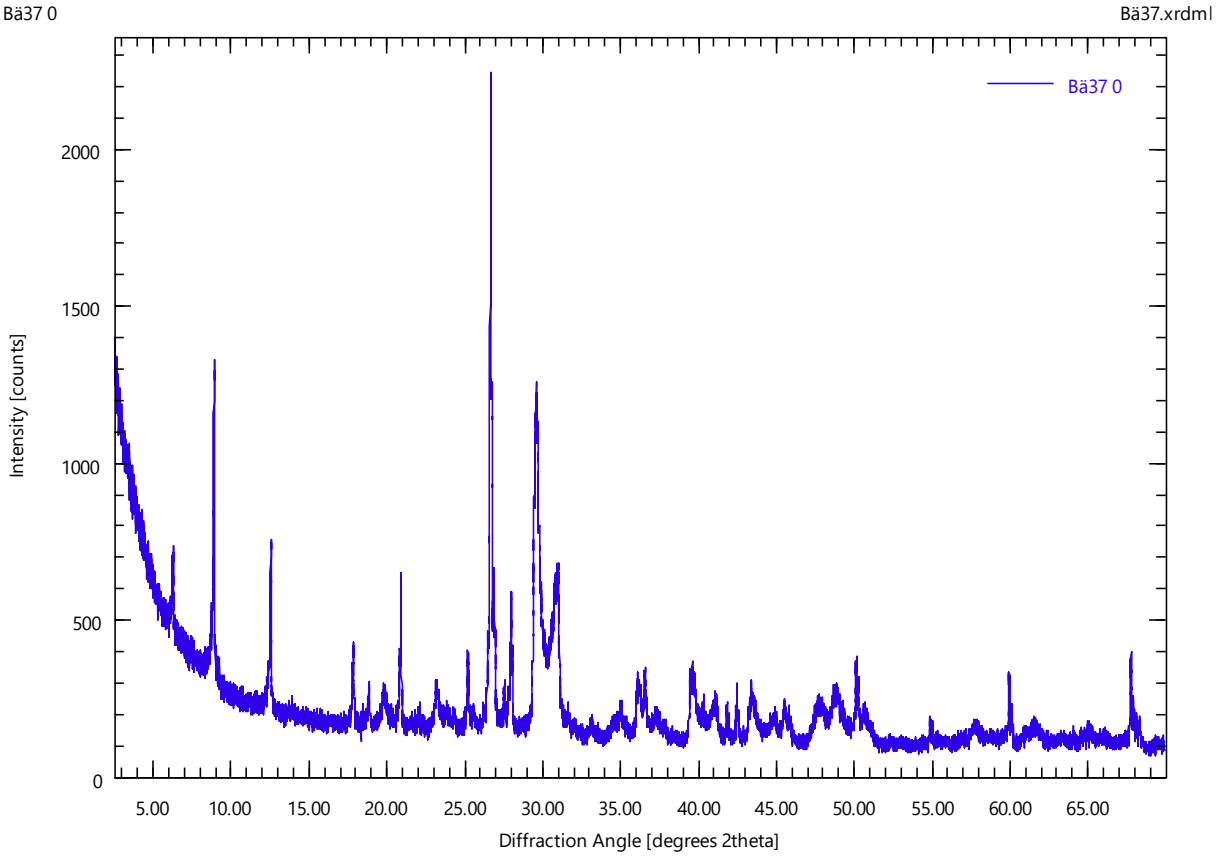
Bä37 0
Bä37.xrdml
Bä37 0
Intensity [counts]
0
500
1000
1500
2000
5.00
10.00
15.00
20.00
25.00
30.00
35.00
40.00
45.00
50.00
55.00
60.00
65.00
Diffraction Angle [degrees 2theta]

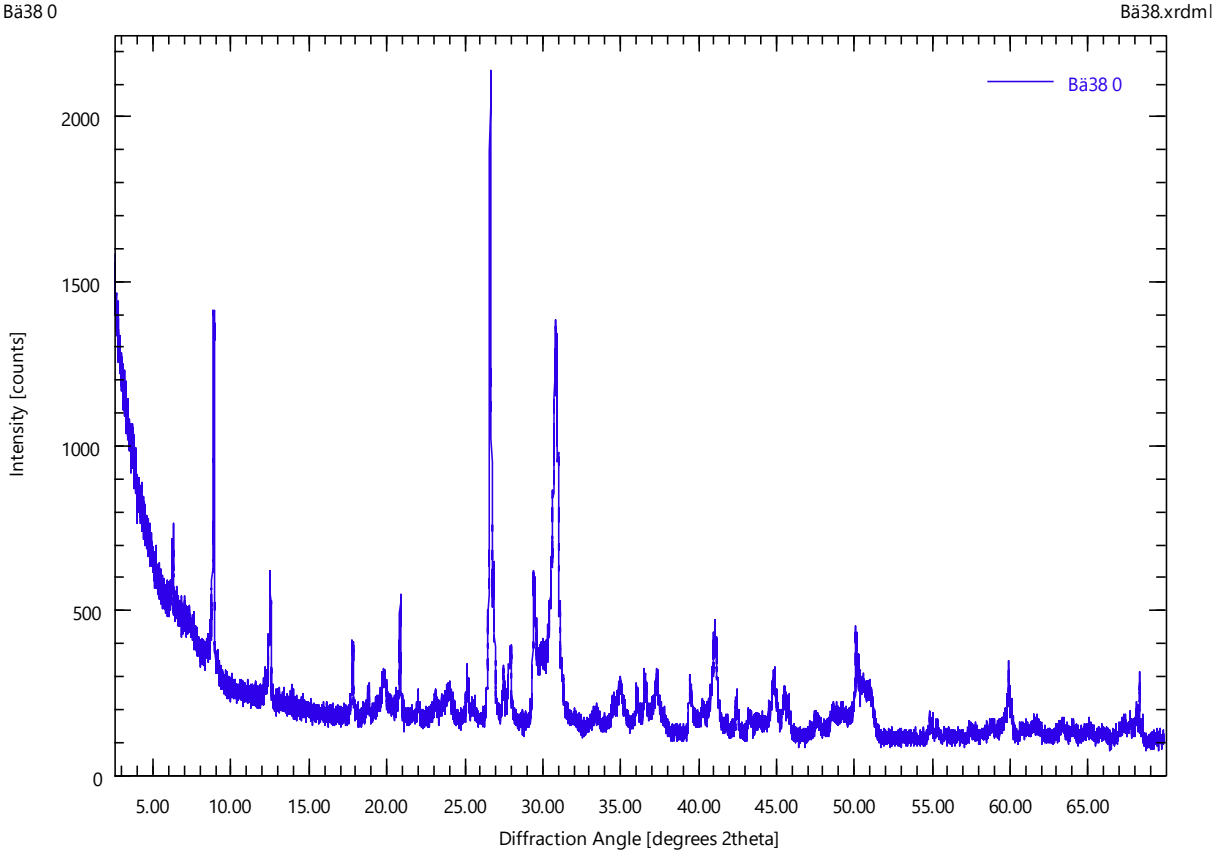
Bä38 0
Bä38.xrdml
Bä38 0
Intensity [counts]
0
500
1000
1500
2000
5.00
10.00
15.00
20.00
25.00
30.00
35.00
40.00
45.00
50.00
55.00
60.00
65.00
Diffraction Angle [degrees 2theta]

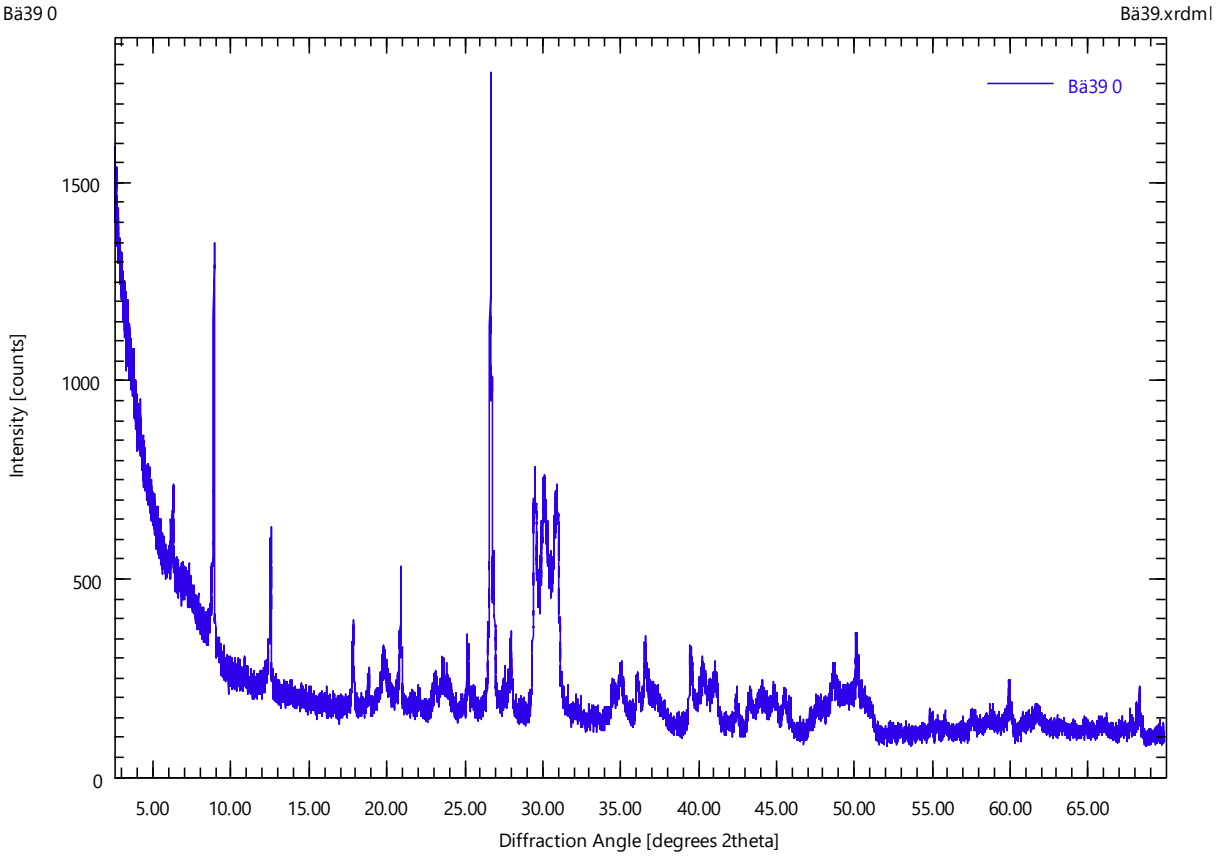
Bä39 0
Bä39.xrdml
Bä39 0
Intensity [counts]
0
500
1000
1500
5.00
10.00
15.00
20.00
25.00
30.00
35.00
40.00
45.00
50.00
55.00
60.00
65.00
Diffraction Angle [degrees 2theta]

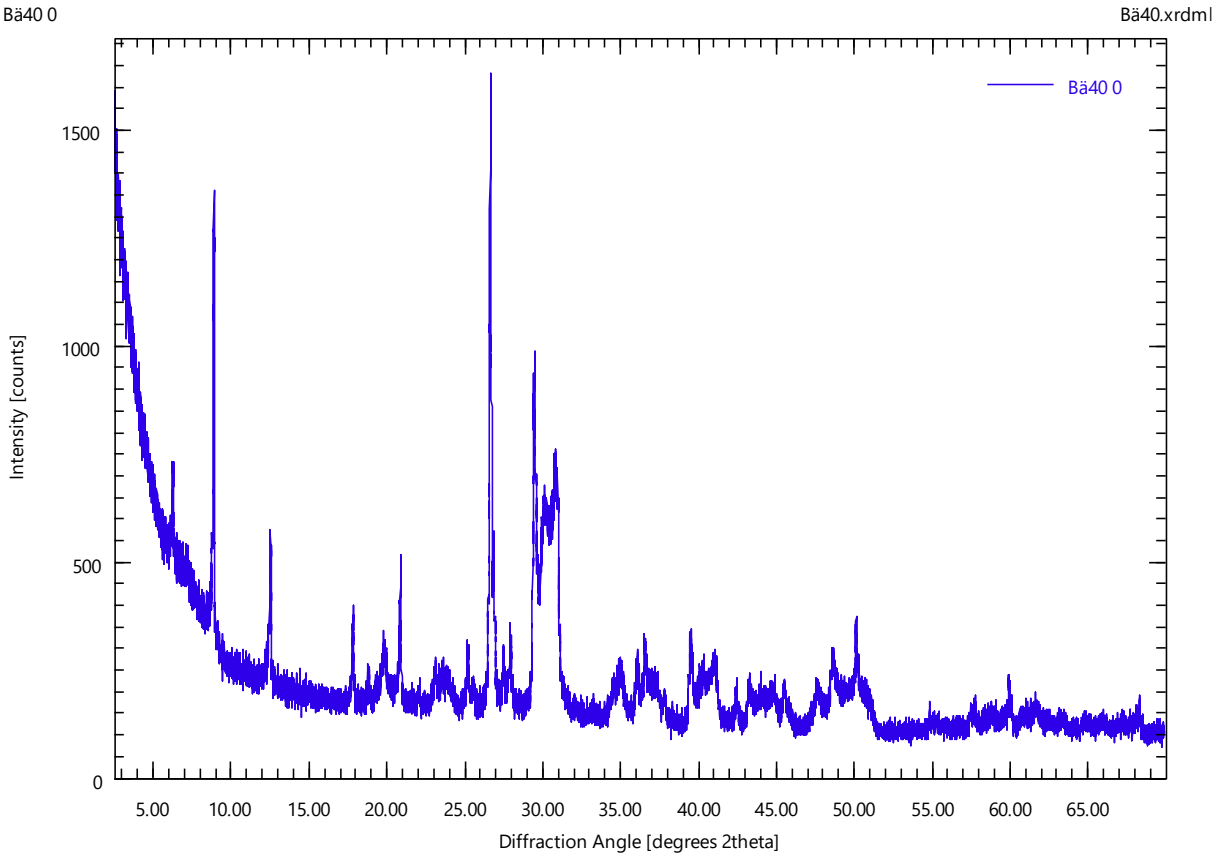
Bä40 0
Bä40.xrdml
Bä40 0
Intensity [counts]
0
500
1000
1500
5.00
10.00
15.00
20.00
25.00
30.00
35.00
40.00
45.00
50.00
55.00
60.00
65.00
Diffraction Angle [degrees 2theta]

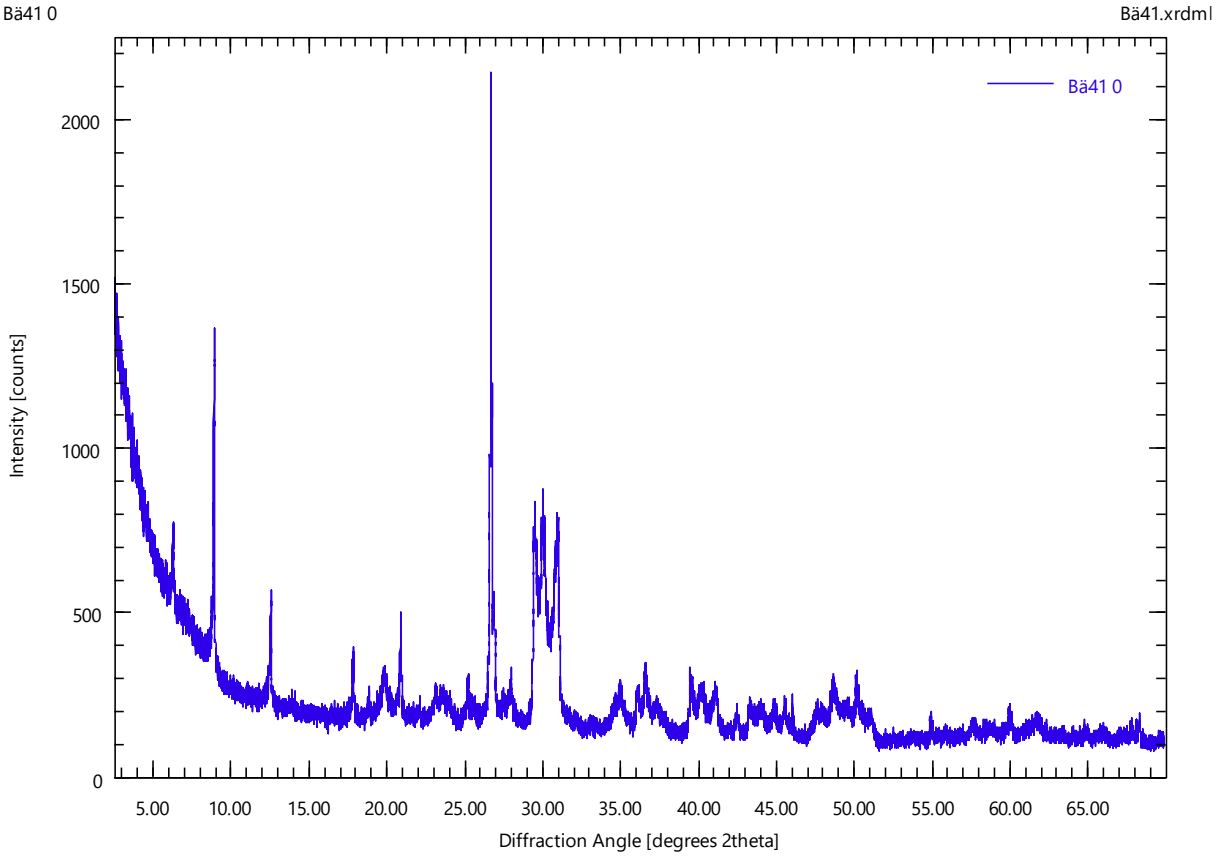
Bä41 0
Bä41.xrdml
Bä41 0
Intensity [counts]
2000
1500
1000
500
0
5.00
10.00
15.00
20.00
25.00
30.00
35.00
40.00
45.00
50.00
55.00
60.00
65.00
Diffraction Angle [degrees 2theta]

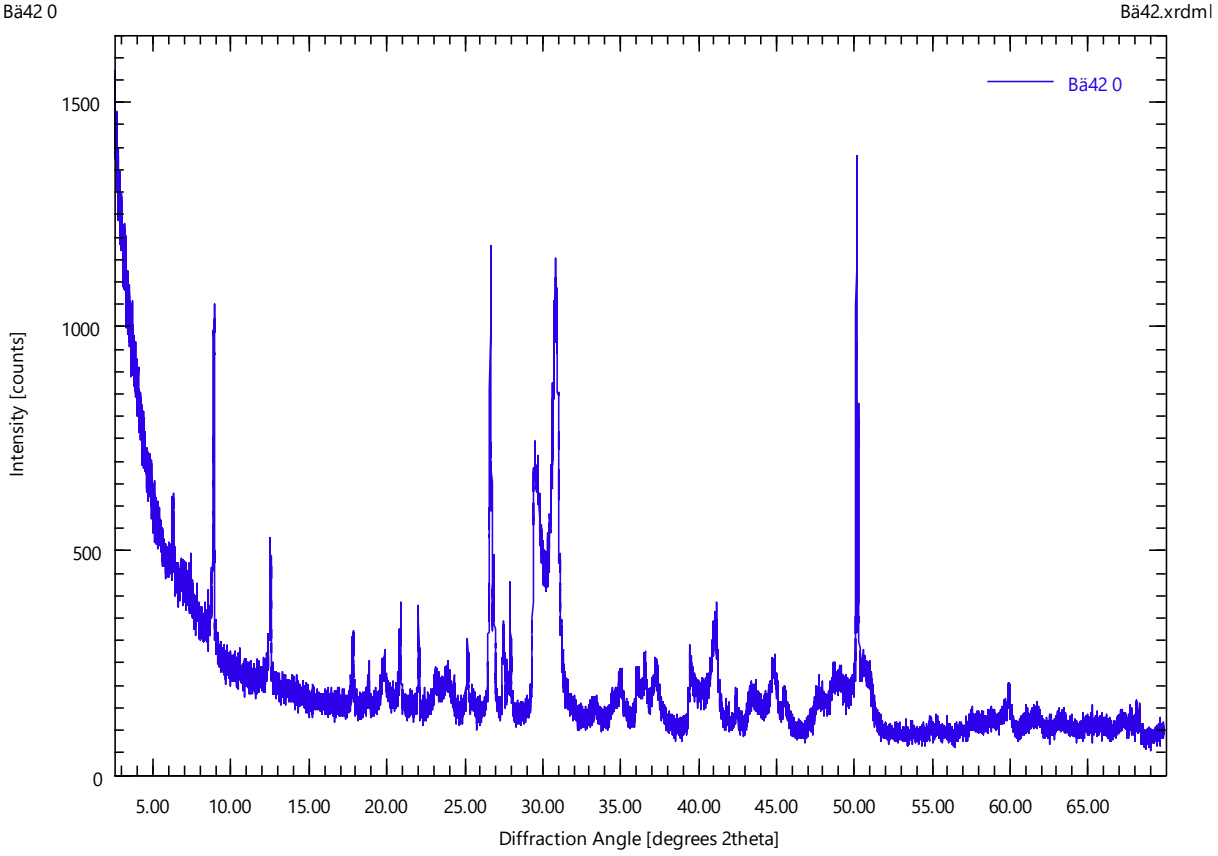
Bä42 0
Bä42.xrdml
Bä42 0
Intensity [counts]
1500
1000
500
0
5.00
10.00
15.00
20.00
25.00
30.00
35.00
40.00
45.00
50.00
55.00
60.00
65.00
Diffraction Angle [degrees 2theta]

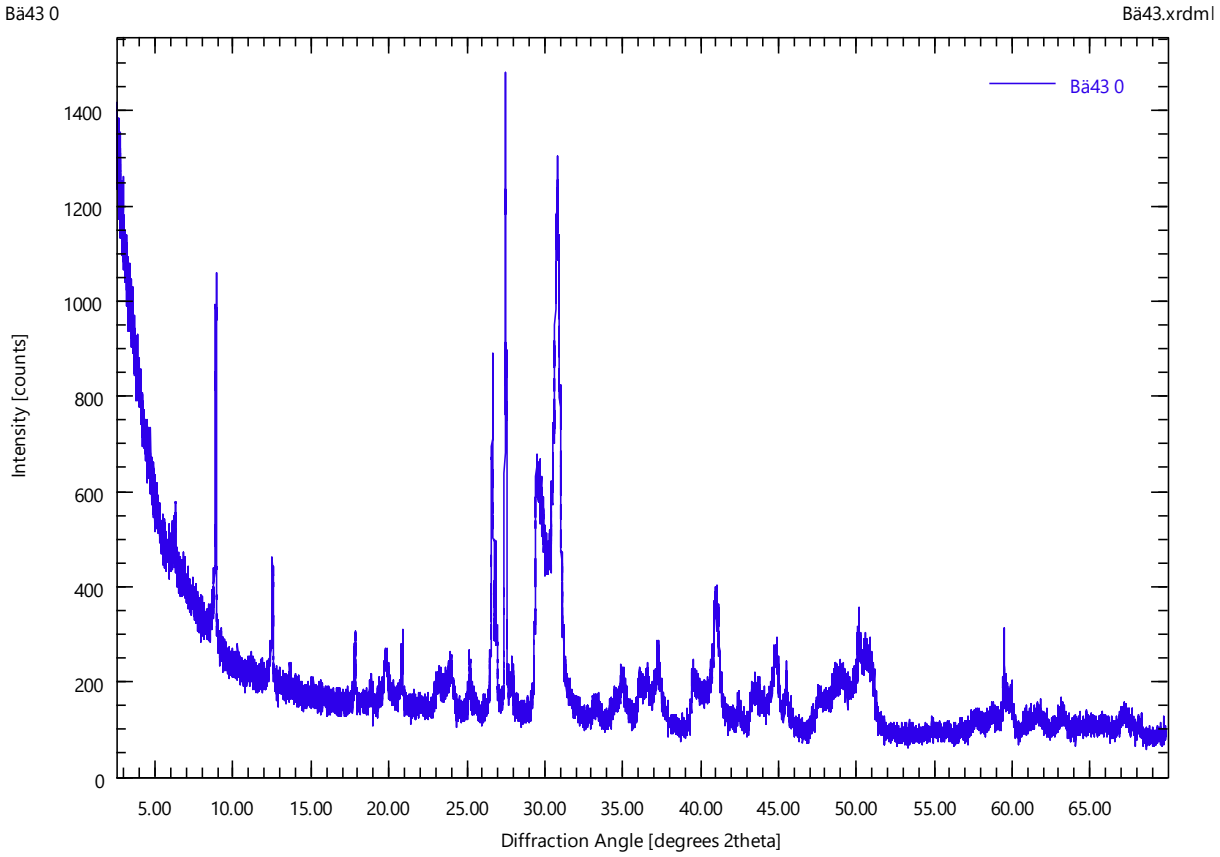
Bä43 0
Bä43.xrdml
Bä43 0
Intensity [counts]
0
200
400
600
800
1000
1200
1400
5.00
10.00
15.00
20.00
25.00
30.00
35.00
40.00
45.00
50.00
55.00
60.00
65.00
Diffraction Angle [degrees 2theta]

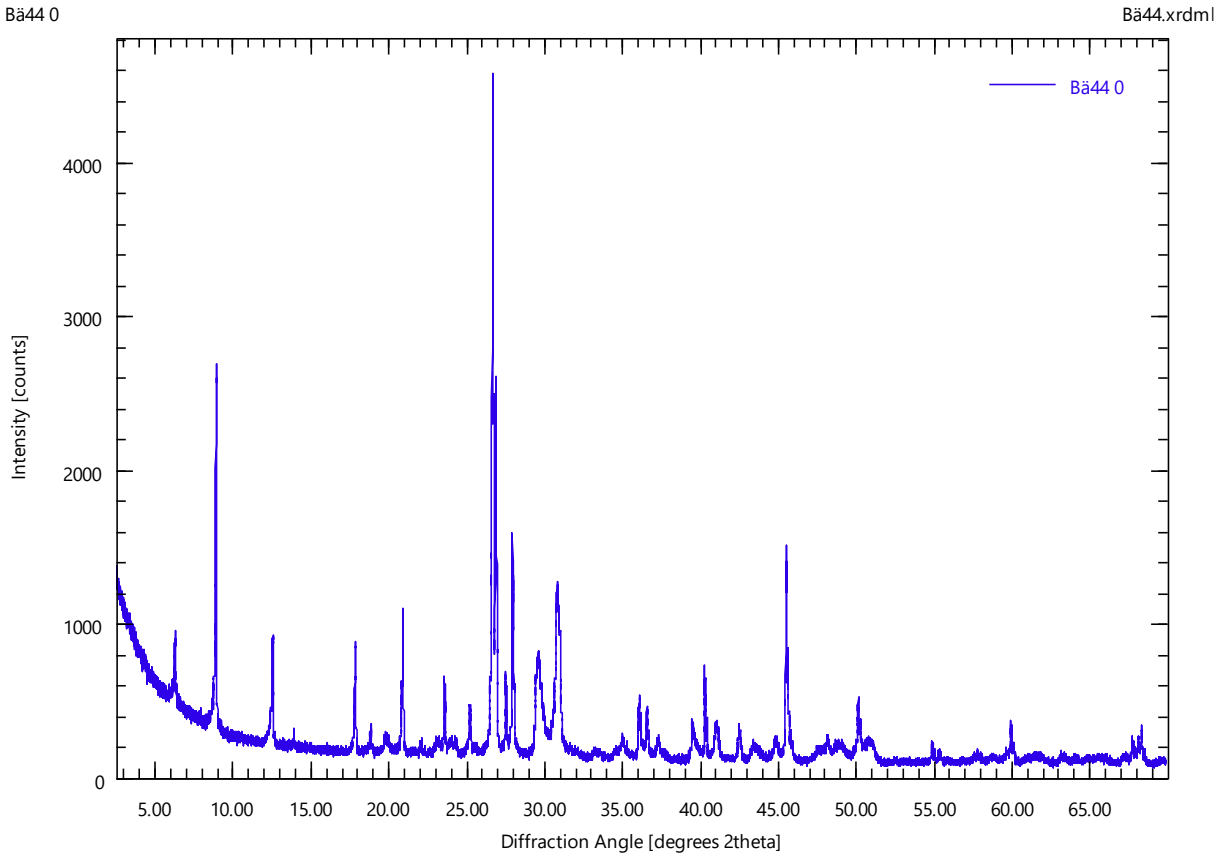
Bä44 0
Bä44.xrdml
Bä44 0
Intensity [counts]
0
1000
2000
3000
4000
5.00
10.00
15.00
20.00
25.00
30.00
35.00
40.00
45.00
50.00
55.00
60.00
65.00
Diffraction Angle [degrees 2theta]

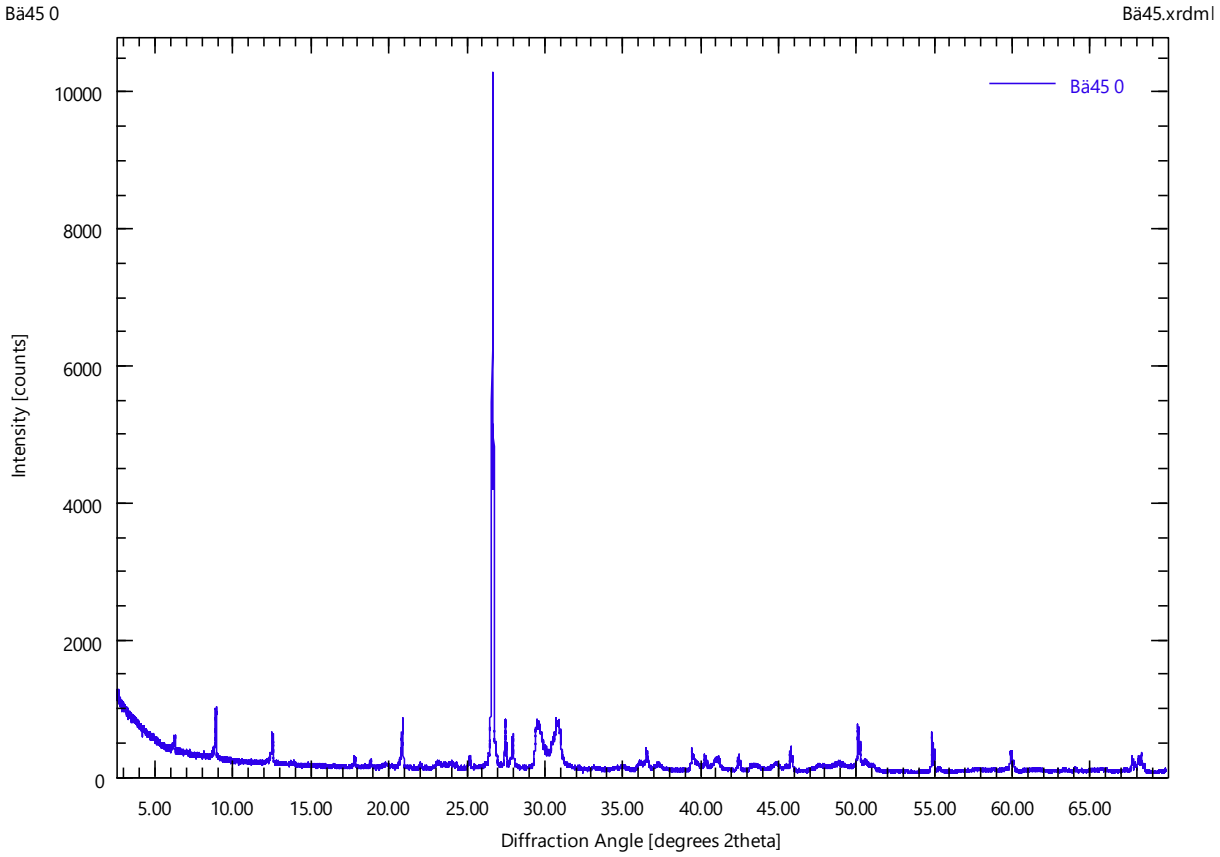
Bä45 0
Bä45.xrdml
Bä45 0
Intensity [counts]
Diffraction Angle [degrees 2theta]

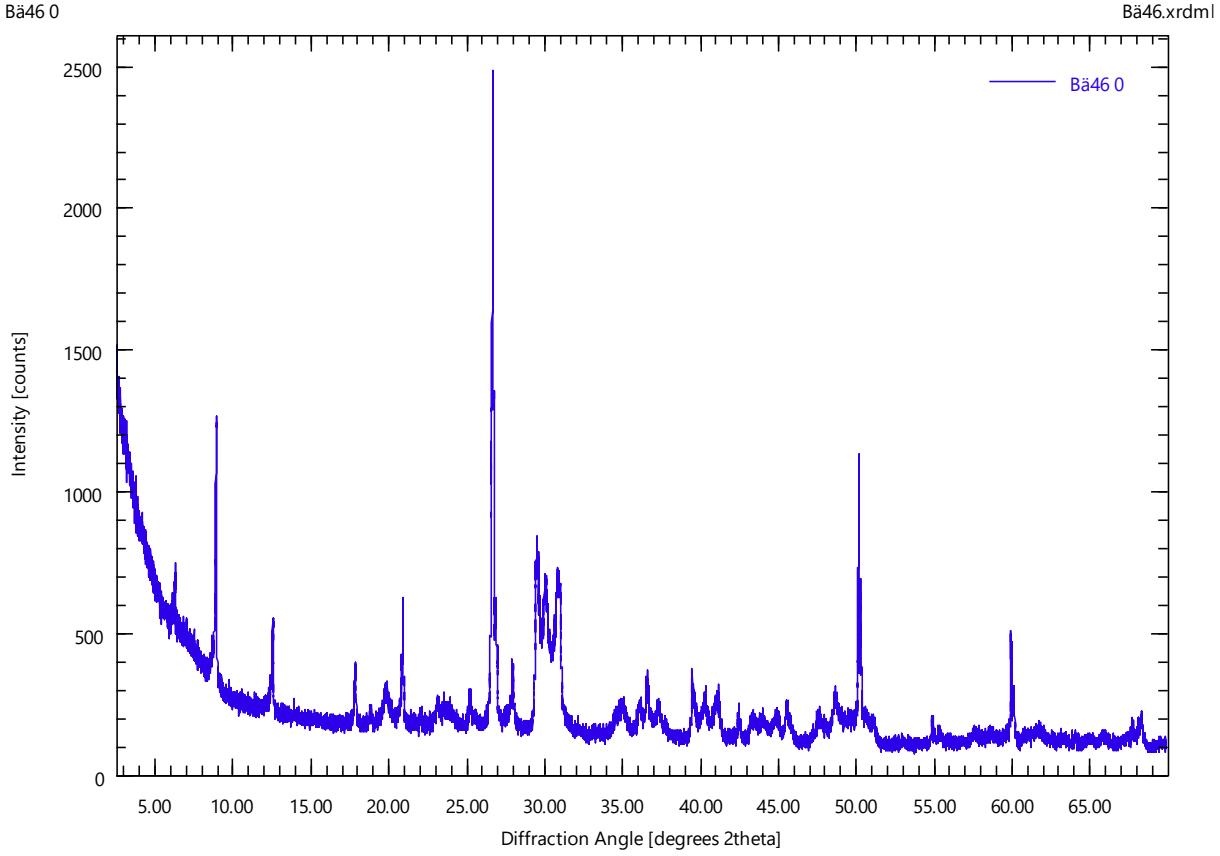
Bä46 0
Bä46.xrdml
Bä46 0
Intensity [counts]
Diffraction Angle [degrees 2theta]

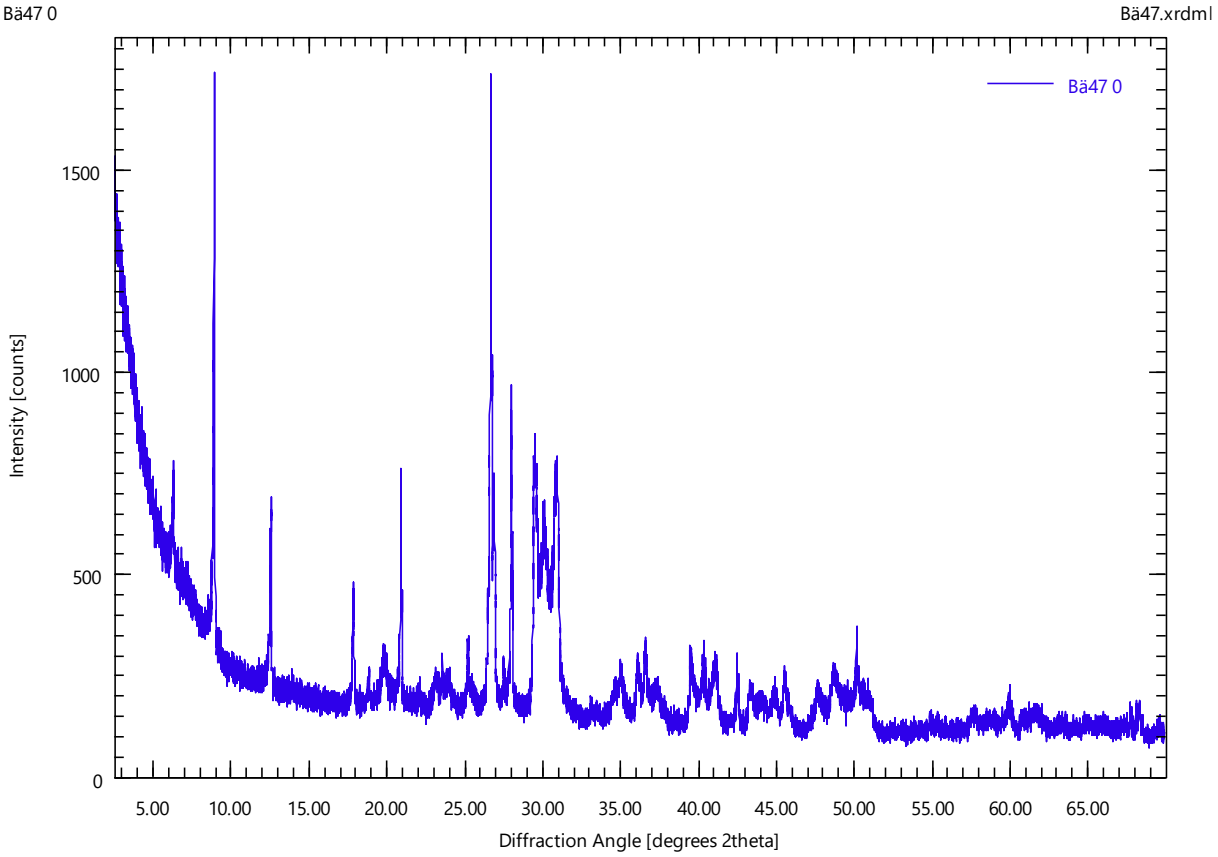
Bä47 0
Bä47.xrdml
Bä47 0
Intensity [counts]
0
500
1000
1500
5.00
10.00
15.00
20.00
25.00
30.00
35.00
40.00
45.00
50.00
55.00
60.00
65.00
Diffraction Angle [degrees 2theta]

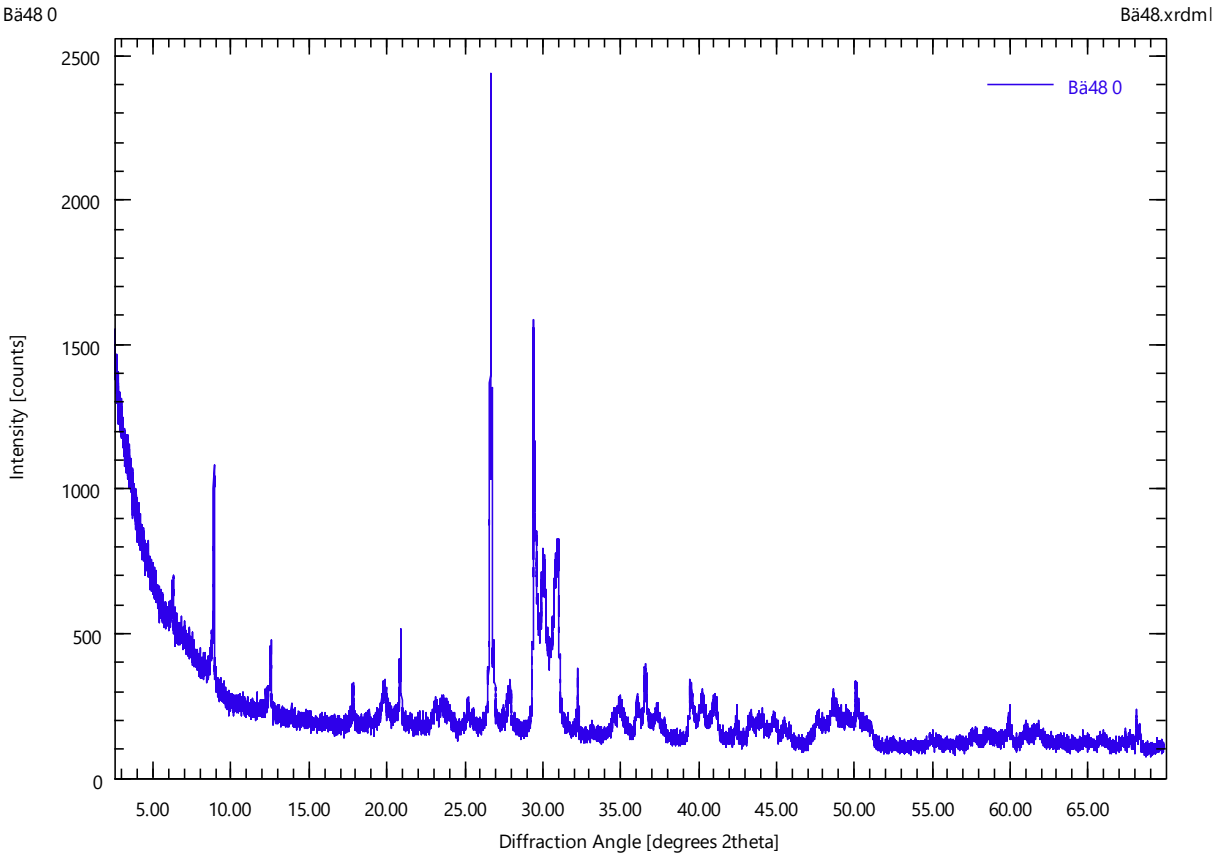
Bä48 0
Bä48.xrdml
Bä48 0
Intensity [counts]
0
500
1000
1500
2000
2500
5.00
10.00
15.00
20.00
25.00
30.00
35.00
40.00
45.00
50.00
55.00
60.00
65.00
Diffraction Angle [degrees 2theta]

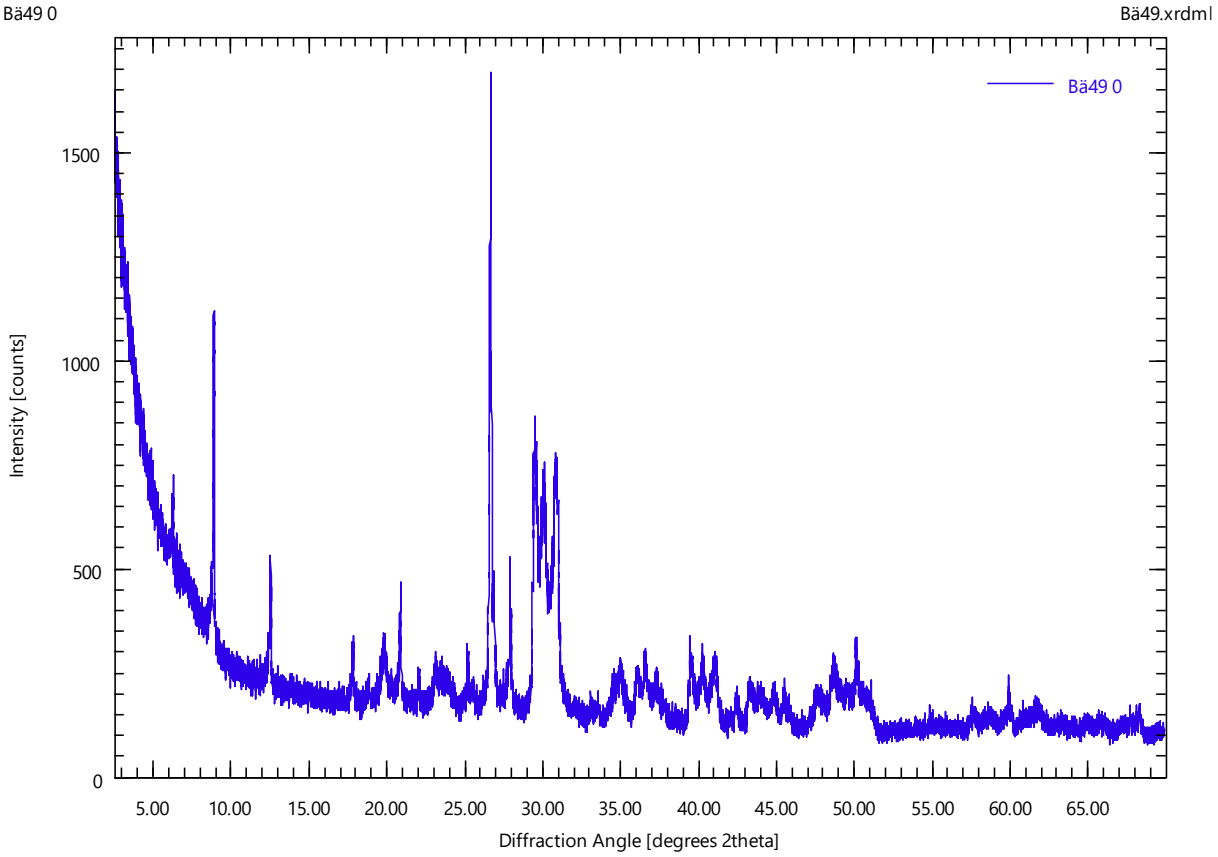
Bä49 0
Bä49.xrdml
Bä49 0
Intensity [counts]
0
500
1000
1500
5.00
10.00
15.00
20.00
25.00
30.00
35.00
40.00
45.00
50.00
55.00
60.00
65.00
Diffraction Angle [degrees 2theta]

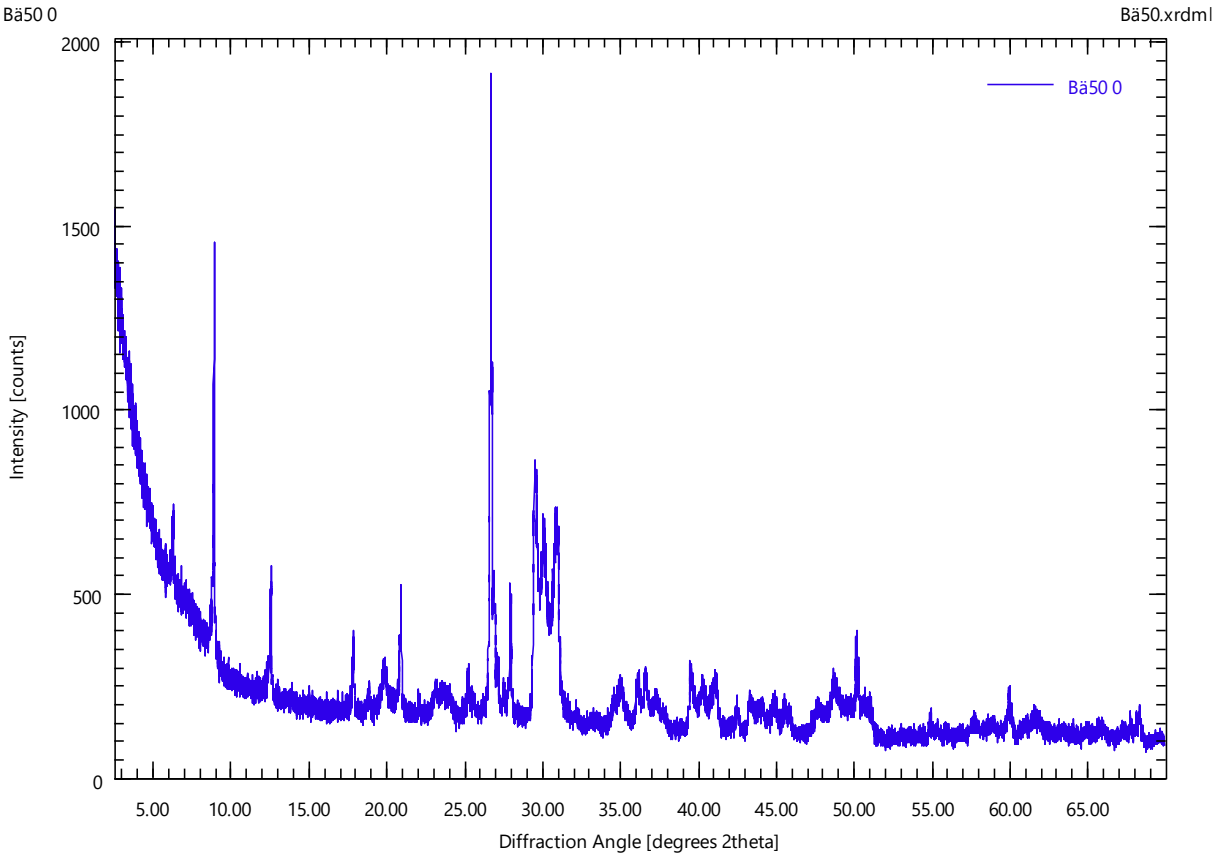
Bä50 0
Bä50.xrdml
Bä50 0
Intensity [counts]
0
500
1000
1500
2000
5.00
10.00
15.00
20.00
25.00
30.00
35.00
40.00
45.00
50.00
55.00
60.00
65.00
Diffraction Angle [degrees 2theta]

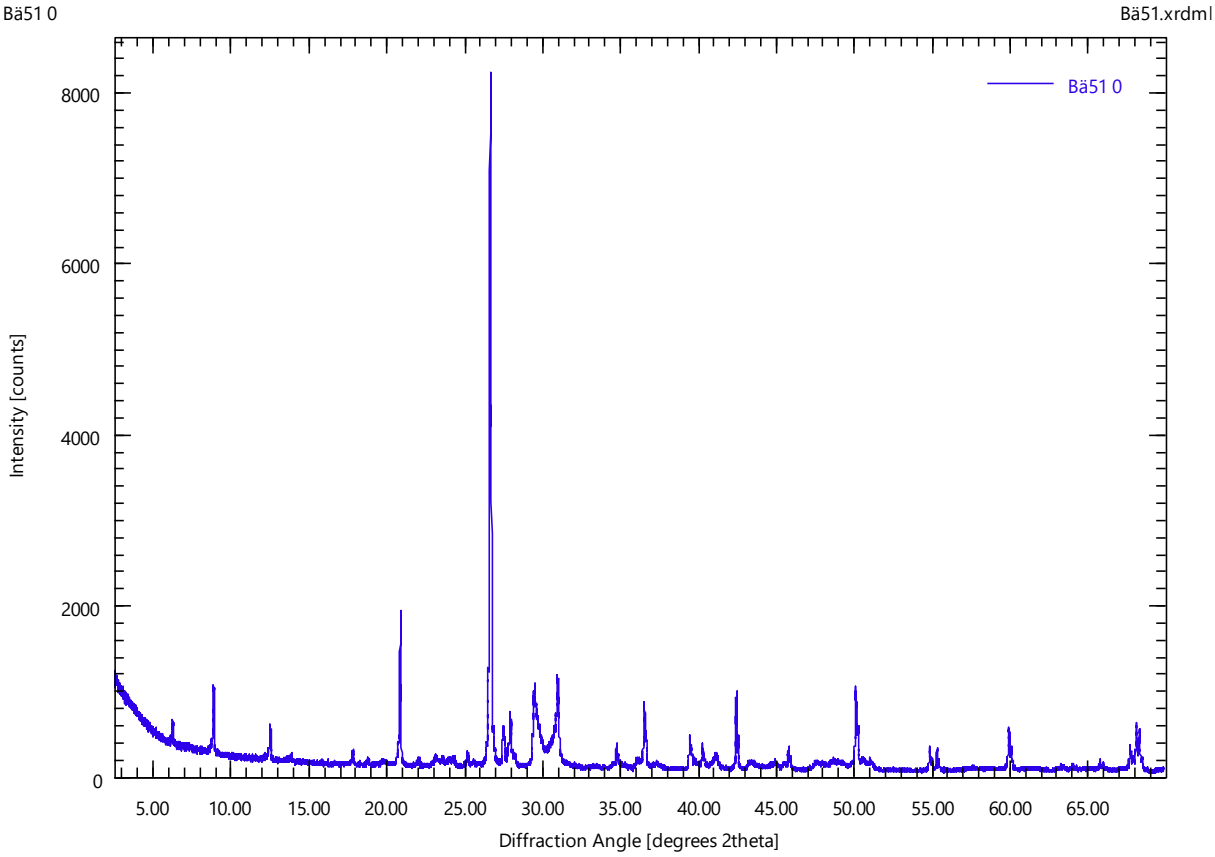
Bä51 0
Bä51.xrdml
Bä51 0
8000
6000
4000
2000
0
Intensity [counts]
5.00
10.00
15.00
20.00
25.00
30.00
35.00
40.00
45.00
50.00
55.00
60.00
65.00
Diffraction Angle [degrees 2theta]

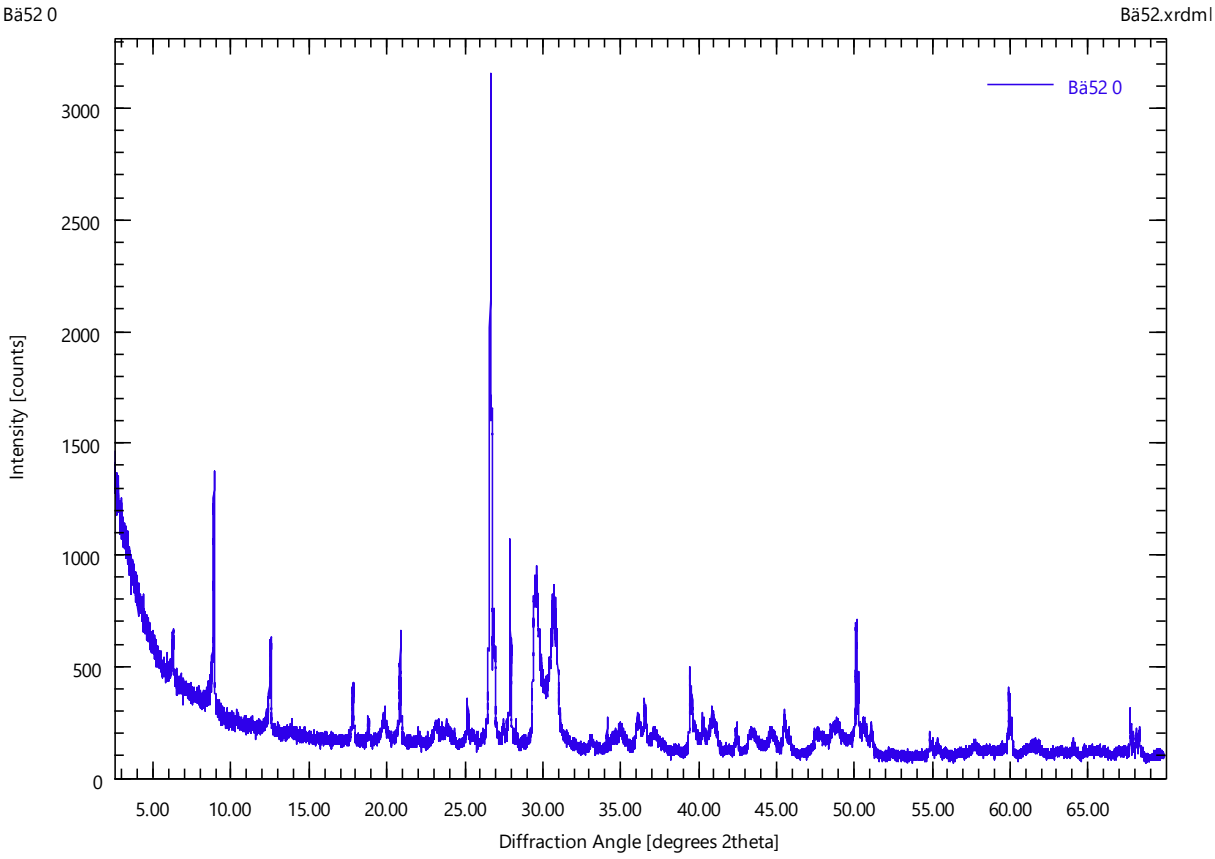
Bä52 0
Bä52.xrdml
Bä52 0
3000
2500
2000
1500
1000
500
0
Intensity [counts]
5.00
10.00
15.00
20.00
25.00
30.00
35.00
40.00
45.00
50.00
55.00
60.00
65.00
Diffraction Angle [degrees 2theta]

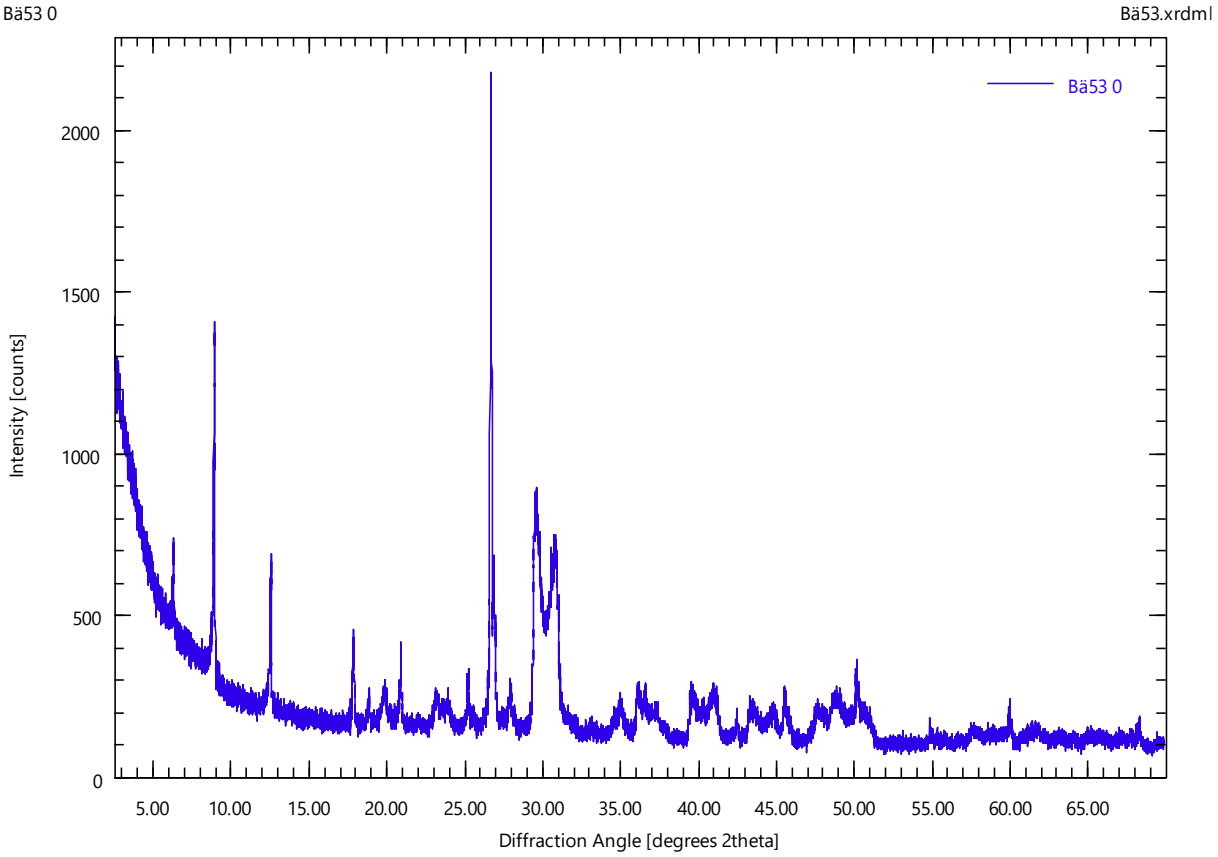
Bä53 0
Bä53.xrdml
Bä53 0
Intensity [counts]
Diffraction Angle [degrees 2theta]
0
500
1000
1500
2000
5.00
10.00
15.00
20.00
25.00
30.00
35.00
40.00
45.00
50.00
55.00
60.00
65.00

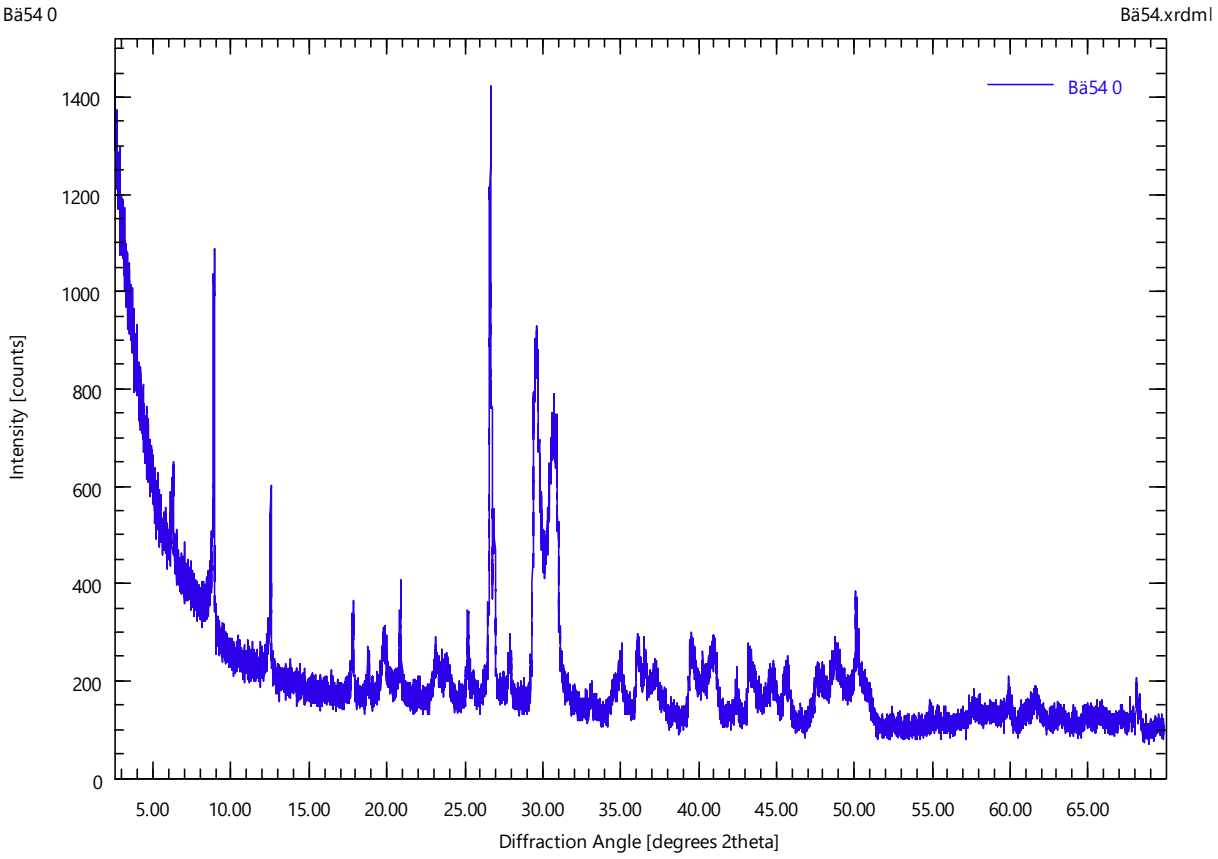
Bä54 0
Bä54.xrdml
Bä54 0
Intensity [counts]
Diffraction Angle [degrees 2theta]
0
200
400
600
800
1000
1200
1400
5.00
10.00
15.00
20.00
25.00
30.00
35.00
40.00
45.00
50.00
55.00
60.00
65.00

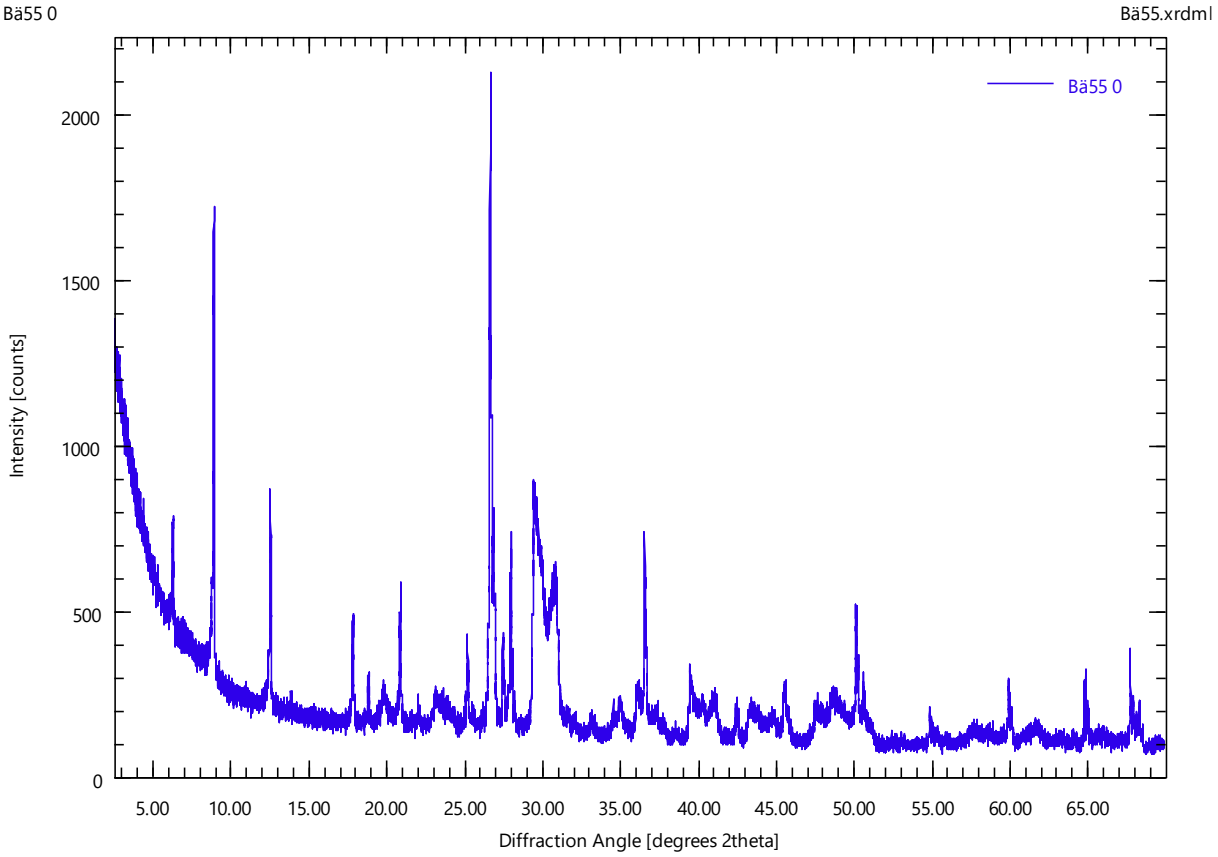
Bä55 0
Bä55.xrdml
Bä55 0
Intensity [counts]
0
500
1000
1500
2000
5.00
10.00
15.00
20.00
25.00
30.00
35.00
40.00
45.00
50.00
55.00
60.00
65.00
Diffraction Angle [degrees 2theta]

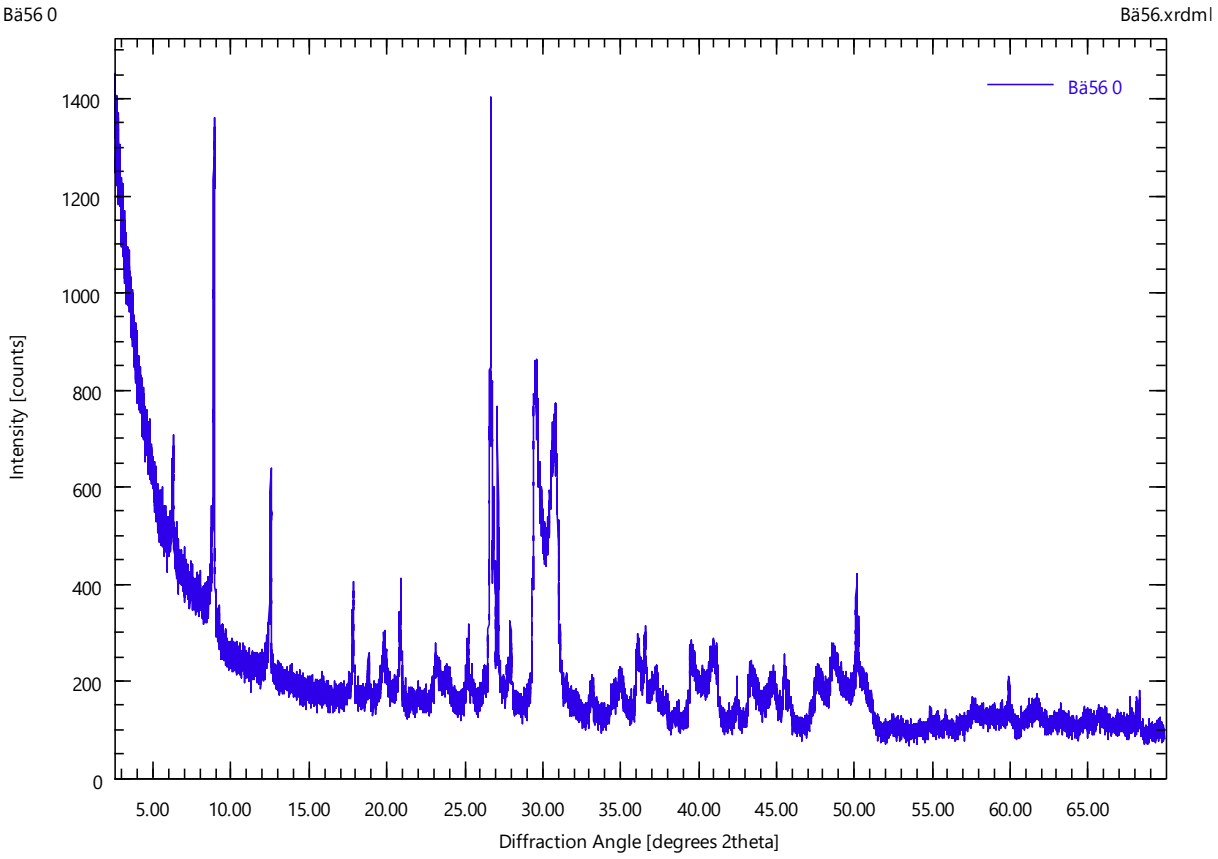
Bä56 0
Bä56.xrdml
Bä56 0
Intensity [counts]
0
200
400
600
800
1000
1200
1400
5.00
10.00
15.00
20.00
25.00
30.00
35.00
40.00
45.00
50.00
55.00
60.00
65.00
Diffraction Angle [degrees 2theta]

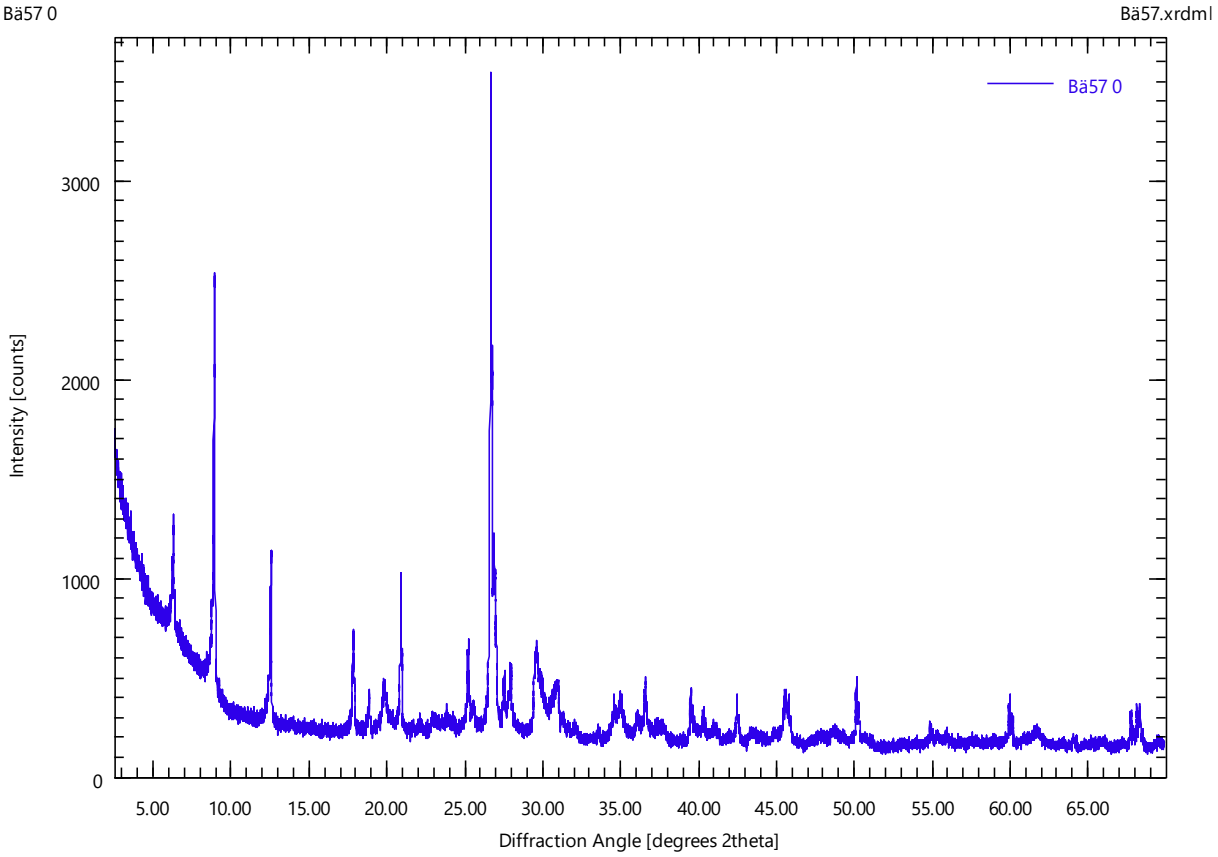
Bä57 0
Bä57.xrdml
Bä57 0
3000
2000
1000
0
Intensity [counts]
5.00
10.00
15.00
20.00
25.00
30.00
35.00
40.00
45.00
50.00
55.00
60.00
65.00
Diffraction Angle [degrees 2theta]

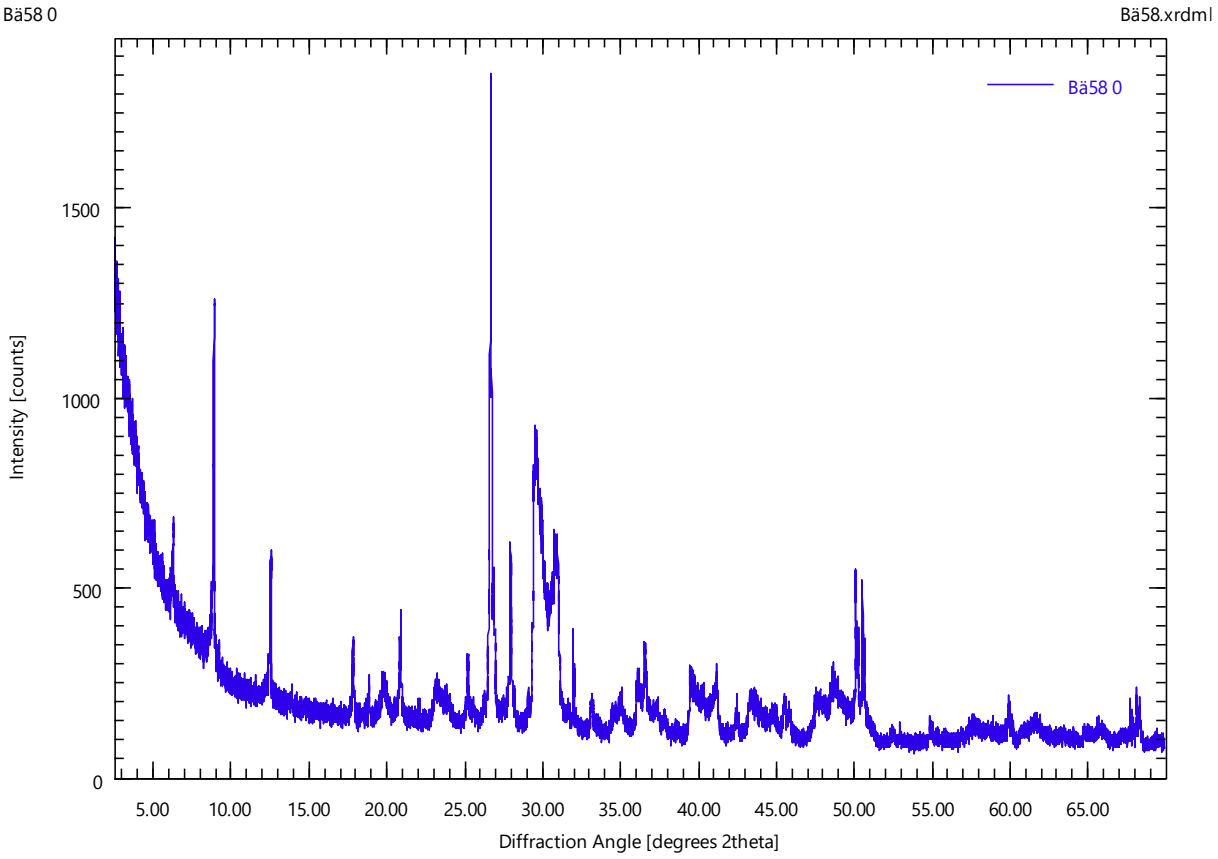
Bä58 0
Bä58.xrdml
Bä58 0
1500
1000
500
0
Intensity [counts]
5.00
10.00
15.00
20.00
25.00
30.00
35.00
40.00
45.00
50.00
55.00
60.00
65.00
Diffraction Angle [degrees 2theta]

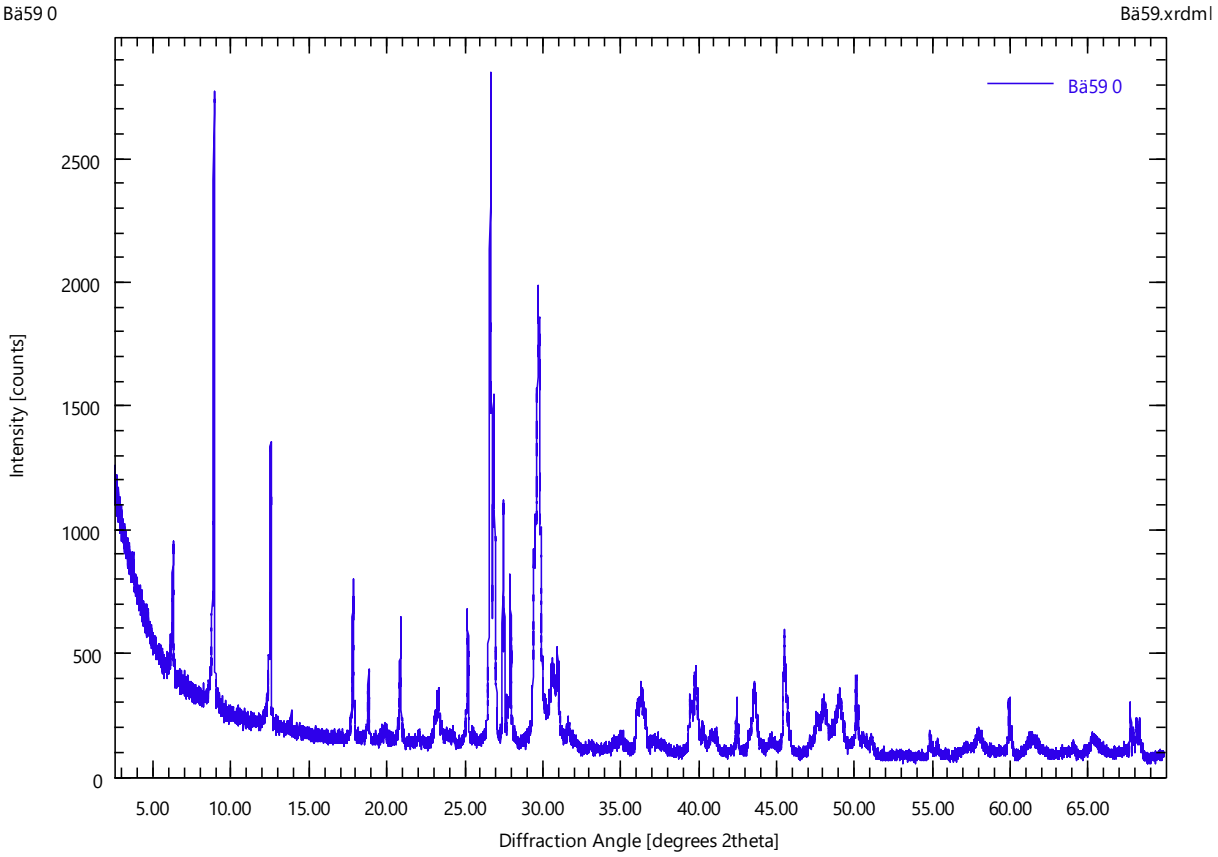
Bä59 0
Bä59.xrdml
Bä59 0
Intensity [counts]
0
500
1000
1500
2000
2500
5.00
10.00
15.00
20.00
25.00
30.00
35.00
40.00
45.00
50.00
55.00
60.00
65.00
Diffraction Angle [degrees 2theta]

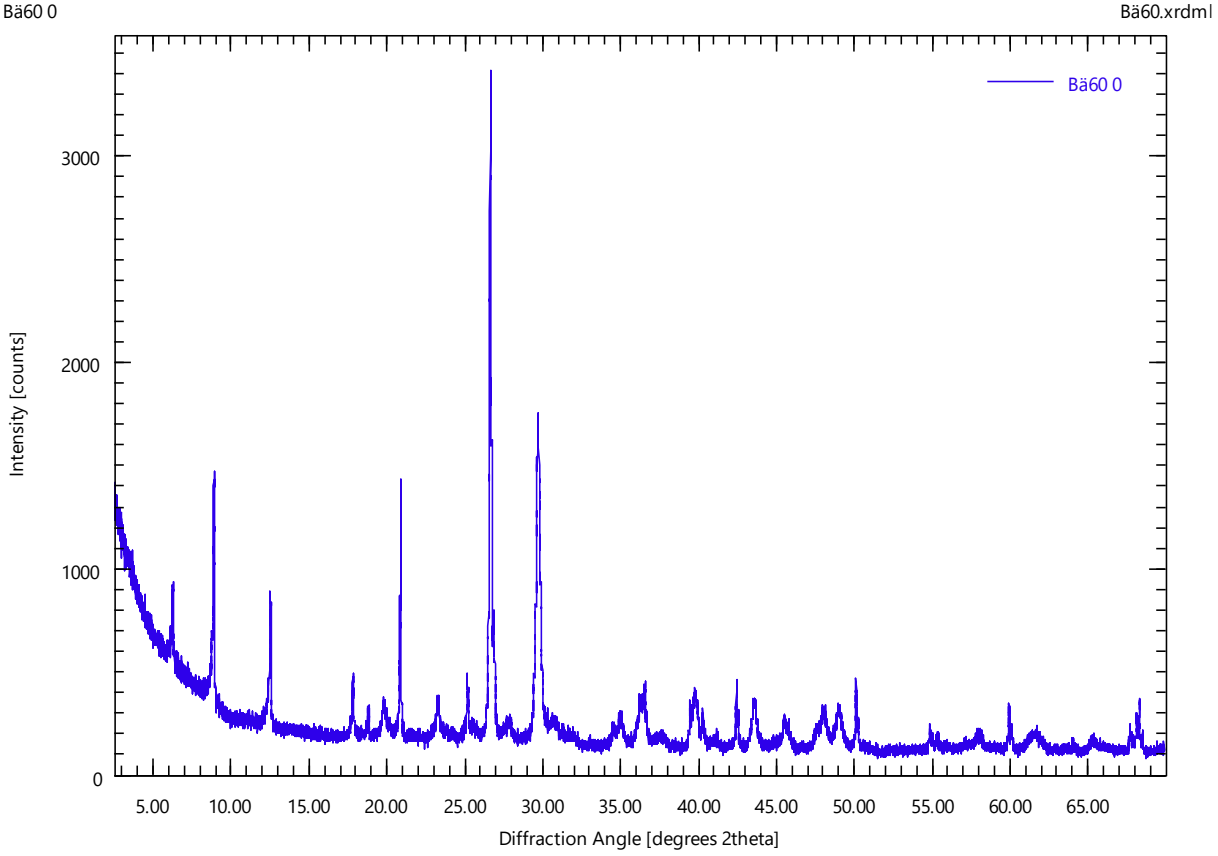
Bä60 0
Bä60.xrdml
Bä60 0
Intensity [counts]
0
1000
2000
3000
5.00
10.00
15.00
20.00
25.00
30.00
35.00
40.00
45.00
50.00
55.00
60.00
65.00
Diffraction Angle [degrees 2theta]

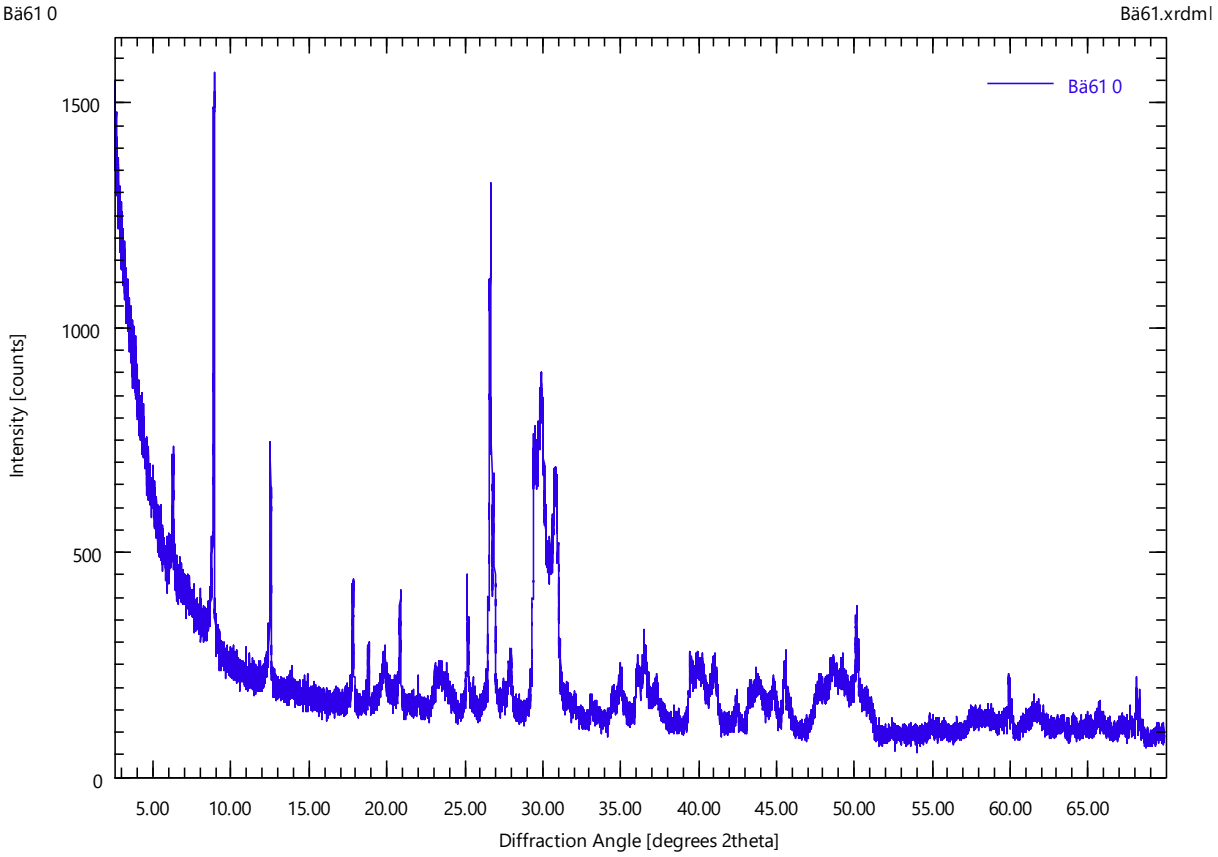
Bä61 0
Bä61.xrdml
Bä61 0
Intensity [counts]
0
500
1000
1500
5.00
10.00
15.00
20.00
25.00
30.00
35.00
40.00
45.00
50.00
55.00
60.00
65.00
Diffraction Angle [degrees 2theta]

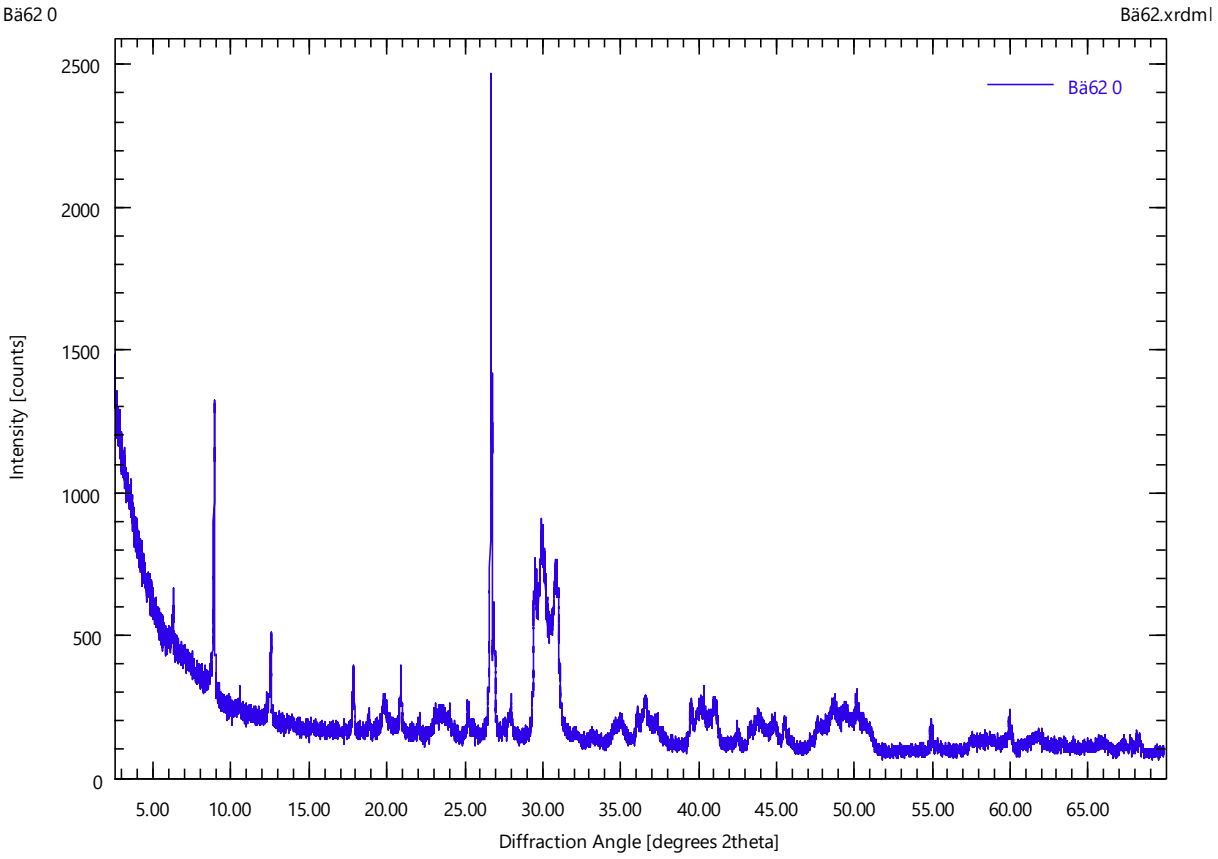
Bä62 0
Bä62.xrdml
Bä62 0
Intensity [counts]
0
500
1000
1500
2000
2500
5.00
10.00
15.00
20.00
25.00
30.00
35.00
40.00
45.00
50.00
55.00
60.00
65.00
Diffraction Angle [degrees 2theta]

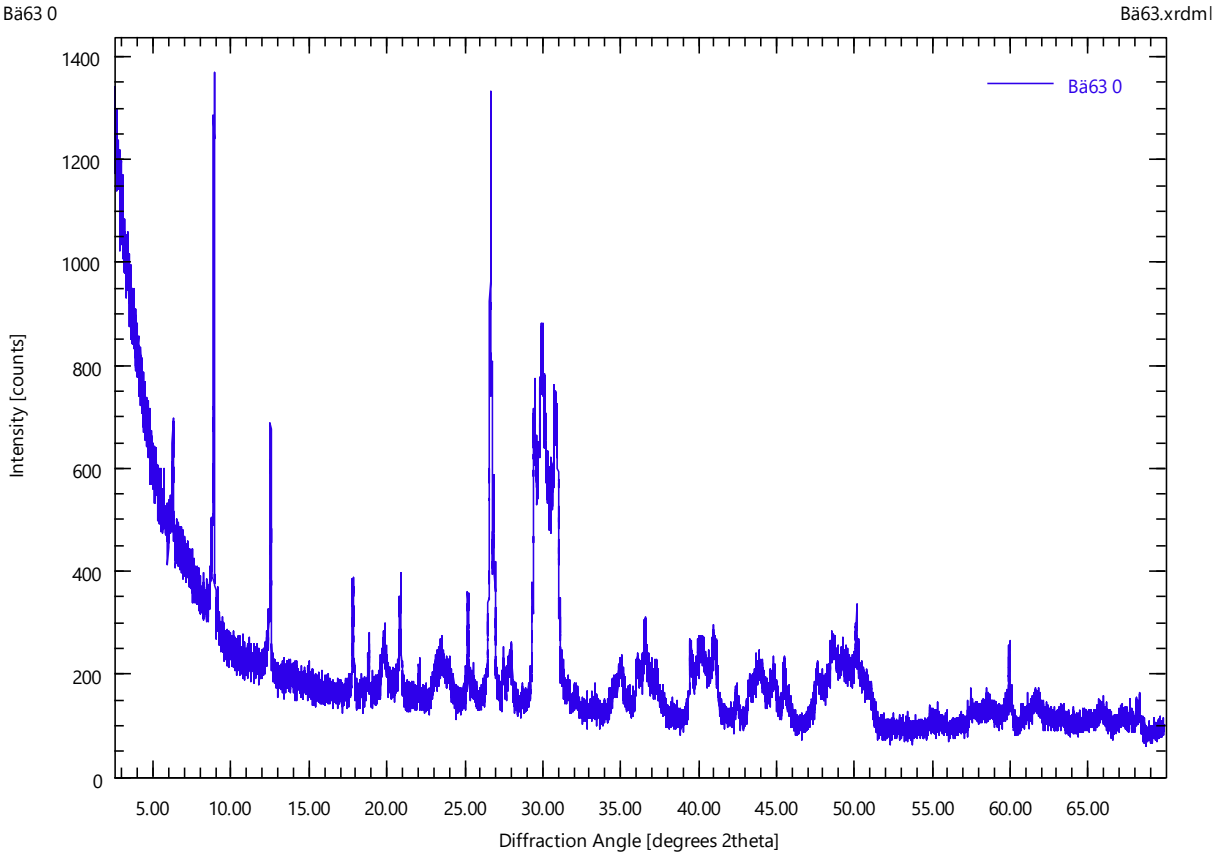
Bä63 0
Bä63.xrdml
Bä63 0
Intensity [counts]
Diffraction Angle [degrees 2theta]
0
200
400
600
800
1000
1200
1400
5.00
10.00
15.00
20.00
25.00
30.00
35.00
40.00
45.00
50.00
55.00
60.00
65.00

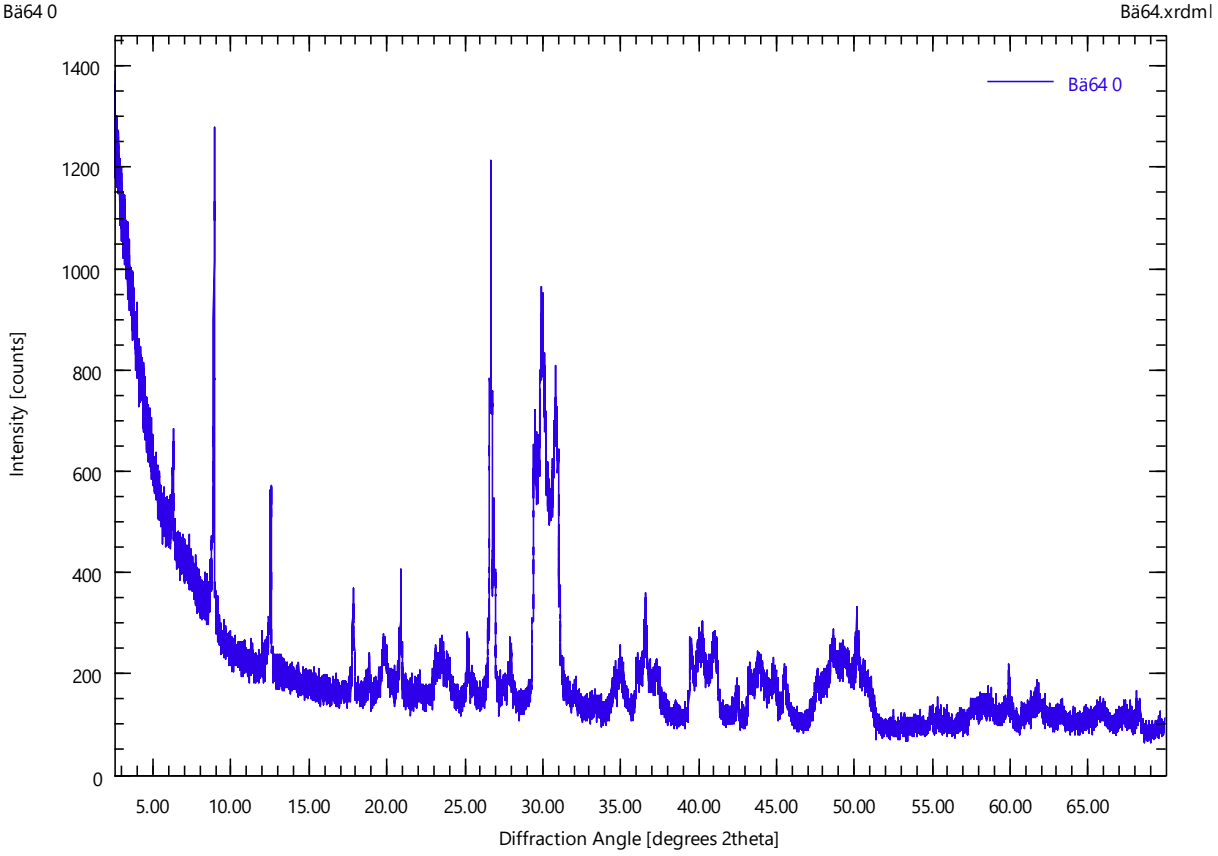
Bä64 0
Bä64.xrdml
Bä64 0
Intensity [counts]
Diffraction Angle [degrees 2theta]
0
200
400
600
800
1000
1200
1400
5.00
10.00
15.00
20.00
25.00
30.00
35.00
40.00
45.00
50.00
55.00
60.00
65.00

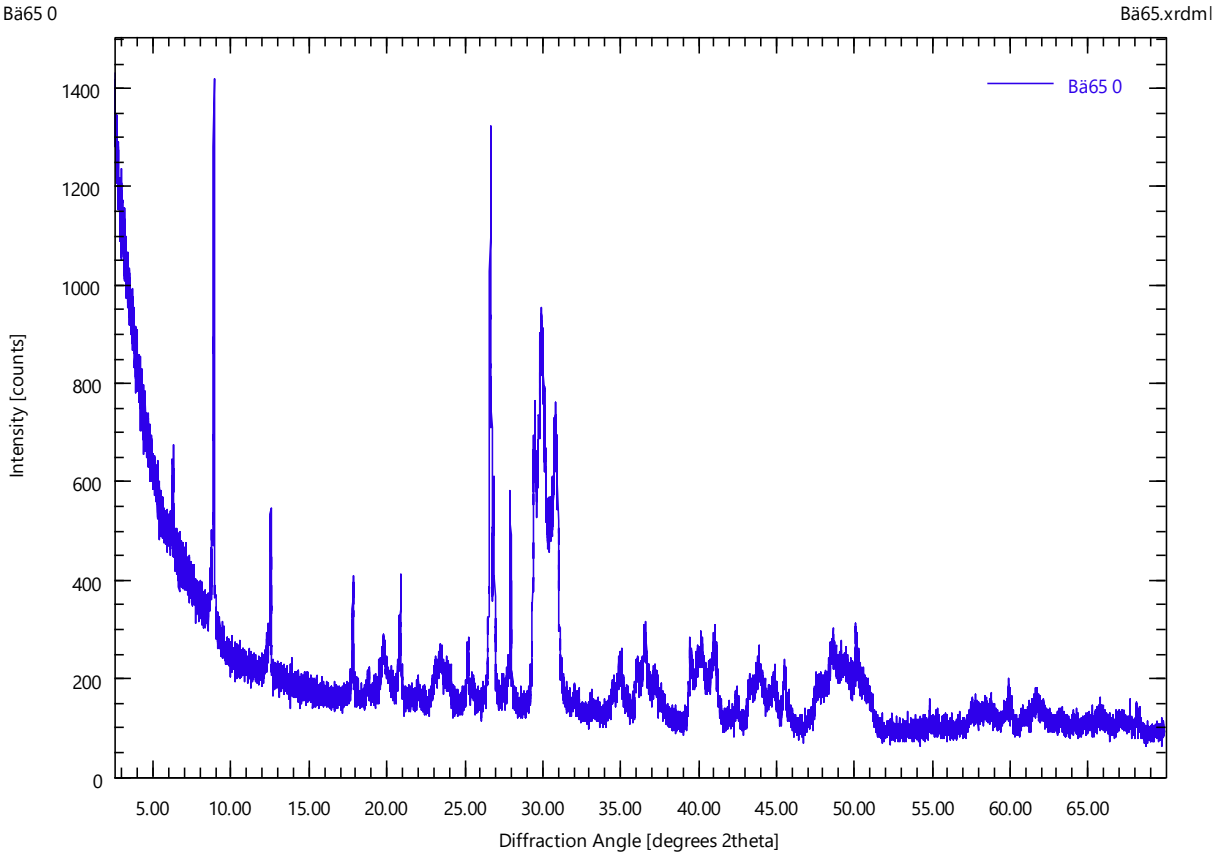
Bä65 0
Bä65.xrdml
Bä65 0
Intensity [counts]
Diffraction Angle [degrees 2theta]
0
200
400
600
800
1000
1200
1400
5.00
10.00
15.00
20.00
25.00
30.00
35.00
40.00
45.00
50.00
55.00
60.00
65.00

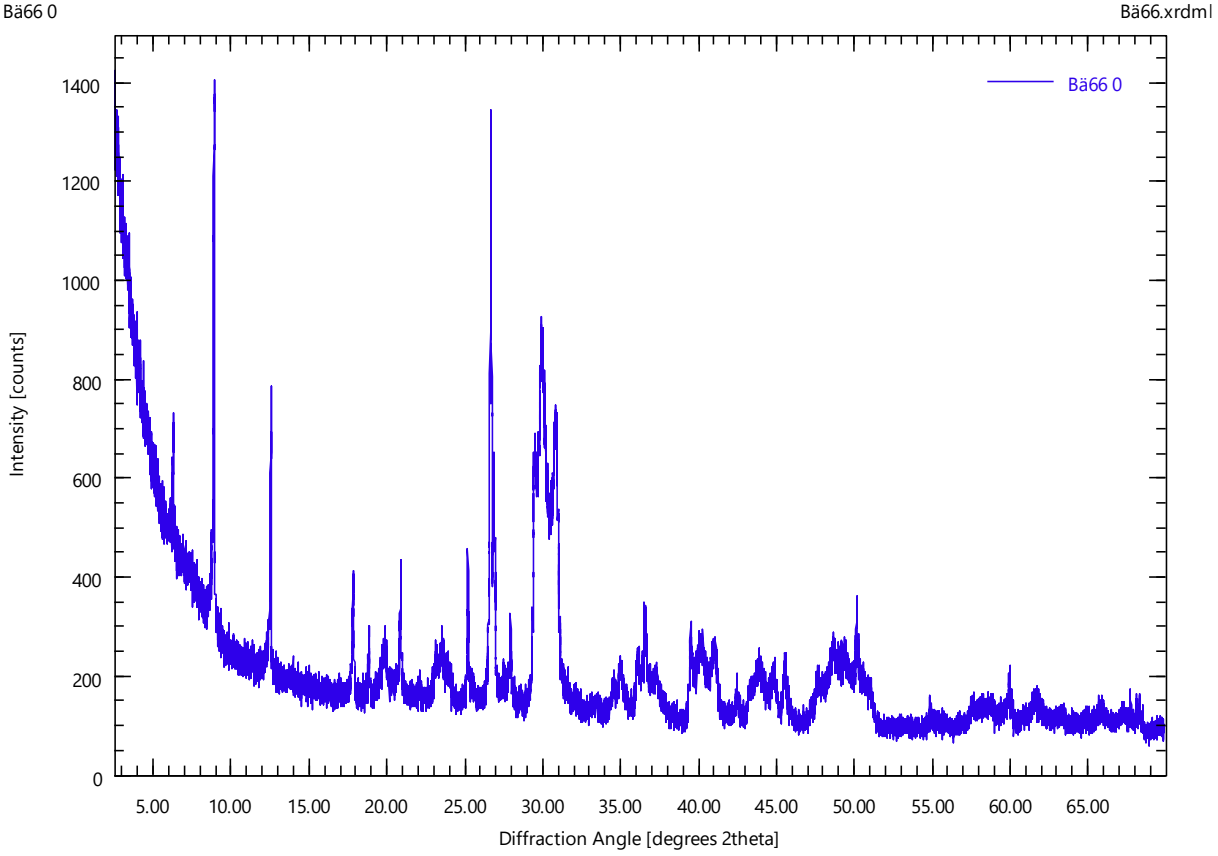
Bä66 0
Bä66.xrdml
Bä66 0
Intensity [counts]
Diffraction Angle [degrees 2theta]
0
200
400
600
800
1000
1200
1400
5.00
10.00
15.00
20.00
25.00
30.00
35.00
40.00
45.00
50.00
55.00
60.00
65.00

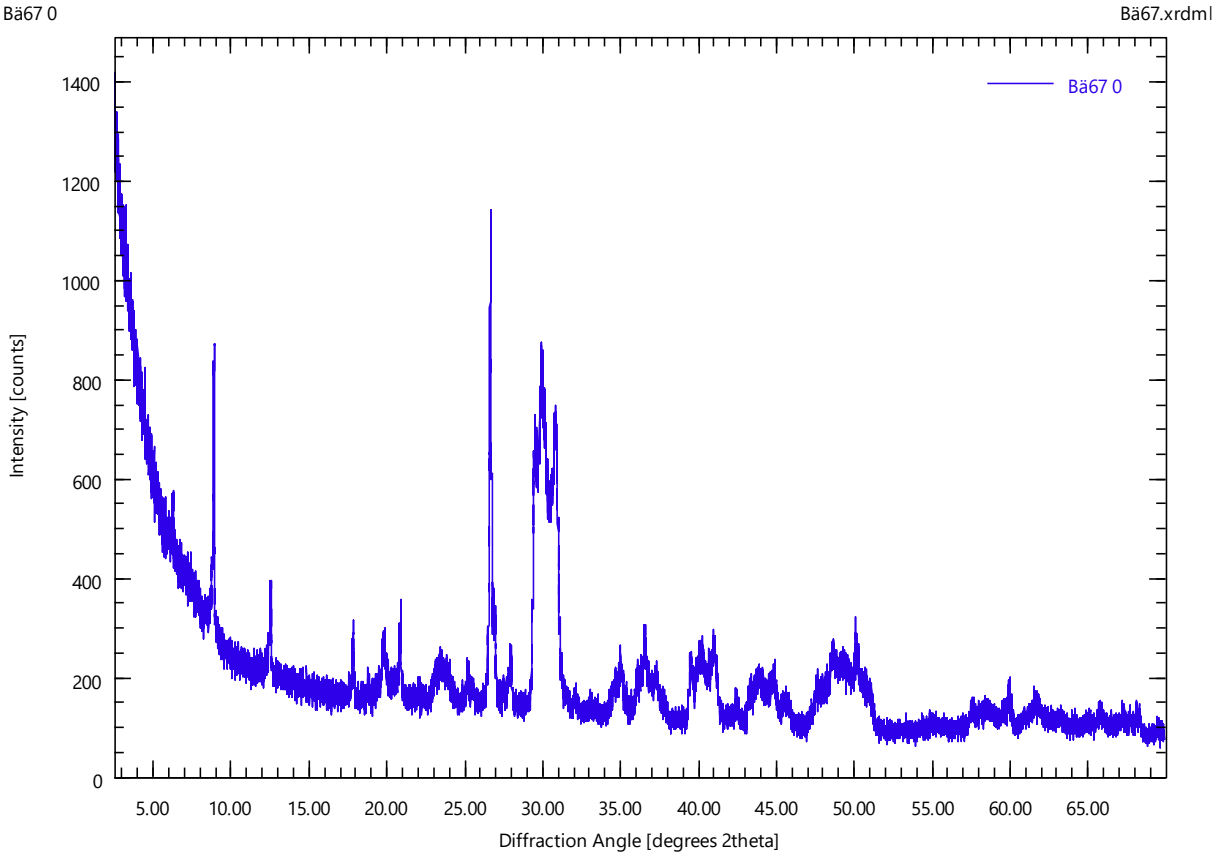
Bä67 0
Bä67.xrdml
Bä67 0
Intensity [counts]
Diffraction Angle [degrees 2theta]
0
200
400
600
800
1000
1200
1400
5.00
10.00
15.00
20.00
25.00
30.00
35.00
40.00
45.00
50.00
55.00
60.00
65.00

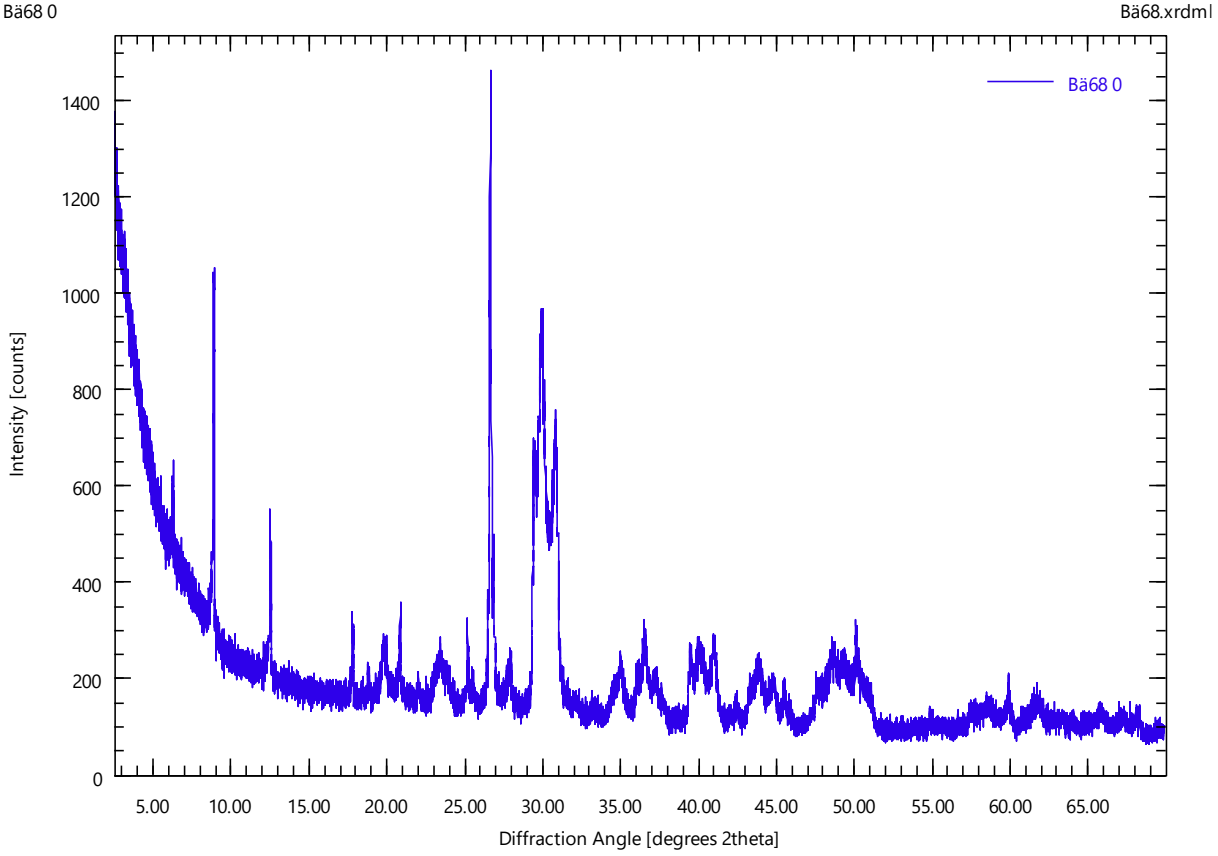
Bä68 0
Bä68.xrdml
Bä68 0
Intensity [counts]
Diffraction Angle [degrees 2theta]
0
200
400
600
800
1000
1200
1400
5.00
10.00
15.00
20.00
25.00
30.00
35.00
40.00
45.00
50.00
55.00
60.00
65.00

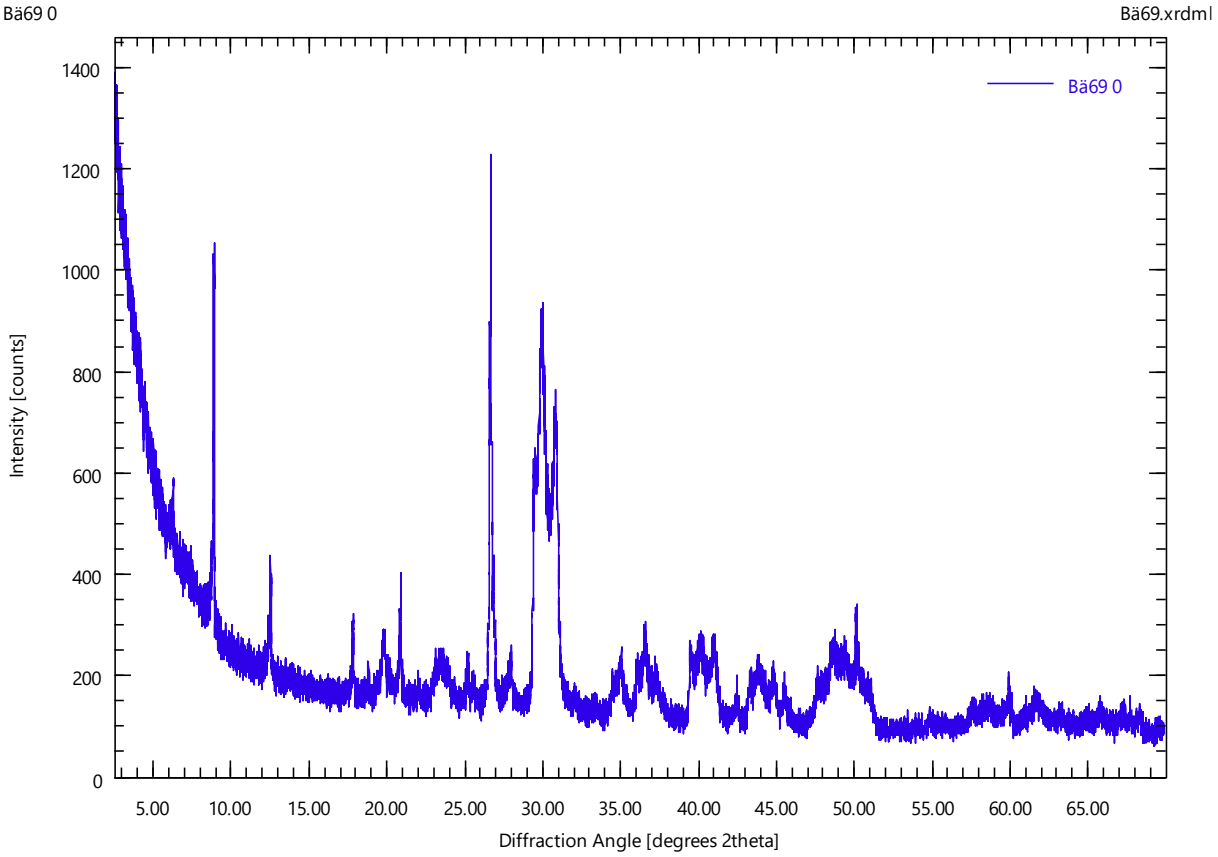
Bä69 0
Bä69.xrdml
Bä69 0
Intensity [counts]
Diffraction Angle [degrees 2theta]
0
200
400
600
800
1000
1200
1400
5.00
10.00
15.00
20.00
25.00
30.00
35.00
40.00
45.00
50.00
55.00
60.00
65.00

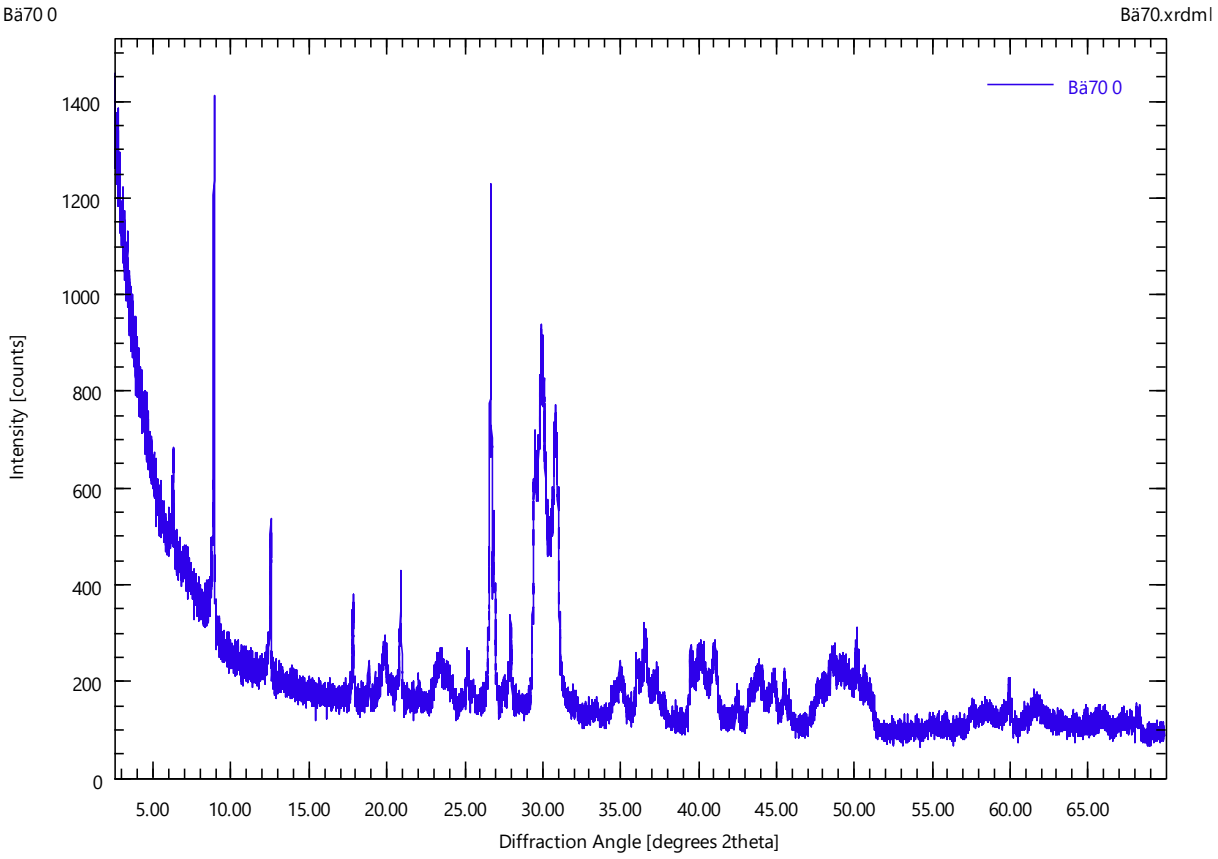
Bä70 0
Bä70.xrdml
Bä70 0
Intensity [counts]
Diffraction Angle [degrees 2theta]
0
200
400
600
800
1000
1200
1400
5.00
10.00
15.00
20.00
25.00
30.00
35.00
40.00
45.00
50.00
55.00
60.00
65.00

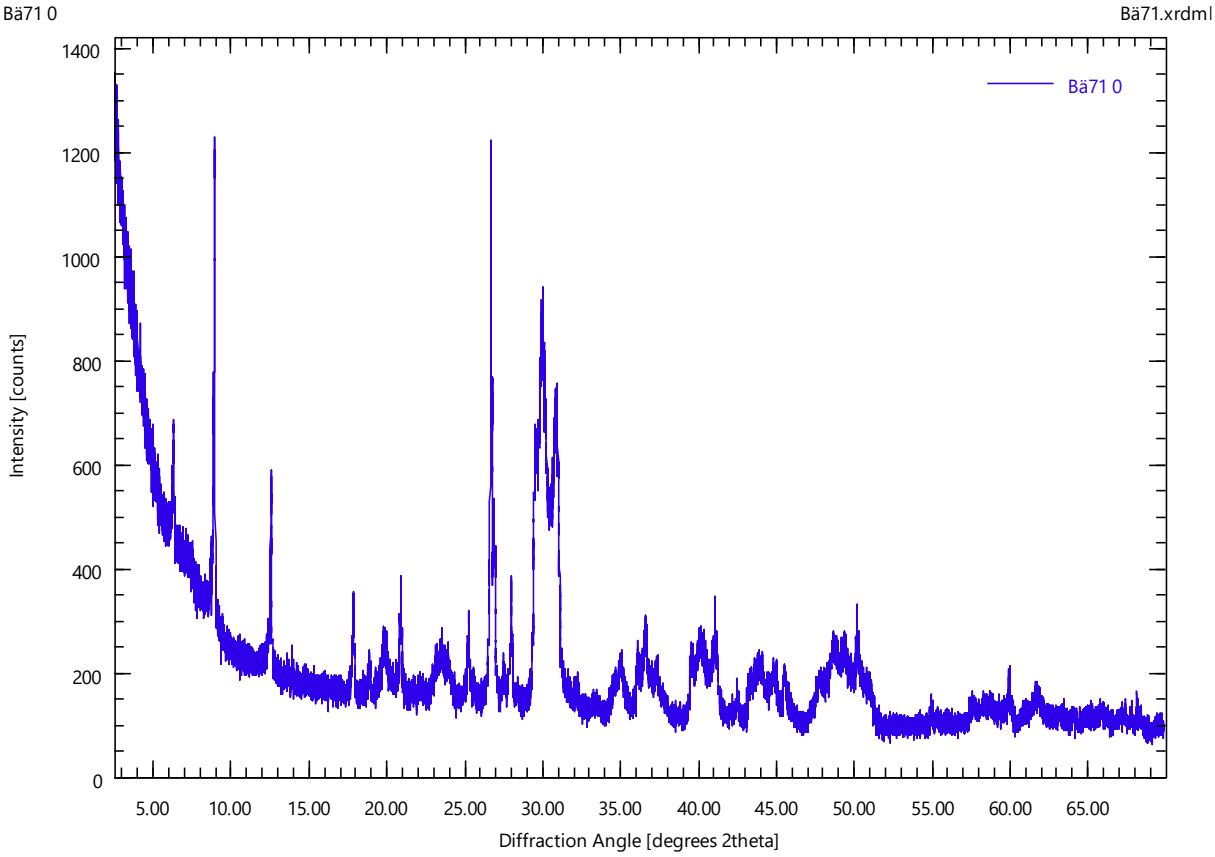
Bä71 0
Bä71.xrdml
Bä71 0
Intensity [counts]
Diffraction Angle [degrees 2theta]
0
200
400
600
800
1000
1200
1400
5.00
10.00
15.00
20.00
25.00
30.00
35.00
40.00
45.00
50.00
55.00
60.00
65.00

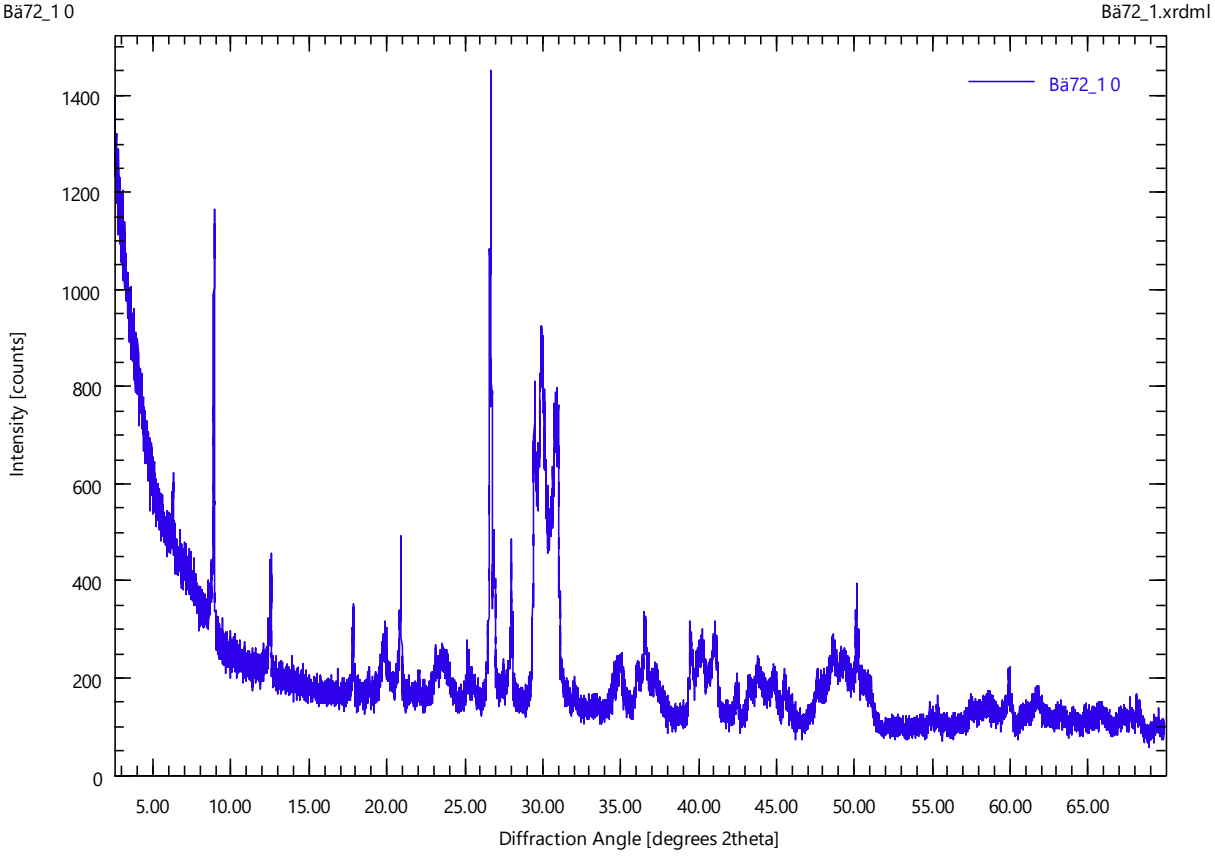
Bä72_1 0
Bä72_1.xrdml
Bä72_1 0
Intensity [counts]
Diffraction Angle [degrees 2theta]
0
200
400
600
800
1000
1200
1400
5.00
10.00
15.00
20.00
25.00
30.00
35.00
40.00
45.00
50.00
55.00
60.00
65.00

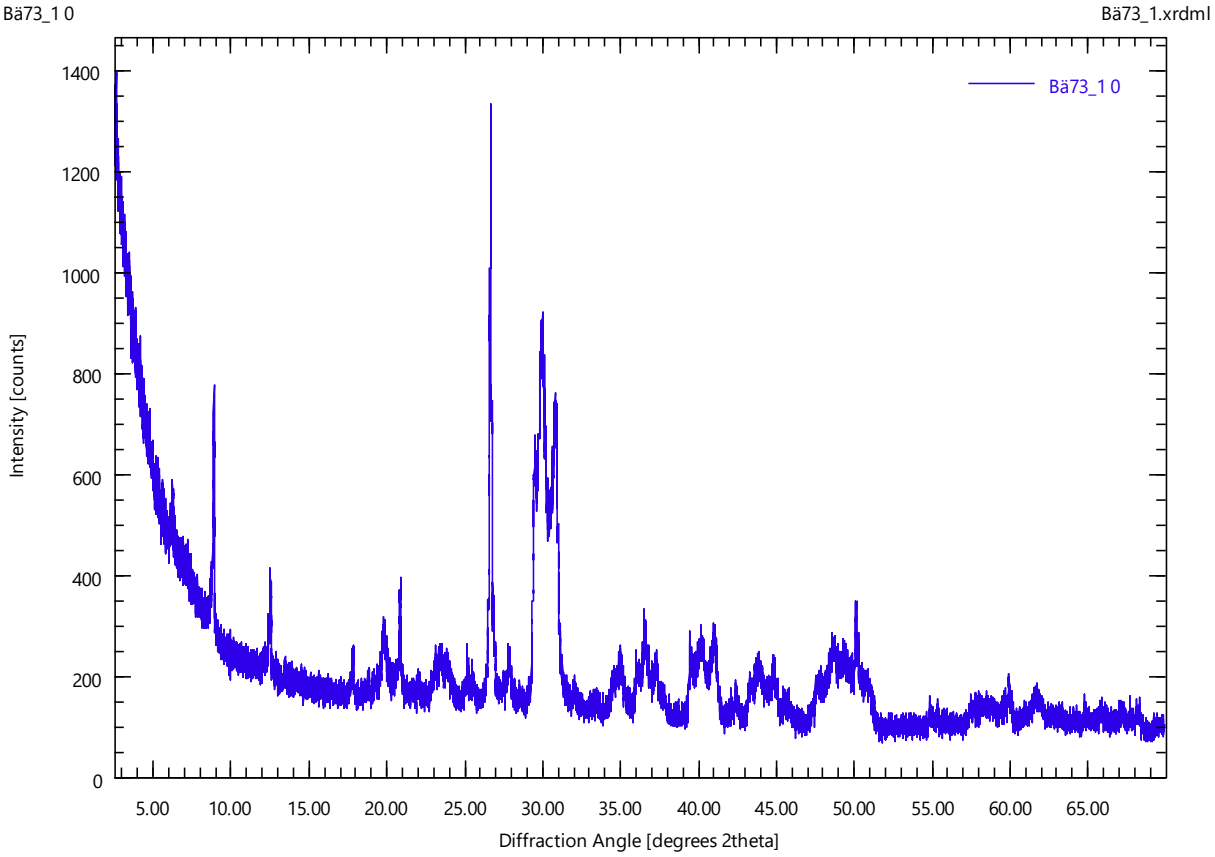
Bä73_1 0
Bä73_1.xrdml
Bä73_1 0
Intensity [counts]
Diffraction Angle [degrees 2theta]
0
200
400
600
800
1000
1200
1400
5.00
10.00
15.00
20.00
25.00
30.00
35.00
40.00
45.00
50.00
55.00
60.00
65.00

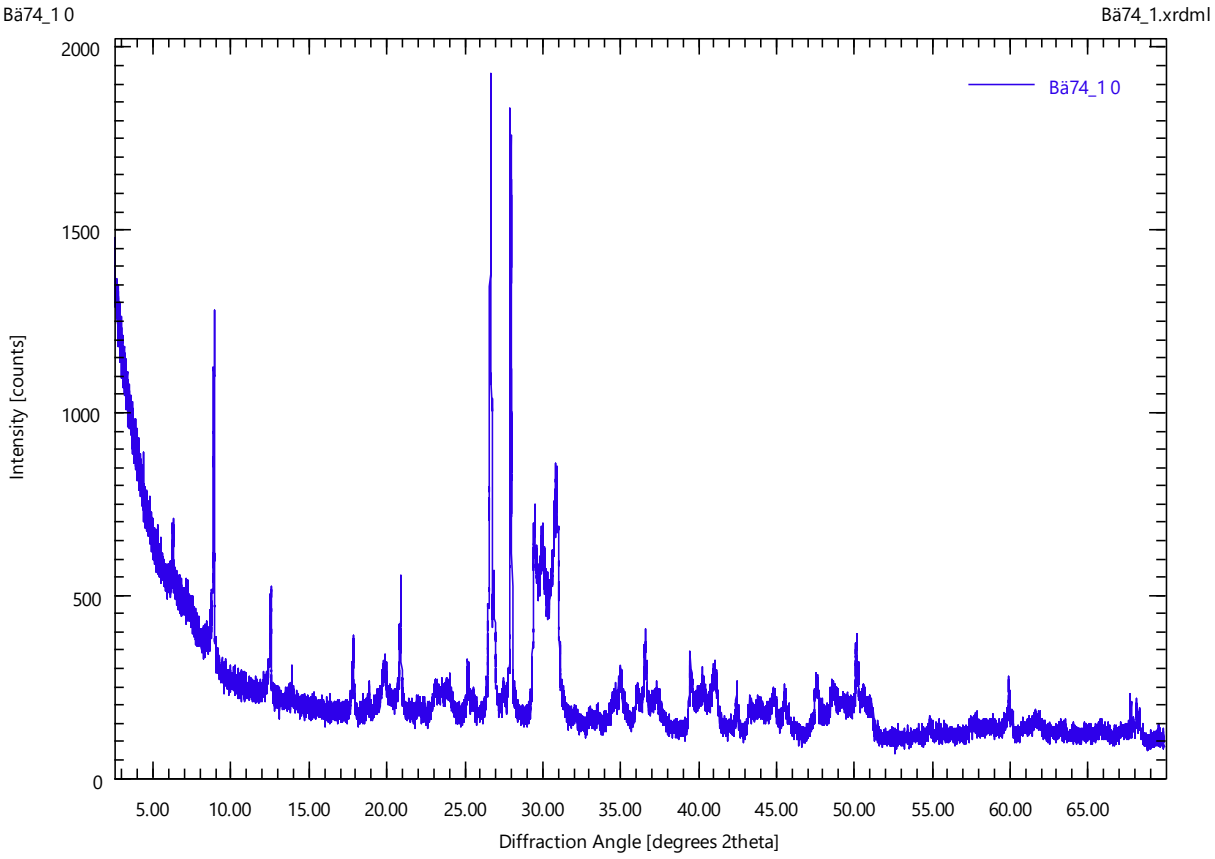
Bä74_1 0
Bä74_1.xrdml
Bä74_1 0
Intensity [counts]
Diffraction Angle [degrees 2theta]
0
500
1000
1500
2000
5.00
10.00
15.00
20.00
25.00
30.00
35.00
40.00
45.00
50.00
55.00
60.00
65.00

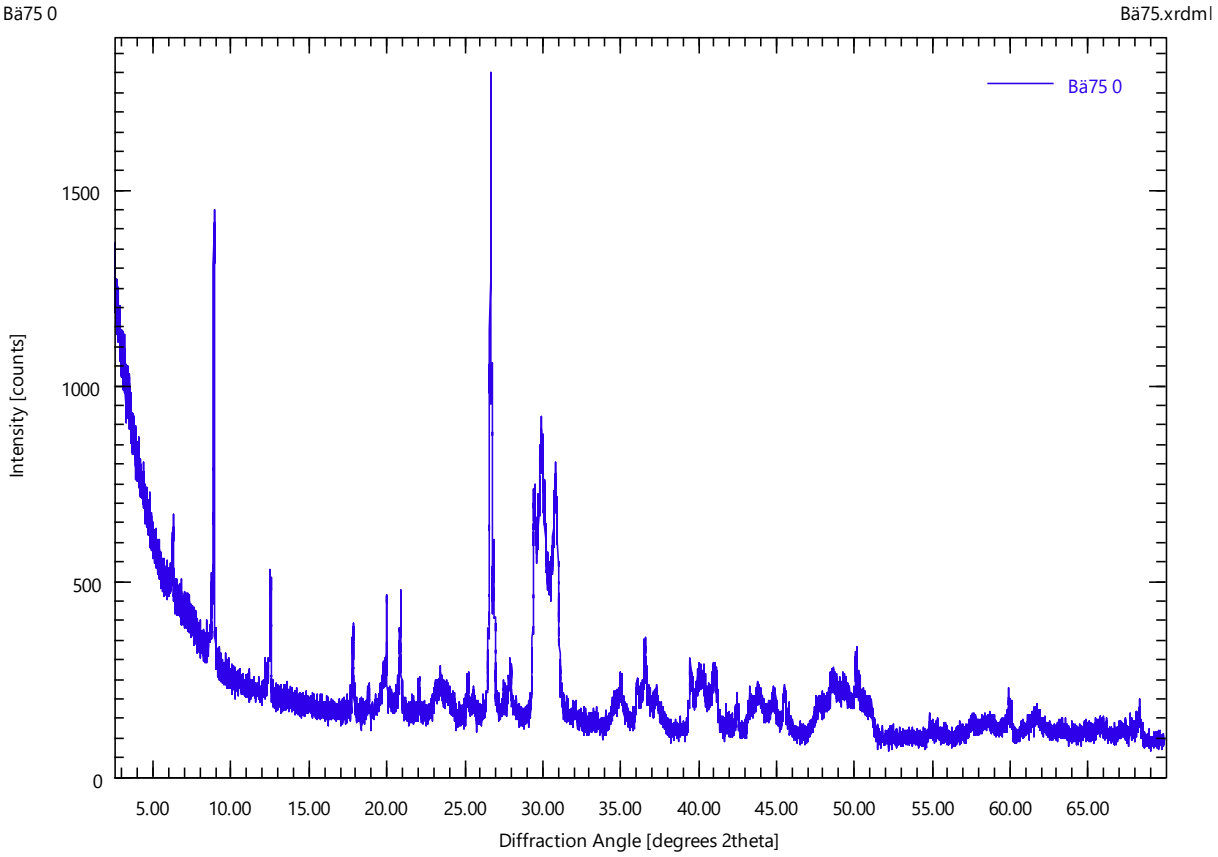
Bä75 0
Bä75.xrdml
Bä75 0
Intensity [counts]
0
500
1000
1500
5.00
10.00
15.00
20.00
25.00
30.00
35.00
40.00
45.00
50.00
55.00
60.00
65.00
Diffraction Angle [degrees 2theta]

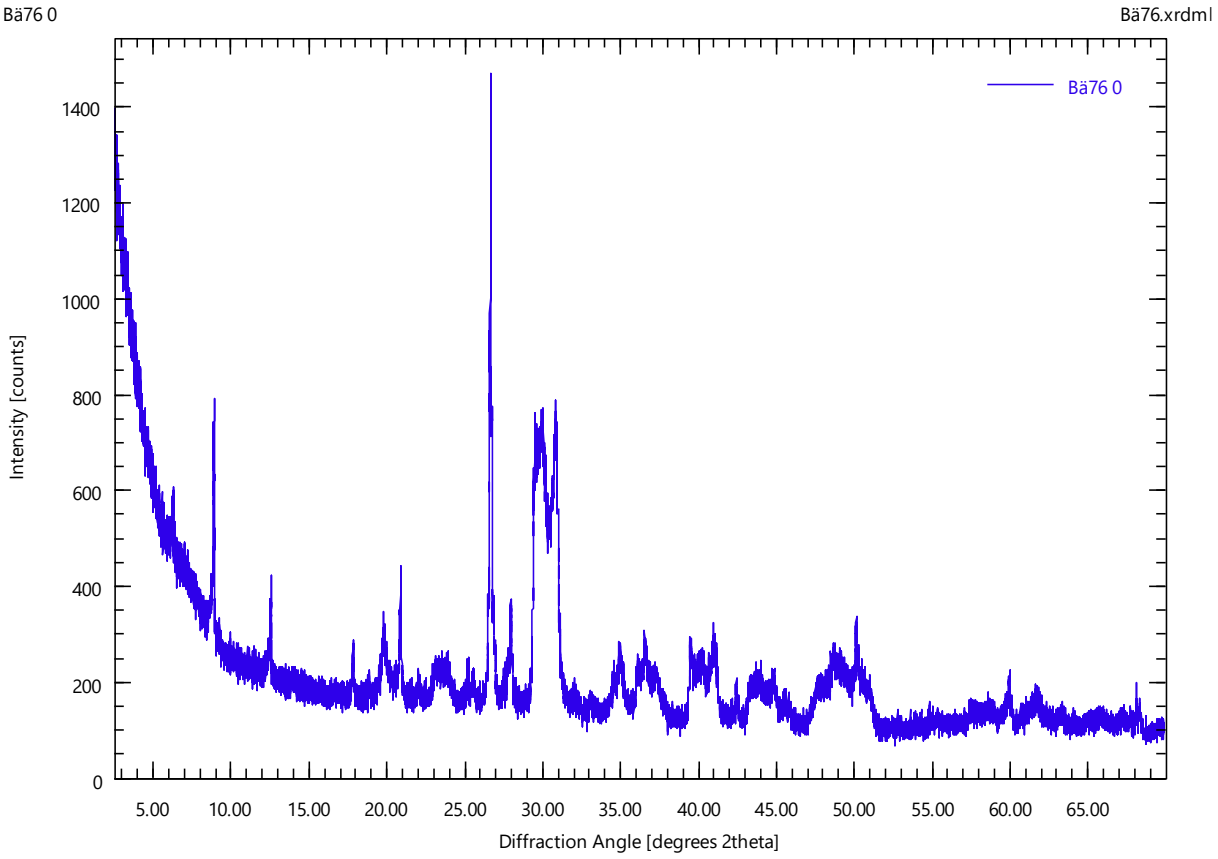
Bä76 0
Bä76.xrdml
Bä76 0
Intensity [counts]
0
200
400
600
800
1000
1200
1400
5.00
10.00
15.00
20.00
25.00
30.00
35.00
40.00
45.00
50.00
55.00
60.00
65.00
Diffraction Angle [degrees 2theta]

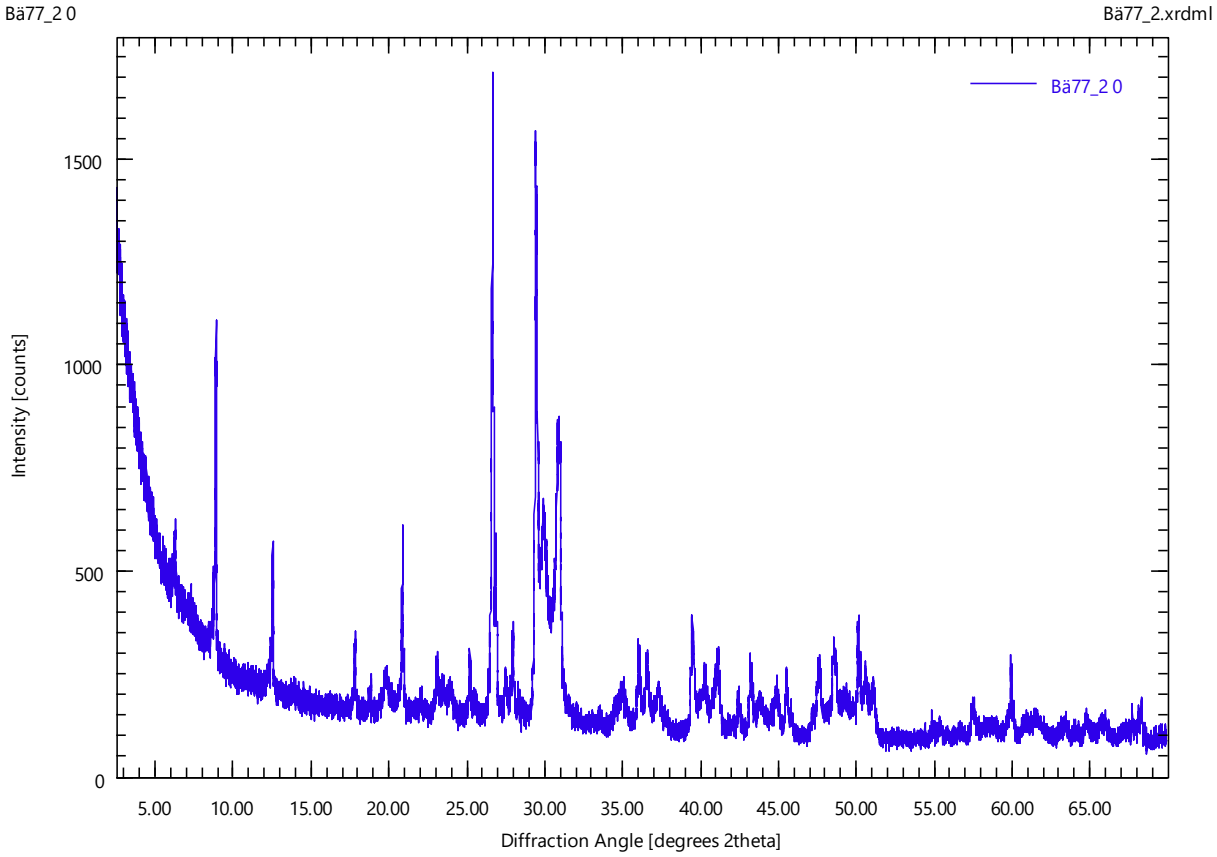
Bä77_2 0
Bä77_2.xrdml
Bä77_2 0
Intensity [counts]
0
500
1000
1500
5.00
10.00
15.00
20.00
25.00
30.00
35.00
40.00
45.00
50.00
55.00
60.00
65.00
Diffraction Angle [degrees 2theta]

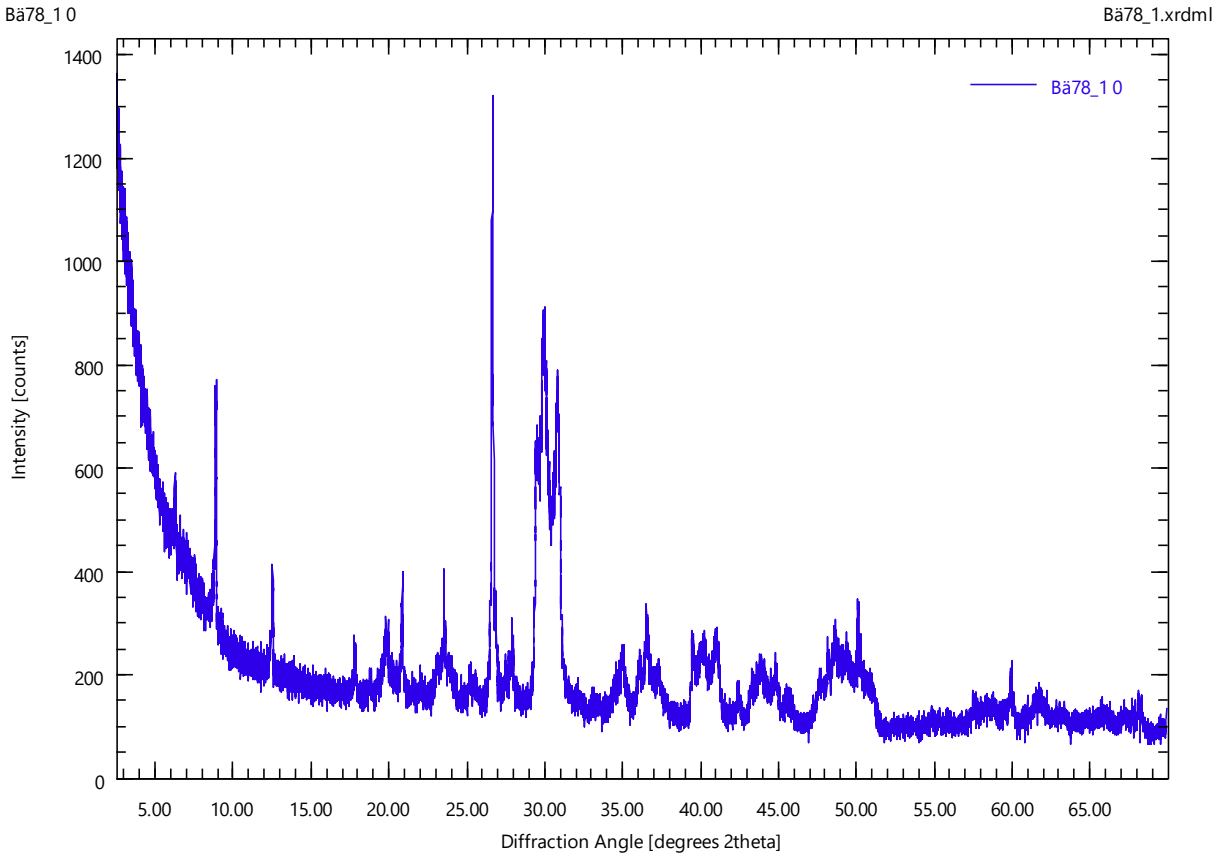
Bä78_1 0
Bä78_1.xrdml
Bä78_1 0
Intensity [counts]
0
200
400
600
800
1000
1200
1400
5.00
10.00
15.00
20.00
25.00
30.00
35.00
40.00
45.00
50.00
55.00
60.00
65.00
Diffraction Angle [degrees 2theta]

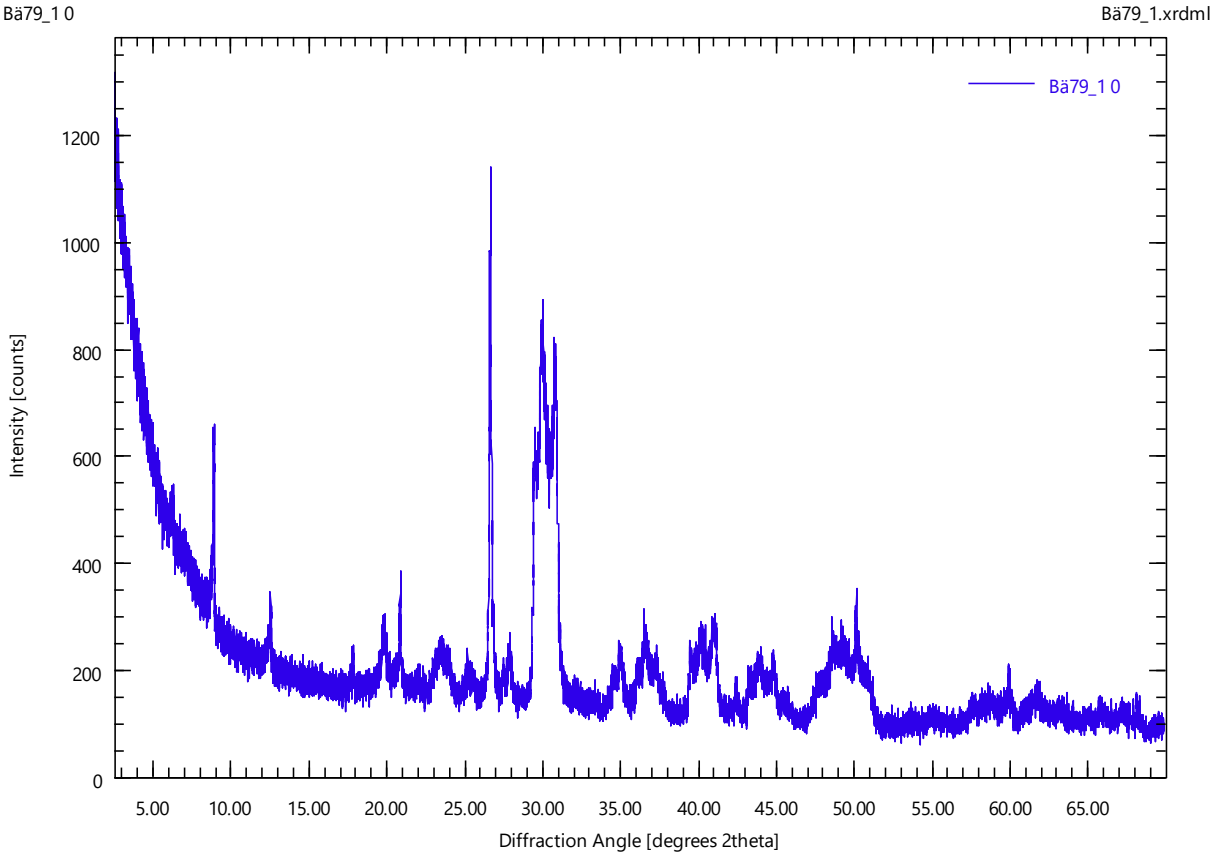
Bä79_1 0
Bä79_1.xrdml
Bä79_1 0
Intensity [counts]
0
200
400
600
800
1000
1200
5.00
10.00
15.00
20.00
25.00
30.00
35.00
40.00
45.00
50.00
55.00
60.00
65.00
Diffraction Angle [degrees 2theta]

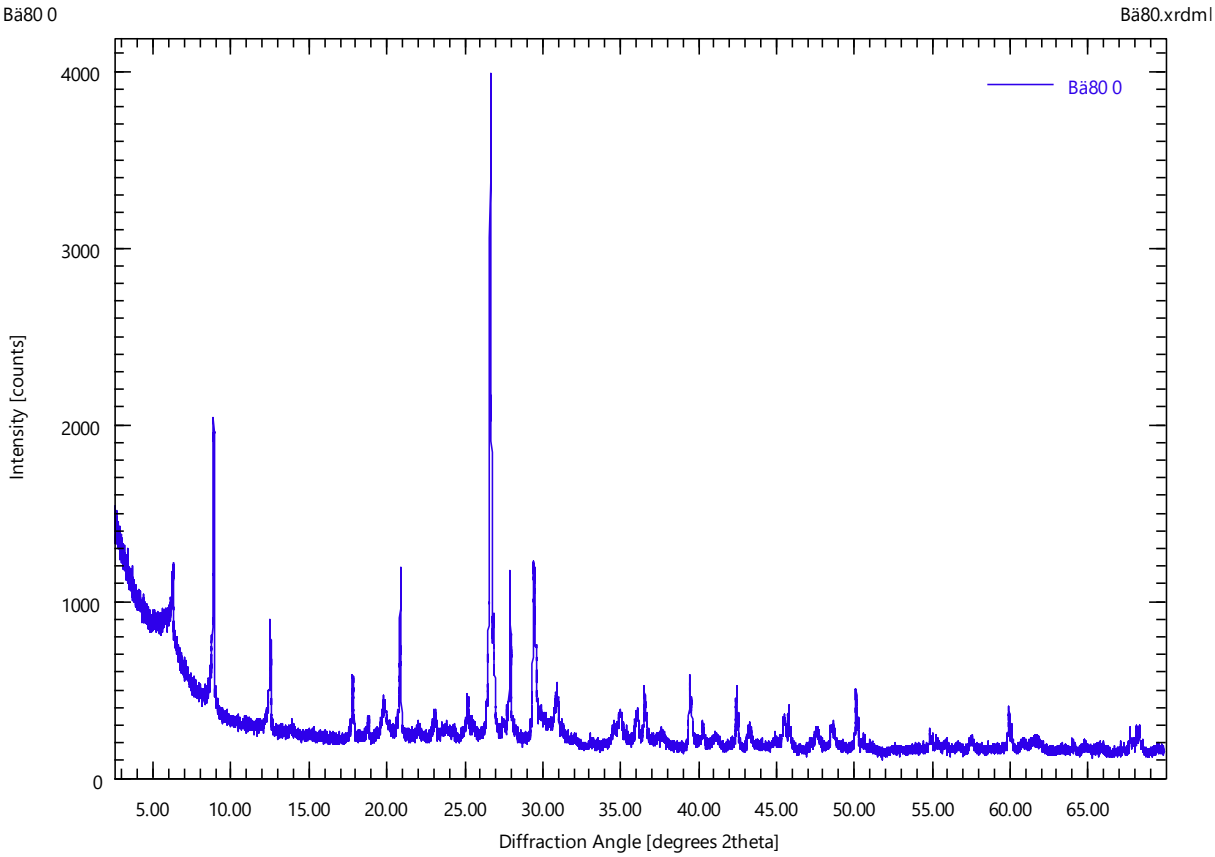
Bä80 0
Bä80.xrdml
Bä80 0
Intensity [counts]
0
1000
2000
3000
4000
5.00
10.00
15.00
20.00
25.00
30.00
35.00
40.00
45.00
50.00
55.00
60.00
65.00
Diffraction Angle [degrees 2theta]

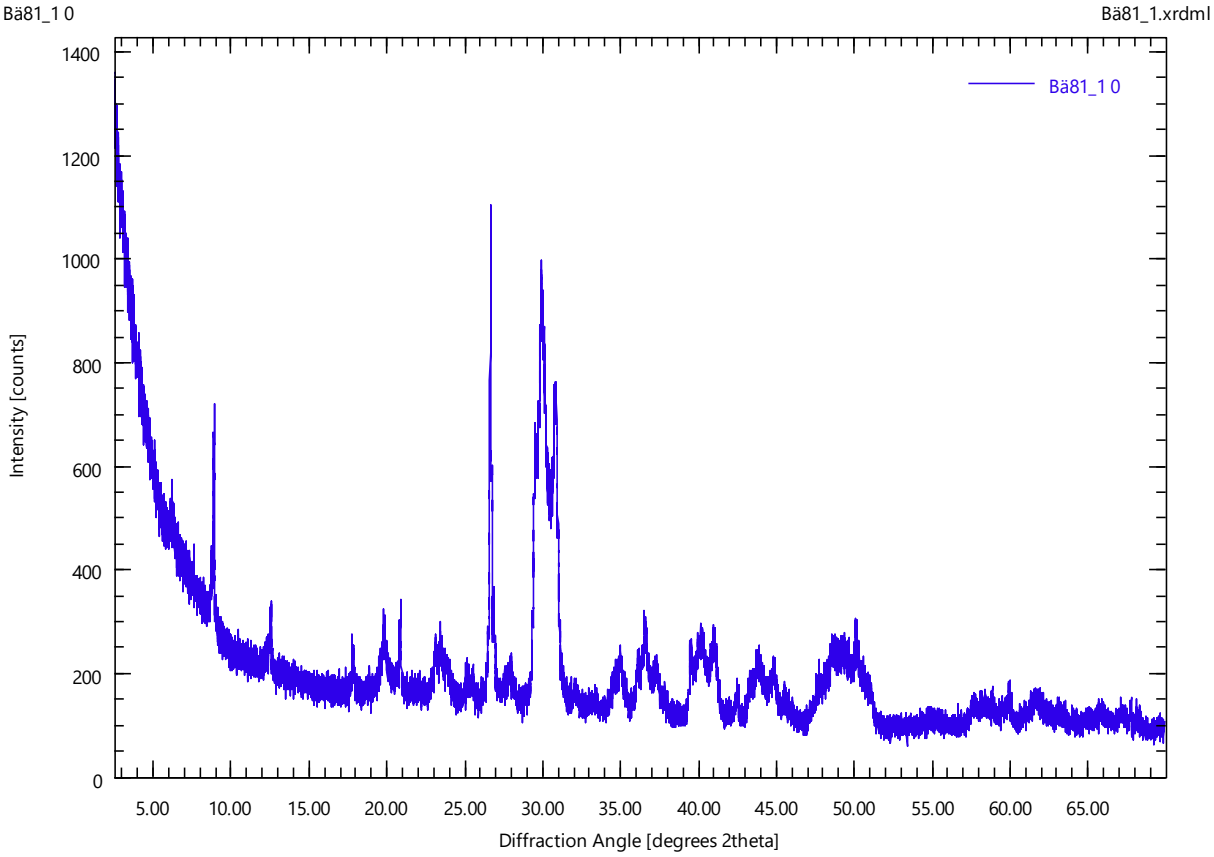
Bä81_1 0
Bä81_1.xrdml
Bä81_1 0
Intensity [counts]
Diffraction Angle [degrees 2theta]
0
200
400
600
800
1000
1200
1400
5.00
10.00
15.00
20.00
25.00
30.00
35.00
40.00
45.00
50.00
55.00
60.00
65.00

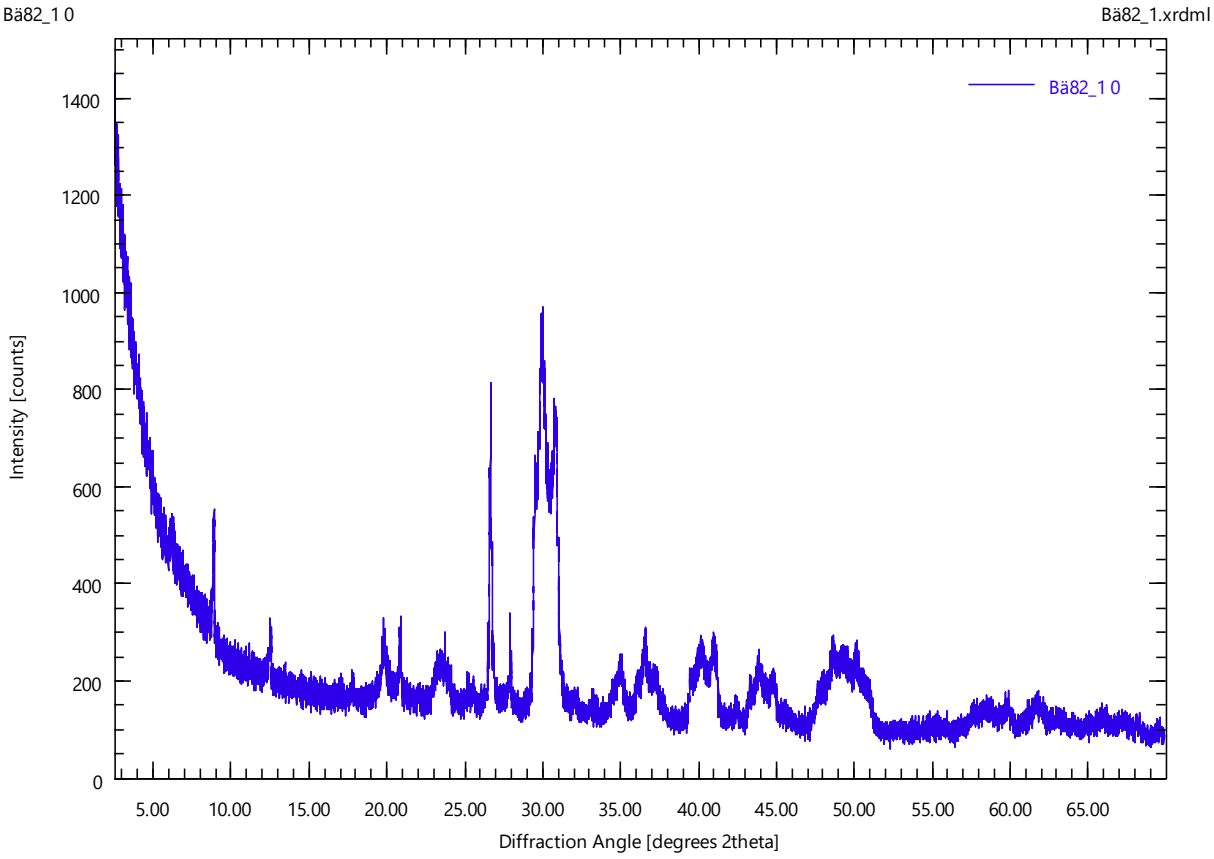
Bä82_1 0
Bä82_1.xrdml
Bä82_1 0
Intensity [counts]
Diffraction Angle [degrees 2theta]
0
200
400
600
800
1000
1200
1400
5.00
10.00
15.00
20.00
25.00
30.00
35.00
40.00
45.00
50.00
55.00
60.00
65.00

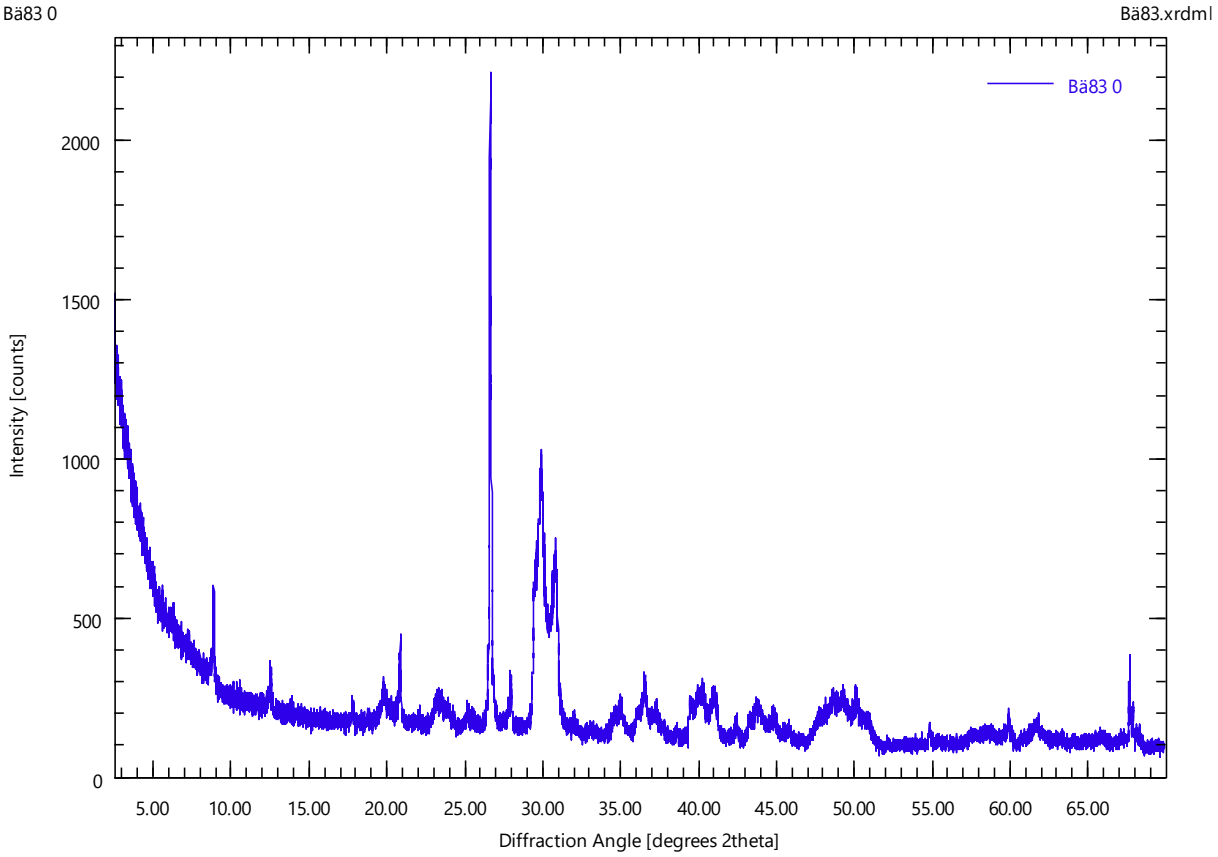
Bä83 0
Bä83.xrdml
Bä83 0
Intensity [counts]
0
500
1000
1500
2000
5.00
10.00
15.00
20.00
25.00
30.00
35.00
40.00
45.00
50.00
55.00
60.00
65.00
Diffraction Angle [degrees 2theta]

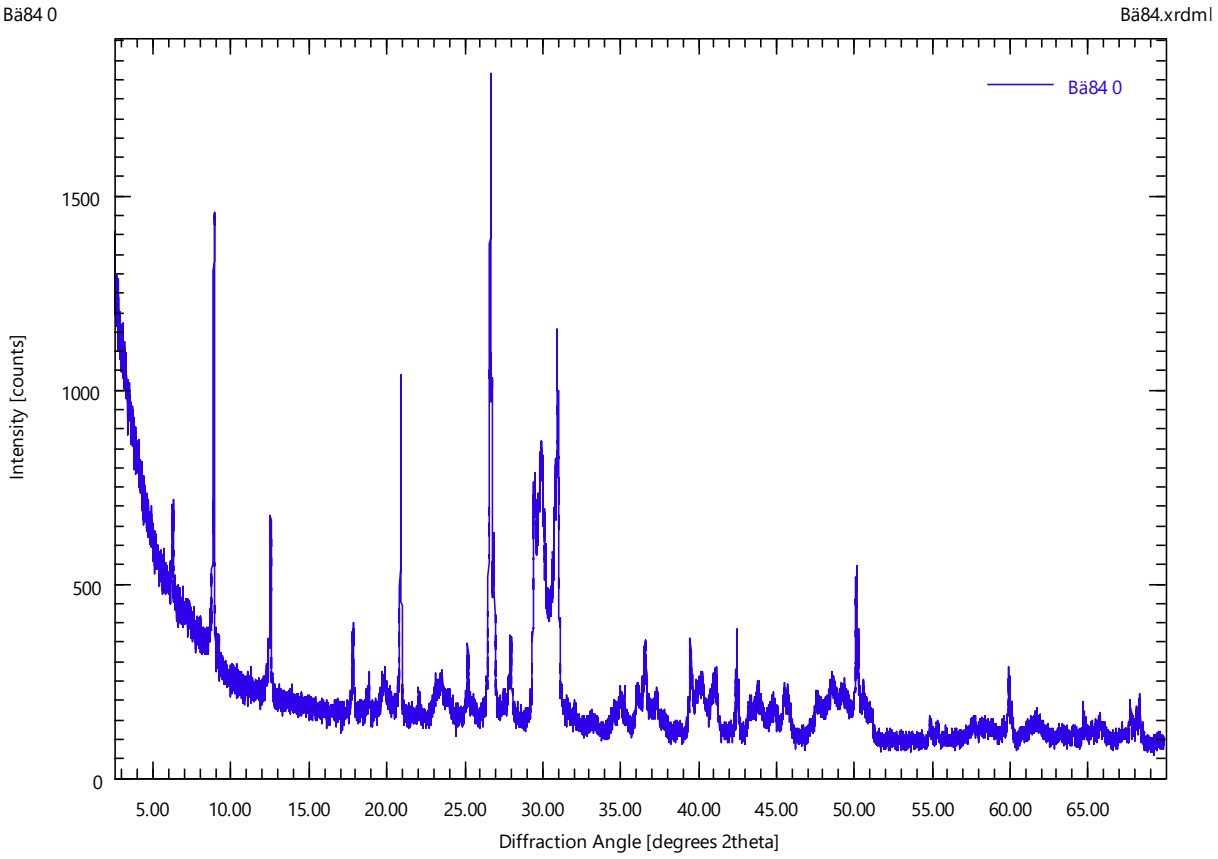
Bä84 0
Bä84.xrdml
Bä84 0
Intensity [counts]
0
500
1000
1500
5.00
10.00
15.00
20.00
25.00
30.00
35.00
40.00
45.00
50.00
55.00
60.00
65.00
Diffraction Angle [degrees 2theta]

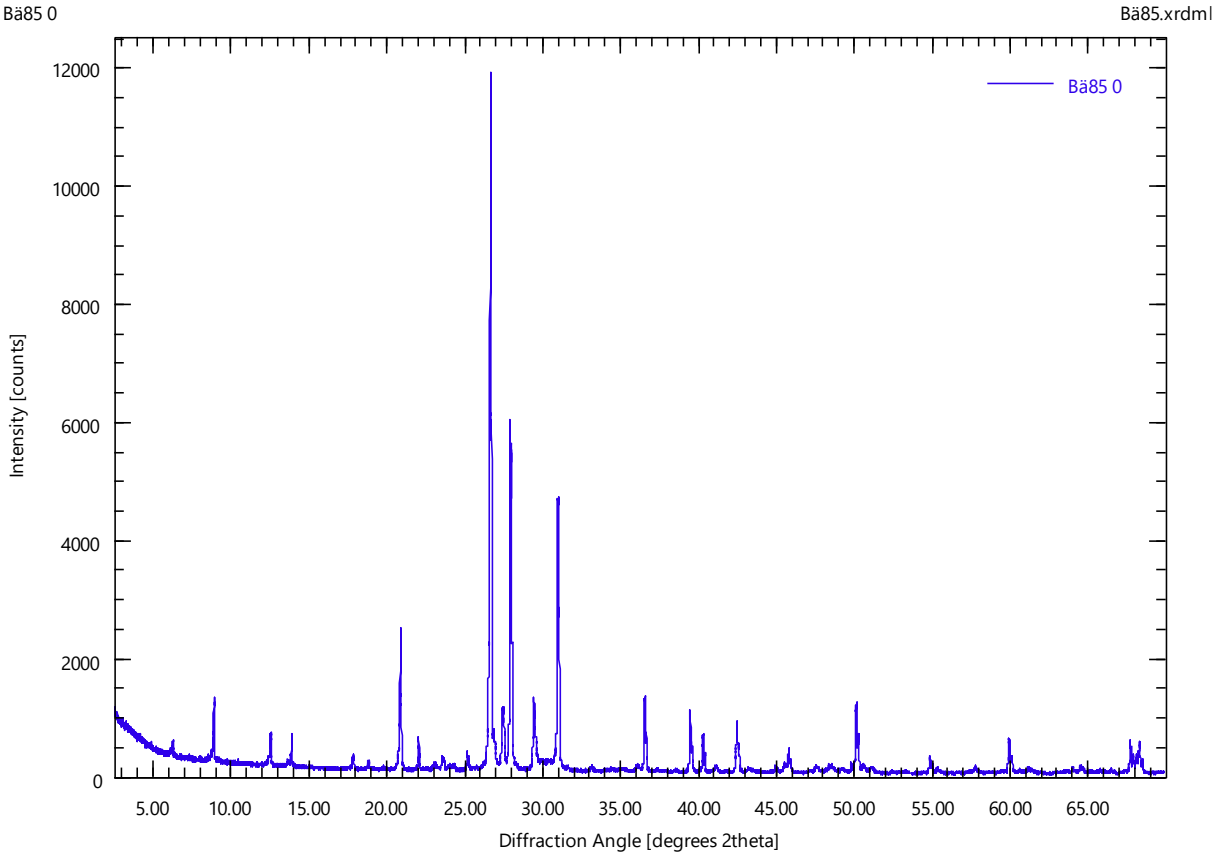
Bä85 0
Bä85.xrdml
Bä85 0
Intensity [counts]
Diffraction Angle [degrees 2theta]

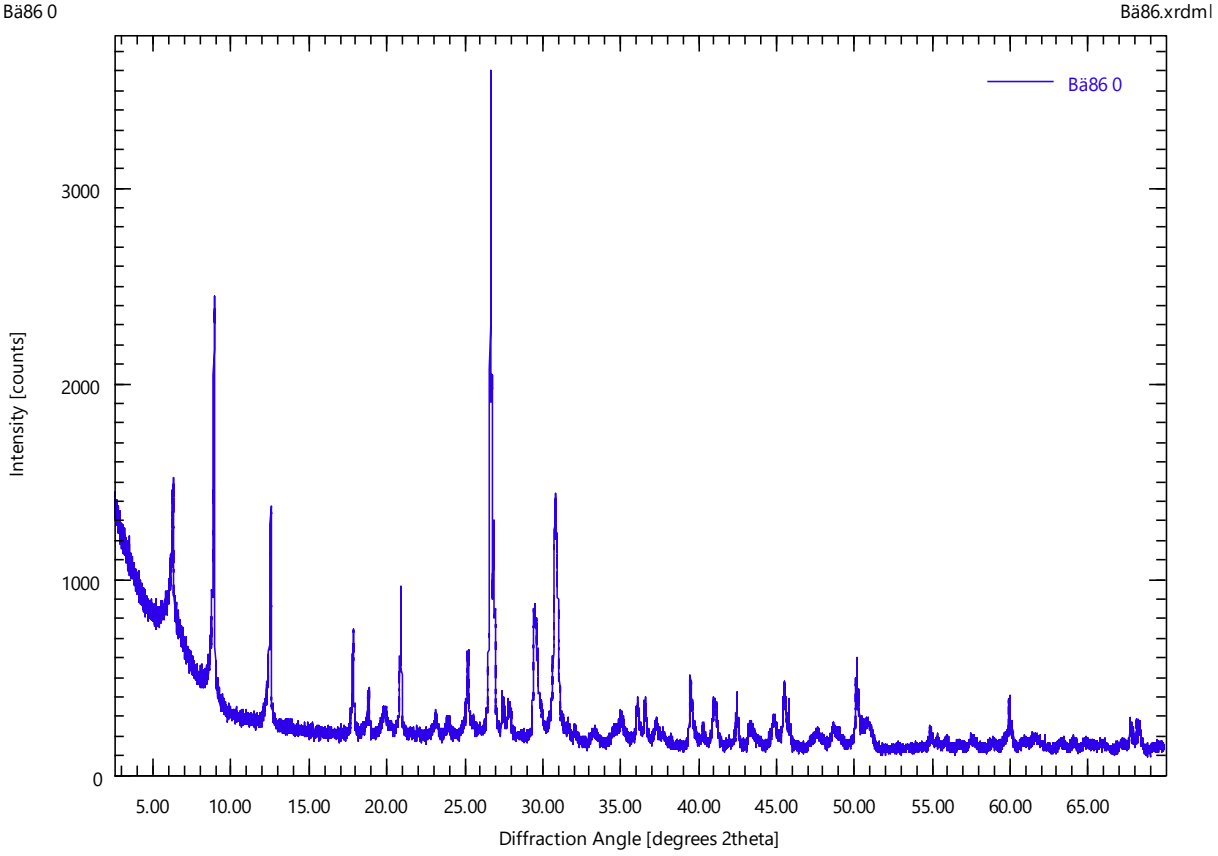
Bä86 0
Bä86.xrdml
Bä86 0
Intensity [counts]
Diffraction Angle [degrees 2theta]

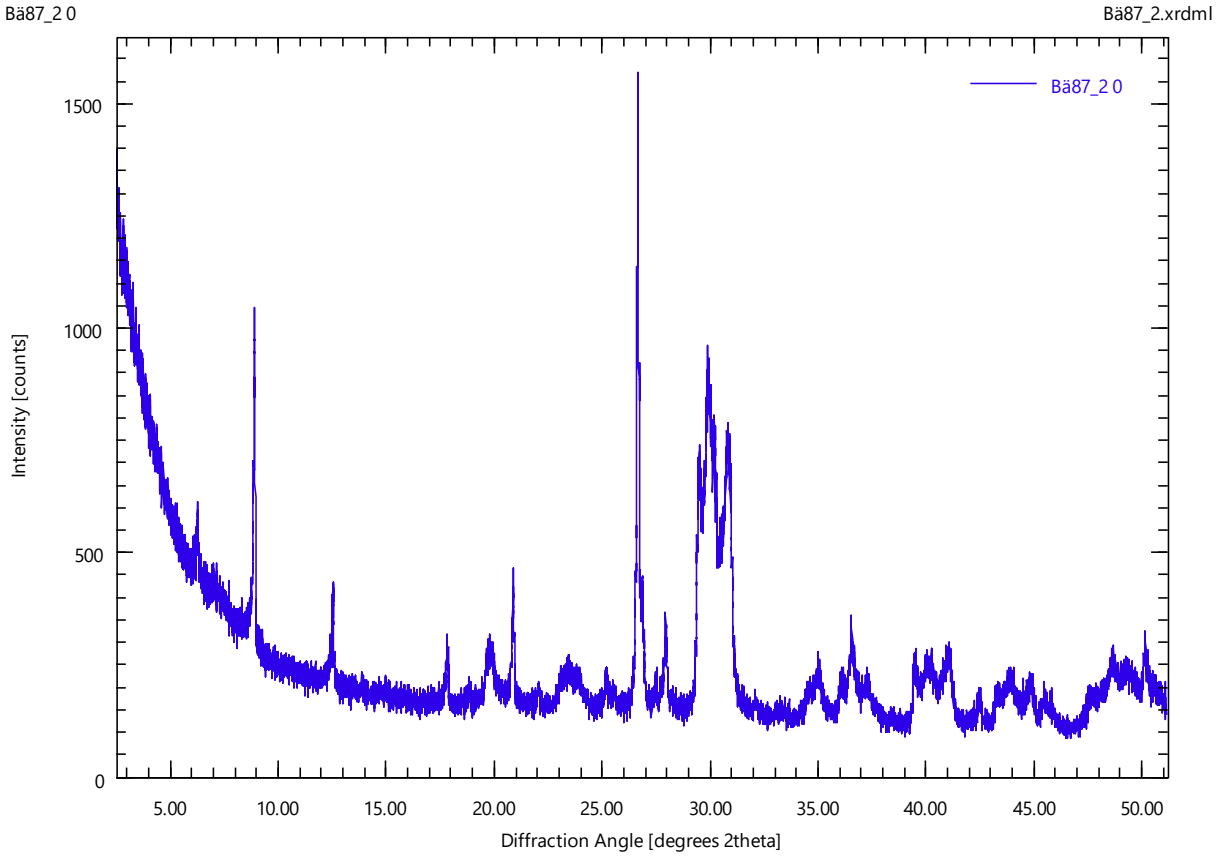
Bä87_2 0
Bä87_2.xrdml
Bä87_2 0
Intensity [counts]
0
500
1000
1500
5.00
10.00
15.00
20.00
25.00
30.00
35.00
40.00
45.00
50.00
Diffraction Angle [degrees 2theta]

II. X-ray Diffractograms textured mounts

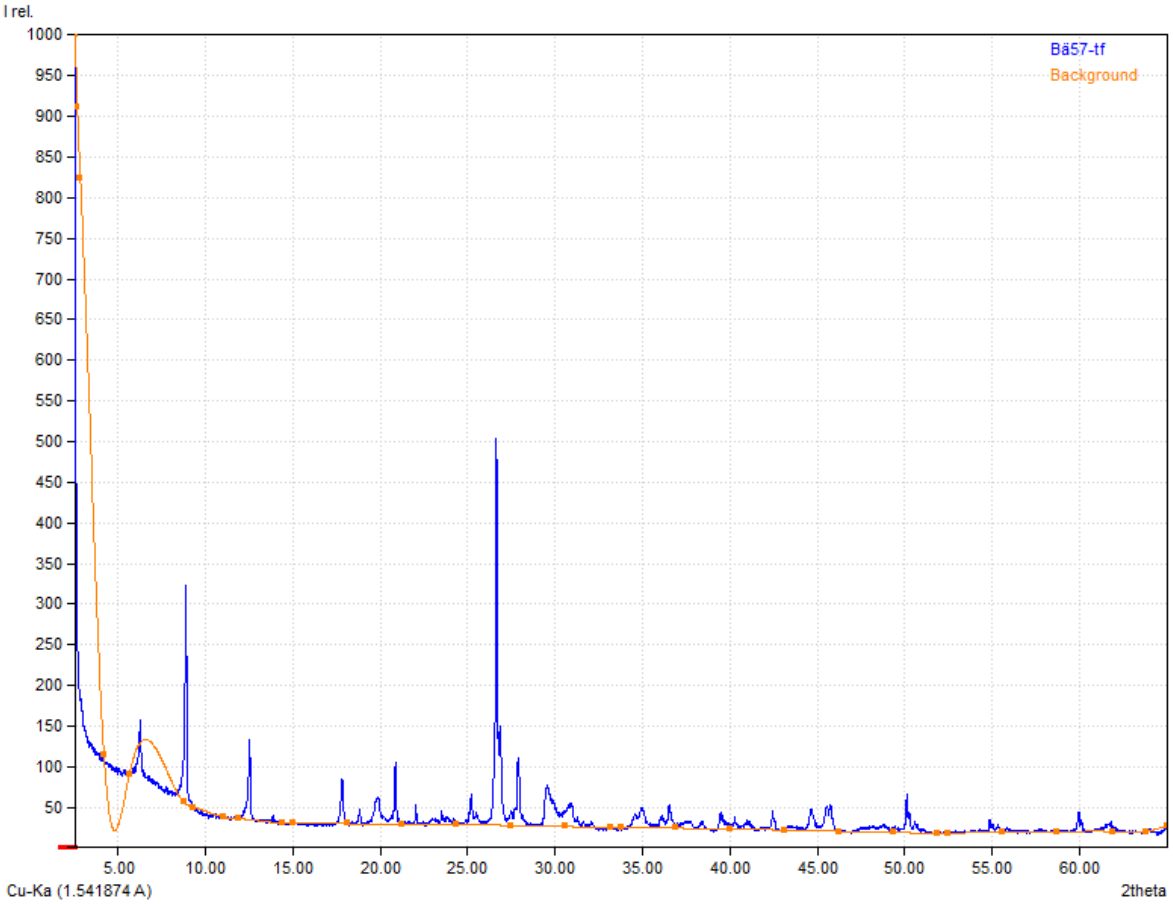
I rel.
Bä57-tf
Background
Cu-Ka (1.541874 A)
2theta

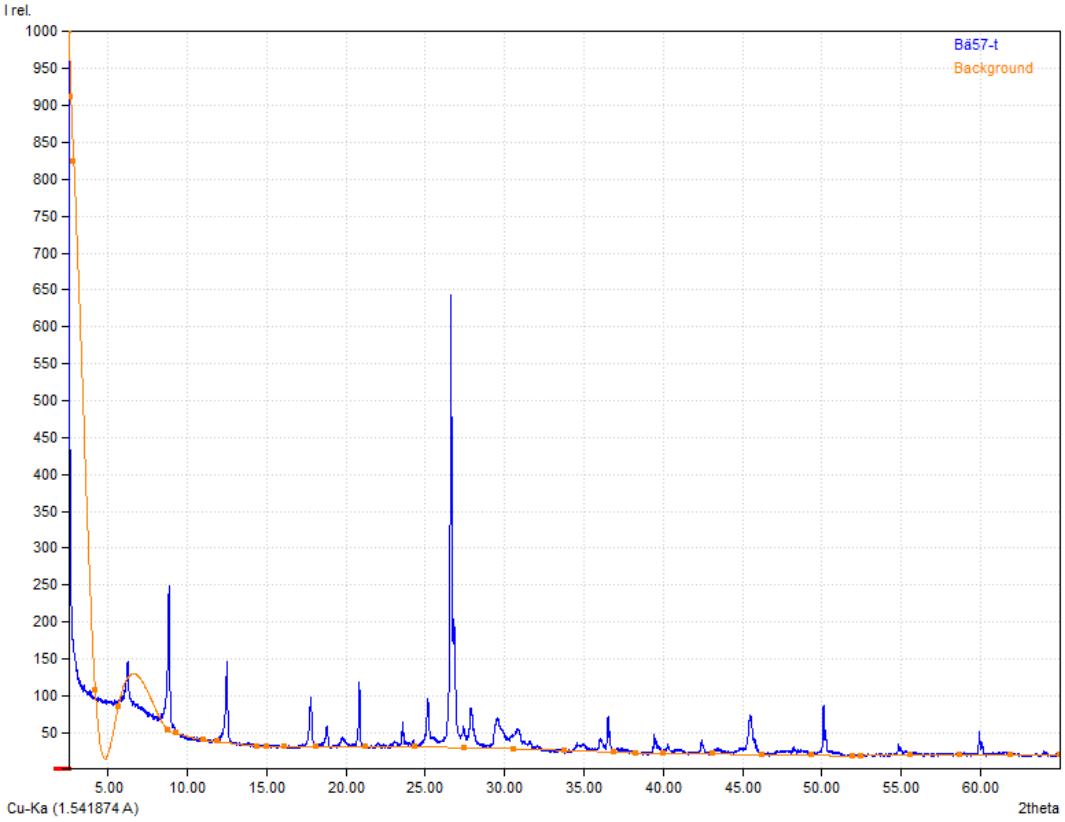
I rel.
Bä57-t
Background
Cu-Ka (1.541874 A)
2theta

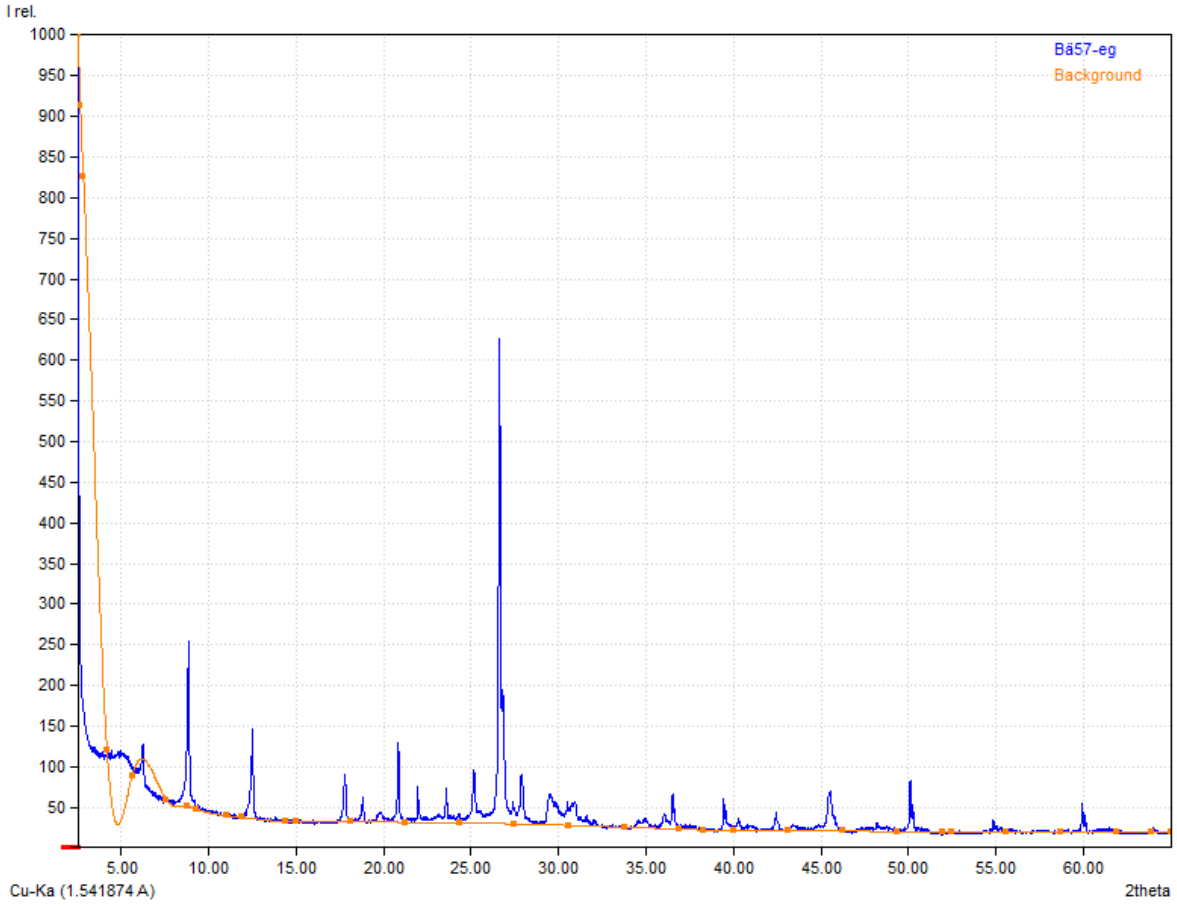
I rel.
Bä57-eg
Background
Cu-Ka (1.541874 A)
2theta

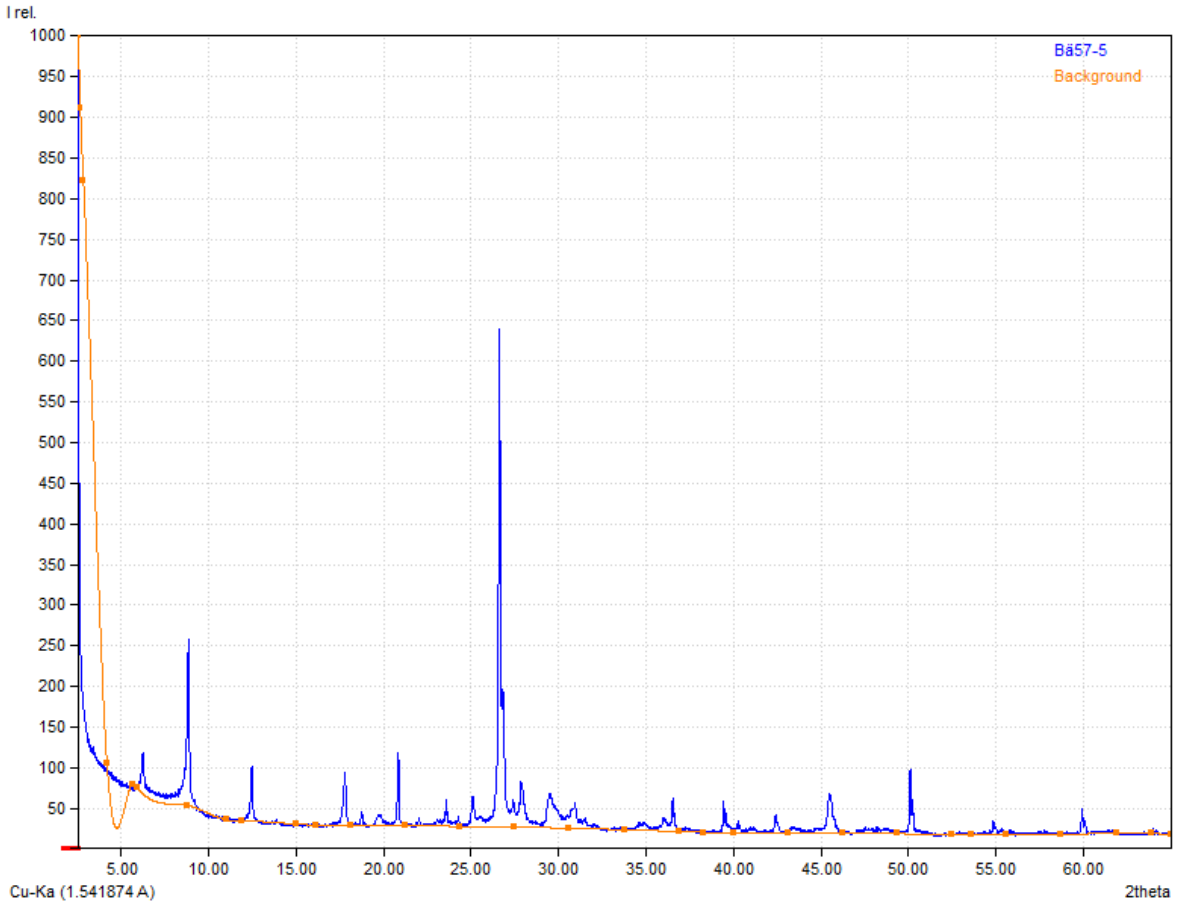
I rel.
Bä57-5
Background
Cu-Ka (1.541874 A)
2theta

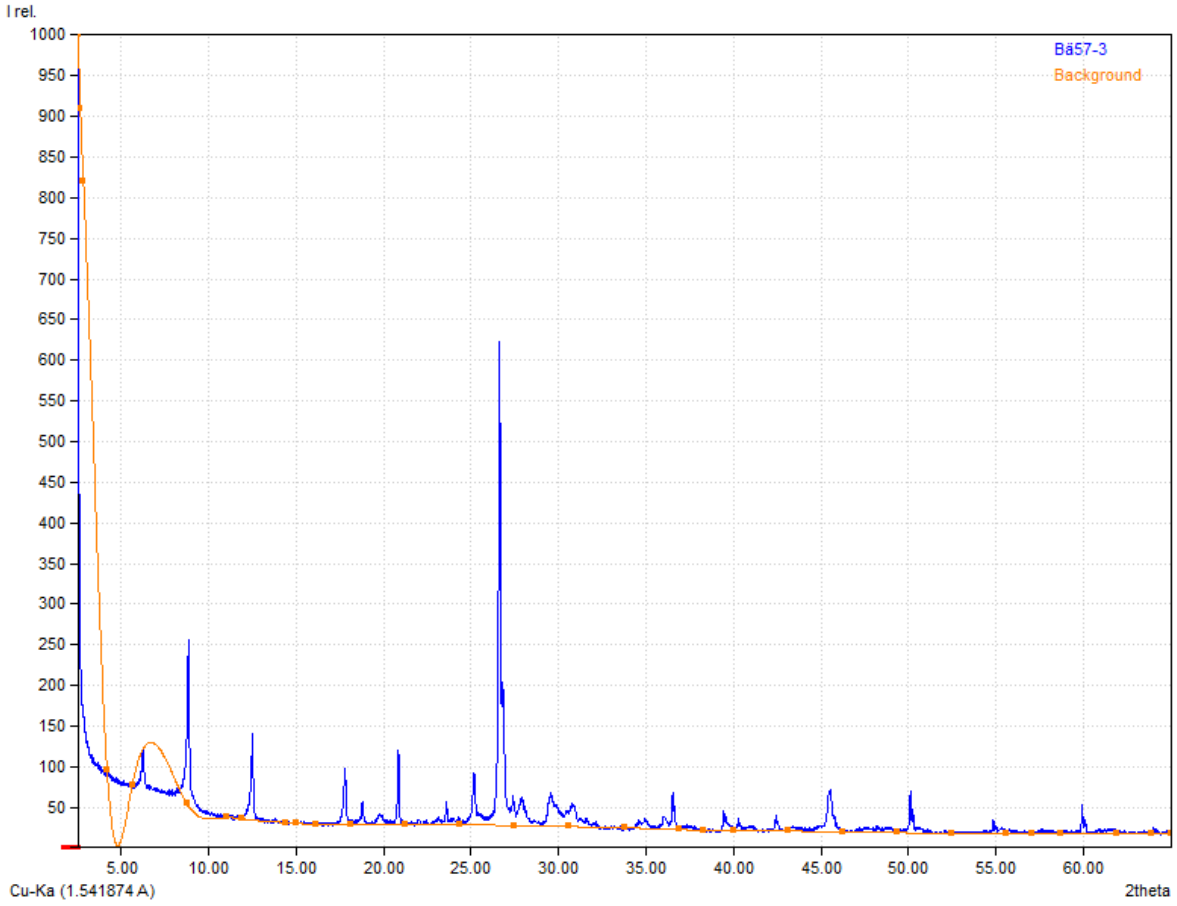
I rel.
Bä57-3
Background
Cu-Ka (1.541874 A)
2theta

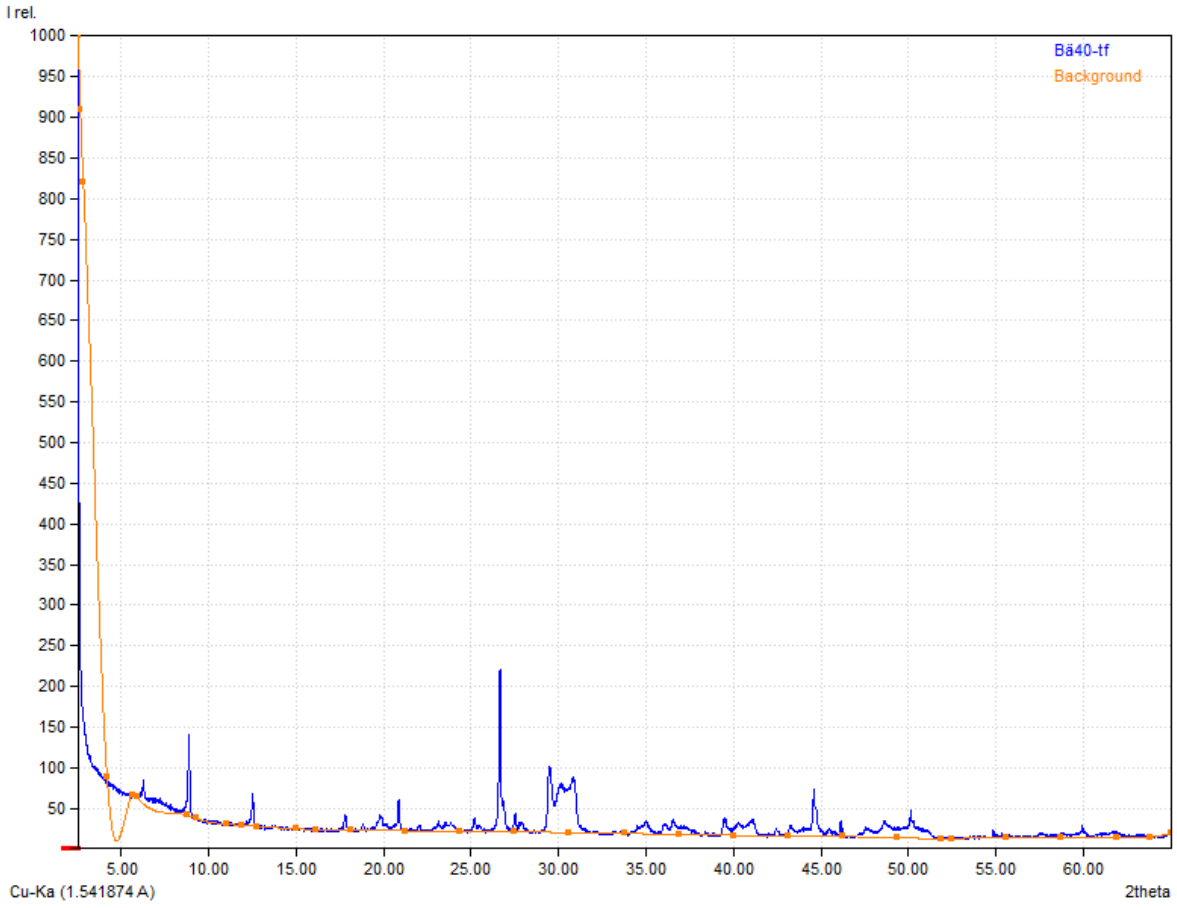
I rel.
Bä40-tf
Background
Cu-Ka (1.541874 A)
2theta

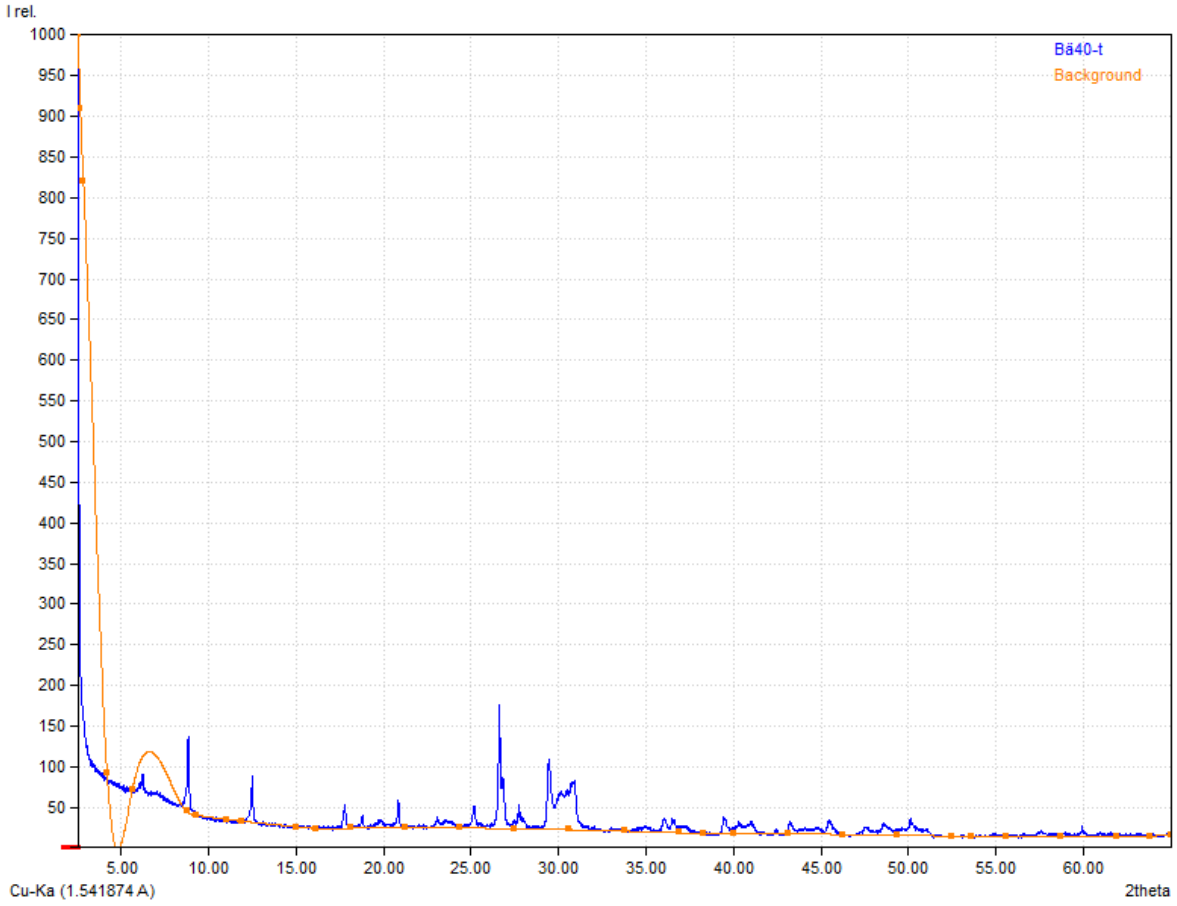
I rel.
Bä40-t
Background
Cu-Ka (1.541874 A)
2theta

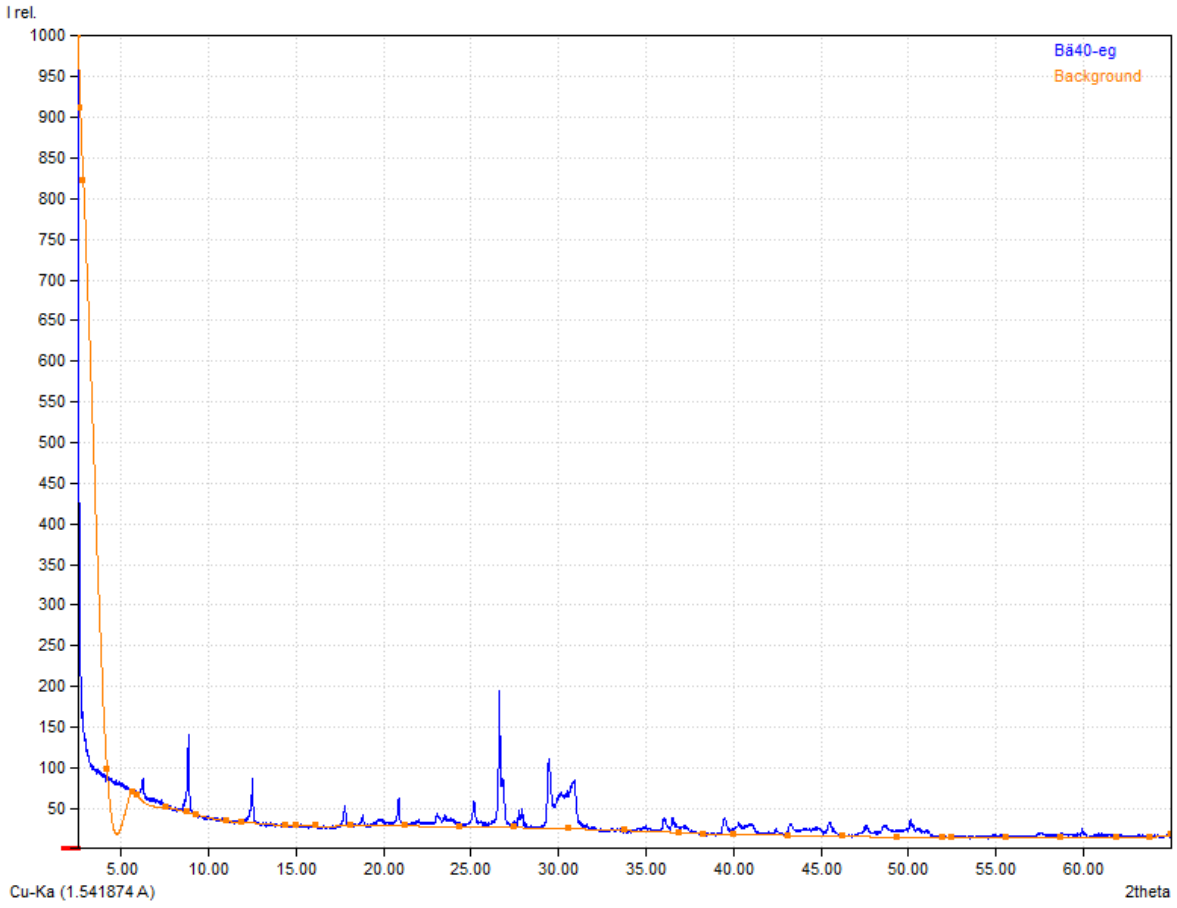
I rel.
Bä40-eg
Background
Cu-Ka (1.541874 A)
2theta

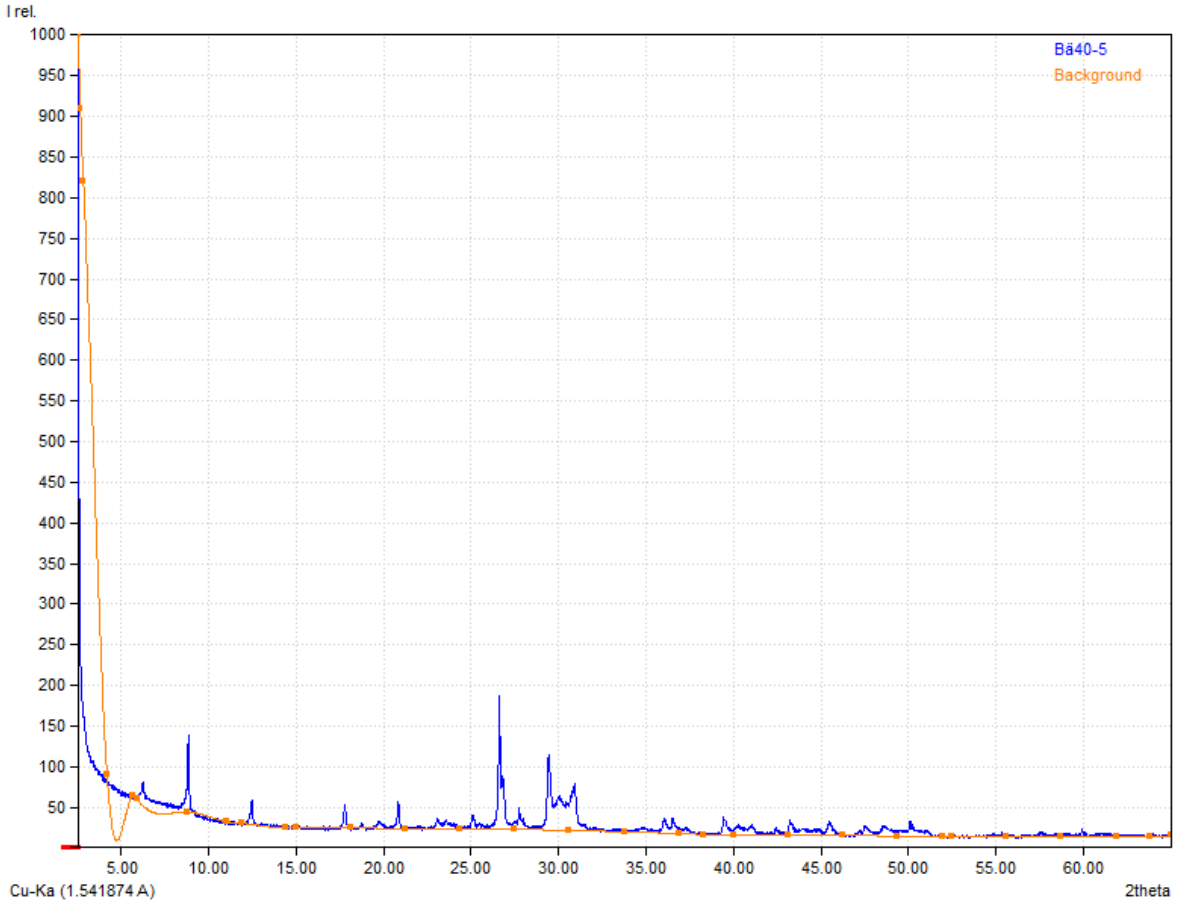
I rel.
Bä40-5
Background
Cu-Ka (1.541874 A)
2theta

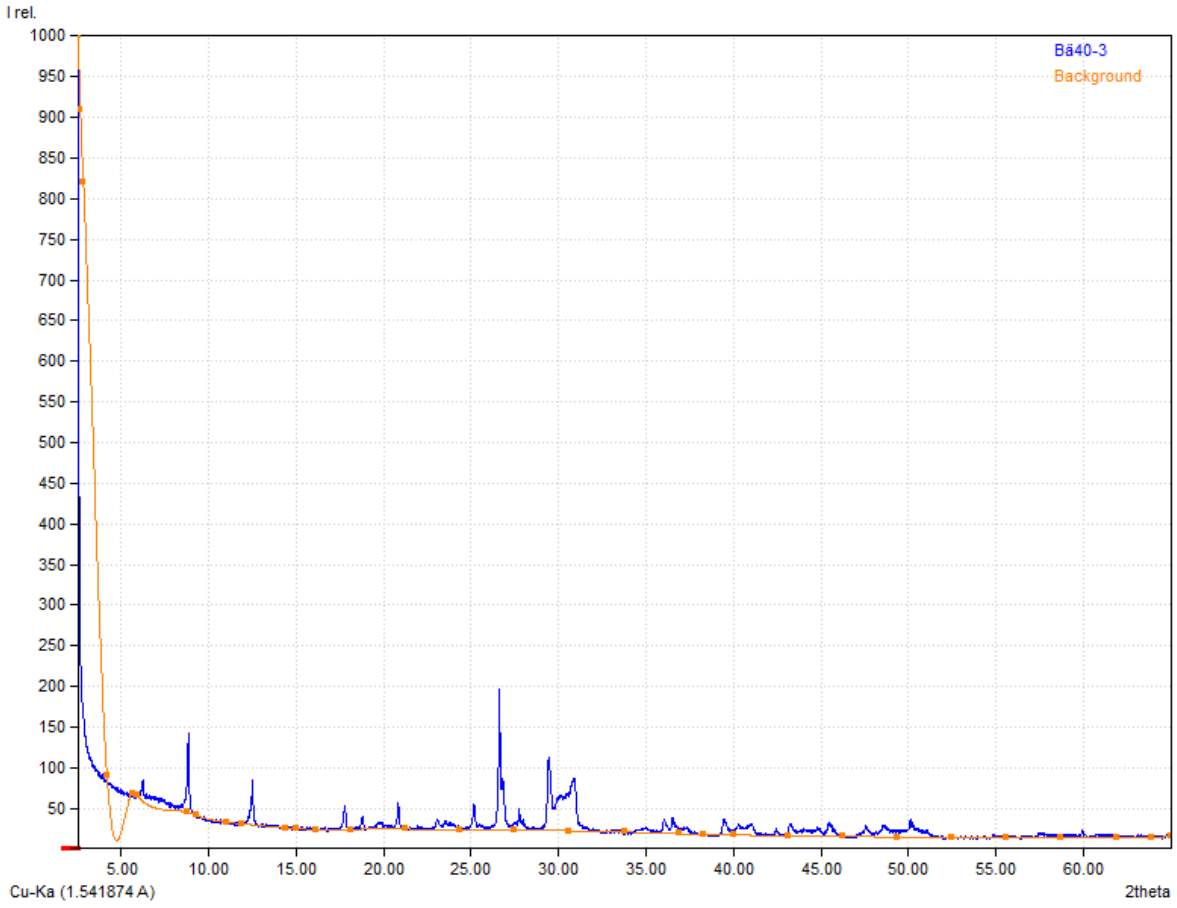
I rel.
Bä40-3
Background
Cu-Ka (1.541874 A)
2theta

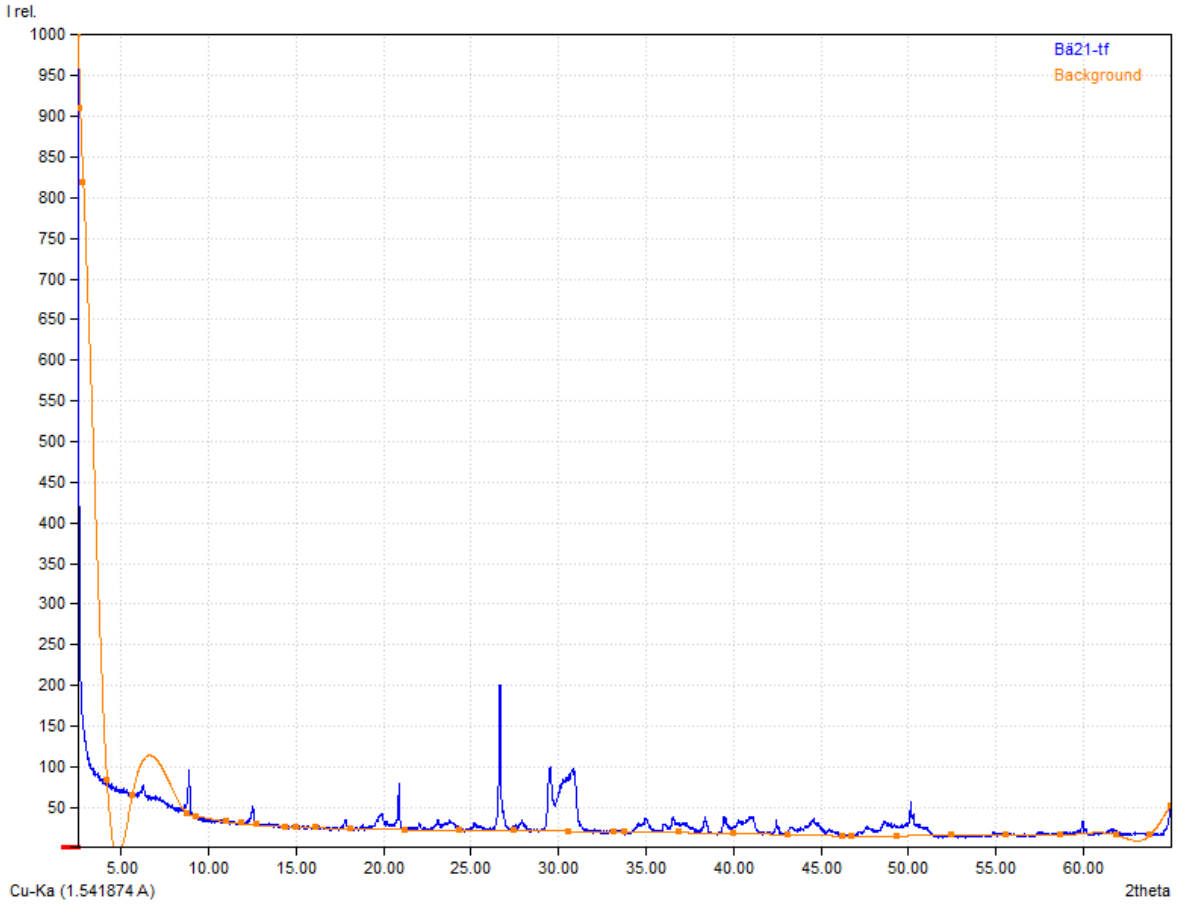
I rel.
Bä21-tf
Background
Cu-Ka (1.541874 A)
2theta

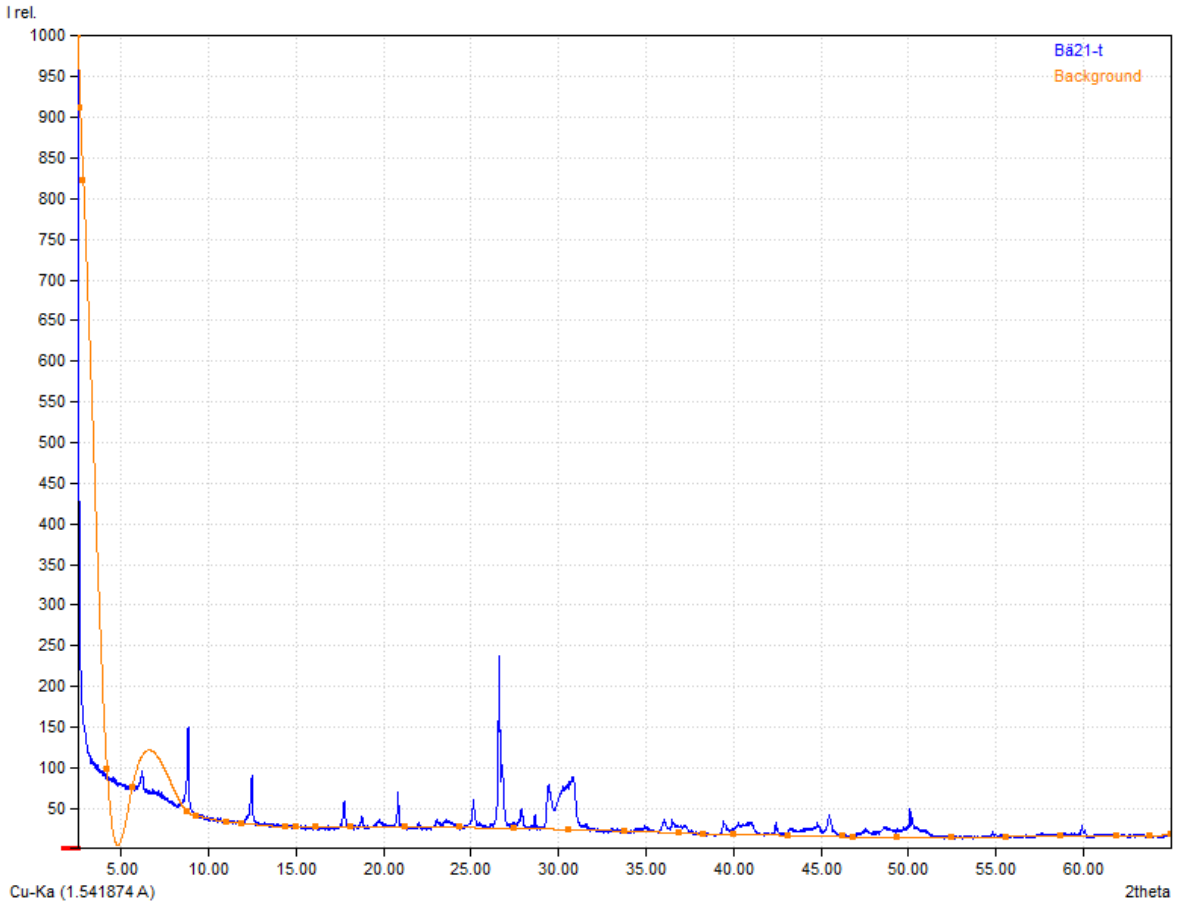
I rel.
Bä21-t
Background
Cu-Ka (1.541874 A)
2theta

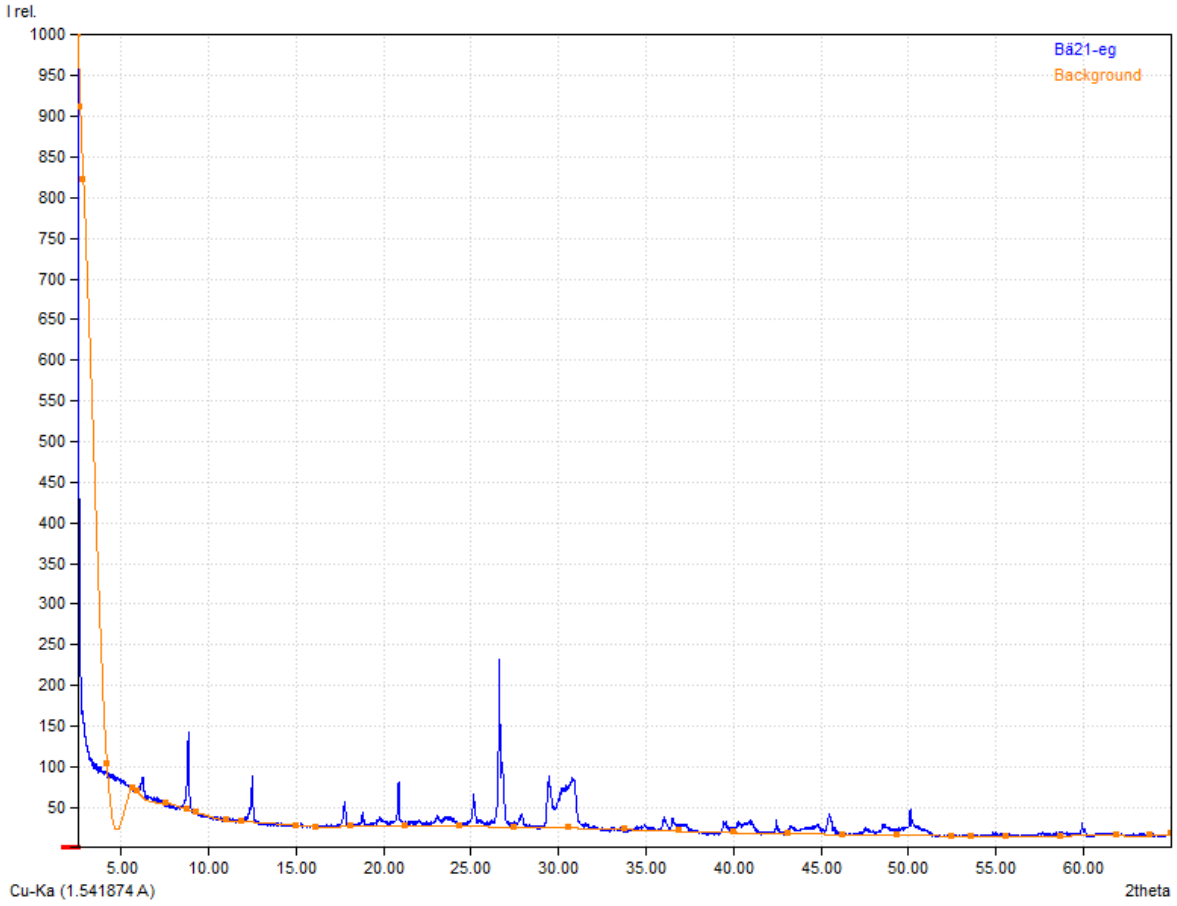
I rel.
Bä21-eg
Background
Cu-Ka (1.541874 A)
2theta

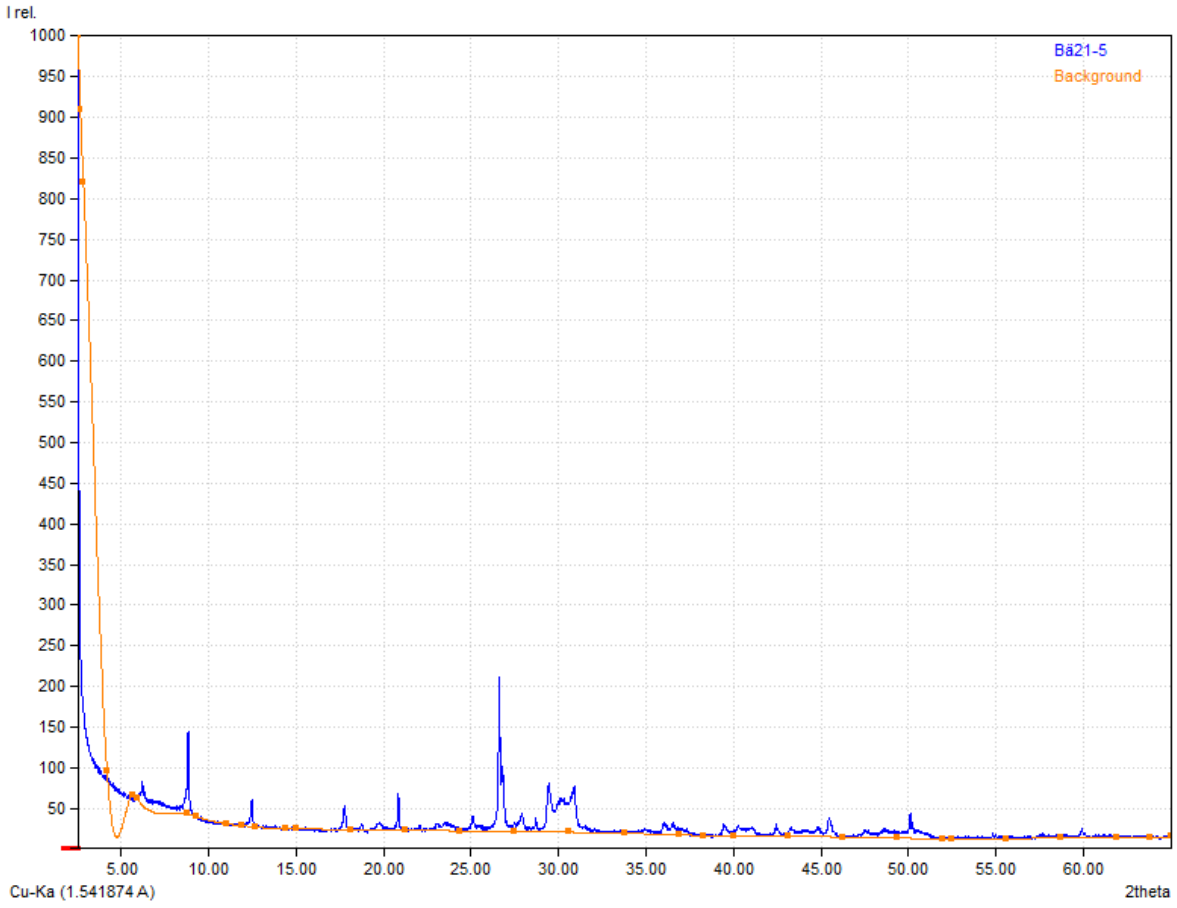
I rel.
Bä21-5
Background
Cu-Ka (1.541874 A)
2theta

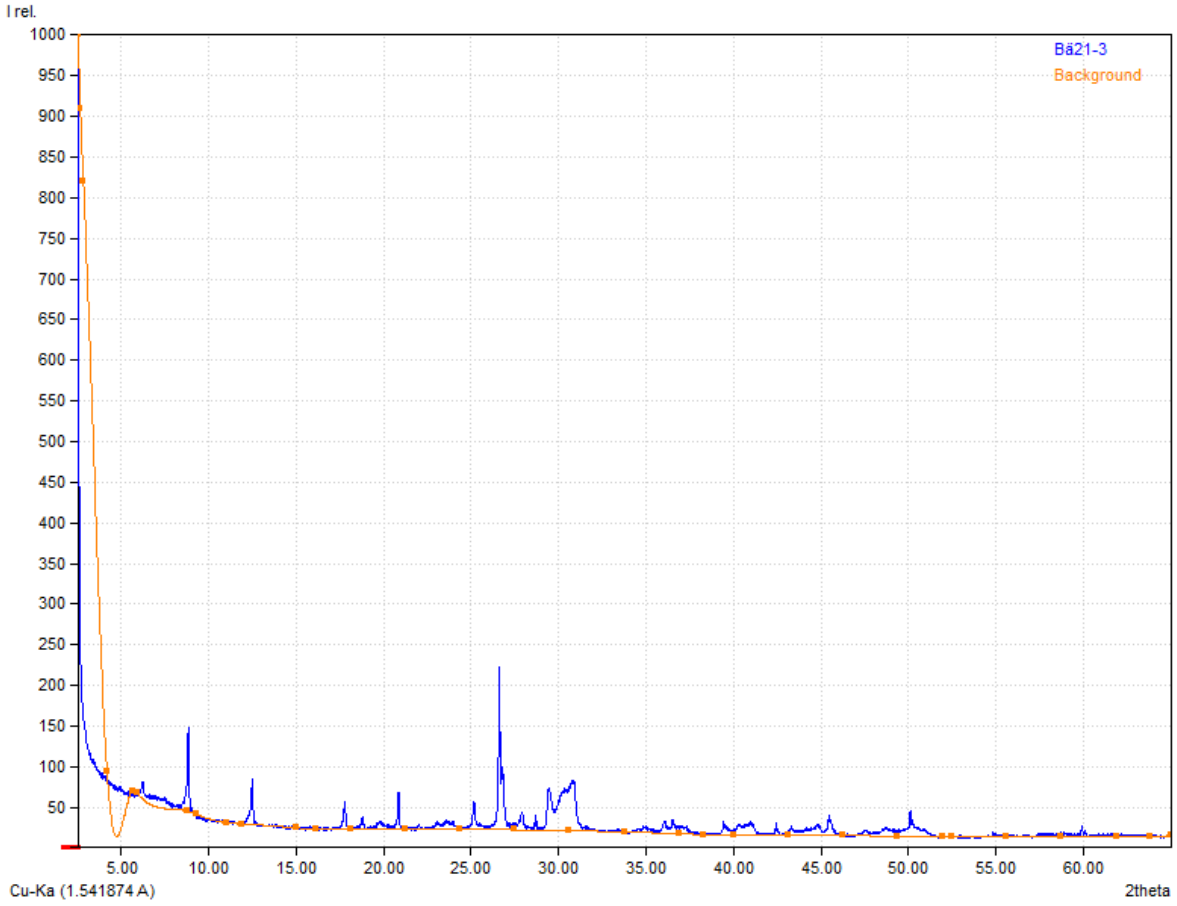
I rel.
1000
950
900
850
800
750
700
650
600
550
500
450
400
350
300
250
200
150
100
50
Bä21-3
Background
5.00
10.00
15.00
20.00
25.00
30.00
35.00
40.00
45.00
50.00
55.00
60.00
Cu-Ka (1.541874 A)
2theta

III. Tables

Profile 1		
	Coordinates [WGS84]	
Sample Nr	**Latitude**	**Longitude**
Pod41	47°53.248'	016°46.498'
Pod42	47°53.304'	016°46.480'
Pod43	47°53.359'	016°46.465'
Pod44	47°53.414'	016°46.459'
Pod45	47°53.467'	016°46.446'
Pod46	47°53.524'	016°46.436'
Pod47	47°53.577'	016°46.425'
Pod48	47°53.633'	016°46.419'
Pod49	47°53.687'	016°46.406'
Pod50	47°53.741'	016°46.396'
Pod51	47°53.795'	016°46.375'
Pod52	47°53.847'	016°46.355'
Pod53	47°53.902'	016°46.337'
Pod54	47°53.955'	016°46.315'
Pod55	47°54.008'	016°46.298'
Pod56	47°54.063'	016°46.264'
Pod57	47°54.117'	016°46.246'
Pod58	47°54.169'	016°46.222'
Pod59	47°54.222'	016°46.202'
Pod60	47°54.272'	016°46.181'
Pod61	47°54.324'	016°46.165'
Pod62	47°54.376'	016°46.149'
Pod63	47°54.429'	016°46.121'
Pod64	47°54.478'	016°46.101'
Pod65	47°54.533'	016°46.086'

Pod66	47°54.581'	016°46.068'
Pod67	47°54.629'	016°46.055'
Pod68	47°54.687'	016°46.046'
Pod69	47°54.744'	016°46.028'
Pod70	47°54.808'	016°46.021'
Pod71	47°54.865'	016°46.011'
Profile 2		
POD1	47°51.187'	016°49.353'
POD2	47°51.227'	016°49.290'
POD3	47°51.267'	016°49.232'
POD4	47°51.297'	016°49.165'
POD5	47°51.324'	016°49.094'
POD6	47°51.352'	016°49.026'
POD7	47°51.379'	016°48.956'
POD8	47°51.405'	016°48.886'
POD9	47°51.425'	016°48.811'
POD10	47°51.450'	016°48.740'
POD11	47°51.478'	016°48.669'
POD12	47°51.504'	016°48.597'
POD13	47°51.531'	016°48.527'
POD14	47°51.555'	016°48.457'
POD15	47°51.581'	016°48.386'
POD16	47°51.606'	016°48.308'
POD17	47°51.629'	016°48.234'
POD18	47°51.660'	016°48.166'
POD19	47°51.688'	016°48.097'
POD20	47°51.723'	016°48.034'
POD21	47°51.749'	016°47.966'
POD22	47°51.786'	016°47.889'

POD23	47°51.814'	016°47.834'
POD24	47°51.855'	016°47.778'
POD25	47°51.888'	016°47.712'
POD26	47°51.913'	016°47.642'
POD27	47°51.947'	016°47.579'
POD28	47°51.985'	016°47.523'
POD29	47°52.007'	016°47.449'
POD30	47°52.042'	016°47.387'
POD31	47°52.075'	016°47.325'
POD32	47°52.107'	016°47.258'
POD33	47°52.143'	016°47.195'
POD34	47°52.169'	016°47.128'
POD35	47°52.202'	016°47.054'
POD36	47°52.231'	016°46.991'
POD37	47°52.265'	016°46.938'
POD38	47°52.294'	016°46'869'
POD39	47°52.332'	016°46.820'
POD40	47°52.384'	016°46.784'
Sediment samples gas sampling locations		
Rust1	47°48.481'	016°42.759
Rust2	47°48.488'	016°42.766'
Rust3	47°48.597'	016°42.913'
Rust6	47°48.782'	016°42.859'
Rust7	47°49.113'	016°43.214'
Rust8	47°47.980'	016°42.472'
Rust9	47°48.081'	016°42.349'
Rust10	47°48.597'	016°42.913'
Mörbisch	47°45.091'	016°41.847'
Purbach	47°54.329'	016°42.517'

Breitenbrunn1	47°54.960'	016°45.925'
Breitenbrunn2	47°54.954'	016°45.917'
Neusiedl	47°55.673'	016°50.328'
Weiden	47°55.045'	016°51.083'
Podersdorf	47°51.118'	016°49.224'
Illmitz	47°45.370'	016°44.534'
Gas samples		
Rust1	47°48.481'	016°42.759
Rust2	47°48.488'	016°42.766'
Rust3	47°48.597'	016°42.913'
Rust4	47°48.789'	016°42.788'
Rust5	47°48.794'	016°42.790
Rust6	47°48.782'	016°42.859'
Rust7	47°49.113'	016°43.214'
Mörbisch	47°45.091'	016°41.847'
Purbach	47°54.329'	016°42.517'
Breitenbrunn1	47°54.960'	016°45.925'
Breitenbrunn2	47°54.954'	016°45.917'
Neusiedl	47°55.673'	016°50.328'
Weiden	47°55.045'	016°51.083'
Podersdorf	47°51.118'	016°49.224'
Illmitz	47°45.370'	016°44.534'

Profile 1			
Sample Nr.	**Carbonates [wt.%]**	**Quartz+Feldspar [wt.%]**	**Clay Minerals [wt.%]**
Pod41	59	8	33
Pod42	74	8	18
Pod43	71	14	15
Pod44	47	19	33
Pod45	51	33	17
Pod46	57	19	23
Pod47	50	19	31
Pod48	54	13	33
Pod49	59	11	30
Pod50	56	14	30
Pod51	42	38	20
Pod52	45	24	31
Pod53	61	12	27
Pod54	69	5	26
Pod55	45	26	29
Pod56	65	10	25
Pod57	34	10	56
Pod58	44	25	31
Pod59	49	11	40
Pod60	17	27	57
Pod61	64	12	24
Pod62	70	9	21
Pod63	65	12	23
Pod64	62	10	28
Pod65	65	15	20

Pod66	77	6	17
Pod67	64	12	24
Pod68	76	7	18
Pod69	41	18	40
Pod70	66	6	27
Pod71	60	5	35
Profile 2			
POD1	19	47	34
POD2	34	55	11
POD3	63	17	20
POD4	66	14	19
POD5	71	13	16
POD6	51	25	24
POD7	61	14	25
POD8	62	12	25
POD9	64	11	26
POD10	62	10	27
POD11	68	11	22
POD12	61	20	19
POD13	65	8	27
POD14	76	6	18
POD15	56	17	27
POD16	66	14	20
POD17	53	24	22
POD18	66	12	23
POD19	68	8	24
POD20	57	20	23

POD21	67	9	24
POD22	64	15	21
POD23	63	14	23
POD24	66	7	27
POD25	69	13	18
POD26	64	15	21
POD27	68	8	24
POD28	64	15	20
POD29	62	15	24
POD30	60	14	25
POD31	69	11	20
POD32	71	6	24
POD33	71	11	19
POD34	58	16	26
POD35	59	12	29
POD36	75	7	17
POD37	60	6	34
POD38	61	12	27
POD39	57	18	25
POD40	59	15	26

Profile 1		
Sample Nr.	**pH**	**Temperature [°C]**
Pod41	7,5	22,3
Pod42	7,6	22,5
Pod43	7,8	23,3
Pod44	7,9	23,2
Pod45	8,0	23,1
Pod46	7,7	22,8
Pod47	7,5	23,3
Pod48	7,7	23,0
Pod49	7,7	22,8
Pod50	7,6	22,9
Pod51	7,9	23,3
Pod52	8,0	23,0
Pod53	7,7	23,2
Pod54	7,8	23,2
Pod55	7,7	23,4
Pod56	7,8	23,0
Pod57	7,5	23,4
Pod58	7,8	23,0
Pod59	8,1	23,0
Pod60	8,1	22,8
Pod61	7,7	23,1
Pod62	8,3	22,8
Pod63	7,8	22,8
Pod64	7,7	22,8
Pod65	8,3	22,7

Pod66	8,3	23,2
Pod67	8,1	22,8
Pod68	8,3	23,2
Pod69	8,2	23,2
Pod70	8,2	23,3
Pod71	8,1	23,3
Profile 2		
POD1	8,2	22,6
POD2	8,4	22,4
POD3	8,4	22,5
POD4	8,4	22,6
POD5	8,7	22,7
POD6	7,5	22,3
POD7	7,9	22,7
POD8	8,1	22,6
POD9	7,7	22,8
POD10	7,8	22,3
POD11	7,6	23,2
POD12	7,7	22,6
POD13	7,7	22,7
POD14	7,7	22,4
POD15	7,8	22,7
POD16	7,9	22,9
POD17	8,1	22,6
POD18	8,1	22,6
POD19	8,1	23,0
POD20	7,9	22,7

POD21	7,7	22,8
POD22	8,0	22,6
POD23	7,9	22,4
POD24	8,0	22,2
POD25	8,0	22,3
POD26	8,0	22,5
POD27	7,9	22,5
POD28	8,0	22,3
POD29	8,0	22,8
POD30	7,9	22,7
POD31	7,8	22,3
POD32	7,6	22,2
POD33	7,7	22,5
POD34	7,8	22,4
POD35	7,6	22,5
POD36	7,9	22,4
POD37	7,4	22,8
POD38	7,5	22,5
POD39	7,5	22,8
POD40	7,6	22,6

Sample Nr.	Total Carbon2 [wt.%]	Total Carbon2 [wt.%]	Total Carbon3 [wt.%]	Sulfur1 [wt.%]	Sulfur2 [wt.%]	Sulfur3 [wt.%]
Pod-01	2,38	2,40		0,00	0,00	
Pod-02	3,72	3,83		0,00	0,00	
Pod-03	7,83	7,93		0,00	0,01	
Pod-04	7,24	7,15		0,00	0,00	
Pod-05	9,59	9,87		0,00	0,00	
Pod-06	7,57	7,91		0,01	0,01	
Pod-07	7,09	7,04		0,01	0,01	
Pod-08	8,02	8,17		0,01	0,01	
Pod-09	7,75	7,90		0,00	0,01	
Pod-10	8,27	8,24		0,00	0,01	
Pod-11	7,89	8,00		0,01	0,01	
Pod-12	6,28	6,43		0,01	0,01	
Pod-13	7,89	7,96		0,00	0,00	
Pod-14	8,22	8,18		0,01	0,01	
Pod-15	8,11	8,12		0,00	0,00	
Pod-16	7,17	7,31		0,01	0,00	
Pod-17	6,64	6,87	6,74	0,00	0,00	0,00
Pod-18	8,73	8,75		0,00	0,00	
Pod-19	9,21	9,13		0,00	0,00	
Pod-20	8,30	8,33		0,00	0,01	
Pod-21	8,49	8,38		0,01	0,01	
Pod-22	8,29	8,41		0,01	0,00	
Pod-23	8,35	8,38		0,00	0,00	
Pod-24	7,85	7,64		0,01	0,00	
Pod-25	8,32	8,34		0,00	0,01	
Pod-26	7,98	8,33	8,26	0,01	0,01	0,00

Pod-27	8,24	8,31		0,00	0,01	
Pod-28	8,09	7,90		0,01	0,00	
Pod-29	8,18	8,36		0,00	0,00	
Pod-30	7,92	8,10		0,00	0,00	
Pod-31	8,49	8,21		0,00	0,01	
Pod-32	8,42	8,54		0,01	0,00	
Pod-33	8,46	8,51		0,01	0,01	
Pod-34	8,19	8,15		0,00	0,00	
Pod-35	8,17	8,01		0,01	0,01	
Pod-36	8,46	8,45		0,00	0,00	
Pod-37	7,56	7,80	7,53	0,00	0,00	0,00
Pod-38	7,07	7,10		0,00	0,00	
Pod-39	8,71	8,95		0,01	0,00	
Pod-40	8,90	8,71		0,01	0,00	
Pod-41	9,64	9,66		0,02	0,01	
Pod-42	8,73	8,70		0,00	0,00	
Pod-43	9,30	9,35		0,00	0,00	
Pod-44	5,53	5,51		0,00	0,00	
Pod-45	6,00	5,98		0,00	0,00	
Pod-46	7,72	7,77		0,01	0,01	
Pod-47	9,26	10,70	9,15	0,01	0,01	0,01
Pod-48	9,20	9,47		0,01	0,01	
Pod-49	9,32	9,50		0,01	0,01	
Pod-50	8,96	9,12		0,01	0,01	
Pod-51	4,60	4,71		0,00	0,00	
Pod-52	6,71	6,72		0,00	0,00	
Pod-53	7,96	8,15		0,00	0,00	

Pod-54	8,67	8,48		0,00	0,01	
Pod-55	7,63	7,57		0,01	0,01	
Pod-56	9,23	9,24		0,00	0,00	
Pod-57	5,02	4,99		0,01	0,01	
Pod-58	8,50	8,36		0,00	0,01	
Pod-59	7,30	7,15		0,00	0,00	
Pod-60	4,99	5,35	5,01	0,00	0,00	0,00
Pod-61	8,58	8,70		0,01	0,00	
Pod-62	9,20	9,32		0,01	0,00	
Pod-63	9,47	9,56		0,01	0,01	
Pod-64	9,79	9,78		0,01	0,01	
Pod-65	9,54	9,64		0,00	0,00	
Pod-66	9,49	9,40		0,01	0,01	
Pod-67	9,62	9,73		0,01	0,01	
Pod-68	9,51	9,53		0,01	0,01	
Pod-69	9,56	9,50		0,01	0,01	
Pod-70	9,47	9,36		0,01	0,01	
Pod-71	9,68	9,69		0,01	0,01	
Pod-72	8,91	9,04		0,01	0,01	
Pod-73	9,34	9,38		0,01	0,01	
Pod-74	8,79	8,76		0,01	0,01	
Pod-75	8,92	9,11		0,01	0,01	
Pod-76	9,21	9,21		0,01	0,01	
Pod-77	8,86	9,17		0,01	0,01	
Pod-78	9,00	9,19		0,01	0,01	
Pod-79	9,74	9,72		0,01	0,01	
Pod-80	5,49	5,49		0,01	0,01	

Pod-81	9,99	10,11		0,01	0,01	
Pod-82	10,24	10,41		0,01	0,01	
Pod-83	9,53	9,71		0,01	0,01	
Pod-84	7,99	8,05		0,01	0,01	
Pod-85	2,50	2,58		0,00	0,00	
Pod-86	5,15	5,07		0,00	0,00	
Pod-87	8,85	9,10		0,01	0,01	

Sample Nr.	Total organic carbon1 [wt.%]	Total organic carbon2 [wt.%]	Total organic carbon3 [wt.%]
Pod-01	0,14	0,14	
Pod-02	0,06	0,12	0,07
Pod-03	1,44	1,51	
Pod-04	0,39	0,41	
Pod-05	0,69	0,63	
Pod-06	2,32	2,35	
Pod-07	1,21	1,27	
Pod-08	1,55	1,57	
Pod-09	1,49	1,63	1,56
Pod-10	1,64	1,66	
Pod-11	1,56	1,59	
Pod-12	1,44	1,05	1,09
Pod-13	1,41	1,44	
Pod-14	1,51	1,53	
Pod-15	1,73	1,80	
Pod-16	1,77	1,53	1,45
Pod-17	0,30	0,33	
Pod-18	0,68	0,64	
Pod-19	1,05	1,40	0,97
Pod-20	1,89	1,89	
Pod-21	1,78	1,87	
Pod-22	1,68	1,78	
Pod-23	1,56	1,63	
Pod-24	1,59	1,61	
Pod-25	1,67	1,70	
Pod-26	1,65	1,71	
Pod-27	1,54	1,59	

Pod-28	1,46	1,48	
Pod-29	2,54	1,54	1,55
Pod-30	1,49	1,60	1,51
Pod-31	1,74	1,73	
Pod-32	1,63	1,71	
Pod-33	1,74	1,83	
Pod-34	1,63	1,65	
Pod-35	2,02	2,06	
Pod-36	**0,92**	**1,02**	0,96
Pod-37	0,80	0,96	0,86
Pod-38	0,65	0,67	
Pod-39	2,21	2,27	
Pod-40	2,24	2,10	
Pod-41	3,35	3,50	
Pod-42	0,68	0,74	
Pod-43	0,71	0,78	
Pod-44	**0,53**	**0,43**	0,41
Pod-45	0,22	0,20	
Pod-46	2,39	2,43	
Pod-47	2,79	2,97	2,77
Pod-48	3,16	3,21	
Pod-49	3,13	3,09	
Pod-50	2,78	2,76	
Pod-51	0,32	0,32	
Pod-52	0,63	0,63	
Pod-53	1,04	1,02	
Pod-54	**1,44**	**0,51**	1,26

Pod-55	1,19	1,10	
Pod-56	1,76	1,84	
Pod-57	2,37	2,40	
Pod-58	1,18	1,24	
Pod-59	0,36	0,40	
Pod-60	0,48	0,55	0,44
Pod-61	1,53	1,58	
Pod-62	1,82	1,87	
Pod-63	1,84	1,91	
Pod-64	1,92	1,90	
Pod-65	1,81	1,83	
Pod-66	1,87	1,90	
Pod-67	1,98	1,99	
Pod-68	1,92	1,86	
Pod-69	1,96	1,96	
Pod-70	1,81	1,89	
Pod-71	1,89	1,96	
Pod-72	1,76	1,79	
Pod-73	1,84	1,85	
Pod-74	2,63	2,54	
Pod-75	1,80	1,71	
Pod-76	1,97	2,00	
Pod-77	1,91	1,84	
Pod-78	1,82	1,85	
Pod-79	2,27	2,30	
Pod-80	2,08	2,01	
Pod-81	2,31	2,37	

Pod-82	2,25	2,28	
Pod-83	2,80	2,84	
Pod-84	1,50	1,47	
Pod-85	0,18	0,15	
Pod-86	0,18	0,21	
Pod-87	1,81	1,82	

Gas composition [ppm]							
Location	**H_2S**	**H_2**	**CO_2**	**O_2**	**N_2**	**CH_4**	**sum**
Mörbisch		9,52	1994,27	211869,37	761946,53	24180,30	1000000
Rust1		10,75	841,80	214372,93	772035,27	12739,24	1000000
Rust2		8,05	666,96	211723,86	766589,19	21011,94	1000000
Rust3		9,42	492,86	217809,88	780421,80	1266,04	1000000
Rust4		8,09	785,10	214291,28	771916,87	12998,67	1000000
Rust5		8,94	1201,84	209813,41	761887,45	27088,37	1000000
Rust6		9,22	3214,23	207877,58	742941,34	45957,64	1000000
Rust7	313,24	7,53	46069,02	141634,15	516984,32	294991,74	1000000
Purbach		8,56	1822,13	214048,87	765785,11	18335,34	1000000
Breitenbrunn1	0,04	6,98	11050,99	162692,77	594897,86	231351,35	1000000
Breitenbrunn2	1,72	8,42	19184,92	165782,75	608837,50	206184,69	1000000
Neusiedl		9,46	2104,86	207180,62	750744,59	39960,47	1000000
Weiden		9,65	1645,70	209954,03	754450,67	33939,96	1000000
Podersdorf	0,55	9,39	9152,18	212165,55	758965,81	19706,51	1000000
Illmitz		8,89	3627,15	210902,50	756880,90	28580,57	1000000

Stable isotopes			
Location	**$\delta^{13}C$ of CH_4 [‰]**	**δD of CH_4 [‰]**	**$\delta^{13}C$ of CO_2 [‰]**
Mörbisch	-66,4	-213	-10,65
Rust1	-57,5		-16,48
Rust2	-56,9		
Rust3	-21,1		
Rust4	-79,2		
Rust5	-80,3		-15,57
Rust6	-57,6	-268	
Rust7	-59,7	-334	-7,53
Purbach	-57,8		
Breitenbrunn1	-68,5	-307	-7,05
Breitenbrunn2	-61,4	-309	-9,59
Neusiedl	-61,6	-229	
Weiden	-61,5		-13,61
Podersdorf	-57,4	-138	-6,60
Illmitz	-57,5		